Identifying novel regulators of ciliogenesis

Alice Verity Rosalind Lake

Submitted in accordance with the requirements for the degree of
PhD Medicine

The University of Leeds
Faculty of Medicine
Leeds Institute of Medical Research at St. James's

April, 2020

The candidate confirms that the work submitted is her own and that appropriate credit has been given where reference has been made to the work of others.

Acknowledgements

For their guidance and encouragement I would like to give endless thanks to my supervisors; Prof. Colin A. Johnson, Dr. Jacquelyn Bond, and Dr. Ewan Morrison. My supervisors not only helped me to develop my research interests and broader perspective, but also encouraged my personal development for which I am very grateful.

The research presented in Chapter 4 of this thesis has been carried out by a team which has included myself and Dr. Basudha Basu. My own contributions, fully and explicitly indicated in the thesis, have been all the work that contributed to figures: 4.1 through to 4.10 in addition to 4.16. Furthermore my work included the analysis and interpretation of all data presented except for Figure 4.11. Dr Basudha Basu's contributions have been as follows: intellectual input and experimental design that contributed to Figures 4.11 through to 4.15, lab work that contributed to 4.11, 4.12 and 4.15, and identification of the exemplar images and videos presented in 4.11, 4.12 and 4.15.

I would also like to thank Dr. Katarzyna Szymanska, Dr. Claire E Smith, and the rest of the Johnson Cilia Lab group for their contributions to academic discussion, help with lab issues and insightful advice. I would also like to extend thanks to my lab partner in crime Rebecca Perrin, who without the laughs would have made this whole process so much harder. Then a further thanks to my friends Dr. Ringaile Zaksauskaite and Dr. Lucia Sedlackova who never failed to be there for me when I needed them.

For his unwavering support, love, patience, and motivation I would like to thank my darling partner Dr. Thomas White. For their support and love I would also like to thank my family far and wide, and especially my Grandad, Jim Russell, who has always championed my academic achievements.

Abstract

Primary cilia are microtubule-based “antennae-like” organelles extending from the apical surface of most mammalian cells. They integrate mechanical or chemical signals essential for cell homeostasis and differentiation through several cooperating compartments. Mutations in genes that encode ciliary proteins or proteins essential for correct ciliary function are the cause of a major group of inherited and variable developmental disorders known as ciliopathies. Functional interactions between ciliary compartments, the molecular basis of variable clinical phenotypes, and the mechanisms of cilia formation are all still poorly understood.

The presence or absence of cilia can be easily imaged and quantitated. This lends itself to high-throughput, high-content imaging in reverse genetic screens of cellular phenotypes. siRNA reverse genetic screens were performed to assess increased cilia incidence and identified that ROCK2 is a key negative regulator of ciliogenesis. Analysis showed ROCK2 acts through a mechanism involving actin remodelling and acto-myosin contraction. Pharmacological inhibition of ROCK2 may therefore comprise a novel therapeutic approach for treatment of a broad group of ciliopathy disease classes. Further screening of a data-set for supernumerary primary cilia, added to the evidence that cytokinesis is not a prerequisite for ciliogenesis. Disruption of the centralspindilin complex caused mitotic failure and maturation of supernumerary centrosomes, leading to the formation of the supernumerary cilia, a known cellular phenotype of severe ciliopathies. Finally, a combinatorial screening approach to generate double genetic perturbations of ciliary genes identified reciprocal synthetic genetic interactions between anterograde intraflagellar transport (the IFT B complex) and the transition zone.

Reverse genetics screening techniques have identified novel regulators and pathways of ciliogenesis, and a potential therapeutic target for ciliopathies. Furthermore, combinatorial screening has highlighted a novel and complex interaction in ciliary biology, that may provide potential new insights into ciliary organisation and disease pathomechanisms.

Table of Contents

List of Tables

List of Figures

Abbreviations

4-HT	4-hydroxytamoxifen
ACTR3	Actin related protein 3
AurA	Aurora A
Bcl10	B-cell lymphoma leukaemia 10
BioID	Proximity-dependent biotin identification
Cdk1	Cyclin dependant kinase 1
CRISPR/Cas9	Clustered regularly spaced short palindromic repeats/Cas9
DAPs	Distal appendages
DNA	Deoxynucleic acid
dsRNA	Double stranded ribonucleic acid
ECV	Extracellular vesicles
ER	oestrogen receptor
ERK/JNK	Extracellular signal-related kinase/c-jun N-terminal kinase
Fancd2os	Fanconi anaemia opposite strand transcript protein
Foxj1	Forkhead box protein J1
FRAP	Fluorescence recovery after photobleaching
GAP	GTPase Activating Protein
GFP	Green fluorescent protein
GO	Gene Ontology
GPCR	G protein coupled receptor
gRNA	Guide RNA
GSN	Gelsolin
HDAC6	Histone deacetylase 6
Hectd2	HECT Domain E3 Ubiquitin Protein Ligase 2
HR	homologous repair
IMCD3	Inner medullary collecting duct
Indels	Insertions/deletions
INPP5E	Inositol polyphosphate-5-phosphatase E
InterPro	Integrative protein signature database
JBTS	Joubert Syndrome
KD	Kinase domain
KEGG	Kyoto encyclopaedia of genes and genomes
MEFs	Mouse embryonic fibroblasts
mIMCD-3	Mouse inner medullary collecting duct cells
MLC	Myosin light chain

MLC^{TASA}	MLC (Thr18>Ala18, Ser19>Ala19)
MIP	Maximum intensity projection
mRNA	Messenger RNA
NFκB	Nuclear factor kappa B
NHEJ	Non-homologous end joining
PAM	Protospacer adjacent motif
PCM	Peri-centriolar matrix
PCR	Polymerase chain reaction
PFAM	Protein families database
PIP3	Phosphatidylinositol (3,4,5)-trisphosphate
Plk1	Polo-like kinase 1
Q-SNARE	Gluatamine donating soluble NSF attachment receptor
RACGAP1	Rac GTPase activating protein 1
RBD	RhoA binding domain
RISC	RNAi-induced silencing complex
ROCK	RhoA-associated protein kinase
RPE-1	Retinal pigment epithelial cells
RTK	Receptor tyrosine kinase
RT-PCR	Reverse transcriptase-polymerase chain reaction
Shh	Sonic hedgehog
shRNA	Small hairpin ribonucleic acid
siRNA	Small interfering ribonucleic acid
STRING	Search tool for recurring instances of neighbouring genes
T7 Assay	T7 Endonuclease I Digestion Assay
TAP	Tandem Affinity Purification
TEM	Transmission electron microscopy
TCF/LEF	Transcription factor/lymphoid enhancer-binding factor
TGFβ	Transforming growth factor beta
TZ	Transition zone
UPS	Ubiquitin/proteasome system
Wnt	Wingless-related integration site
WT	wild-type
YAP/TAZ	Yes associated protein/transcriptional coactivator with PDZ binding motif

Chapter 1
Introduction

1.1 The primary cilium

The hair-like organelles, that protrude from the surface of most types of eukaryotic cells, were first noted by Anthony van Leeuwenhoek in 1675 as “little legs” on the protozoa he was observing, thus making cilia the oldest known cellular organelle. These “little legs” were later called cilia, after the Latin for eyelash, by Otto Muller in 1786. However, the distinction between motile, flagella-like cilia observed by Leeuwenhoek and non-motile cilia was first described in the 19th century (1). As a consequence, early research on cilia focused on motile cilia and their similarities to the eukaryotic flagellum, leaving the primary cilium mostly ignored and perceived as a vestigial cellular structure. In retrospect, this seems to be a strange view because early researchers knew that primary cilia were highly conserved organelle across major animal phyla, albeit with some variations in function and structure. It is only in the last 20 years that the importance of these fascinating organelles has been fully appreciated, following the many recent seminal discoveries of their involvement in many essential signalling and developmental pathways in humans. Primary cilia are now part of the scientific mainstream in modern biomedical research (1).

1.1.1 Primary vs motile cilia

There are two main types of cilia: motile cilia and primary cilia (Figure 1.1). Motile cilia include sperm flagella and the numerous cilia of airway epithelial multi-ciliated cells. The latter mediate the muco-ciliary escalator that moves mucus up and out of the respiratory tract. In contrast, primary cilia are static and known to have a more specialised sensory role. Primary cilia are present on nearly all cells within the human body except hepatocytes (2) and leukocytes.

A) Primary Cilium **B) Motile Cilium**

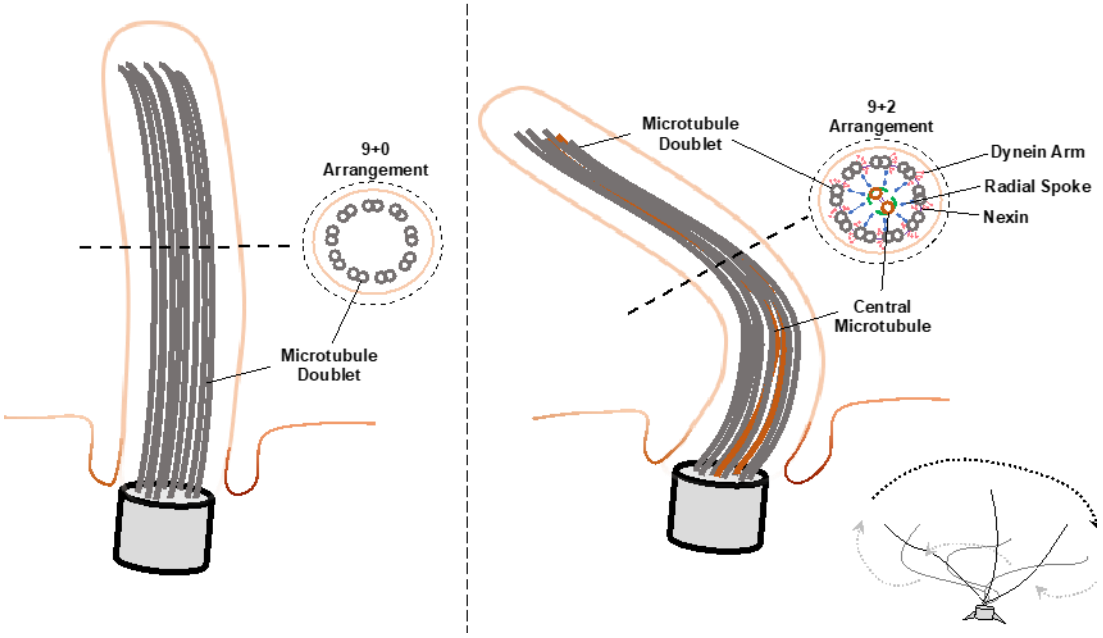

Figure 1.1 Primary vs motile Cilia

A) The primary cilium is an hair-like structure that protrudes from the apical membrane of many eukaryotic animal cells. It has a 9+0 microtubule doublet arrangement in the axoneme that protrudes from the basal body. **B)** A motile cilium also protrudes from the membrane of cells. but differs in its internal microtubule structure. The majority of motile cilia have a pair of central microtubules making a 9+2 arrangement (exceptions include nodal cilia). Dynein arms and radial spokes allow the microtubules to slide against each other to generate movement. An example ciliary beat pattern of tracheal cilia is represented in the bottom right corner, consisting of a whipping-like motion.

1.1.1.1 Motile cilia

Motile cilia are an essential organelle conserved in many animals and are ubiquitous in vertebrates, large animals such as mammals, and humans (3). To facilitate their beat patterns the majority of motile cilia have a different structural arrangement of microtubules, comprising a 9+2 arrangement (4), and different motor proteins in the ciliary axoneme. Spermatozoa have a single motile cilium required for movement, although most cells in mammalian adults with motile cilia form arrays of these motile cilia. These cells are terminally differentiated because of the vast number of centrioles (from 30 up to 300 (5)) required to produce the ciliary arrays. Motile cilia when in arrays, synchronise their beat patterns within cells and tissues to produce directional fluid flow (6). This fluid

flow is essential in tissues such as the lungs, nasal passage and fallopian tubes for correct tissue function (6).

1.1.1.2 Primary cilia

Primary cilia are static and have a major sensory role in cells (7), with a different ultrastructure to motile cilia, including a 9+0 microtubule doublet arrangement in the axoneme (Figure 1.1) (4). They also protrude from the apical membrane of cells, but in some cases are held within a deep membrane invagination known as the ciliary pocket (8). They are able to sense chemical and mechanical stimuli and transduce signals into the cell.

1.1.2 Specialised cilia

There are several specialised cilia that have essential roles for correct organ function. Renal cilia and kinocilia, displayed on hair cells of the inner ear, mediate mechanosensation (9, 10) . Renal cilia are displayed as solitary organelles on renal epithelial cells in order to detect fluid flow (9), whereas kinocilia cooperate with actin-rich stereocilia in order detect mechanosensation of soundwaves and also fluid flow in the utricular macula for balance (10). Other specialised cilia include olfactory cilia that are essential for chemosensation in the nasal mucus (11), the photoreceptor connecting cilium essential for phototransduction (12, 13), and nodal cilia in embryogenesis (14).

1.1.2.1 Photoreceptor connecting cilium

The outer segments of retinal photoreceptors mediate phototransduction (12). These highly-specialised neurons have a highly modified primary cilium termed the connecting cilium, which attaches the inner and outer segments of the photoreceptor (12). The base of the cilium is in the inner segment and the cilium then joins to the outer segment where the ciliary axoneme extends (15). This cilium is required for the phototransduction cascade and transport of rhodopsin and other essential proteins and lipids from the cell body to the outer segment (Reviewed in Khanna, 2015 (15)).

Since the photoreceptor and connecting cilium is vastly complex, this is the likely reason that the retina is highly susceptible to the effect of mutations in

ciliary genes and, as a result, inherited retinal dystrophy is a common phenotype across the spectrum of ciliopathies.

1.1.2.2 Nodal cilia

Single motile cilia are present in the developing embryo and are essential for the initiation and maintenance of asymmetric flow in the embryonic node. This asymmetric flow is required for distribution of morphogens at the embryonic node and subsequent correct left/right patterning in the developing embryo (14, 16). These mono-motile cilia generate leftward flow in the vertebrate embryonic node (in mammals) and Kupffer's vesicle (in fish) in order to establish gradients of developmental proteins and to produce patterning across the embryo (14, 16). These mono-motile cilia are found around the pit of the node, however there is a second type of nodal sensory cilia which have an important role in breaking embryo symmetry (17).. These primary cilia are non-motile and are found on the crown cells which surround the edges of the indentation in the node (17). With such essential roles in embryogenesis, it is not surprising that mutations in ciliary genes cause complex, multi-organ developmental defects that include laterality defects.

1.2 Primary cilia structure

1.2.1 Ultra-structure

Most of ciliary ultra-structure was determined from early transmission electron microscopy (TEM) studies in the 60s and 70s (18-22). The cilium is made up of distinct compartments that each contribute to overall structure and function. The ciliary membrane is an extension of the apical plasma membrane, but has a unique composition of proteins and lipids (23). The cilium is therefore a cellular organelle that is not completely membrane bound. It originates from a mature mother centriole in the cytoplasm (24, 25), and forms an axonemal structure that protrudes from the cell (Figure 1.2).

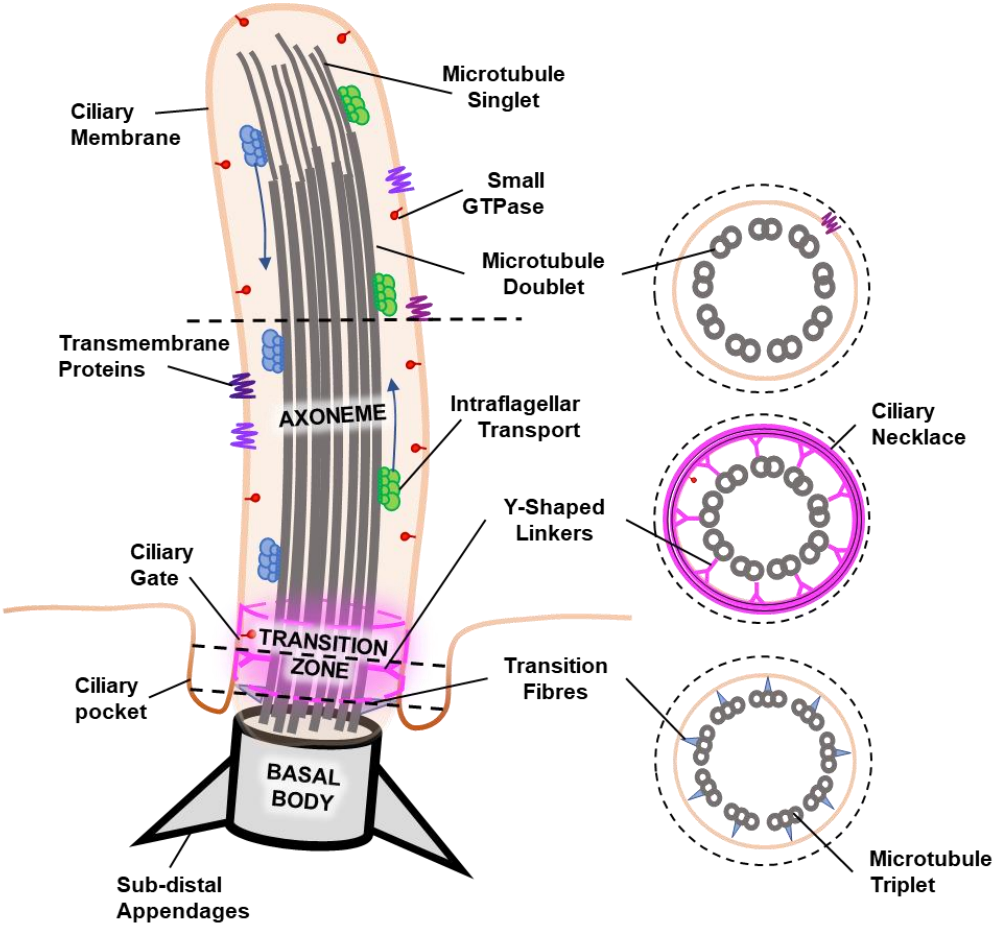

Figure 1.2 Ultra-structure of the primary cilium

The primary cilium is formed from the mother centriole (termed basal body when docked to the membrane),, that attaches to the cell membrane with support from distal appendages. Microtubules extend from the basal body and form a 9+0 microtubule doublet arrangement at the transition zone and becomes singlet microtubules at the ciliary tip. The transition zone tethers the ciliary membrane to the microtubules using distinctive Y-shaped linkers. The ciliary membrane is a continuation of the cell membrane but is highly specialised, containing a different complement of phospholipids and signalling receptors.

1.2.1.1 Ciliary pocket

The part of the membrane that surrounds the lower portion of the cilium and connects directly to the cell membrane is called the ciliary pocket (also known as the ciliary pit in older literature). It is primarily seen as a full membrane invagination in non-polarized cell types, such as hTERT-immortalized Retinal Pigment Epithelial cell line (RPE-1). In polarized cells, however, it also present at low incidence, for example in ~10% of mouse inner medullary collecting duct (IMCD3) cells (8). This region of the cilium mediates the interactions of the

ciliary membrane with the basal body via the distal appendages (23, 24), and the ciliary pocket therefore reflects the positioning of the basal body (8).

The ciliary pocket is relatively poorly defined. However, it is known to be very dynamic, due constant endocytosis which recycles ciliary receptors and for fusion of ciliary vesicles delivering membrane proteins (8, 26). The ciliary pocket is also surrounded by actin bundles which help to deliver ciliary-targeted vesicles and maintain the shape and depth of the pocket (27). As this is the fusion site for the delivery of new membrane proteins, the ciliary pocket also works to regulate transport into and out of the cilium in association with the transition zone.

1.2.1.2 Basal body and appendages

The basal body is the name given to the matured mother centriole when it has docked and formed a cilium. The mother centriole has a stable 9+0 microtubule triplet arrangement and is approximately 500 x 250 nm (28, 29). These microtubule triplets extend to become the ciliary axoneme.

When docked at the cell membrane the basal body is supported by the distal and/or sub-distal appendages anchoring it to the ciliary pocket in vertebrate cells (30). In cells with submerged cilia, such as non-polarised cells including RPE-1 cells, the basal body and cilium is submerged within the ciliary pocket (31). The basal body in these cells, as with most vertebrate cells, is associated with the Golgi apparatus (32). This positioning of the cilium is maintained by centrosome cohesion and the presence of sub-distal appendages. The sub-distal appendages are not essential for cilia assembly, unlike the distal appendages, and therefore the role of sub-distal appendages varies between cell types. However, they are generally thought to give further ciliary stability and contribute to centriole linkage (33).

RPE-1 cells with mutations in both centrosome cohesion linkers (*CEP128*$^{-/-}$) and sub-distal appendages (*C-NAP*$^{-/-}$), cilia are able to surface as they are no longer restrained to the Golgi apparatus or associated with a deep ciliary pocket (33). Surfaced cilia have exacerbated signalling responses (Figure 1.3) in their ability to detect flow or to accumulate signalling receptors such as Smoothened (33). Therefore, the overall positioning of the cilium is regulated by both the sub-distal

appendages and centriole cohesion complex, as single mutants of one or the other structure cause the cilium to remain submerged (33). Therefore, regulation of these structures may be responsible for the surfacing of cilia in polarised cell types. This, in turn, informs the choice of cell model for ciliary research into signalling and mechanosensation, as well as the light microscopy method used to visualize ciliary processes.

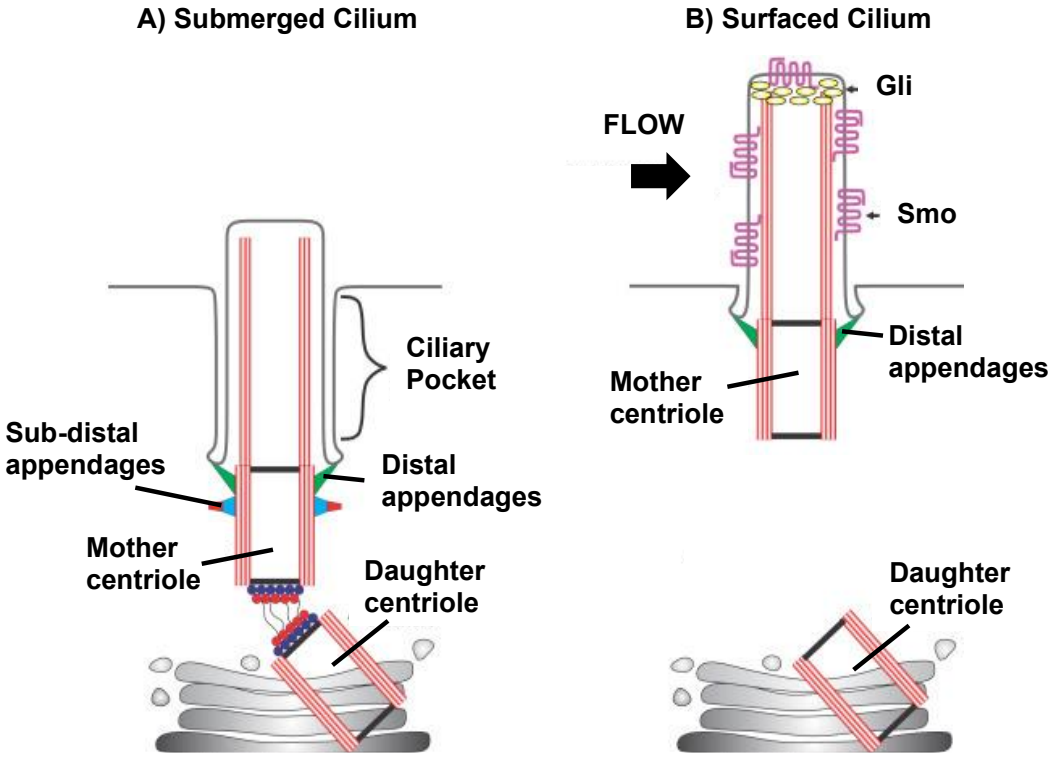

Figure 1.3 Positioning of the basal body contributes to ciliary function

A) Sub-distal appendages and centriole cohesion are required for cilia to be submerged and close to the Golgi apparatus. These cilia usually occur in non-polarised cells and have reduced signalling capabilities. **B)** The positioning of the basal body with a small ciliary pocket is held by distal appendages. Without centrosome cohesion the cilium can surface. These cilia have full signalling capacity, seen by increased localisation of signalling receptors and also increased mechanosensation. Image adapted from (30) Figure 1, and used with copyright permissions.

1.2.1.3 The transition zone

Just above the basal body is the transition zone (TZ), a highly complex structure that acts as the ciliary gate, regulating the movement of proteins into and out of the cilium. The TZ starts 10nm above the distal appendages (34) of the basal body and extends into the base of the axoneme. It is approximately 300-350nm wide and follows the 9 fold symmetry of the axoneme microtubules (34). It is in

the TZ that the microtubule arrangement changes from the 9 triplet microtubules to the signature 9+0 microtubule doublet arrangement (35). TEM has also revealed clear Y-shaped linkers in the TZ that appear to tether the membrane the microtubule doublets (36).

1.2.1.4 The axoneme

The central structure of the cilium is a microtubule arrangement that extends from the basal body in the 9+0 formation previously mentioned, with the plus end of the microtubules at the tip of the cilium. The axoneme of primary cilia can vary from 1-9μm in length, dependant on cell type (37), and is surrounded by the ciliary membrane. As there is no translational machinery within the cilium, proteins that are made in the cytoplasm or cell body must be trafficked into and along the axoneme to build, maintain and disassemble the cilium throughout the cell cycle. The microtubules act as tracks to allow trafficking of transport trains to and from the ciliary tip (38) .

1.2.2 Molecular structure

There are over 1000 known ciliary proteins (39, 40) that contribute to the cilium's diverse functions, and recent publications have identified several hundred further candidate proteins (40, 41). The cilium must therefore have a highly organized molecular structure, where the localisation of and translocation of these proteins are tightly regulated. Despite a well-characterized ultra-structure, defined by electron microscopy studies, the molecular organisation of proteins within the cilium is still relatively undefined. This is due to the limitations of traditional protein-protein interaction studies and the restricted resolution of confocal microscopy techniques. Recent advances in super-resolution microscopy, and proximity labelling methods such as the "APEX" method (42) and use of localization reagents such as nanobodies or tagged non-antibody binding proteins ("Affimers") (43), should soon lead to a more defined molecular organisation of the cilium (44).

1.2.2.1 Ciliary membrane

There are an abundance of different signalling receptors that make up the specific composition of the ciliary membrane, reflecting the cilium's role in a

wide range of signalling pathways (23). The ciliary membrane has several sub-compartments, each with an individual composition of proteins, associated with the ciliary pocket, axoneme and ciliary tip (23). Furthermore, lipid composition differs not only compared to the cell membrane but even throughout the sub-regions of the ciliary membrane (23).

Despite high levels of endocytic activity, specific signalling receptors are not found to localise to the ciliary pocket, although they may be present transiently. The current opinion is that the pocket is primarily a site of vesicle docking that transports new membrane proteins during maintenance of the cilium (8). This model therefore predicts that soluble NSF attachment receptor (SNARE) proteins and vesicle regulators such as Rabin8 and exocyst localise to the ciliary pocket (45-47).

The main length of the axoneme is the location for the majority of signalling receptors that are responsible for the many functions of the primary cilium. Once trafficked, the distribution of proteins along the ciliary membrane and anchoring of ciliary membrane proteins is partially regulated by the small GTPase ARL13B. ARL13B interacts with actin (48) and tubulin (49) to ensure the correct distribution of membrane proteins along the axoneme, and possibly mediates the interactions between membrane proteins and the axoneme during signal transduction (49). Separate to this, ARL13B has roles in recruitment of proteins to the ciliary membrane (49) through endocytic trafficking of ciliary cargo (48).

The ciliary tip is known to have a different composition of proteins, including clathrins and actin, because the ciliary tip can also be a source of extracellular vesicles (ECV) (50). The most well-investigated of these ECVs are from the retina outer segment, which allow recycling of opsins through endocytosis of ECVs by the retinal pigment epithelial cells (51). In other cell types, ECVs are poorly characterised, but purified ECVs have been shown to contain ciliary proteins and transmembrane signalling molecules (52, 53). Therefore, ECVs may be used as a type of ciliary paracrine signalling between cells, or as a way for the cilium to rapidly regulate the levels of signalling proteins during signalling responses (50).

1.2.2.2 The axoneme and intraflagellar transport

The axonemal microtubules are post-translationally modified as they extend. The main stem of the axoneme is made up of alpha/beta tubulin heterodimers in which the alpha tubulin is acetylated (54). The plus end of the tubules are at the ciliary tip and are unmodified until incorporated into the main axoneme. Axonemal extension and transport of cargo along these tubules is controlled by intraflagellar transport (IFT) proteins. IFT proteins are split into two types, IFT-A and IFT-B, which form macromolecular complexes to continuously traffic cargo throughout the cilium (55).

Although peripheral and core IFT proteins are highly conserved between different organisms the IFT-A and IFT-B complexes have different compositions of proteins. First characterised in 2009 in mice (56), the mammalian IFT-B complex is made up of 10 core IFTB proteins and a further 6 peripheral proteins (57). The core and peripheral proteins form a large complex through interactions of IFT52 and IFT88 from the core complex, with IFT38 and IFT57 from the peripheral complex (57). Across IFT proteins, most domains are not required for complex formation and stability, and as most do not have enzymatic activity (58). An exception to this would be IFT140 in the stabilisation and formation of the IFTA complex However the complexes have a range of domains available for protein-protein interactions with an assortment of cargos (55, 59). The difference between these domains and the few stability domains are reviewed in Bhogaraju *et al*., 2013 (58).

IFT-B has been shown to gather in two distinct pools around the transition zone, at the sub-distal appendages and distal to the transition zone, presumably for collection of cargo (60). The exact interactions between IFT and cargos is not well-defined and is thus an area of on-going research. It is currently known that ciliary cargo is trafficked by motor proteins that travel along the ciliary microtubules. IFT-B works in complex with kinesin motors to facilitate anterograde transport to the ciliary tip (61). To select the cargo, IFT works in conjunction with the BBSome, an eight-membered protein complex that regulates the stability of IFT trains (multiple cargo associated with IFT and motor proteins) (62, 63). The BBSome complex also has a non-specific binding motif which allows it to select and carry a variety of ciliary cargos with IFT (64),

of which much work provides evidence for a BBSome role in exit of cargo selectively. For entry and trafficking, Tulp3 has also been shown to act as an adaptor for g-protein coupled receptors in the ciliary membrane to be carried by and IFT-A (65). Highlighting a surprising role for IFT-A in transport of protein into the cilium rather than solely in retrograde transport.

Once at the tip, cargo is collected by IFT-A which work with dynein motor proteins for retrograde transport (66). IFT-A is a complex of at least six proteins (67) and transport of cargo also occurs in association with the BBSome. If not shuttled back down the axoneme, cargo accumulates and forms a bulbous ciliary tip, as seen in mutants of IFT-A proteins (68). IFT-A is not only important in transport within the cilium, but has been implicated in proper ciliogenesis (69).

There is evidence that shows IFT-A proteins are involved in the recruitment of proteins during ciliogenesis not just ciliary retrograde transport. In RPE-1 and HEK293 mutants of the IFT-A protein IFT121, membrane proteins ARL13B, INPP5E and SSTR3 were not observed in the cilium (70). SMO localisation was also defective in the presence of Sonic Agonist (SAG) in MEF with null mutations (71). This is further supported by evidence in C. elegans where IFT-A has also been implicated in the recruitment of transition zone proteins during ciliogenesis (72).

1.2.2.3 Transition zone

The transition zone (TZ) is a highly protein dense region of the cilium that makes up the ciliary gate, separating the cilium from the cell cytoplasm. The TZ is separated into different functional modules: the NPHP module, the core and peripheral MKS modules, the JBTS module and the Inversin compartment (73) (Figure 1.4), although these do not directly correspond to the structural arrangement in the cilium. The TZ is known to be made up of at least 87 proteins (associated with the Gene Ontology term (74, 75) “transition zone” found using AmiGo database (http://amigo.geneontology.org/amigo/search/bioentity) (76)), and a further 600 proteins are currently being screened as potential TZ proteins (personal communication, Dr Katarzyna Szymanska, University of Leeds). Many of these may only localise transiently, but it is clear that the molecular organisation must

be precise and tightly regulated. Although these functional modules have been defined, our understanding of the molecular organisation of the transition zone is limited to a few recent super-resolution microscopy studies (44, 60, 77).

2D stimulated emission depletion (STED) microscopy was used in RPE-1 cells to describe the lateral localisations of RPGRIP1L, CEP290, MKS1, TMEM67 and TCTN2 in relation to centrin, a centrosomal protein, and CEP164, distal appendage protein (60). CEP290 was the only protein tested that did not have distinct peak localisations on either side of the axoneme and instead localised throughout the whole axoneme of the cilium, proximal to the other proteins imaged (60). RPGRIP1L has a similar localisation throughout the axoneme but more consistently showed intensity peaks on the edges of microtubules. TMEM67 and TCTN2 had a larger radial diameter and were also seen in some images to extend into the ciliary axoneme. MKS1 was located between these two groups of proteins (Figure 1.4B) (60).

Independently it has been shown from an cross section view that the MKS and NPHP modules form concentric rings, each with individual 9-fold symmetry of punctate staining, presumably due to microtubule association (34).

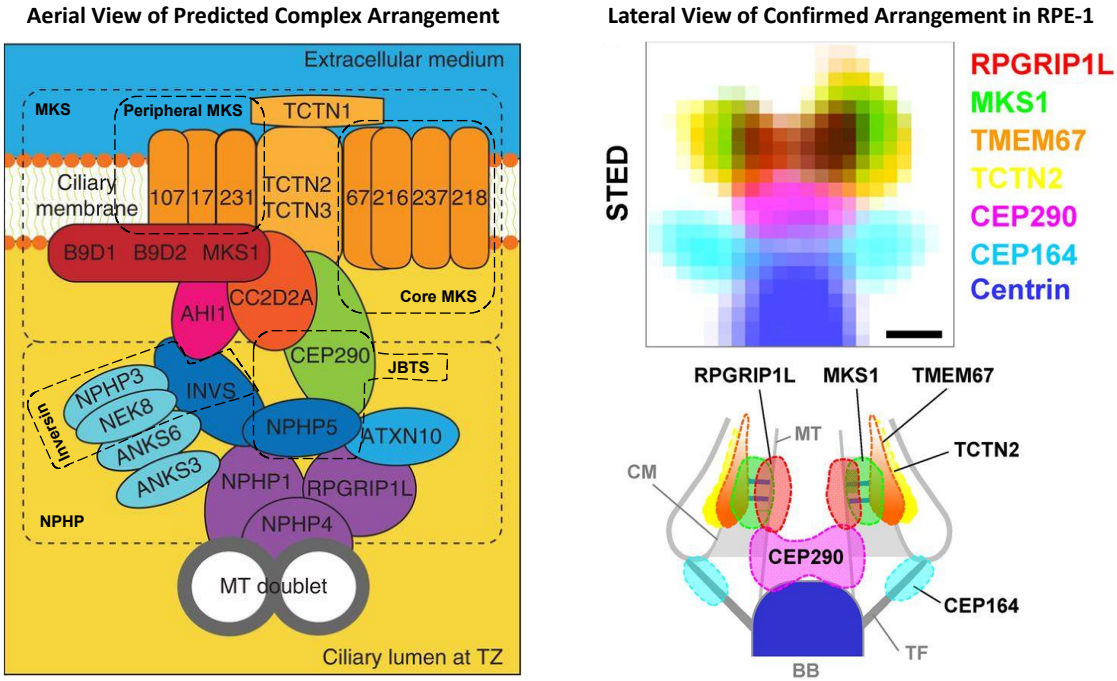

Figure 1.4 Molecular organisation of the transition zone

A) The primary cilium transition zone is made up of several functional complexes, or modules. The MKS modules, (core and peripheral) are made up of transmembrane (TMEM) proteins. The NPHP module is in the ciliary lumen and binds to the microtubule doublets. It is primarily made up of NPHP1, NPHP4 and RPGRIP1L, and then further includes the Inversing module made up of NEK8 and NPHP3, and the JBTS module made up from NPHP5 and CEP290. Adapted from (35) Figure 3C with copyright permissions. **B)** Confirmed localisation of a selection of transition zone proteins in relation to centrosomal proteins in RPE-1 cells from STED microscopy. RPGRIP1L is associated with the microtubules in the ciliary lumen, MKS1 is central in the ciliary lumen whereas both TMEM67 and TCTN2 are associated with the ciliary membrane, TMEM67 is spatially positioned more internally on the membrane than TCTN2. Adapted from (60) Figure 3, and used with copyright permissions.

1.2.2.3.1 Hierarchy of organisation

The hierarchy of proteins in the TZ ensures correct molecular organisation and recruitment of other transition zone proteins, which is key for function. RPGRIP1L is at the top of this hierarchy (summarised in Figure 1.5) (78). RPGRIP1L self-assembles and then is able to recruit and assemble the proper composition of the TZ cells in a cell-dependant manner (79). However NPHP1, also high in the hierarchy, appears to have a minor role in aiding the recruitment of RPGRIP1L (78). SIM microscopy of *Nphp1*$^{-/-}$ mouse embryonic fibroblasts had 15% less RPGRIP1L localised to the transition zone compared to controls (34). However, the determination of proteins in functional modules and their hierarchy of organisation in the TZ was mostly defined through genetic interaction studies in *C.elegans* (80, 81).

The TZ and its interaction with the ciliary membrane and pocket make up the ciliary gate (80). The main proteins in the TZ that contribute to ciliary gate function are RPGRIP1L and CEP290 (82), although the correct amount of CEP290 in the TZ is regulated by RPGRIP1L (82) . The other ciliary luminal-localised proteins, such as inversin and the NPHPs are located within the ciliary membrane and outside of the microtubules and are not essential for ciliary gate function (78). This, in turn, suggests that the hierarchy of proteins in the TZ does not reflect the importance of their function. NPHP4, which is high in the ciliary hierarchy (Figure 1.5), is not essential for ciliary gate function (82).

This also highlights some functional redundancy within the TZ and ciliary gate. As a functional TZ can still be formed and maintained even with complete knock-outs of proteins, during the evolution of mammalian cilia it is possible that proteins have evolved to compensate in the absence of another or where genetically duplicated.

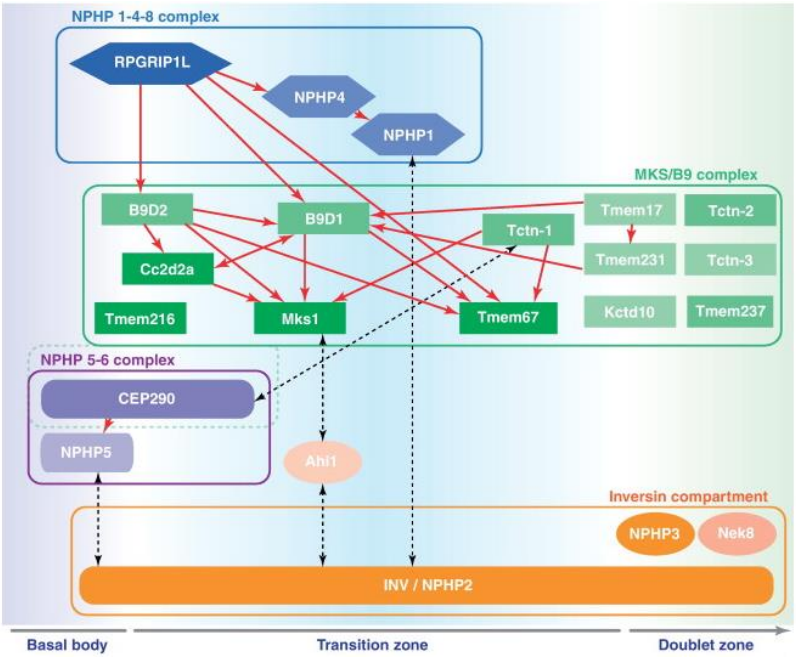

Figure 1.5 Hierarchy of organisation in the transition zone

RPGRIP1L is the primary organising protein of the transition zone and localises independent of other TZ proteins. RPGRIP1L recruits NPHP4, B9D2, B9D1 and TMEM67, which in turn ensure the organisation of the MKS complexes. However proteins at the bottom of this hierarchy (TMEM216, MKS1 and TMEM67) are associated with severe ciliopathies such as Meckel syndrome and Joubert syndrome. Proteins with saturated colour represent greater association with severe phenotypes. The inversin complex spans from the basal body to the above the transition zone and into the ciliary axoneme. It physically interacts (black arrows) with all other modules, and has been suggested to act as a bridge for interactions between modules (78). Image presented is from (78), Figure 2 and used with copyright permissions.

1.3 Primary ciliogenesis

Primary ciliogenesis is tightly linked to the cell cycle, since the basal body functions as both the mitotic spindle and is derived from the mother centriole (28). Cilia were originally thought to form in cells during both G1 or post-mitotically at G0 in quiescent cells. However, recent work in mouse cell models presented evidence that ciliogenesis can occur throughout the cell cycle and was not restricted to G1 as previously thought (83). Subsequently, it was hypothesised that the capacity of daughter cells to ciliate is inherited, and that cells are pre-primed for ciliogenesis based on the inheritance of the mother centriole (83, 84).

The full molecular mechanism of ciliogenesis is yet to be fully defined, however two pathways have been described. The first is an extracellular pathway where the centriole matures and migrates straight to the plasma membrane, where it docks though distal appendages and extends its axoneme through IFT (Figure 1.6) (25). The second pathway is an intracellular pathway, by which a ciliary vesicle initially forms at the mature centrosome, ciliary proteins are recruited, and a nascent cilium forms within the cell, prior to docking at the plasma membrane and before fully extending (Figure 1.6) (25).

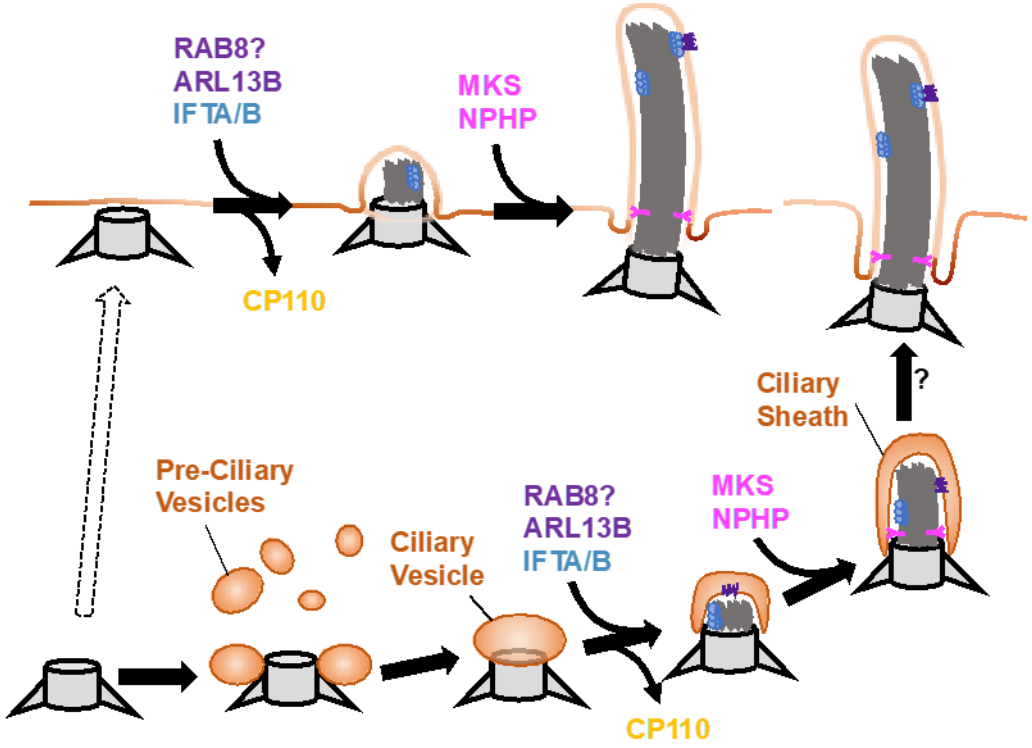

Figure 1.6 Two pathways of primary ciliogenesis

There are two suggested pathways for ciliogenesis: **A)** Extracellular ciliogenesis occurs after the mature mother centriole is localised to the apical plasma membrane. CP110 is removed from the centrosome which allows the recruitment of membrane proteins and IFT for axoneme extension. A transition zone forms and after full axoneme extension the primary cilium is formed. **B)** The intracellular pathway describes the first stage of ciliogenesis as comprising the recruitment of pre-cilliary vesicles to the distal appendages. Once fused these form a ciliary vesicle, which is associated with the loss of CP110. Recruitment of membrane proteins and IFT allows the formation of a nascent cilium into the ciliary vesicle. Once a transition zone forms the cilium docks and fuses with the plasma membrane. Adapted from (25) Figure 4 with Copyright permissions.

1.3.1 Centriole to centrosome conversion

A pre-requisite to ciliogenesis is the conversion of the inherited centrioles into a full mature centrosome (25). The centrosome is made up two linked centrioles surrounded by a dynamic matrix of proteins that control the centrosome's functions (25). The proximal end of the centriole recruits peri-centriolar matrix (PCM), made up of hundreds of proteins that form an amorphous mass around the centrioles, however it has been shown using 3D-structured illumination that there are distinct rings of proteins, such as pericentrin and CEP215 amongst the PCM (85). Following the PCM, centriole satellites are recruited. These satellites include proteins such as PCM1, alongside proteins found elsewhere in the cilium such as CEP290 and BBS4 (86). The PCM and satellites interact to allow the satellites to shuttle proteins the PCM for and the recruitment of other ciliary proteins from the cytosol (87).

Once the PCM is accumulated, the distal end of the mother centriole also forms distal appendages (DAPs) that attach to the main microtubule structure (24). Furthermore, in some cell types the centriole also recruits sub-distal appendages as discussed in Section 1.2.1.2. As it is only the mother centriole that recruits DAPs, DAP proteins such as CEP164 (88), are often used as a mother centriole markers to allow researchers to distinguish the two centrioles. siRNA knock-downs of DAPs such as *CEP164* show that these are essential for the docking of the centriole (24).

1.3.2 Pre-ciliary vesicles

The first stage of intracellular ciliogenesis is the formation of a pre-ciliary vesicle. It has been demonstrated in human RPE-1 cells that RAB11-associated vesicles recruit Rabin8 to the centrosome, which in turn is able to recruit and locally activate RAB8 (89). These vesicles are first trafficked using dynein along microtubules to the PCM (90). At the PCM, the vesicles use myosin-Va to travel along the branched actin network associated with the centrosome to the DAPs (90). Here, the RAB11-associated vesicles then become associated with each of the DAPs. These distal vesicles are remodelled by EPS15-homology-domain-containing proteins to increase the proximity to the vesicles (46). The vesicles are then able to fuse together to form a pre-ciliary vesicle, a process mediated by SNAP29 (46).

After the pre-ciliary vesicle has formed, the membrane extends and ciliary-specific proteins are recruited. As the axoneme extends through active IFT, transition zone proteins are also recruited for the formation of a transition zone and a full nascent cilium (Figure 1.6).

1.3.3 Basal body docking

Although it has been shown that during initial ciliogenesis, vesicle transport required for ciliogenesis is dependent on myosin-Va as described in 1.3.2, the transport mechanism of the centrosome to the apical membrane or the transport of a whole nascent cilium is not understood. Once at the membrane, docking only occurs after TTBK2 is targeted to the mother centriole through cell cycle cues (24). This is required to signal the removal of the CP110 distal protein, which acts as a cap to the distal region of the centriole. This distal cap is stabilised by Kif24 to prevent inappropriate ciliary assembly, which also acts to destabilise microtubules as a further preventative mechanism against ciliary formation (91). This removal of CP110 and TTBK2 is essential for basal body docking at the plasma membrane (24).

Through an unknown mechanism, the distal appendages then bind to the plasma membrane to support and dock the mother centriole. Once docked, the centriolar microtubules are able to extend to begin the formation of the ciliary axoneme.

1.3.4 Actin remodelling in ciliogenesis

Actin remodelling factors have recently been shown to negatively regulate ciliogenesis (92-94). The timing of these actin dynamics and their exact role in ciliogenesis still requires further research, as it is poorly understood and currently only modelled with global actin changes, which do not reflect the likely local and nuanced changes during normal ciliogenesis. In general, actin depolymerisation, through either siRNA knock-down of actin regulators or chemical inhibition of actin polymerisation with cytochalasin D, promotes ciliogenesis in all cell culture conditions (confluency and presence/absence of serum).

As discussed in section 1.3.2, actin is also required around the centrosome for delivery of ciliary vesicles and cargo. Furthermore, acto-myosin contraction, in co-ordination with microtubule remodelling, has been implicated in the movement of the basal body to the apical membrane during ciliogenesis (95). Although these structural changes to the actin cytoskeleton promote ciliogenesis, actin remodelling has also been shown to transcriptionally control the negative regulators of ciliary disassembly Aurora A and Plk1 through YAP-mediated Hippo signalling (92).

A whole genome siRNA screen that was published in 2010 sought to identify modulators of ciliogenesis and cilia length (96). The two main regulators that were further investigated were gelsolin (GSN), a positive regulator, and actin-related protein 3 (ACTR3), a negative regulator. Both are involved in the regulation of actin filament stabilisation: GSN severs actin filaments and ACTR3 inhibits branching. Knock-downs of these genes, in parallel with cytochalasin D treatment (a chemical inhibitor which depolymerises F-actin by binding actin monomers), suggested an important role of branched F-actin in modulating ciliogenesis, with dynamic or destabilised actin promoting ciliogenesis and increased cilia length. Cytochalasin D has also independently been shown to rescue ciliogenesis under siRNA knock-down conditions of *CEP290*, *NPHP5* and *IFT88* (70, 97). These observations provide additional evidence to support the essential role of actin cytoskeleton regulation in modulating ciliogenesis. Additionally, a follow-on paper by researchers who were involved in the 2010 genome screen further investigated actin regulators. This included LIMK2 and TESK1, separate actin regulators (98). When either of these proteins were knocked-down by siRNA there was a significant increase in cilia incidence (98). The authors linked this to increased vesicle trafficking, which in-turn signalled changes in Yes-associated protein/tafazzin (YAP/TAZ) localisation and Hippo signalling (98).

It was proposed by Kim *et al*. 2010, that destabilised F-actin allows for increased vesicle trafficking, whereas stabilised F-actin would create a physical barrier to ciliary vesicle trafficking around the base of the cilium or centrosome during ciliogenesis (92). However, both the screen and downstream work did not take into account the over-expression of Smo (their ciliary marker) (96, 98). When Smo is overexpressed it artificially activates the Shh pathway, and Smo

overexpression causes excessive GLI activation which is linked to cancer progression and cell cycle dysregulation (99), thus potentially interfering with the ciliary phenotypes assessed.

As actin cytoskeleton remodelling had been implicated in the regulation of ciliogenesis initiation, separate studies assessed the possible role of non-muscle myosins in the remodelling of actin during ciliogenesis (100). A study by Rao *et al*. found that the myosin heavy chains *Myh10* and *Myh9* acted antagonistically to modulate ciliogenesis (101). *Myh10*-dependent actin dynamics were shown to regulate the correct localisation of pre-ciliary complex proteins PCM1 and CEP290, and promote ciliogenesis. Interestingly, loss of cilia following *Myh10* knock-down could be rescued by treatment with blebbistatin (100), a chemical inhibitor of acto-myosin contraction.

An interacting partner of CEP290 at the centrosome, CP110, has also been linked to F-actin destabilisation through microRNA regulation (102). F-actin destabilisation was described as stimulating the accumulation of pericentrosomal pre-ciliary compartment proteins to the mother centriole, an important prerequisite stage of ciliogenesis (102).

Although there is increasing evidence for the role of actin destabilisation in promoting ciliogenesis, in multi-ciliated cells these is support for the opposite (103). F-actin stabilisation and an enriched actin web supports the docking of basal bodies in mouse tracheal epithelial cells, promoting ciliogenesis (103). This was induced by Forkhead box protein J1 (FOXJ1), which promoted RhoA activity during ciliogenesis (103), and thus is likely to regulate the activation of ROCK-mediated actin remodelling. However, as discussed by Kim et. al. 2010 (98), this process may be downstream of initial dynamic actin remodelling which allows centriole migration.

1.3.5 Maintenance of cilia

Due to the high volume of traffic into and out of the cilium during normal cell homeostasis, ciliary maintenance and stability is essential for its function. The constant renewal of ciliary membrane proteins and transduction of signal requires functional IFT and delivery of cargo from the cytoplasm to the cilium.

1.3.5.1 Vesicle trafficking maintains ciliary signalling and membrane composition

Currently the mechanism for the delivery of ciliary membrane proteins is not fully understood. It is thought that ciliary cargo is arranged into ciliary-specific vesicles at the trans Golgi network (TGN) (104). On these vesicles, proteins containing ciliary targeting sequences (CTS) (105) are recognised and mark the vesicles to be trafficked to the cilium (Figure 1.7). These CTS are highly variable between proteins, and a set consensus sequence has yet to be found, possibly reflecting the non-specific binding region in the BBSome that is able to recognise a wide range of cargos (64). The specificity of cargos could be regulated through the recognition of these sequences by small GTPases such as ARL13B and RABs, which in turn interact with the BBSome, however evidence has also been published refuting this hypothesis (64). There is further evidence suggesting that the BBSome interacts with Rabin8 to regulate RAB8- and RAB11-marked vesicles (106). RAB8 directly interacts with RAB11 (106), and this marks vesicles as ciliary-specific. These marked vesicles are thought to be trafficked along the actin cytoskeleton (92, 102, 107) rather than microtubules, and would therefore move by association with myosin motors (108). These vesicles then accumulate at the ciliary base where Rabin8, in co-ordination with the exocyst complex, tethers the vesicles to the periciliary membrane or ciliary pocket and membrane proteins are deposited by fusion, mediated by SNARE proteins, allowing lateral diffusion of proteins into the cilium (45, 47, 109). Furthermore, CEP290 has also been shown to interact with RAB8 (86), possibly recruiting the vesicles to the base of the cilium. Another transition zone protein CC2D2A has also been shown to facilitate protein transport through RAB8-dependant processes in photoreceptors, highlighting that many ciliary components have multiple roles in ciliogenesis and ciliary maintenance. This vesicle trafficking mechanism is also important in initial ciliogenesis as discussed in (Section 1.3).

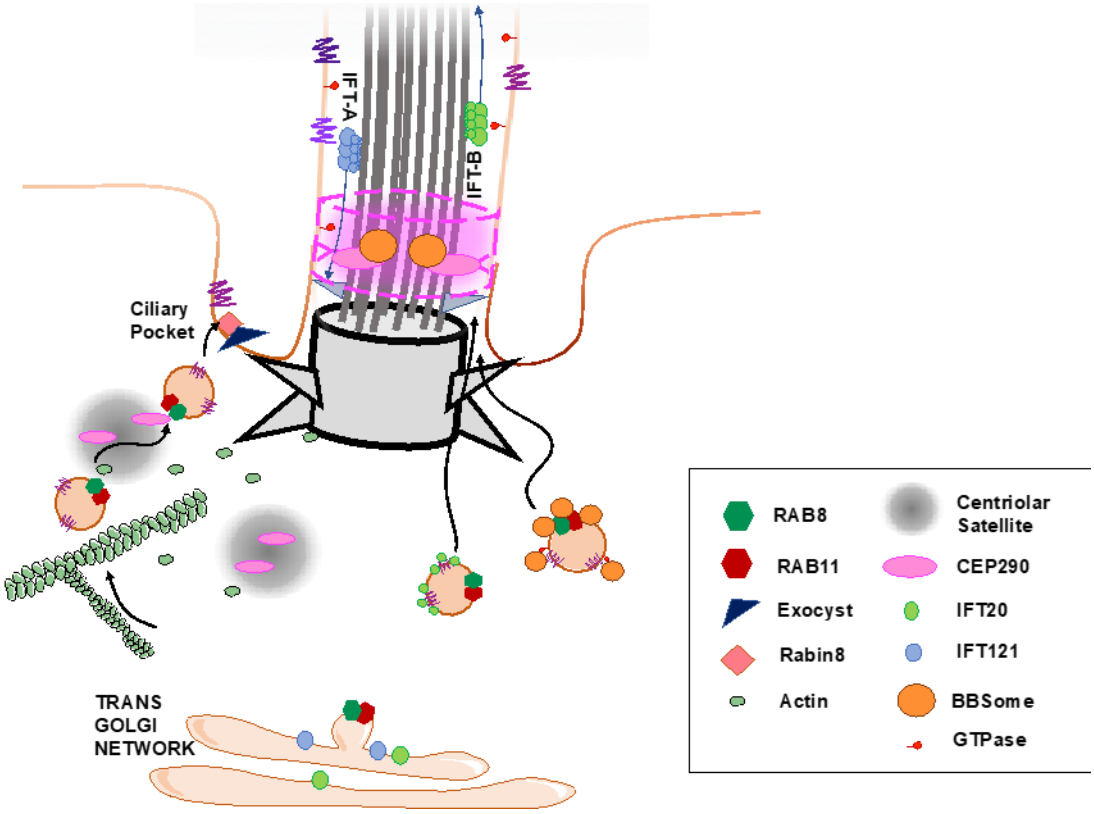

Figure 1.7 Vesicular transport to the cilium

Vesicle transport to the cilium. RAB8- and RAB11- marked vesicles are formed at the trans Golgi network. These vesicles can then be trafficked along actin filaments to the ciliary pocket, where they tether to the membrane through interaction with Rabin8 and exocyst, before fusion and delivery of membrane protein cargo. Other proteins implicated in vesicle transport include the BBSome and IFTs. Figure adapted from (110) Figure 1.3 and use licensed under CC BY-ND 2.0 with Copyright.

Another hypothesis for ciliary transport emphasises a role for IFT-B in targeting ciliary cargo. IFT20 has been shown to be directly associated with the TGN and mediates transport of polycystin-2 in mammalian cilia (104). It was hypothesised that IFT20 interacts with PKD-2 and marks vesicles for ciliary transport, and this direct binding to an IFT-B protein allows it to remain attached and to be shuttled in ciliary membrane (111). IFT-A has also been implicated in ciliary vesicle trafficking; IFT121 mutant RPE-1 cells have reduced formation of RAB8 vesicles and delivery of membrane proteins (70, 71), suggesting a role for IFT-A in transport outside of the cilium.

1.3.5.2 Actin stabilisation maintains ciliary structure and function

The ultrastructure and function of the ciliary pocket is maintained by stable and dynamic actin filaments. This membrane invagination is maintained by stable and dynamic actin filaments, where more dynamic actin is found at the distal end of the ciliary pocket to facilitate vesicle trafficking of ciliary cargo (112).

Alongside actin negatively regulating ciliogenesis and cilia length, it has also been implicated in ciliary stability (113). Human and mouse mutant models of *KDM3A*$^{-/-}$, a multifunctional protein shown to have roles as a transcription factor for free actin, have reduced cellular actin levels and an associated increase in cilia. As there is reduced actin around the base of the cilium in KDM3A mutants, it was proposed that the loss of this physical gate would allow for an increase in IFT at the cilium, disrupting the balance of transport proteins (113). This dysregulation is further compounded by actin instability causing an increase in cilia length, further disrupting the balance and regulation of IFT (113).

RhoA is the activator of ROCK, a key actin remodelling regulator (114, 115). RhoA has been shown to contribute to the molecular pathology of ciliopathies: increased RhoA levels were observed in dermal fibroblasts from ciliopathy patients with *TMEM216* mutations (99). Independently, RhoA has also been shown to mislocalise in patients with JBTS syndrome (specifically caused by *TMEM237* mutations), and patient fibroblasts had increased actin stress fibres (116).

Cellular phenotypes observed in many ciliopathies are caused by defects of the actin cytoskeleton (99, 117, 118). A study into Bardet-Biedl syndrome found *Bbs4*- and *Bbs6*-deficient renal epithelial cells derived from mutant mice had very low cilia incidence, associated with increased focal adhesions and abnormal actin stress fibres (117). These aberrant changes in the actin cytoskeleton were ascribed to highly up-regulated RhoA expression (119). RhoA-GTP is a direct activator of ROCK2, and thus increased ROCK2 activity would lead to increased stress fibre formation and F-actin stabilisation. When these cells were treated with Y27632, a non-specific inhibitor of ROCK and ribosomal S6 kinase (RSK) families, cilia incidence was rescued. Thus, it was suggested that the actin cellular phenotype was the cause of the loss of cilia in the *Bbs4* and *Bbs6* mouse mutants (117).

1.3.5.3 IFT-A maintains the ciliary transition zone

Furthermore, the delivery of proteins is also regulated at the ciliary gate. The transition zone must be stable in order to correctly allow the necessary proteins to diffuse into and out of the ciliary axoneme, maintaining the highly specialised composition of the ciliary membrane. IFTA-dynein, mediating retrograde IFT, has been implicated in the recruitment and building of a functional transition zone during ciliogenesis (113), as well as for maintenance of the transition zone in *C. elegans* (72). Dynein mutants were shown to have high concentrations of ectopic, mis-assembled transition zone proteins which were able to diffuse out of the transition zone and localise at the tip of a short bulbous cilium (72, 120), highlighting an important function for IFT-A in transition zone assembly and stability.

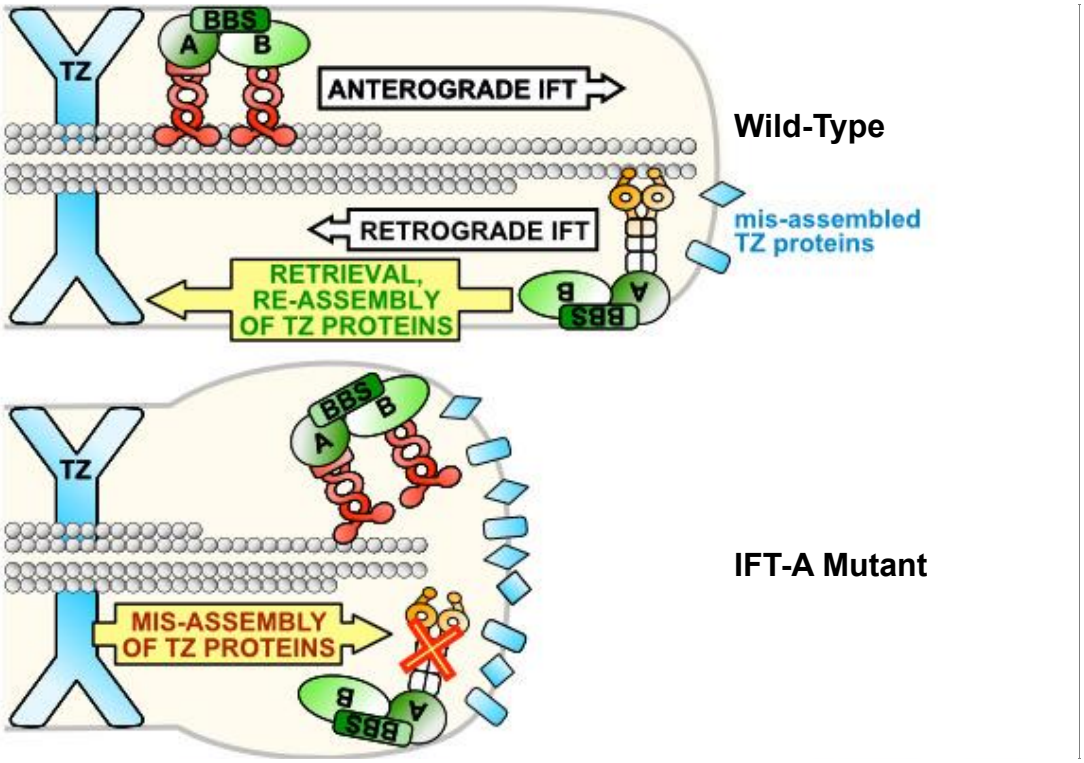

Figure 1.8 IFT-A maintains transition zone integrity

In wild-type cilia some transition zone proteins diffuse along the ciliary membrane and mis-localise at the base of the cilium. These are retrieved by IFT-A/dynein retrograde transport to maintain the transition zone. IFT-A mutants present with a short and bulbous cilium, with an accumulation of transition zone proteins at the tip of the cilium. These cannot be retrieved by IFT-A, and therefore compromise the transition zone's integrity. Figure adapted from (72) and used with Copyright permissions.

1.3.6 Disassembly of cilia

As cilia are tightly linked to the cell cycle, complete disassembly must occur by the end of G2 to allow the centriole to be repurposed as a spindle pole in mitosis. Until recently it has been thought that ciliary resorption occurs by S-phase prior to centriole duplication. However new evidence from mouse cells expressing a fluorescence ciliary marker and cell cycle biosensor shows that ciliary retention can occur until late G2 (83).

Although the timing of ciliary resorption varies and can occur throughout the cell cycle, presumably the signalling pathways that activate it are constant. Studies into cilia resorption add serum to cell cultures to trigger the restart of the cell cycle, and have characterised resorption to occur in two waves, the first occurring before S phase and the second occurring in G2 (121). However, the full molecular mechanisms behind these waves of resorption are still poorly understood.

It is known that signalling for ciliary resorption is regulated by Aurora A (AurA), a centrosomal kinase that signals for mitosis. Aurora A activation leads to the direct phosphorylation of histone deacetylase 6 (HDAC6) (122). This in turn deacetylates the ciliary axoneme, promoting ciliary disassembly.

Inositol polyphosphate-5-phosphatase E (INPP5E) has also been linked to the regulation of ciliary disassembly. INPP5E dephosphorylates PI(3,4,5)P3 and PI(4,5)P2 in the ciliary membrane, and is thought to maintain the ratios of these phospholipids to confer ciliary stability (123). Loss of INPP5E is associated with more rapid ciliary disassembly, likely due to unbalanced levels of phospholipids and the ciliary response to cell cycle signals.

Research over the last 5 years has further revealed that disassembly of cilia occurs after an initial de-capping step. This de-capping is controlled by intraciliary F-actin and PI(4,5)P2, to bud off the tip of the cilium (50). This budding has been hypothesised as a mechanism to quickly dispose of ciliary membrane proteins at the ciliary tip (53). This de-capping step then signals, through an unknown mechanism, to initiate full ciliary disassembly (50). The full resorption of the remaining cilium is also poorly defined. It is unknown if the cilium is resorbed from the base, or is disassembled from the tip down.

There is also recent evidence that mammalian cilia are lost in a whole-cilium shedding event (124). It was shown by Mirvis *et al*. that intracellular calcium levels controlled IMCD3 cells decision to de-ciliate. The deciliation occurred via resorption as discussed above or by whole cilium shedding, which could then be recovered from cell growth media (124).

1.4 Primary cilia function

Primary cilia have a variety of roles in many cellular signalling pathways, and also have many important functions throughout the stages of embryo development by establishing the flow of morphogens through nodal cilia (14, 125), but also in many developmental signalling pathways (126). As previously mentioned they have an essential for phototransduction in photoreceptors and have diverse roles in mechanosensation of flow in vessels, ducts and tubules in several organ types. Alongside these dedicated roles, cilia are also involved in more general cell homeostasis(126).

1.4.1 Signalling

Primary cilia are often described as antennae-like (7), not only for their structural shape but because they mediate a diverse range of signalling pathways they are involved in, such as; Hedgehog (Hh) (127, 128), Wnt signalling (129), mammalian target of rapamycin (mTOR) (130), Hippo (131), G protein coupled receptor (GPCR) (132), extracellular signal-related kinase/c-jun N-terminal kinase (ERK/JNK) (133), and transforming growth factor beta (TGFβ) (134) signalling.

Cilia have a known role in the mammalian target of rapamycin mTOR signalling, which regulates cell proliferation, autophagy and protein production (135). mTOR signalling is implicated in the aetiology of kidney cysts in mouse models (136). The presence and size of these kidney cysts can be reduced with rapamycin, which inhibits the mTOR signalling which is dysregulated by cilia loss (135, 137).

The Hippo signalling pathway, a conserved pathway regulating cell proliferation, has also been linked to cilia (131). NPHP proteins and interactors negatively regulate Hippo signalling in relation to cell proliferation and ciliary disassembly

(131, 138, 139). Other signalling pathways that have been linked to ciliopathy pathology or cilia regulation include GPCR signalling (reviewed in (132)), receptor tyrosine kinase (RTK) signalling (Reviewed in Christensen *et al*., 2017 (140)), and ERK/JNK signalling which has been linked to polycystic kidney disease pathology (133) and regulation of ciliary length (141). Furthermore, TGFβ signalling pathways are thought to be transduced through the ciliary pocket, and receptors have been shown to localise to the ciliary tip (134, 142).

1.4.1.1 Hedgehog (Hh) signalling

Hedgehog (Hh) signalling is a conserved pathway essential for embryo development and tissue regeneration. When dysreglated Sonic Hh signalling can also lead to inherited cancers such as Gorlin syndrome (143).

There are three mammalian ligands: Indian hedgehog (Ihh), Desert hedgehog (Dhh), and Sonic Hedgehog (Shh). The best characterised of this family is Sonic Hedgehog (Shh) (144), which is essential in generation of the anterior-posterior axis, axial skeleton, spinal cord and developing limb bud, as well as regulating neural tube cell fate (145).

Patched (Ptch1), a 12 transmembrane domain glycoprotein is the signal transducer of Hh signalling, and is located in the ciliary membrane and ciliary pocket. Here, Ptch1 can inhibit the translocation of Smoothened (Smo) into the cilium. While Smoothened is excluded, full length Gli (GliFL) is transported into and out of the cilium normally. GliFL is sequestered by the key Shh regulator SuFu. Once sequestered, GliFL is phosphorylated and targeted for proteasomal cleavage in the cytoplasm, turning it into the Gli transcriptional repressor (GliR). GliR translocates to the nucleus and suppresses the expression of Shh target genes such as cyclins (146).

When Shh is present, it binds to Ptch1. This initiates Ptch1 to move out of and be excluded from the ciliary membrane, allowing the translocation of Smo into the ciliary membrane. GliFL is then differentially phosphorylated and activated (termed GliA) by an unknown mechanism. GliA is transported out of the cilium where it then acts as a transcriptional activator, turning on genes and initiating a feedback loop by expressing Ptch1 and protein regulators of Gli degradation. It is also thought that cytosolic GliFL is activated to GliA by a separate poorly

described mechanism (146). This pathway is the most common one tested in assays of ciliary function.

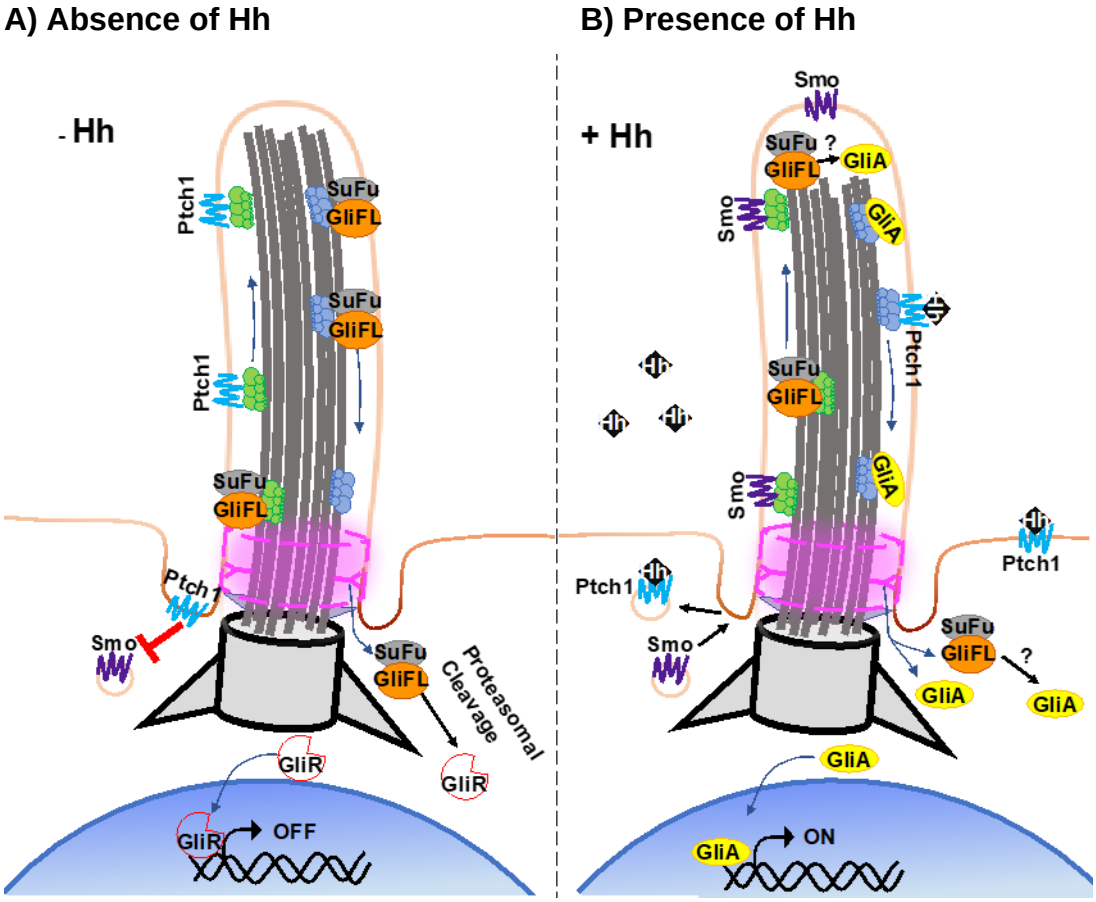

Figure 1.9 Hedgehog signalling in cilia

A) Schematic diagram shows the localisation of signalling components without the presence of Hedgehog (Hh). Ptch1 prevents translocation of Smo into the cilium. This leads to full length Gli (GliFL) being transported out of the cilium and cleaved into the repressor form (GliR). This represses gene expression of target genes. **B)** In the presence of Hh, this binds to Ptch1 and thus allows Smo translocation into the ciliary membrane. Smo presences leads to activation of Gli (GliA). This is transported out of the cilium and activates target genes once in the nucleus. Adapted from (146) Figure 1 with copyright permissions.

1.4.1.2 Wnt Signalling

Wnt signalling is a highly-conserved signalling pathway that regulates a plethora of cellular processes such as; motility, stem cell renewal, polarity and organogenesis (Reviewed in Logan and Nusse, 2004 (129)). Dysregulated Wnt signalling is associated with severe embryogenesis defects such as spina bifida (147) and in adults, can lead to several types of cancer (reviewed in Zhan et. al, 2017 (148)). There are two main arms of the Wnt signalling pathway: the

canonical and non-canonical, both of which are initiated by the binding of a Wnt ligand to a Frizzled (Fzd) receptor. Canonical Wnt signalling leads to the activation of Wnt targeted gene expression, whereas the non-canonical Wnt pathway either turns on Wnt targeted genes or leads to actin remodelling.

1.4.1.2.2 Canonical Wnt signalling

In canonical Wnt signalling, Wnt binds to a seven transmembrane Frizzled receptor, of which there are 10 in humans (149). Once Wnt is bound, Frizzled associates with its co-receptor LRP5/6, leading to the recruitment and phosphorylation of Dishevelled (Dvl) at the plasma membrane. This activation of Dishevelled recruits and disassembles the destruction complex through binding axin. The destruction complex, made up of axin, casein kinase 1α (CK1α), adenomatous polyposis coli (APC) and glycogen synthase kinase 3β (GSK3β) is responsible for β-catenin degradation in the absence of Wnt. Once the destruction complex is disassembled, this allows the accumulation of β-catenin levels in the cytoplasm, leading it to translocate into the nucleus (150). Once in the nucleus, β-catenin acts with co-transcriptional activators and transcription factor/lymphoid enhancer-binding factor (TCF/LEF) proteins, to turn on genes such as cyclin D 1 (151).

In the absence of Wnt, CK1α and GSK3β of the destruction complex phosphorylate β-catenin. This phosphorylation targets β-catenin for degradation through the proteasome (150).

1.4.1.2.3 Non-canonical Wnt signalling

There are two sub-arms of non-canonical Wnt signalling. The first is the Wnt/Ca^{2+} pathway in which the signal is transduced by calcium signalling which also leads to the transcription of Wnt activated genes and calcium-sensitive kinases (eg. protein kinase C). The second sub-arm is the Wnt/planar cell polarity (PCP) pathway, which controls cell migration and orientation. This pathway occurs through different co-receptors, which cause the activation of RhoA, leading to changes in actin regulation and the cytoskeleton (152).

1.4.1.2.1 Wnt signalling through primary cilia

It has been controversially suggested that loss of cilia, due to *Ift88* mutations in mice, was associated with an increase in both cytoplasmic and nuclear β-catenin levels (153), suggesting an over activation of canonical Wnt signalling. It has also been noted that suppression or silencing of *BBS1*, *BBS4* or *Kif3a* causes stabilisation of β-catenin. However, loss of cilia in zebrafish, a lower eukaryote, has been shown to affect Hh signalling but not Wnt signalling (154). This suggest, although refuted (154, 155) that the association between Wnt signalling and cilia could be specific to mammals.

Inversin has been shown to be essential in recruiting Dishevelled in response to Wnt binding of Frizzled receptors. Inversin is localised to the basal body of cilia and interacts with NPHP proteins in the transition zone. When mutated, these genes cause nephronophthisis, a ciliopathy that has developmental (microcystic) and degenerative kidney defects correlated to excessive Wnt signalling (156).

Once recruited to the membrane by Inversin, both Inversin and NPHP4 can antagonise Dishevelled and reduce the downstream transduction of signal, allowing levels of the destruction complex to remain active and reduce the accumulation of β-catenin (Figure 1.10). However, this is still a disputed topic as zebrafish ciliopathy models such as IFT mutants still have normal regulation of Wnt signalling. This is further disputed in the IFT mouse models, with reports of normal responses to Wnt in the mouse embryonic fibroblasts (MEFs) (155). The complexity of this pathway makes dissecting the exact role of cilia in Wnt signalling difficult. It may be that compensatory mechanisms are at play, or fine

control of Wnt signalling through the cilium is dispensable. It may also be a time-dependant process and, only be important in the initial stages of development, rather than postnatal growth or tissue function (157, 158).

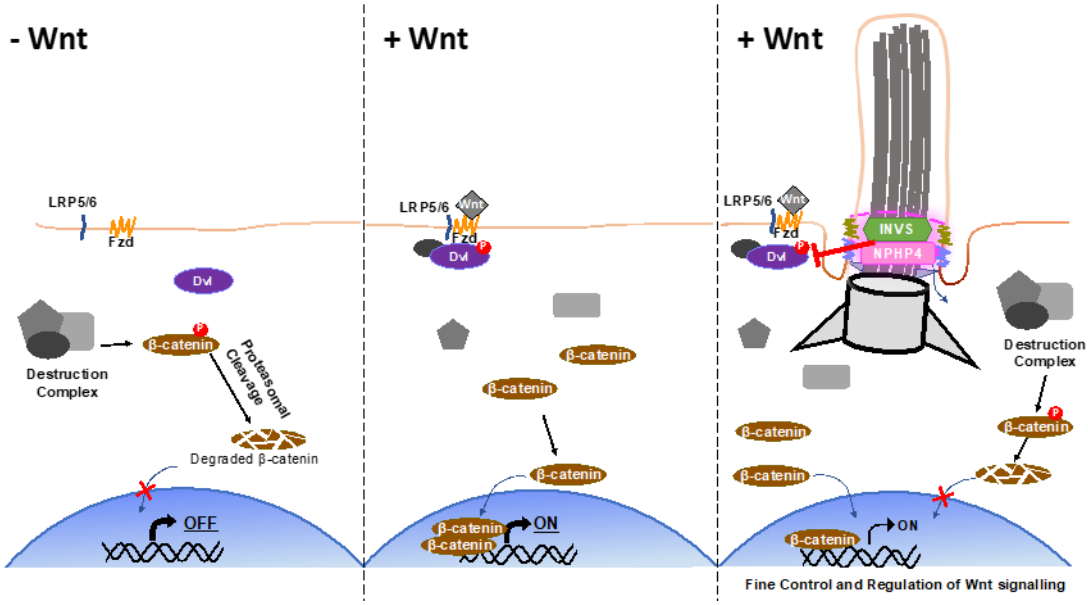

Figure 1.10 Cilia in canonical Wnt singalling

Schematic diagram showing canonical Wnt signalling with and without the presence of a cilium. Under normal conditions β-catenin is degraded by the destruction complex in the cytoplasm. When Wnt binds to the Frizzled receptor (Fzd), along with its co-receptor LRLP5/6 it recruits Dishevelled (Dvl) to the membrane and activates it. This in turn causes the destruction complex to be recruited to the membrane, therefore allowing β-catenin to accumulate and translocate into the nucleus to work with transcriptional activators to turn on Wnt activated genes. In the presence of the primary cilium, inversin (INV) and NPHP4 inhibit the activation of Dvl and therefore modulate the level of signal transduction, giving fine control in response to Wnt signalling. Adapted from (159) Figure 4, use licensed under the Creative Commons Attribution 4.0 International License.

1.5 Ciliopathies and disease

1.5.1 Non-motile ciliopathies

Non-motile ciliopathies are a spectrum of usually autosomal recessive disorders that are caused by mutations that affect ciliary structure or function. Due to the presence of primary cilia on most cells in the body, the phenotypic spectrum and multi-system pathology of ciliopathies greatly varies. This spectrum ranges from isolated retinal degeneration to a collection of more severe phenotypes including perinatal death. Examples of non-motile ciliopathy phenotypes include

retinal degeneration, polycystic kidneys, polydactyly, obesity, neural tube defects, learning disabilities, skeletal dysplasia, hypoplasia of essential organs and laterality defects.

Ciliopathies are an expanding class of disorders, as an increasing number of previously defined and new conditions become associated with the dysregulation of primary ciliary processes. Individually, ciliopathies are rare, but as a group of inherited disorders, ciliopathies are comparatively common compared to other inherited diseases.

Management of ciliopathy patients focuses on systematic therapy. There are however, no clear guidelines for the management of these patients, likely due to the pleiotropy of phenotypes. The best studied are listed with their associated mutated genes and phenotypes in Table 1.1.

Table 1.1 Ciliopathy genes and phenotypes

Mutations in genes highlighted in bold cause more than one ciliopathy, phenotypes highlighted in bold are common across several ciliopathies. Human Phenotype data source: Online Mendelian Inheritance in Man, OMIM®; Associated Genes data source: U.S. National Library of Medicine. This is not an extensive list of phenotypes. Other phenotypes may be present in individual families or are less common amongst patients. List generated from the most common ciliopathies, as recognised by the Ciliopathy Alliance (160). Autosomal Dominant form of the disease is denoted by (AD), Autosomal Recessive by (AR) and X-linked by (XL).

Ciliopathy	**Associated Genes**	**Summary of Human Phenotypes**
Alström Syndrome	*ALMS1, RYR2*	Short stature, **Obesity**, **Hearing loss, Retinal degeneration**, **Blindness**, Gingivitus, Dilated cardiomyopathy, Asthma, Gynecomastia, **Hypotonia**, Atherosclerosis, **Renal abnormalities**, **Renal failure**, **Skeletal abnormalities**, **Developmental delay**, Diabetes, Hyperthyroidism,
Bardet-Biedl Syndrome	***ARL6,*** *BBS1,* ***BBS2****, BBS4, BBS5, BBS7, BBS9, BBS10, BBS12,* ***CEP290****, MKKS****, MKS1****, TRIM32, TTC8*	**Obesity**, **Retinal degeneration**, **Renal anomalies**, Dental abnormalities, **Developmental delay**, **Mental retardation**, **Polydactyly**, **Hypogenitalism**, **Ataxia**
Jeune Asphyxiating thoracic dystrophy	***CEP120****,* ***CSPP1****, DYNC2H1, IFT80,* ***IFT140****,* ***IFT172****,* ***TTC21B****,* ***WDR19****, WDR34, WDR35, WDR60*	**Skeletal abnormalities**, **Polydactyly**
Joubert Syndrome	*AHI1, ARL13B,* ***B9D1, B9D2,*** *C2CD3,* ***CC2D2A,*** *CEP41, CEP104,* ***CEP120****,* ***CEP290****, CPLANE1,* ***CSPP1****,* ***IFT172****, INPP5E, KIF7,* ***MKS1, NPHP1****, OFD1, PDE6D, POC1B,* ***RPGRIP1L****, TCTN1, TCTN2, TCTN3,* ***TMEM67****, TMEM107, TMEM138,* ***TMEM216****, TMEM231, TMEM237,* ***TTC21B****, ZNF423*	Macrocephaly, Ptosis, Breathing dysregulation, **Ataxia**, **Hypotonia**, Molar Tooth Sign (on MRI), Brainstem hypoplasia and malformation, **Mental Retardation**
Leber congenital amaurosis	*AIPL1,* ***CEP290****, CRB1, CRX, GUCY2D,* ***IMPDH1****,* ***IQCB1****, LCA5, LRAT, NMNAT1,* ***PRPH2,*** *RD3, RDH12, RPE65, RPGRIP1, SPATA7, TULP1*	Hepatomegaly, **Mental retardation, Blindness, Retinal Degeneration**, **Sensory hearing loss**, **Retarded growth**
Meckel Syndrome	***B9D1, B9D2, CC2D2A****,* ***CEP290****,* ***MKS1****,* ***RPGRIP1L****,* ***TMEM67, TMEM216***	Anencephaly, Cleft palate/lip, Pulmonary hypoplasia, Cardiovascular defects, **Polydactyly**, **Skeletal**

		abnormalities, **Hypogenitalism, Polycystic kidneys,** Perinatal Death
Nephronophthisis	*ANKS6, CEP83, CEP164, GLIS2, INVS, NEK8,* ***NPHP1****, NPHP3,* ***NPHP4****,* ***TMEM67****,* ***TTC21B, WDR19****, ZNF423*	**Nephronophthisis**, Tubular atrophy, **End stage renal disease**, **Polyuria, Anemia**, **Retarded Growth**
Polycystic Kidney Disease	AD: *DNAJB11*, *GANAB, PKD1, PKD2* *AR: DZIP1L*, *FCYT*, *PKHD1*	**Polycystic kidney, Renal failure,** Hepatic cysts, Intracranial aneurysm
Retinitis Pigmentosa	AD: *ABCA4, ARL3, BEST1, CA4*, *CRB1, FSCN2, GUCA1B,* ***IMPDH1,*** *KIF3B, KLHL7, NR2E3, NRL, PRPF3, PRPF4, PRPF6, PRPF8, PRPF31,* ***PRPH2****, RDH12 RHO, ROM1, RP9, RGR, SEMA4A, SNRNP200, TOPORS* AR: *ABCA4, AGBL5, AHR, ARHGEF18, ARL2BP,* ***ARL6, BBS2****, C2ORF71, C8ORF37, CDHR1, CERKL, CLCC1,* ***CLRN1****, CNGA1, CNGB1, CRB1, CWC27, DHDDS, DHX38, EYS, FAM161A, HGSNAT, HK1, IDH3B, IFT43,* ***IFT140, IFT172****, IMPG2, KIAA1549, KIZ, MAK, MERTK, NEK2, NR2E3, PDE6A, PDE6B, PDE6G, POMGT1, PRCD, PROM1,* ***PRPH2*** *RBP3, REEP6, RDH12, RGR, RHO, ROM1, RP1L1, RPE65, SAG, SEMA4A, SLC7A14, TTC8, TULP1,* ***USH2A****, ZNF408, ZNF513* XL: *OFD1, RP2, RPGR*	**Retinitis pigmentosa,** Constricted visual fields, Night blindness
Senior-Løken Syndrome	***CEP290****,* ***IQCB1****,* ***NPHP1, NPHP4****, SDCCAG8,* ***WDR19***	**Nephronophthisis, End stage renal disease, Retinal degeration**, **Polyuria, Anemia**
Usher Syndrome	*ADGRV1, AR, ARSG, CDH23, CEP250, CIB2,* ***CLRN1****, ESPN, GPR98, HARS1, MYO7A, PCDH15, PDZD7, SANS, USH1C, USH1E, USH1H, USH1K,* ***USH2A****, WHRN*	**Hearing loss, Retinitis pigmentosa,** Delayed motor development,

1.5.1.1 Genetic heterogeneity and pleiotropy

As can be seen in Table 1.1, different mutations in the same gene can cause different disorders and phenotypes. This phenomenon is known as pleiotropy, where a single gene/allele can produce two or more unrelated affects. In addition, mutations in over 30 different genes can cause the same disorder, as observed for Joubert Syndrome (JBTS). There is also a high-level of genetic heterogeneity, with extensive phenotypic overlap between ciliopathies (phenotypes highlighted in bold), but also extensive phenotypic variation within each disorder. It has even been documented that members of the same family

can present with phenotypic variation (161). For example in family members with the same mutation in *TMEM216*, one member was diagnosed with MKS whereas a sibling was diagnosed with JBTS (99). Another extreme example is *CEP290*: mutations in this gene can either cause isolated retinal degeneration (162)(such as in some cases of Leber Congenital Amaurosis), or result in the far more severe MKS (163) which often presents with anencephaly, skeletal abnormalities and cardiovascular defects. Phenotype variation can sometimes be explained by simple genotype-phenotype correlations (for example, the difference in effect between a severe frame-shift causing a null allele in comparison to a hypomorphic missense mutation). However, this simple explanation does not provide a satisfactory explanation of the full spectrum of phenotype variation across ciliopathies generally. This gap in our understanding and the extent of variation makes diagnosis and clinical management of ciliopathies a continuing clinical challenge.

1.5.2.1.1 Expressivity and penetrance

Expressivity describes a given genotype not being expressed homogenously across a population, such that there is a spectrum of a phenotype. A simple example of this is seen in the autosomal dominant disease Marfan syndrome, where there is variable expressivity of the *FBN1* gene. Heterozygous individuals often present with elongated digits (arachnodactyly), but amongst this patient population digit length is highly variable. Some patients present with extremely long digits and associated loose joints, whereas others have fingers just at the higher end of the average range (164). These highly variable phenotypes are usually attributed to modifier alleles or environmental factors.

Penetrance describes the presence or absence of a given pathogenic phenotype in a population that all carry the same genotype. In contrast to expressivity, the expression of phenotypic features does not vary. An example of this is Huntington's disease, where alleles are defined by the number of CAG repeats. Alleles with <27 repeats are associated with a normal phenotype, whereas alleles with >40 repeats are fully penetrant, such that 100% of people with that allele present with the disease (165). There are also incompletely penetrant alleles: 36-38 CAG repeat alleles present with the disease in only

0.25% of people with that allele. These alleles have also been shown to be at a high frequency throughout the general population (166).

Epistasis describes the interactions between genes. It is a well-defined mechanism that affects expressivity and penetrance of diseases. For normal cellular function genes must interact positively and negatively for regulation of expression, responses to signalling, and developmental pathways. As a consequence, epistasis is likely to be ubiquitous in complex disease phenotypes (167). Ciliopathies are likely to have a combination of both variable expressivity and penetrance (Figure 1.11).

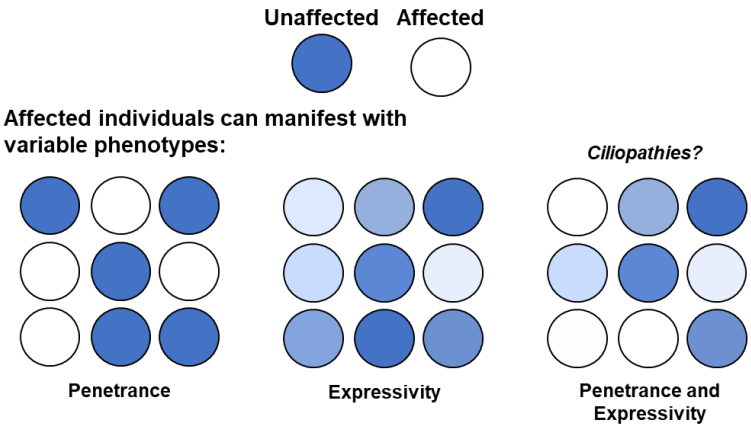

Figure 1.11 Penetrance vs expressivity

The penetrance of a dominant allele determines if the phenotype expresses or not, represented as either blue or white in the schematic. Expressivity of a dominant allele determines the extent that a dominant phenotype is expressed, represented as a range of colours between blue and white. Ciliopathies are thought to have a combination of both variable penetrance and expressivity across the disease causing genes.

1.5.2.1.2 Modifier alleles in ciliopathies

Ciliopathies are mostly diagnosed as autosomal recessive Mendelian conditions, for which a biallelic genotype at a single locus is causative for the disease phenotype. However, several studies have suggested that the additional inheritance of modifier alleles can be an explanation for the phenotypic variability in ciliopathies (161, 168). Modifier alleles are variants of one gene which modify the molecular expression or function of a separate, causative disease locus (reviewed in Kousi and Katsanis, 2015 (169)). Modifier allele studies in mice have shown that they affect penetrance, expressivity and pleiotropy through epistasis (170), causing the spectrum of phenotypes.

Modifier alleles are not to be confused with protective alleles, which instead modify an individual's susceptibility to a non-inherited disease. Modifier alleles have been described in autosomal dominant polycystic kidney disease (ADPKD). Mice trans-heterozygous for *Pkd1* and *Pkd2* have a far more severe phenotype than single heterozygote mice, suggesting a synergistic epistatic interaction between the two genes (171).

Several retinal degeneration phenotypes have also been associated with modifier alleles. RPGR mutant mice were found to have a more severe retinal degeneration phenotype with a non-disease causing heterozygous mutation in *CEP290* (172). The *RPGRIP1L* A229T allele has also been shown to be enriched in BBS and Senior-Løken syndrome (SLS) patients with retinal degeneration, compared to an unaffected ethnic-matched population. Khanna *et al*., 2010, described this allele as a modifier that determines retinal degeneration in ciliopathy patients (173).

A group of proteins called molecular chaperones are also considered as more global disease modifiers. Chaperones, such as the stress induced heat shock proteins (HSP) 70 and HSP90, are essential for the correct assembly of proteins (reviewed in Li and Srivastava, 2004 (174)). They have been implicated in the expressivity of different mutations because of their role in protein folding, and therefore acting as global modifiers of different alleles through widespread epistasis (175). Different functional polymorphisms of chaperones therefore interact with all variations of alleles differently, which in turn can cause protein mis-folding (176). Furthermore, *BBS6*, *10* and *12* encode are described as chaperonin-like proteins, but their role is thought to be specifically for the correct assembly and stability of the BBSome. BBS6 evolved from a cytosolic chaperonin subunit and acquired a specialised PCM function, so that it can encapsulate substrates but is not involved in protein folding (177). Phenotypes caused by mutations in these genes have been described as a "chaperonopathies', and it is recognised that these phenotypes are more severe than other BBS types, for example in individuals with *BBS1* mutations (178). Thus, it seems reasonable to hypothesize that different alleles of these genes may differentially interact with the BBSome, leading to different expressivity of other BBS mutations. However, the molecular data to support this hypothesis is lacking at the present time.

Over the last decade there has been conflicting evidence for existence of modifier alleles in ciliopathies, and despite the isolated examples discussed above there are still not widespread systemic functional studies to support these hypotheses, there are also too few families with defined alleles that are discordant for disease phenotypes for a meaningful study. However, modifier alleles still provide a possible explanation of pleiotropy in ciliopathies, but human whole-exome or genome sequencing data from ciliopathy patients has not yet shown enrichment for secondary, potential modifier alleles in ciliopathy genes (179, 180). This does not exclude the possibility of modifier alleles located in non-ciliopathy genes or in non-coding regions.

1.5.2.1.3 Triallelism in ciliopathies

Triallelic inheritance is a phenomenon by which a phenotype only manifests if an individual carries three mutant alleles. This is a type of oligogenic inheritance, which refers to a trait that is determined by more than one gene locus. Note that this is different to polygenic inheritance which highly complex and involved multiple genes and environmental factors.

Ciliopathies, in particular BBS (181, 182), are one of the few disorders with evidence of this digenic triallelic inheritance pattern (three mutant alleles inherited between two gene loci), with all three mutant alleles necessary for expression of the phenotype. This is therefore a different phenomenon to modifier alleles and expressivity discussed above, because biallelic alleles in the primary disease locus are not necessary and sufficient for expression of the disease phenotype.

Beales *et al*., 2003 (183), analysed 259 individual BBS families to investigate oligogenic disease inheritance. They identified the *BBS1* p.M30R allele, which is present in the general population, and that individuals biallelic for p.M30R are asymptomatic. In rare instances, the BBS phenotype did not manifest until at least one of these alleles in *BBS1* is inherited with two mutations at another locus, such as *BBS2* or *BBS4*. In another study, an affected family with a compound heterozygote mutation in *BBS2*, only manifested the BBS phenotype when inherited with a single p.M30R *BBS1* allele (183). The possible genotypes and expression of triallelic inheritance is summarised in Table 1.2.

Table 1.2 Digenic triallelic Inheritance in BBS

This table provides an example of triallelic inheritance, based on the results of Beales *et al*., 2003 (183), summarizing the possible genotypes in two loci and the possible combinations of inherited alleles. For the phenotype to manifest (+), three mutant alleles (b) must be inherited across both loci. Therefore only three of nine possible combinations of allele inheritance are causative for BBS, and biallelic inheritance for at least one gene locus must occur. Therefore, both parents must be carries of mutant alleles at one locus, and at least one parent carries a mutant allele at the second locus.

Gene Locus 1 (BBS 1 M30R)	Gene Locus 2 (BBS2)	Combined Genotype	Phenotype manifestation
BB	BB	BBBB	-
BB	Bb	BBBb	-
BB	bb	BBbb	-
Bb	BB	BbBB	-
Bb	Bb	BbBb	-
Bb	**bb**	**Bbbb**	**+**
bb	BB	bbBB	-
bb	**Bb**	**bbBb**	**+**
bb	**bb**	**bbbb**	**+**

1.5.2 Primary cilia in cancer

The role of the cilium in essential signalling and developmental has already been discussed, but the strong link to cell cycle progression also implicates cilia in both sporadic and inherited forms of cancer. Cilia formation and disassembly are very tightly linked to the cell cycle, and one of the hallmarks of cancer is deregulation of the cell cycle causing over-proliferation cells, hence a logical link to cilia dysregulation in contributing to cancer cell phenotypes. The cilium has been described as the “tumour suppressor organelle”. A clear example of cilia loss correlating with increased cell proliferation has been noted in tumour cells and surrounding stromal cells in the early stages of breast cancer (184), although does not directly imply that the cilia loss was the cause of cell proliferation.

As well as cell cycle disruption, changes to ciliary-regulated signalling such as Wnt and mTOR also have links to cancer progression (148, 185). Cilia loss has been specifically described as a mechanism for tumour survival through drug resistance, specifically in medulloblastoma (186). By removing the targeting signalling response, the drugs are no longer effective. However, in contradiction

to this, some tumours develop due to de-regulated ciliary signalling such as Smoothened-dependant tumours, and therefore require persistence of cilia to develop (186). This highlights a complicated association between cilia incidence and cancer development, with each disease association specific to the tumour type. Alongside these complications, cancer research is a very broad field of study and thus the ciliary role in cancer is still poorly understood and under-studied. The current knowledge is further discussed in several excellent recent reviews (187-189).

1.5.3 Primary Cilia in other disease

There is strong recent evidence that suggests ciliary function has an important role in diabetes. Cilia are associated with regulating hormonal signals in the hypothalamus (190) and are present on α and δ-cells in the pancreas of mice and rats (191). Ciliary dysfunction in some mouse models (including *Rpgrip1l*$^{+/-}$ (192), *BBS2*$^{-/-}$ and *Bbs4*$^{-/-}$ (193)), is reported to be associated with excessive eating, possibly through ciliary dysregulation in the hypothalamus, the brain centre for weight regulation. These mice have also been shown to have impaired insulin secretion, possibly regulated by pancreatic cilia (194), causing glucose tolerance to decrease. These symptoms are the pre-requisite for type two diabetes. Thus it has been proposed (195) that cilia have a metabolic role in the onset of diabetes through weight regulation and insulin secretion. Interestingly, diabetes and obesity are often present in ciliopathy patients and these phenotypes are part of the primary diagnostic criteria for BBS (196). It has been very recently shown that pancreatic islet B cells lacking cilia are unable to respond to glucose and thus regulate intracellular Ca^{2+} levels which in turn, regulates insulin secretion (197) providing the mechanistic link between cilia and diabetes pathology.

Cilia have a clear role in development and definition of laterality, and therefore congenital heart defects are a frequent clinical feature of some ciliopathies (198). However, cilia have also been implicated in sporadic and complex forms of heart disease such as vascular aneurisms, atherosclerosis and heart disease (199). As previously described in 1.4, primary cilia are mechanosensors of flow in many organ systems (200), which appears to include blood vessels. Mouse models with conditional endothelial knock out of *Ift88* have shown a direct

correlation between flow rate and presence of primary cilia (201). Areas of high shear stress such as the aorta in the mice displayed short or had absence of cilia on endothelial cells, whereas areas of lower flow rates allowed cilia elongation. This is turn was associated with the presence of atherosclerosis plaques (201).

1.5.4 Models of Ciliopathies

As the evidence for a ciliary role in a wider range of conditions expands, the need for more diverse disease models increases. This is further confounded when modelling disorders with a range of expressivity of disease phenotype. Several well-characterised eukaryotic models such as *Chalmydomonas*, *Xenopus*, zebrafish and mouse are used for different areas of ciliary research despite the range of models for ciliary biology, the differences in genetics and physiology can limit the relevance of each model for a human disease state.

Bardet-Biedl Syndrome (BBS) is an example of a pleiotropic ciliopathy that has a phenotypic spectrum, as discussed in Section 1.5, which makes traditional animal modelling of this condition difficult. It is also often reported that full phenotypes are not fully reiterated in murine models (202). Furthermore, human dermal fibroblasts and derived induced pluripotent stem cells (iPSCs) have clonal variation even for the same individual, presumably due to epigenetic changes (203). As a consequence, despite well-studied murine models, many aspects of ciliopathy pathogenesis will remain unexplored until more physiological or relevant models of disease states can be generated.

The high conservation of ciliary proteins and ease of study makes many of these model organisms ideal for investigating the basis of ciliary structure, function and formation. Therefore these models gives reliable if not precise insight into the molecular basis behind human disease mechanisms.

1.5.4.1 Unicellular eukaryotic models

Simple single-cell models such as *Chlamydomonas* and *Tetrahymena* have greatly contributed to our understanding of ciliary biology. For example, highly conserved IFT complexes were first identified in *Chlamydomonas* flagella (204), and the use of electron microscopy in this model provided essential insight into

ciliogenesis and protein trafficking within the cilium (205). *Tetrahymena* is also commonly used in structural and protein work as it has 1000 cilia per cell (206).

1.5.4.2 Caenorhabditis Elegans

Validation work and studies into other orthologues of ciliary genes have also been extensively researched in higher multicellular organisms such as in C. *elegans* which have neuronal sensory cilia (207). These nematode worms are a great model for studying developmental biology as every cell division and differentiation throughout the nematodes worm has been described and documented. They are also quick to grown and easily to genetically maniputlate. However, conservation between human and nematode worms is low with many essential proteins in mammalian cilia not having a orthologue in the worm to study.

1.5.4.3 Zebrafish Models

Zebrafish are a vertebrate model that has cilia on nearly all their cell types. Zebrafish are useful to study ciliary effects during development because the embryos are transparent and can be genetically manipulated by either morpholino oligonucleotide knock-down or transgenesis (208). However, the interpretation of zebrafish models of human ciliopathies must be carefully considered, because the zebrafish do not manifest a full renal cyst phenotype, despite having the characteristic curved tail seen in ciliopathy models (209). Furthermore, unlike human renal cilia which are immotile, zebrafish have motile renal cilia (16).

The zebrafish genome has also caused issues for researchers when modelling disease. The genome is duplicated and there are many genes that do not have orthologues in other species, making it harder to specifically and accurate knock-down gene expression but to also accurately sequence and align the zebrafish genome. This lead to genetic studies in zebrafish being behind other model organisms.

1.5.4.4 Mouse Models

Out of all commonly used laboratory models, mice have the most similar genome to humans (upwards of 99% (210)). Despite this similarity, ciliopathy

gene knock-outs in murine models often show varied phenotypic severity and organ specificity differences compared to the human condition. For example, mutant mouse models of JBTS genes do not usually display the molar tooth sign, the diagnostic feature of JBTS patients (211). The *Nphp1* knock-out mouse, modelling the most common gene mutated in nephronophthisis (212), does not present with kidney cysts as in the human disease but does display other ciliopathy-like features such as retinal dystrophy and male infertility (213). Thus, although the closest model organism to humans, further supporting work needs to be carried out in a human model system to confirm the relevance of findings. Despite these differences, mouse models are the most comprehensive mammalian model we have to work with commonly in a laboratory setting. They provide essential insight and act and pre-clinical models for potential therapeutics.

1.5.4.5 Mouse and Human Cell Lines

Immortalised mammalian cell lines can offer well-characterised *in vitro* models that can be used for validation of research findings that are observed in other eukaryotic models, but without the expense of maintaining a mouse model. Murine inner medullary collecting duct cells (mIMCD3) are easy to culture, can form polarized monolayers and display long cilia that can be useful for immunofluorescence microscopy and protein localization studies. As an alternative, the hTERT-immortalized Retinal Pigment Epithelial cell line (hTERT RPE-1) is a human immortalized diploid cell model with shorter primary cilia. As a human cell line these can be used to confirm findings from other eukaryotic models and are particularly useful for studying ciliopathies with a retinal phenotype. However, it is important to consider that RPE-1 cells are not functioning RPE and have adapted to grow in cell culture. Many other commonly used cell models no longer genetically resemble their donor as they can become ploidy over time or when immortalised.

Non-immortalised patient-derived primary cells, usually dermal fibroblasts, can offer molecular insight into patient mutations and pathological mechanisms. However cellular phenotypes in fibroblasts can change under culture conditions and fibroblasts do not present an overt disease phenotype in ciliopathy patients. Therefore, more relevant models would use cell lines from affected tissue types.

Biopsies from patients can be an intrusive means of cell collection for research studies, but recent work has exploited urine-derived human epithelial cells as a more acceptable means of collecting patient tissue (214). However, these cells do not proliferate in culture and are derived from mixed renal cell populations. Genome editing technology such as the CRISPR/Cas9 system (discussed in 1.6.5.1 and 1.6.7), offers the ability to make both cell models of specific ciliary gene knock-outs, or exactly model patient mutations, in many different cell-types. The other advantage is that cell-lines are isogenic, which is a presumably a confounding factor in the use of patient-derived dermal fibroblasts. Therefore cell models make an affordable and simpler model for investigating ciliogenesis regulators and the molecular mechanisms, without the influence of potential of variable epistatic effects due to different genetic backgrounds. However, a single mother cell line should be used throughout experiments as it is common to note clone to clone variation between laboratories.

1.5.4.6 iPSCs and organoids

Different patient genetic backgrounds can affect the interpretation of results when investigating epistasis in primary cells, and the lack of this phenotypic diversity in animal models or immortalised cell lines is apparent across ciliopathy research. Using immortalised cell lines in this thesis allowed interpretation to be attributed to the administered genetic perturbations only, and therefore phenotypes could be ascribed to the specific genetic interactions due to introduced mutations rather than unknown epistatic effects.

Another benefit to patient-derived iPSCs is that the retrieval of cells is not an invasive procedure compared to direct tissue biopsies. Alongside being a directly relevant human model, research with iPSCs and derived organoids does not require government licencing, unlike work with animal models. Organoids resemble a middle ground between animal models and cell lines, as they resemble tissues but still lack the complexity of a full animal models. Many clinical development compounds have the desired effect on cell lines, but the majority do not progress to clinical trials because they do not provide a therapeutic effect or have additional deleterious effects when tested in pre-clinical model organisms. So, although not generally suitable for high-throughput work, they are an ideal pre-clinical model for investigating the

molecular pathology of ciliopathies, and potentially model to test therapeutics (215).

However, for future work in the field of ciliopathies, patient-derived primary cells would be invaluable for investigating patient-specific epistatic interactions. These phenotypes could be accurately modelled in patient-derived induced pluripotent stem cells (iPSCs), which can then be differentiated into appropriate disease-affected cells and organoids. However, patient derived cell lines would have high-variability. A more time consuming option would be to induce patient specific mutations into a control mother iPSC cell line using CRISPR/Cas9 editing so that the genetic background is consistent through experiments.

First developed for intestinal tissue (216), ciliopathy organoid models include optic cups to study LCA (217) and kidney organoids to model cysts in polycystic kidney disease (PKD) (218). These organoids could be a future research tool for helping to gain a more accurate understanding of complex ciliary biology. This is a highly specialised, expensive and committing technique in terms of both time and effort. These limitations made organoids unsuitable for use in this thesis and high-throughput screening.

1.6 Genetic manipulation in biomedical research

1.6.1 History of Genetics

A rudimentary understanding of genetics and inheritance began as early as the Ancient Greek era, when Hippocrates described pangenesis as the process that determines the inheritance of specific traits (219). Following the advances of cell theory and the invention of the microscope in 1595, Charles Darwin elaborated the theory of pangenesis by suggesting that each organ gave off small “germules” that then accumulated in the mother after intercourse to form the foetus (220).

In the mid-19th century the first use of experimental genetics was performed by Gregor Mendel. Mendel used cross-pollination of pea plants to describe strong individual hereditary factors, each of which were present in pairs. Each single factor, one from each parent, was responsible for a trait that was passed on to the next generation of pea plant (221). Mendel is now known as the “father of

genetics", and his experimental work provided evidence that contradicted the previous ideas put forward by the pangenesis theory. This work is the basis of Mendelian inheritance and the foundation of modern genetics.

Following Mendel, Boveri's experiments described "chromatic elements", which were later named chromosomes. He described the inheritance pattern of chromosomes, which exactly followed Mendel's theory of inheritance (222).

1.6.2 Forward Genetics

A rise in experimental genetics and interest in hereditary factors came about after Boveri's experiments in 1900, when Mendel's work was rediscovered by Hugo De Vries, who then went on to develop mutation theory (223). Following De Vries, Thomas Hunt Morgan worked to prove Mendel and De Vries' theories by using mutational screening in the Drosophila fly. Morgan's group used either natural mutants or, in later studies, randomly mutated the fruit fly using chemicals or radiation, then observed resulting phenotypes. This is a technique now called forward genetics, in which the phenotype is identified first and then linked back to the causative gene that was mutated. These experiments also provided the first evidence that genes were associated with chromosomes, and that genes in close proximity on a chromosomes were inherited together (the phenomenon called genetic linkage). Following Morgan, George Beadle and Edward Tatum developed the "one gene one enzyme hypothesis" in 1941 (224), the concept that allowed genes to be characterized based on the enzyme they produced. All of these discoveries went on to win Nobel Prizes.

1.6.3 Molecular genetics

During the early 1950s Rosalind Franklin and Raymond Gosling were carrying out x-ray diffraction experiments on fibres of deoxynucleic acid (DNA). Their now famous Photo 51 was shared with Watson and Crick who went on to describe the molecular structure of DNA in 1953 (225). Once the structure of DNA was defined new technologies quickly developed, ushering in the era of molecular genetics. This was soon followed by the discovery of restriction enzymes 1968 and the development of Sanger sequencing in 1977.

Furthermore, gene delivery was developed which allowed exogenous genes to transferred into organisms and allowed scientists to make genetically modified bacteria that produced insulin in 1978. The Polymerase chain reaction (PCR) was developed by Kary Banks Mullis and Randall Saiki in 1983 which allowed easy amplification of target DNA (226), followed by early attempts at genome engineering and the manipulation of gene expression. The completion of the first draft of the Human Genome project in 2003 (227), ushered in the most recent advances in next generation sequencing technologies. This in turn led to new gene discoveries, rare disease alleles being identified and a diagnosis given to patient families and to the era of personalised medicine.

1.6.4 Reverse Genetics

A major gap in knowledge in the new genomic era is the capacity to infer correlations between genotypes and phenotypes. Earlier methods to delineate these genotype-phenotype correlations used forward genetics, which worked from the observed phenotype in order to identify the causative genotype in the mutated gene. With the completion of the Human Genome Project, the reverse of this workflow could now be implemented, which works by targeting or mutating known sequences in a specific gene of interest, then observing the resulting phenotype. This methodology was termed reverse genetics.

1.6.4.1 RNA Interference and Genome Screening

RNA interference (RNAi), the endogenous mechanism for post-translation silencing of mRNA, was discovered in the early 1990s (228) and the mechanism of function was elucidated in the early 2000s from research in plants (229). In 1998, double stranded small interfering RNA (siRNA) was found to be more efficient at producing gene knock-down in *C.elegans* (230) and thus was eventually adopted and optimised for use across many different model organisms and cell models. In 2003, a whole genome RNAi library was generated for *C.elegans (231),* allowing for the full genome-wide analysis of gene function in a high-throughput format using the so-called “reverse genetics” workflow. This was the first systematic use of this methodology, and it allowed for unbiased analysis of all genes in a single high-throughput experiment. This provides specific phenotype data in a much quicker time scale, which has

accelerated researcher capacity to infer genotype-phenotype correlations and define gene function.

siRNAs also provide researchers with a transient/acute knock-down of gene expression. This differs from the chronic depletion seen in a knock-out model. When using siRNA this does not allow for genetic compensation to act in the model being tested, often presenting different results to a complete knock-out model.

1.6.5 Modern molecular genetics

1.6.5.1 Genome engineering

Before the era of modern genetics, genome engineering (generating specific changes to a target genome) was a laborious process that required significant investment of time and effort. In 1985, zinc finger nucleases were discovered which are a fusion of a DNA nuclease (Fok1), which generates double strand breaks, with a DNA binding domain that can be specifically engineered by changing 4 key amino-acids in its alpha helix to recognise different DNA sequences (232). In 2011 similar technology in transcription activator-like effector nucleases (TALENs) was discovered. TALENS also require protein engineering in order to determine the specificity of DNA cleavage (233). The original methods of genome engineering was therefore complicated and time consuming.

The clustered regularly spaced short palindromic repeats/Cas9 (CRISPR/Cas9) system was originally discovered in 1987, but molecular genetics had a breakthrough in 2012 when Jennifer Doudna and Emmanuelle Charpentier were able to describe its molecular mechanism (234). They also realised the potential to use CRIPSR/Cas9 in other organisms, outside of the prokaryotes it was discovered in, to specifically target genes of interest. The system could be used to induce insertions and/or deletions (indels) through non-homologous end-joining. This error prone repair allowed for quick, efficient and specific genome editing in almost any animal or cell model. Then, in 2013 Feng Zhang's research group published a protocol describing how they adapted CRISPR/Cas9 for use as a programmable genome editing tool in eukaryotic cells (235), not long after TALENs were being adopted. CRISPR/Cas9 is

arguably one of the biggest impacts in molecular biology and genetics research in the last 10 years and has even been translated into early-stage clinical trials since 2018.

1.6.6 Modern Reverse Genetics Tools

1.6.6.1 Small interfering RNA (siRNA) and small hairpin RNA (shRNA)

Experimentally designed small hairpin ribonucleic acid (shRNA) or small interfering RNAs (siRNAs) can be delivered to animals or cell models through injection, transfection or by generating a transgenic model. These small RNAs take advantage of the endogenous cellular mechanism of RNA interference for gene silencing and control of gene expression (Figure 1.12).

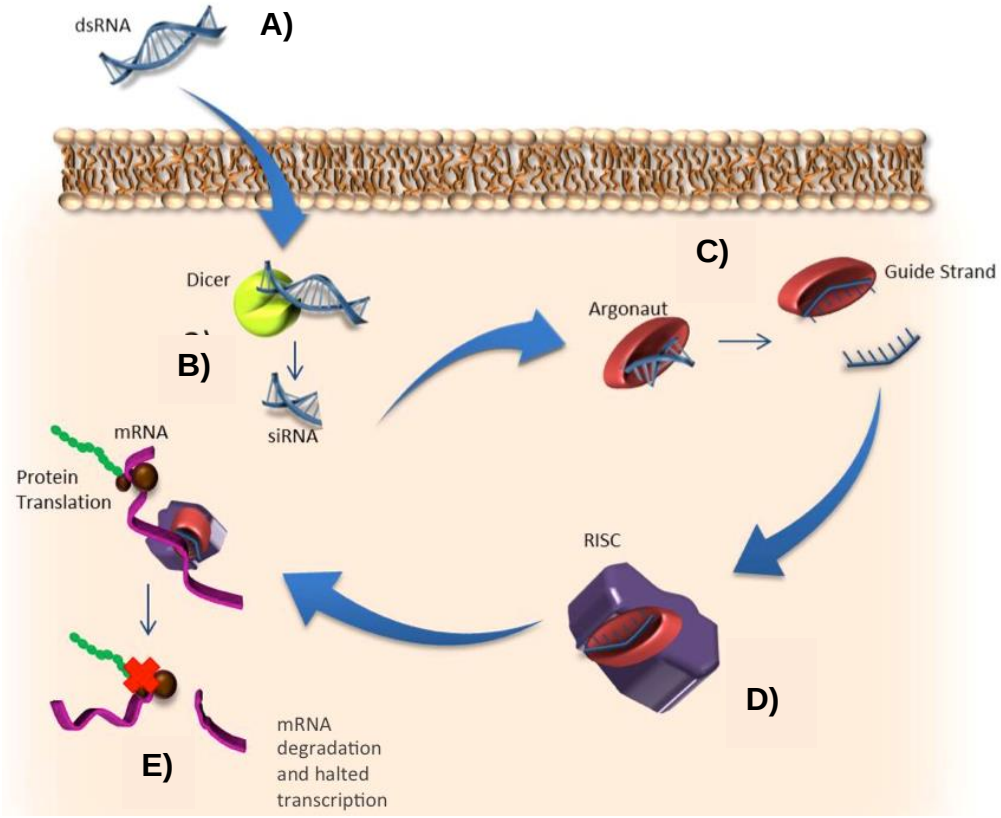

Figure 1.12 RNAi and Experimental Knock-down

> **A)** siRNA or shRNA is delivered to the cell. **B)** dsRNA is recognised and cleaved by dicer. **C)** Argonaut binds to the guide stand of the cleaved RNA. **D)** Argonuat and the guide stand form a complex which is targeted to the complementary mRNA. **E)** Targeted mRNA is cleaved by RISC and degraded. This halts transcription and creates a protein knock-down.

When shRNA is expressed experimentally, it is processed by a protein called Dicer to create 21 base-pair double stranded RNA (dsRNA) (236). This 21 base-pair RNA is similar to siRNA, which is usually transiently transfected into

cells directly as a short dsRNA oligonucleotide. Argonaute binds to a single guide strand of the dsRNA and signals the formation of the RNAi-induced silencing complex (RISC). The antisense guide strand of the RNA specifically targets complementary mRNA to be bound by RISC. The targeted messenger RNA (mRNA) is then cleaved by Argonaute and degraded (236). Recurrent targeting and degradation of the targeted mRNA suspends protein translation, leading to a functional knock-down of expression of the targeted gene. Depending on the stability and turnover of the protein expressed from that gene, a functional knock-down can occur within a few hours or a few days.

Experimental siRNAs are small and modified and can induce RISC without inducing a full viral response, which, if activated, would non-specifically reduce total protein expression (237). By overcoming this innate response that was described when RNAi was discovered, this provides the experimental means to impose specific knock-down of only the targeted gene. This makes siRNA an ideal molecular tool to specifically manipulate gene expression.

Viral transduction and *in vitro* reverse transcription of a virally-integrated shRNA gene can provide a constitutive knock-down of the targeted gene. This technique can also provide another level of control if the shRNA is expressed under an inducible promoter. Viral transduction can often deliver shRNA to difficult-to-transfect cell types (such as SH-SY5Y the human neuroblastoma cell line and patient primary cells), increasing the options for more relevant cell models. However, viral insertion mutagenesis of actively-transcribing regions of the genome, and the potential off-target effects of using only a single shRNA, have to be taken into consideration. Viral particle production, optimisation and final cell line validation are time-consuming and require more stringent Genetically Modified Organisms Class II working conditions, making it a less convenient method to set up. However, a key advantage is the ability to investigate longer-term processes and the effects of time-dependant knock-down.

1.6.6.2 High-throughput siRNA screening

As the specificity and popularity of siRNA as a molecular tool increased, siRNA screening was developed (231). Whole genome libraries of siRNAs were produced commercially so that in a high-throughput format, every gene in the

genome of interest could be specifically knocked-down. It allowed a non-biased approach to be taken when identifying genes that contribute to the cellular phenotype of interest, which in turn increases the chances of novel discoveries.

Screening requires a lot of optimisation because of the high experimental variation that can arise from the high-throughput setup of a cell-based assay, unless many processes are carried out robotically. Furthermore, under ideal experimental circumstances, siRNAs should be individually optimised for concentration and knock-down time for each gene to ensure functional knock-down. However, this is impossible in a high-throughput setup, and so siRNAs are either induced for the same length of time (stable transfection) or transfected at the same concentration (transient transfection) across the whole panel of siRNAs being screened. Screening therefore requires several validation steps and downstream work to ensure that a specific knock-down of the target gene was achieved in the set time-frame and concentration. It should be considered as a “hypothesis generating” approach to identify further avenues of investigation.

1.6.6.3 Advantages and disadvantages of experimental siRNA knock-downs

As RNA is relatively unstable, several nanomoles of dsRNA are required for a functional knock-down in experimental conditions, which can increase experimental costs and off-target effects. The use of transfected siRNA also only provides a transient knock-down, and therefore limits the experimental use of this technique to investigate shorter term effects. Short-term knock-down can also be an advantage, since it has been shown that full knock-outs in model organism such as mice and zebrafish induce compensatory mechanisms that can affect phenotypes and thus mask the function of the targeted gene (238).

Knock-downs are a well-optimised methodology and due to their transient effects are a short-term experiment that can be easily scaled-up for high-throughput approaches. This allows screening of several genes quickly to identify primary hits of interest for further investigation. Experimentally, rather than induce the full endogenous RNAi response, which can cause non-specific knock-down of all gene expression, direct transfection of siRNA is used. This double stranded 21nt RNA bypasses the normal immune response induced by

foreign RNA. Despite this, non-specific off-target effects remain one of the biggest drawbacks of siRNA knock-downs as a reverse genetics technique. Thus, for many whole genome screens unless each siRNA has previously been confirmed to be specific, either during optimisation or is purchased and validated commercially, some phenotypic changes may be due to off-target effects. This is a major potential source of skew in data that confound meaningful analysis. To reduce these effects, pools of several different siRNAs targeting the same mRNA were used throughout this project. Each siRNA in a pool is therefore at a lower concentration but the total RNA is at working concentrations. This dilutes off-target effects of each individual siRNA, whilst the total pool of siRNAs still provides a functional knock-down. Throughout this thesis siRNA pools were therefore used in experiments to increase the specificity and accuracy of the experiments.

1.6.7 CRISPR/Cas9

CRISPR/Cas9 is an endonuclease driven by a designed guide RNA (gRNA) which targets a gene-specific 20 nucleotide sequence, upstream of a protospacer adjacent motif (PAM) sequence (NGG for *Streptococcus*-derived Cas9) within the target gene (Figure 1.13). Once the gRNA is bound to the target sequence, Cas9 recognises the PAM sequence and cleaves the DNA to generate a double strand break 3 base-pairs upstream. DNA repair mechanisms, such as non-homologous end joining (NHEJ), are then recruited to repair the break, but the mechanism is error-prone because the nuclease remains attached to the DNA and interrupts repair machinery (239). The error in repair therefore generates random insertions/deletions (Indels) at the cleavage site, creating frame-shifts and functional knock-outs of the targeted gene. If the system is delivered with an engineered repair template, homologous recombination can insert (“knock-in”) exact patient mutations (240) (Figure 1.13).

The main drawbacks of this technology are delivery in certain cell models, potential off-target effects, and editing efficiency. Editing efficiency further decreases when using the homologous repair (HR) system, and improvements in efficiency are the subject of many recent studies and advances in the CRISPR/Cas9 field (241, 242).

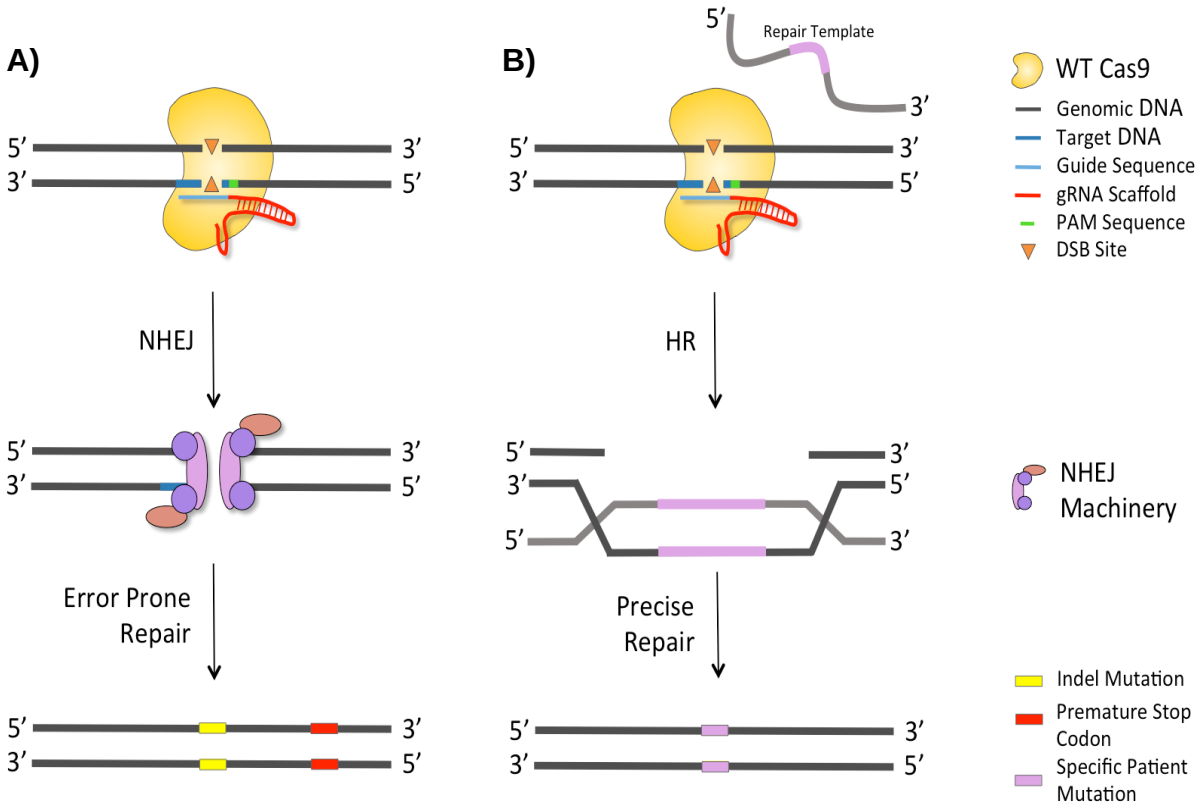

Figure 1.13 CRISPR/Cas9 and DNA repair pathways

A) Cas9 cleaves target DNA and is repaired by non-homologous end joining (NHEJ). This error-prone repair pathway causes random insertions or deletions at the Cas9 targeted site. This can then generate a frameshift in the target gene, leading to a knock-out of the gene, or expression of a non-functional protein. **B)** The same system can be used to insert exact patient mutations by using the homologous recombination repair pathway; an engineered DNA repair template is delivered to the cells alongside the CRISPR/Cas9 system to allow precise repair at the targeted region. Adapted from (235) Figure 2 with Copyright permissions.

1.6.7.1 Advances and uses of CRISPR/Cas9

With the exponential advances made in CRISPR/Cas9 technology, since the work in this thesis was completed, it could soon be performed on a similar timescale to siRNA experiments (as little as 72hours). Viral delivery systems can also be used for primary cells, or cell lines that are difficult to transfect. Alongside improvements in delivery methods, the reagents have also improved. One popular method is to form a ribonucleotide protein complex of purified Cas9 protein with guide RNA. The guide RNA can be in the form of a synthetic single guide (sgRNA), or separate CRISPR RNA (crRNA) associated with fluorescently tagged *trans*-activating CRISPR RNA (tracrRNA). This allows reagents to be directly targeted to the nucleus without the expression delay that

occurs with the use of older plasmid-based approaches and which also requires self-assembly of the protein and RNA after expression. Fluorescently tagged tracrRNA also allows for fluorescent-associated cell sorting (FACS) of transfected cells for single cell clone selection.

Different species of endonucleases, such as Cpf1 (243) or Cas9 engineered with nuclear localisation signals (244), have also been developed to improve transport and localisation into the nucleus upon delivery. However, there are mixed reports on the relative benefit of improved nuclear localisation for increased editing efficiency (245). Cas9 has also been engineered to have variable PAM recognition sequences (including NG, GAT and GAA) to increase potential editing target sites (246). Therefore, there are more potential target regions that can be edited with a much higher efficiency and specificity than before.

1.6.7.2 Homology-directed repair and precision editing

Homology directed repair (HDR) is used to model patient mutations, repair mutations, make fusion proteins, or knock-in whole expression cassettes and remains the most versatile technique to generate specific edits. However, both knock-ins of small single base changes and larger 1kb regions are far less efficient than generating random indels or base editing. The need for an efficient delivery of a repair template, and to induce the specific HDR pathway reduces the overall number of desired edits. HDR is also not possible in many cell types that are terminally differentiated, non-dividing or do not express HDR machinery. This therefore has been the focus for many contemporary methodologies in improving CRISPR/Cas9 technology.

Initially, Suzuki *et al.* developed a homology independent targeted integration (HITI) method to make edits in non-dividing cells. This takes advantage of the remaining non-homologous end joining (NHEJ) repair pathway that is present in these cell types (244). The system uses CRISPR/Cas9 to cut both the target region and the homology template. The cells are then able to use NHEJ and repair the DSB on the template DNA into the target region. However, in theory the repair template can be knocked into any location with a DSB or it could be knocked-in in either orientation, so clones must be rigorously screened. It is also possible that because NHEJ is error-prone, mutations may occur around

the insert sites, which may cause frame-shifts or deleterious mutations. However, this methodology improves specific knock-in efficiencies from <5% for HDR to >45% for HITI in dividing cells such as HEK293 cells (244).

Later research utilised machine learning to optimise the design of single stranded donor templates by showing that the composition of the 3' arm is key to inducing microhomology-mediated end joining repair rather than HDR and that the distance to the double stand break made a crucial contribution to repair efficiency (247). Over-expression of B-cell lymphoma-extra-large (*BCL-XL*) could improve HDR efficiency 10-fold in stem cells by increasing their survival post-transfection (248). Another approach transfected two donor templates containing selection cassettes, allowing modified clones to be isolated using dual antibiotic selection to increase the specificity and frequency of homozygous edits (249). However, this approach was still limited by transfection efficiency.

These methodologies have the potential to be used for *in vivo* gene therapies (250) and have been used to treat autosomal dominant retinitis pigmentosa in pre-clinical rat models with a premature stop codon substituting the serine codon at 334 in the *Rho* gene (251). The retina is an ideal tissue for gene therapy as shown by the many research groups developing the therapies for retinal disease (reviewed in Cherenk *et al*., 2016 (252)). The retina has even been the subject of an on-going gene therapy clinical trial for a ciliopathy (Leber's congenital amaurosis; ClinicalTrials.gov Identifier: NCT03872479).

1.6.7.2.1 Base editing

Base editing was originally developed for cytidine to thymine (C:G>T:A) base changes, but new subsequent fusion proteins later allowed adenine to guanine (A:T>G:C) changes (253). This new technology was designed as a quicker and easier way to generate specific base changes in order to introduce missense mutations and to overcome the issues of low efficiency in homology-directed repair approaches. C:G>T:A base pair editing was important to develop because C:G>T:A transitions are the most common cause of missense mutations, accounting for half of pathogenic single-nucleotide variants (SNVs) (253). C:G>T:A transitions arise from spontaneous deamination of cytosine, which can happen up to 500 times a day in each human cell (254). In turn the

A:T>G:C base editing system was developed to be able to repair these common mutations in human disease or model pathogenic SNVs that could not be modelled with the C:G>T:A base editor (253).

However, the basic concept is the same for both base editors and is summarised in Figure 1.14. For C:G>T:A editing; nuclease-deficient Cas9 (nCas9) is fused to a cytidine deaminase (such as APOBEC1), a uracil DNA glycosylase inhibitor (UGI), and in some cases a fluorescent tag such as GFP. This fusion protein is targeted to the region of interest in the genome by the guide sequence on the crRNA. Any cytidine within a 5-nucleotide editing window will act as a substrate for the deaminase and will be converted to uracil. This is then protected by the UGI which inhibits base excision repair of the uracil. The Cas9 creates a single strand nick in the DNA to encourage mismatch repair, permanently converting the C:G>T:A (255).

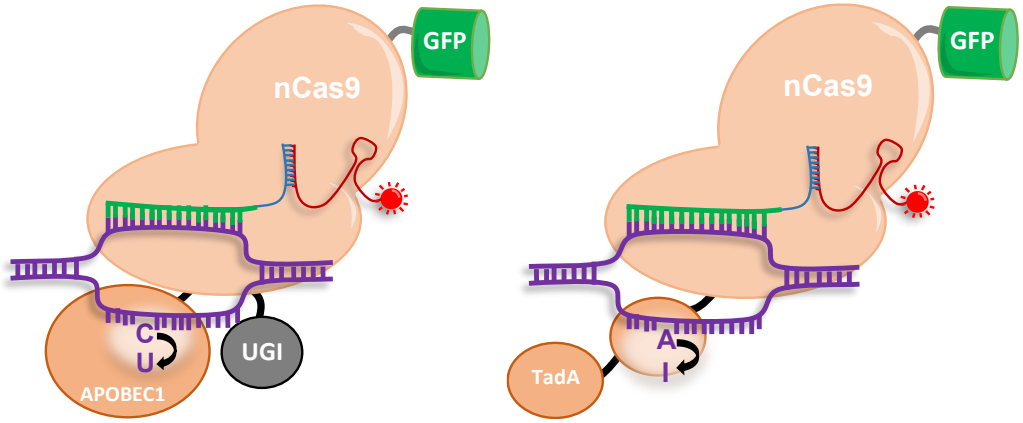

Figure 1.14 CRISPR/Cas9 base editing

A) Nickase-Cas9 (nCas9) is fused to APOBEC1 (cytidine deaminase), UGI (uracil DNA glycosylase inhibitor), and GFP. The guide sequence of a crispr RNA (green) targets the nCas9 complex to the DNA region of interest. Any cytidine bases within the defined editing window of the APOBEC1 fusion protein will be deaminated to uracil. These uracils are protected from base excision repair by UGI. When repaired or copied, the uracil is read as a thymidine and the base pair is changed from C:G>T:A. **B)** nCas9 is fused to two TadA domains. As described in A), the guide specifically targets the nCas9 complex. Adenine is deaminated to inosine, which is recognised as a guanine during repair or replication, therefore changing the base pair from A:T>G:C

For A:T>G:C editing, nCas9 is instead fused to adenine deaminase TadA. It is also targeted to the genome by the guide sequence but has a variable editing window. Adenines are converted to inosine, which are read as guanine by DNA polymerases, thus incorporating the base change during DNA repair or replication (253).

Improvements in base editing have also been developed, and there are now several generations of base editors (256). For example, targeted APOBEC1 mutations were used to change the size and positioning of the editing window in C:G>T:A base editing (257). This approach allows for alternative bases along the target region to be edited with a single guide sequence, expanding the list of possible base changes throughout the genome.

1.6.7.1.2 CRISPR prime editing

Efficiency of HDR and specific editing is such that desired mutations can be screened for in as few as 30 clones, however precision had yet to be optimised. Base editing can cause mutations across the editing window (255), this can lead to unwanted changes within the proximity of the targeted base.

Furthermore, unwanted edits can occasionally occur from HDR and the technologies mentioned above. David Liu’s research group therefore recently developed a new technology that aims improve the precision of specific CRISPR/Cas9 mediated editing called CRISPR Prime editing (258) and is summarised in Figure 1.15

CRISPR prime editing uses a nickase Cas9 to guide a synthetic prime editing RNA (pegRNA) to the target region in the genome. This pegRNA is both a guide RNA and a reverse transcriptase repair template in one single RNA. Once bound, Cas9 nicks the DNA to release the top strand which can then bind to the reverse transcriptase template of the pegRNA. The reverse transcriptase domain then transcribes in the desired edit by directly polymerising DNA to the nicked strand. This heteroduplex DNA is then targeted by a secondary gRNA and nickase Cas9. This nicks the bottom strand in proximity to the edited region to encourage the cell to incorporate the edited strand during repair or replication (258).

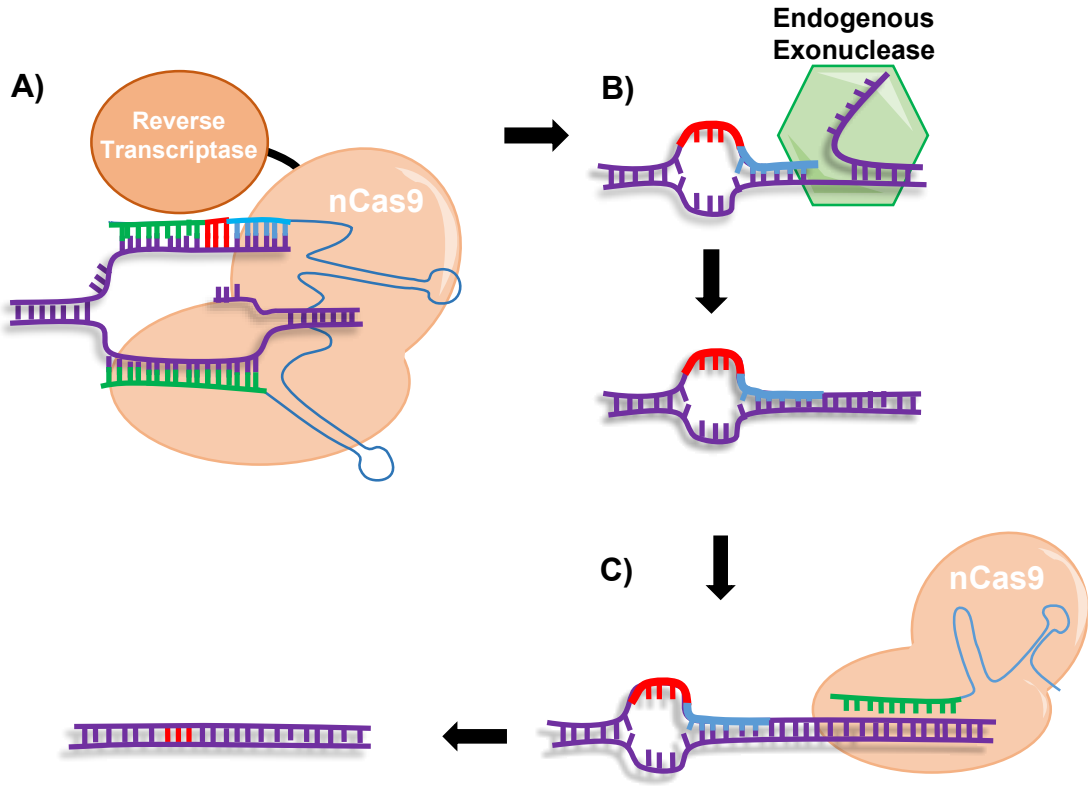

Figure 1.15 CRISPR/Cas9 prime editing

Prime editing occurs by three main steps: **A)** Nickase D10A Cas9 (nCas9) is directed to the target genomic sequence by the guide region in the prime editing guide RNA (pegRNA; green). This region is homologous and binds to the target DNA. nCas9 makes a single-strand break in the DNA, releasing the top strand of the DNA complex. This region is complimentary to the binding region of the pegRNA. Next to the binding region is the desired edit (red), followed by a homologous region to the target sequence (blue). The reverse transcriptase fused to nCas9 extends the nicked DNA to match the pegRNA sequence. **B)** This region of new DNA binds using the new homology region (blue). The 5' flap of the original DNA is then cleaved by endogenous exonucleases, allowing the DNA to repair with a mismatch where the designed precise edit has been inserted. **C)** A different guide RNA recruits nCas9 downstream of the edit on the opposite strand. nCas9 nicks the DNA to promote DNA repair and incorporation of the new designed edit.

This technique extends the editing capacity across the genome because edits can occur up to 30bp from the PAM sequence and PAMs occur approximately every 8bp throughput the genome (258), whereas previous techniques left regions of the genome unreachable for targeted and specific editing (253). More importantly however, this technique does not use an error prone DNA repair

pathway, thus minimises unwanted edits and improved overall precision of editing.

1.6.7.3 Whole genome CRISPR/Cas9 screens

The availability of commercially designed and validated CRISPR gRNA sequences has led to the development of CRISPR/Cas9 whole genome screens. These screens require cells that are stably transfected to expresses Cas9. Unlike siRNA screens, which target the mRNA and transiently knock-down gene expression, CRISPR/Cas9 screens generate random mutations at the genomic DNA level. Therefore, these screens require highly efficient guide sequences to ensure that a high proportion of the cell population have received deleterious mutations in order for accurate assessment of phenotypes. However, further technical developments in precise genome editing such as HDR or base editing would be needed for more researchers to adopt this demanding technique. Currently, the efficiency of high-throughput CRISPR/Cas9 screens is limited and as indel formation is random, there is likely to be inconsistencies in phenotypes across the cell populations being analysed, each of which would not be characterised and attributed to a known mutation. Once the technique becomes more reliable, efficient and specific, these screens could offer a new approach to reverse genetic screening and highlight the differences in phenotype between transient knock-down and genomic level knock-out.

1.6.8 Using Reverse Genetics to Study Cilia and Ciliopathies

1.6.8.1 siRNA screening to study cilia

There are several data sets available that have utilised whole genome siRNA screening as an unbiased technique to investigate ciliary biology, including the mouse genome screen data set that was used throughout this thesis (259). The whole genome screening technique has led to several important findings and the identification of novel mechanisms in ciliary biology. In 2010, a “druggable” genomic screen was published that further implicated actin remodelling as a modulator of ciliary length (260). A genome-wide screen was published in 2013 that focused on human centriole biogenesis and showed that TRIM37 prevents over duplication of centrioles (261). In 2015, a similar screen to that used in this

thesis, but in a human cell line, aimed to identity positive ciliopathy regulators and found a novel JBTS gene (262). In 2016 Kim *et al*. published a whole genome screen investigating links between ciliogenesis and the cell cycle identified and provided further evidence for the role of the ubiquitin proteasome system in ciliary disassembly (93). Furthermore, the role of the proteasome was highlighted in a recent siRNA screen that aimed to identify antagonistic interactions that influence Wnt signalling in a BBS4 Bardet Biedl syndrome cell model (263).

With the advent of CRISPR/Cas9 approaches, there has also been a genome-wide CRISPR/Cas9 screen into ciliary function and Hedgehog signalling (264). This screen identified new transition zone components FAM92A and TTC23, described the novel ciliopathy gene TXNDC15, and defined the role of *FAM92A* and *TTC23*, two previously uncharacterised genes in centriole stability.

1.6.8.2 CRISPR/Cas9 to study cilia

CRISPR/Cas9 genome editing offers a quick and easy-to-use technology that can generate stable human cell models for molecular studies of the cilium and ciliopathies. To combat the variation in phenotypes seen between different patient mutations, CRISPR/Cas9 with HR could be used to model patient-specific mutations in a tissue type of interest, in order to generate a model that is directly relevant to patient phenotypes. Although these models will not have the same genetic background as patients, they offer a quicker and inexpensive model compared to using patient-derived iPSCs. A further advantage is that multiple disease causing mutations can be compared on the same genetic background by deriving a panel of mutant cell lines from the same mother cell line. Patient-derived iPSCs may be more directly relevant to a single patient for therapeutic stem cell replacements, but the different genetic background between patients can be an additional source of pleiotropy for ciliopathy phenotypes. Therefore, a panel of cell models will be a useful tool for high-throughput screening, molecular screening, genetic interaction studies and structural studies of the cilium, complementing published and on-going work in human cell lines.

1.7 Preliminary Work leading to or included in this thesis

1.7.1 Primary Whole Genome siRNA Screen

A primary whole genome siRNA screen was carried out in Prof. Colin A. Johnson's research group as part of a system biology project to identify new regulators of ciliogenesis (259). The screen aimed to identify potential ciliopathy genes and positive regulators of ciliogenesis. The full data set was published in 2015 along with follow-up validation work from the group and collaborators. This data-set was adopted for reanalysis and use throughout Chapters 3 and 4 of this thesis. Screen protocols were also adopted and re-optimised for use throughout Chapters 3-5 of this thesis.

1.7.2 Cell lines

In 2015, my work in Prof. Colin A. Johnson's group included developing and optimising the use of CRISPR/Cas9 technology in RPE-1 to develop cellular models of ciliopathies. A panel of genes were targeted, and both polyclonal and single cell clones were generated. These cells were adopted and validated for use throughout Chapter 5 of this thesis.

Other cell lines included mIMCD3 cells expressing GFP-Life-Act, which were kindly made and gifted by Dr. Chiara Galloni from Dr. Georgia Mavria's Research Group, University of Leeds. Work from the Mavria Research group also included phenotyping the *Rock2*$^{-/-}$ mouse for angiogenesis defects, presented in Dr. Gary Grant's thesis (265). Dr. Grant identified that mouse had ciliary defects and mis-organisation of cilia across vessel lumens. Work with these cells also showed that drugs that affect actin remodelling can increase cilia length or incidence, which supported work presented in Chapter 3 of this thesis.

1.8 Aims & Objectives

The overall aim of this project was to improve ciliopathy patient quality of life through greater understanding of their genetic disease and though identifying potential therapeutic pathways. Furthermore, to understand the molecular and

genetic mechanisms that regulate ciliogenesis, which would give insight into the spectrum of ciliopathy phenotypes seen across each disease.

A secondary aim was to identify novel the regulators of ciliogenesis which is an area of poor characterisation considering its importance across the spectrum of inherited and non-inherited disease. Any identified regulators could then be further investigated, in order to elucidate some of the molecular mechanisms of regulation and contribute to the overall aim of the project.

The hypotheses to be tested in this thesis were therefore:

‘Ciliogenesis is specifically regulated and timed within the cell cycle. It therefore has negative regulatory pathways that have yet to be identified.’

‘The spectrum of phenotypes seen in ciliopathies is not due to the inheritance of many different SNPs throughout the genome and environmental factors, but can be explained through epistatic genetic interactions between ciliary genes’

Therefore the 3 key experimental objectives of this research project were to:

- Identify novel regulators of ciliogenesis using reverse genetics and screening techniques in relevant and well-characterised cell models.
- Design and develop a combinatorial screen with CRISPR/Cas9 edited cell lines to identify potential genetic interactions that contribute to ciliogenesis in known ciliopathy genes.
- Investigate the molecular mechanisms that underlie any identified regulators or interactions.

The first part of this project used a previously published whole genome siRNA screen data-set to identify potential genes that, once perturbed, either increased cilia incidence across a cell population, or increased the number of cilia per individual cell in the population.

The second part of this project developed a new screening methodology designed to identify synthetic genetic interactions that regulate ciliogenesis: specifically cilia incidence and cilia size. The aim was to further understand the hierarchy of proteins in the organisation of cilia during ciliogenesis, following on

from work in *C.elegans* (80), and mice (79). The overall purpose of this part of project was to substantiate the effect of potential modifier alleles of ciliary phenotypes, and to investigate genetic and biochemical interactions between different structural modules of the cilium. This in turn would generate a primary data-set that could be used to understand the potential mechanistic basis for the pleiotropy that is observed in ciliopathies.

Chapter 2
Materials and Methods

2.1 Materials

All materials were supplied by Sigma-Aldrich unless otherwise stated.

2.1.1 Suppliers

Table 2.1 List of suppliers

List of suppliers for all reagents used throughout this thesis. Supplier name and headquarters address is given.

Company Name	Address
Abcam plc.	Discovery Drive Cambridge Biomedical Campus, Cambridge, CB2 0AX, U.K.
Addgene	490 Arsenal Way, Suite 100, Watertown, MA 02472, U.S.A
American Type Culture Collection® (ATCC®)	10801 University Boulevard, Manassas, VA 20110, U.S.A
Applied BIosystems	120 Birchwood Blvd, Birchwood, Warrington WA3 7QH, U.K.
Bethyl Laboratories	25043 FM 1097, Montgomery, TX 77356, U.S.A
Bioline	Edge Business Centre, Humber Rd, London NW2 6EW, U.K.
BIO-RAD	The Junction 3rd And 4th Floor, Station Road, Watford, WD17 1ET, U.K.
Calbiochem	10394 Pacific Center Ct, San Diego, CA 92121, U.S.A
Cayman Chemical	Cayman Chemical, 1180 East Ellsworth Road, Ann Arbor, Michigan 48108, U.S.A
Cell Signalling Technology	Dellaertweg 9b, 2316 WZ, Leiden, The Netherlands
ChromoTek	Am Klopferspitz 19, 82152 Planegg, Germany
Clent Life Science	Suite 3, Faraday House, King William St, Amblecote, Stourbridge DY8 4HD, U.K.
Clontech Laboratories	The Danby Building, Edmund Halley Road, Oxford Science Park, Oxford, Oxon, OX4 4DQ, U.K.
Corning	Elwy House, Lakeside Business Village, St Davids Park Ewloe, Flintshire, CH5 3XD, U.K.
Dako, Agilent Technologies	5301 Stevens Creek Blvd., Santa Clara, CA 95051, U.S.A

Dharmacon, Horizon Discovery Group	Cambridge Research Park, 8100 Beach Dr, Waterbeach, Cambridge CB25 9TL, U.K.
Fisher Scientific UK	Bishop Meadow Rd, Loughborough LE11 5RG, U.K.
FluidX Ltd	Northbank Industrial Park, Gilchrist Road, Irlam, Manchester, M44 5AY, U.K.
Gibco, Life Technologies	3 Fountain Drive, Inchinnan Business Park, Paisley, PA4 9RF, U.K.
Ibidi GmbH	Lochhamer Schlag 11, 82166 Gräfelfing, Germany
Invitrogen	3 Fountain Drive, Inchinnan Business Park, Paisley, PA4 9RF, U.K.
Merck Millipore	Suite 21, Building 6, Croxley Green Business Park, Watford, Hertfordshire, WD18 8YH, U.K.
New England Biolabs	75-77 Knowl Piece, Wilbury Way, Hitchin, Hertfordshire, SG4 0TY, U.K.
Nippon Genetics Europe	Binsfelder street 77, 52351 Dueren, Germany
Perkin Elmer	Chalfont Road Buckinghamshire, Seer Green, HP9 2FX, U.K.
Proteintech Europe	4th Floor, 196 Deansgate, Manchester, M3 3WF, U.K.
Qiagen	Skelton House Lloyd Street North, Manchester, M15 6SH, U.K.
Santa Cruz Biotechnology	Bergheimer Str. 89-2, 69115 Heidelberg, Germany
Scientific Laboratory Supplies	Wilford Industrial Estate, Ruddington Lane, Wilford, Nottingham, NG11 7EP, U.K.
Sigma-Aldrich	The Old Brickyard, New Rd, Gillingham, Dorset, SP8 4XT, U.K.
Thermo Scientific UK	**3**rd Floor 1 Ashley Road, Altrincham, Cheshire, WA14 2DT, U.K.
VWR Chemicals International	Hunter Blvd, Magna Park, Lutterworth, LE17 4XN, U.K.
Ximbio	2 Redman Place, London, E20 1JQ, U.K.
Zymo Research	*17062 Murphy Avenue, Irvine, California, 92614, U.S.A*

2.1.2 General Reagents

- dH_2O
- Ethanol
- Methanol

2.1.3 Buffers

- 1X Phosphate-buffered Saline (PBS) (Autoclaved and filter sterilised)
- 1X Phosphate-buffered Saline 0.05 % [v/v] Tween20 (PBST)
- 1X Tris-buffered Saline (TBS)
- 1X Tris-buffered Saline 0.05 % [v/v] Tween20 (TBST)

2.1.3.1 Lysis Buffer for Protein Extraction

- 50 mM Trizma® hydrochloride pH8
- 1 mM EDTA pH8
- 150 mM NaCl
- 0.01 % [v/v] Triton™ X-100
- 1 % [v/v] Glycerol

Stored at 4 °C. 100X Halt™ Protease Inhibitor Cocktail and 100X Halt™ Phosphatase Inhibitor Cocktail (Thermo Scientific™) were diluted to 1X in the buffer before use.

2.1.3.2 Lysis Buffer for Genomic DNA Extraction

- 10 mM Trizma® hydrochloride pH8
- 100 mM EDTA pH8
- 0.25 % [w/v] Sodium dodecyl sulphate

Stored at 4 °C. Ribonuclease A from bovine pancreas was diluted to 40 ng/ml in the buffer before use.

2.1.3.3 Gel Loading Buffer (6X)

- 1X TAE
- 0.15 % [w/v] Orange G
- 60 % [v/v] Glycerol

2.1.3.4 Co-Immunoprecipitation Dilution Buffer

- 10 mM Tris/Cl pH 7.5
- 150 mM NaCl
- 0.5 mM EDTA

Stored at 4 °C. 100X Halt™ Protease Inhibitors (Thermo Scientific™) were diluted to 1X in the buffer before use.

2.1.3.5 Co-Immunoprecipitation Wash Buffer

- 10 mM Tris/Cl pH 7.5
- 150 mM NaCl
- 0.5 mM EDTA

Stored at 4 °C. 100X Halt™ Protease Inhibitors (Thermo Scientific™) were diluted to 1X in the buffer before use

2.1.3.6 Fluorescent Activated Cell Sorting (FACS) Buffer

- 2 mM EDTA
- 25 mM HEPES
- 1 % [v/v] Heat inactivated Fetal Bovine Serum (FBS)

Made up to 50 ml in 1X PBS (without $CaCl_2$ and $MgCl_2$) and stored at 4 °C.

2.1.4 Specific Reagents

2.1.4.1 PCR

- DreamTaq DNA Polymerase, 5 U/µL (Thermo Scientific™)
- 10X DreamTaq Buffer, includes 20 mM $MgCl_2$ (Thermo Scientific™)
- Primers, 25 nmol (Full list in Appendix A.2, Table A.8)
- dNTPs, 100 mM (Thermo Scientific™)
- Midori Green Advance DNA/RNA stain (Nippon Genetics)

2.1.4.2 Reverse transcriptase-PCR

- Quick-RNA™ Miniprep Kit (Zymo Research)
- SuperScript™ III First-Strand Synthesis SuperMix (Invitrogen™)

- Hotshot Diamond PCR Mastermix (Clent Life Science)

2.1.4.3 Gel Electrophoresis

- Agarose
- 1X Tris-acetate-EDTA (TAE)
- Quick-Load® Purple 1 kb DNA Ladder (New England Bioscience)
- EasyLadder I (Bioline)

2.1.4.4 Sanger Sequencing

- ExoSAP-IT™ PCR Product Cleanup Reagent (Applied Biosystems™)
- BigDye™ Terminator v3.1 Cycle Sequencing Kit (Applied Biosystems™)
- 0.25 M EDTA
- Deionised Hi-Di™ Formamide (Applied Biosystems™)

2.1.4.5 Cloning

- TOPO® TA Cloning® Kit (Invitrogen™)
- Gateway™ LR Clonase™ II Enzyme mix (Invitrogen™)
- Gateway™ BP Clonase™ II Enzyme mix (Invitrogen™)

2.1.4.6 Protein Quantification

- Quick Start™ Bradford Protein Assay (Bio-Rad)

2.1.4.7 Western Blotting (WB)

- NuPAGE™ LDS Sample Buffer (4X) (Invitrogen™)
- 2-Mercaptoethanol
- NuPAGE™ 4-12 % Bis-Tris Protein Gels (Invitrogen™)
- NuPAGE™ MES SDS Running Buffer (Invitrogen™)
- NuPAGE™ Transfer Buffer (Invitrogen™)
- Invitrolon™ PVDF/Filter Paper Sandwich (Invitrogen™)
- Precision Plus Protein™ All Blue Pre-stained Protein Standards (Bio-Rad)
- SuperSignal™ West Femto Maximum Sensitivity Substrate (Thermo Scientific™)
- Restore™ PLUS Western Blot Stripping Buffer (Thermo Scientific™)

2.1.4.8 Co-Immunoprecipitation

- GFP-Trap® Magnetic Beads (Chromotek)

2.1.4.9 Immunofluorescence

- Matrigel Matrix (Corning)
- “Marvel” Non-fat Dried Skimmed Milk (Premier Foods)
- ProLong™ Gold Antifade Mountant (Invitrogen™)

2.1.4.10 Live Cell Imaging

- µ-Dish, 35 mm, High Glass Bottom dish (ibidi)
- DMEM/F-12, with-out Phenol Red (Gibco™)
- HEPES Buffer

2.1.5 Tissue Culture Reagents

- Dubecco’s Modified Essential Medium (DMEM) (Thermo Scientific™)
- DMEM/F-12, GlutaMAX™ Supplement (Gibco™)
- Opti-MEM™ Reduced Serum Medium (Gibco™)
- Foetal Bovine Serum
- Trypsin
- 1X PBS (without Calcium Chloride and Magnesium Chloride)
- Lipofectamine™ 2000 Transfection Reagent (Invitrogen™)
- Lipofectamine™ RNAiMAX Transfection Reagent (Invitrogen™)
- ON-TARGETplus siRNA SMARTpools (Dharmacon™) (Appendix A.1)

2.1.5.1 Cell-Lines

All cell lines were sourced from American Type Culture Collection® (ATCC®). Any other cell lines used in this thesis were derived from these cell-lines. All cell lines were tested every 3 months for mycoplasma. Cells were used for screening between passage 15-25. mIMCD3 and RPE-1 mother cell-lines were previously verified using arrayCGH (266) and RNA-sequencing under different growth conditions. SRA references for RNA sequencing data:

- serum starved mIMCD3 cells: SRX1411364
- proliferating mIMCD3 cells: SRX1353143
- serum starved RPE-1 cells: SRX1411453
- proliferating RPE-1 cells: SRX1411451

This confirmed the presence of all RNAi machinery in both cell lines and allele numbers before CRISPR/Cas9 editing. Cells were not re-sequenced post CRISPR/Cas9 editing.

Table 2.2 Cell-Lines

Cell line species, origin and growth medium are listed. All cells were grown as standard in 10 % [v/v] FBS and serum starved at 0.2 % [v/v] FBS.

Cell-Line	***Catalogue No.***	***Species***	***Medium***	***Origin***
hTERT RPE-1	*CRL-4000™*	*Human*	*DMEM/F12*	*hTERT immortalised retinal pigment epithelial cells*
HEK293T	*CRL-11268™*	*Human*	*DMEM*	*Embryonic kidney cells containing the SV40-T antigen*
mIMCD3	*CRL-2123™*	*Mouse*	*DMEM/F12*	*Inner medullary collecting duct cells that are SV40 transformed*
*Phoenix-AMPHO **	*CRL-3213™*	*Human*	*DMEM*	*Modified HEK293T that stably express amphotropic envelope protein and gag-pol.*

2.1.6 Microbiology Reagents

- “α-Select Gold” DH5α Chemically Competent *E. coli* Cells (Bioline)
- Ampicillin sodium salt
- Kanamycin Sulphate (Fisher Scientific)
- Spectinomycin dihydrochloride (Fisher Scientific)
- 5-bromo-4-chloro-3-indolyl-βD-galactopyranoside (X-gal)
- Isopropyl β-D-1-thiogalactopyranoside (IPTG)

- QIAprep Spin Miniprep Kit (Qiagen)
- QIAfilter Plasmid Maxi Kit (Qiagen)

2.1.6.1 Luria-Bertani Medium (LB)

- 1 % [w/v] Tryptone (VWR Chemicals)
- 0.5 % [w/v] Yeast Extract
- 10 mM NaCl

Make up to 1 L in dH_2O. For LB Agar 15 g Agar-agar (Merck Millipore) was added. Autoclaved to sterilize before use. *supplied by

2.1.6.2 Super Optimal Broth with Catabolite Repression (SOC)

- 2 % [w/v] Tryptone (VWR Chemicals)
- 0.5 % [w/v] Yeast Extract
- 10 mM NaCl
- 2.5 mM KCl
- 10 mM $MgCl_2$
- 10 mM $MgSO_4$
- 20 mM Glucose

Make up to 1 L in dH_2O. Autoclaved to sterilize, aliquoted and stored at –20 °C. Defrosted at room temperature before use.

2.1.7 Antibodies and Stains

2.1.7.1 Primary Antibodies

Table 2.3 List of primary antibodies

List of all the primary antibodies used throughout this thesis and optimized dilutions used in immunofluorescence (IF) and immunoblotting on western blots (WB) are shown. All antibodies listed have species reactivity in both human and mouse samples. *CEP290 mouse monoclonal IgG2a (Clone IC3G10) was a gift from Ciaran Morrison, National University of Ireland Galway. **Living Colors® A.v. Monoclonal Antibody (JL-8). ***TMEM216 antibody as described in (267). ^CST = Cell Signalling Technologies.

Antigen	Clone No	Raised In	Vendor	Cat. #	Blocking Solution	Dilution
Acetylated α-Tubulin	6-11B-1	Mouse	Sigma	T6793-.5ML	Milk	IF 1:4000
ARL13B	N/A	Rabbit	Proteintech	17711-1-AP	Milk	IF 1:2000 WB 1:5000
β-Actin	AC-15	Mouse	Abcam	Ab6276	Milk	WB 1:10000
CEP290 *		Mouse	N/A	N/A	BSA	IF 1:1000 WB 1:200
FLAG	M2	Mouse	Simga	F3165	Milk	WB 1:1500
GAPDH	N/A	Rabbit	CST	2118	BSA	WB 1:5000
GFP **	JL-8	Mouse	Clontech	632380	Milk	WB 1:5000
γ-Tubulin	C-20	Goat	Santa Cruz	sc-7396	Milk	IF 1:50
γ-Tubulin	GTU-88	Mouse	Sigma	T6557	Milk	IF 1:1000
γ-Tubulin	N/A	Rabbit	Abcam	Ab137822	Milk	IF 1:1000
IFT88	N/A	Rabbit	Proteintech	13967-1-AP	Milk	IF 1:200 WB 1:1000
myosin light chain II	N/A	Rabbit	CST^	8505	BSA	IF 1:50
P-myosin light chain II (Ser19)	N/A	Rabbit	CST	3671	BSA	IF 1:50

PP-myosin light chain (Thr18,Ser19)	N/A	Rabbit	CST	3674	BSA	IF 1:50
Polyglutamylated Tubulin	GT335	Mouse	Sigma	T9822	Milk	IF 1:1000
ROCK1	N/A	Rabbit	CST	4035	Milk	WB 1:1000
ROCK2	N/A	Rabbit	Bethyl	A300-046A	Milk	WB 1:1000
RPGRIP1L	N/A	Rabbit	Proteintech	55160-1-AP	BSA	IF 1:500 WB 1:1000
TMEM67	N/A	Rabbit	Proteintech	13975-1-AP	Milk	WB 1:1000
TMEM216 ***	N/A	Rabbit	N/A ***	N/A	Milk	IF 1:100 WB 1:100
Vinculin	VIN-11-5	Mouse	Sigma	V4505	Milk	WB 1:5000

2.1.7.2 Secondary antibodies

Table 2.4 List of secondary antibodies

Table showing all the secondary antibodies used throughout this thesis. Table outlines the target, species raised in, conjugate and optimized dilutions used in in immunofluorescence (IF) and immunoblotting on western blots (WB). Anti-bodies could be used in either Milk or BSA blocking solutions, blocking solution would correlate to match that used during the primary antibody incubation.

Target	Raised in	Conjugate	Vendor	Cat. #	Dilution
Mouse IgG	Goat	Alexa Fluor® 488	Invitrogen	A1102	IF 1:2000
Mouse IgG	Goat	Alexa Fluor® 568	Invitrogen	A11031	IF 1:2000
Mouse IgG	Goat	Alexa Fluor® 647	Invitrogen	A28181	IF 1:2000
Mouse IgG	Goat	Horseradish Peroxidase (HRP)	Dako, Agilent Technologies	P0447	WB 1:10000
Mouse IgG	Donkey	Alexa Fluor® 555	Invitrogen	A31570	IF 1:2000

Rabbit IgG	Goat	Alexa Fluor® 488	Invitroge	A11034	IF 1:2000
Rabbit IgG	Goat	Alexa Fluor® 568	Invitrogen	A11036	IF 1:2000
Rabbit IgG	Goat	Horseradish Peroxidase (HRP)	Dako, Agilent Technologies	P0448	WB 1:10000
Rabbit IgG	Donkey	Alexa Fluor® 488	Invitrogen	A21206	IF 1:2000
Goat IgG	Donkey	Alexa Fluor® 633	Invitrogen	A21082	IF 1:2000
Goat IgG	Donkey	Alexa Fluor® 350	Invitrogen	A21081	IF 1:2000

2.1.7.3 Cell Stains

Table 2.5 List of cell stains

Cell stains with their excitation and emission values. Dilutions listed were used in immunofluorescence (IF) staining of coverslips and screen plates.

Name	Excitation /Emission	Sub-Cellular Localization	Vendor	Catalogue #	Dilution
DAPI	358/461	Nucleus/DNA	Invitrogen™	D1306	IF 1:1000
TOTO®-3 Iodide	642/660	Nucleus/ Nucleic Acids	Invitrogen™	T3604	IF 1:4000
Alexa Fluor™ 488 Phalloidin	495/518	Filamentous Actin (F-Actin)	Invitrogen™	A12379	IF 1:100

2.2 Methods

Room temperature (RT) refers to a variable temperature between 20-22 °C. The following abbreviations are used: hours (hrs), minutes (mins), seconds (s), relative centrifugal force (rcf), revolutions per minute (rpm).

Experimental replicates refers to repeats of experiments that were carried out using different reagents on different days (new vial of cells, freeze thaw or vial of reagents, new dilutions of chemical etc.), whereas technical replicates refers to repeats of experiments done at the same time on the same day, with the same reagents.

2.2.1 Polymerase Chain Reaction (PCR)

PCR reactions were made up of 1 µl of purified genomic DNA (20 ng/µl), 0.5 µl of forward and 0.5 µl of reverse primers (10 µM each) (Appendix A.2, Table A.8), 5 µl dNTPs (2.5 mM of each dNTP), 5 µl 10X DreamTaq Buffer, 0.2 µl DreamTaq DNA Polymerase, made up to 50 µl with dH_2O. PCR reactions were run at 95 °C for 1 min followed by 35 cycles of 95 °C (30 sec), primer optimised annealing temperature (30 sec), 72 °C (1 min) and then followed by a final extension of 5 mins at 72 °C. Completed reactions were held at 4 °C then analysed on a 1.5 % agarose [w/v] gel stained with Midori Green Advance which was run at 120 V for 1 hr in an electrophoresis tank with 1X TAE.

2.2.2 Reverse transcriptase-polymerase chain reaction

2.2.2.1 RNA extraction

RNA was extracted from up to $5x10^6$ cells using a Quick-RNA™ Miniprep Kit (Zymo Research). Cells were pelleted by centrifugation at 200 x rcf for 5 mins. Then resuspended in PBS and re-pelleted. The cell pelleted was resuspended in 300 µl of RNA lysis buffer, transferred to a Spin-Away™ Filter and centrifuged for 30 sec at 13000 x rcf. The flow through was mixed 1:1 (v:v) with 100 % ethanol, transferred to a Zymo-Spin™ IIICG Column and centrifuged for 30 sec at 13000 x rcf. RNA bound to the column was DNAse I treated for 15 mins and then washed with RNA prep and wash buffers before being eluted in 100 µl of DNase/RNase-Free Water. RNA concentration was then quanitified using a NanoDrop™ 3300 Fluorospectrometer (Thermo Scientific™).

2.2.2.2 Generating cDNA

1 µg of whole cell RNA extract was mixed with 1 µl of random hexamers (50 ng/µl), 1 µl of annealing buffer and made up to a total of 8 µl with nuclease free dH_2O. This was then incubated at 65 °C (5 mins) and then immediately placed on ice. 10 µl of 2X First Stand Reaction Mix and 2 µl SuperScript™ III/RNaseOUT™ Enzyme Mix where then added to the reaction. The reaction was vortexed and centrifuged to ensure it was well mixed before incubation at 25 °C (10 mins), followed by 50 °C (50 mins), and then 85 °C (5 mins). cDNA was then stored at -20 °C until use.

2.2.2.3 Reverse transcriptase-PCR

cDNA was diluted 1 in 10 with dH_20. Then PCR reactions were made up of 1 µl of diluted cDNA, 0.5 µl of forward and 0.5 µl of reverse primers (10 µM each) (Appendix A.2, Table A.9), 3 µl HotShot PCR master mix and 5 µl of dH_2O to make a 10 µl reaction. PCR reactions were run at 95 °C for 1 min followed by 50 cycles of 95 °C (30 sec), primer optimised annealing temperature (30 sec), 72 °C (1 min) and then followed by a final extension of 5 mins at 72 °C. Completed reactions were held at 4 °C then analysed on a 2 % agarose [w/v] gel stained with Midori Green Advance which was run at 120 V for 1 hr in an electrophoresis tank with 1X TAE.

Band intensities were to normalised to GAPDH controls to estimate the total mRNA expression level in each sample.

2.2.3 Enzymatic Clean-up of PCR Products

PCR products were purified using ExoSAP-IT® PCR Product Clean-up by following the manufacturer's recommended protocol to digest excess primer and dephosphorylate nucleotides to allow for downstream sequencing reactions.

2.2.4 Sanger Sequencing

Sequencing reactions were made up of 0.5 µl of BigDye Terminator Kit V3.1, 2 µl BigDye Sequencing Buffer (5X), 1 µl of purified PCR product or 250 ng of purified plasmid DNA, 1 µl of sequencing primer (final concentration 0.2 µM) made up to 10 µl in dH2O. Sequencing reactions were run at 96 °C (1 min) followed by 45 cycles of 96 °C (10 sec), 50 °C (5 sec), 60 °C (4 mins) and then held at 4 °C until precipitation. Sequencing reactions were transferred to a 96-well sequencing plate for precipitation. Reactions were precipitated by adding 1 µl of 0.25 M EDTA and 30 µl of 100 % ethanol to each reaction before being centrifuged at 2750 x rcf for 30 mins at 4 °C. Plates were inverted to remove the supernatant, then pellets were washed in 60 µl of 70 % [v/v] ethanol/dH_2O and centrifuged at 2750 x rcf for 15 mins at 4 °C. Plates were inverted onto tissue and centrifuged at 10 x rcf for 10 secs to remove residual EtOH. Pellets were left to dry at 37 °C for 5 mins before being re-suspended in 10 µl of deionised Hi-Di™ Formamide. Sequencing reactions were run on an ABI 3130xl Genetic

Analyzer and base-called using Sequencing Analysis Software 6 (Applied Biosystems).

2.2.5 T7 Endonuclease Mutation Assay

T7 endonuclease assay was used to identify CRISPR/Cas9 edited cell lines with heterozygous and compound heterozygous mutations in the targeted gene (Figure 2.1). The target gene was amplified by PCR and analysed as in Section 2.1.4.1. PCR products were then denatured at 95 °C and slowly reannealed by decreasing the temperature -2 °C/sec until 85 °C, then at a rate of -0.1 °C/sec until reaching 25 °C. 10 µl of reannealed PCR products were then incubated for 15 mins at 37 °C with; 1.5 µl of NEB Buffer 2 and 0.5 µl of T7 endonuclease (15 µl total reaction volume). Digested PCR products were then run on a gel to analyse the presence of mutations as T7 endonuclease cleaves hetero-duplex DNA.

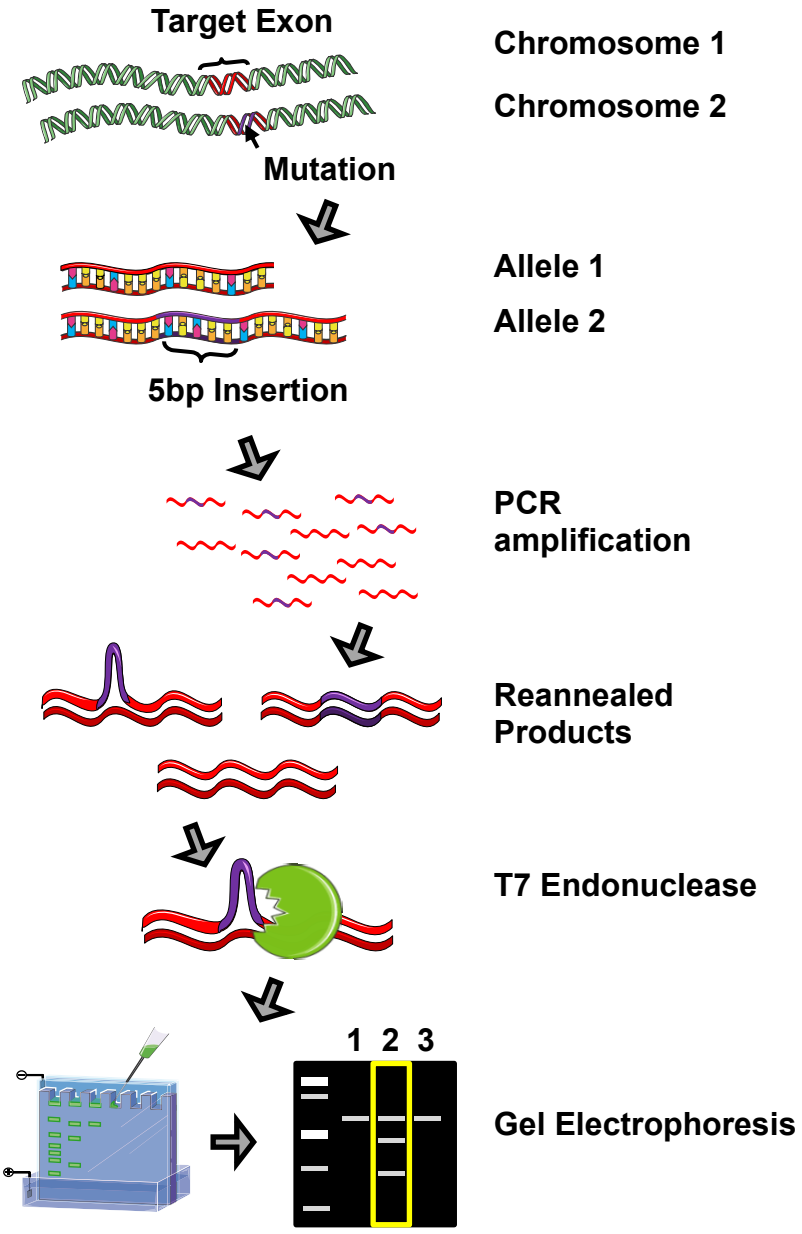

Figure 2.1 T7 Endonuclease assay to detect heterozygous mutations

Schematic of the T7 endonuclease assay. CRISPR/Cas9 targeted DNA is amplified by PCR. Any mutations present are likely to be heterozygous or compound heterozygous. This generates a mixed pool of PCR product. The PCR product is reannealed slowly to allow mismatch DNA (heteroduplexes) to form. T7 endonuclease recognises and cleaves these heteroduplexes which can then be resolved by gel electrophoresis. Therefore DNA digestion represents a mutation present in the targeted gene of that clone, as seen in lane 2 on the imaged gel.

2.2.6 Cloning

2.2.6.1 TA Cloning

Biallelic compound heterozygous mutations that could not be distinguished by initial exon sequencing were taken forward for TA Cloning to sequence each allele individually.

TOPO® TA Cloning® Kit was used following the manufacturer's recommended protocols to clone 4 µl of PCR product (approx. 20-50 ng) of the targeted exon into the pCR™ 2.1-TOPO® vector. After 30 mins reaction time, cloning reactions were transformed into 25 µl of DH5α chemically competent *E. coli* and plated onto kanamycin (50 µg/ml) LB Agar plates with 40 µl of 40 mg/ml X-gal and 40 µl of 100 mM IPTG. Blue/white screening was used to select colonies with successfully cloned vectors and inoculations of white colonies were cultured in 5 ml of LB-kanamycin (50µg/ml) for 16 hr overnight.

2.2.6.2 Gateway Cloning

Expression vectors for co-immunoprecipitation experiments were made using Gateway® technology. Following the manufacturer's protocol, 150 ng of pENTR clones, containing full-length coding sequences (CDS) of genes to be expressed, was mixed with 150 ng of pDEST vectors that contained different C-terminal and N-terminal tags. The plasmids were then made up to a total of 8 µl in TE Buffer, pH 8. 2 µl of the LR clonase was added to make a 10 µl reaction which was incubated at 25 °C for 1 hr. The reaction was stopped by adding 1 µl of 2 µg/µl proteinase K solution and was incubated for 10 mins at 37 °C. Cloning reactions were transformed and cultured as in section 2.2.6.1 but without blue/white selection.

pDONR plasmids were made from linearized pDEST clones as above, but using BP clonase.

2.2.6.3 Plasmid DNA extraction

Cloned vector DNA was extracted from 1 ml of each 5 ml culture using a QIAprep Spin Miniprep Kit (Qiagen) following the manufacturer's protocol. Once sequence verified, cultures were expanded to 200 ml and plasmid DNA was extracted with a QIAfilter Plasmid Maxi Kit (Qiagen) following the manufacturers

protocol and re-suspended in 300 µl of the provided Elution Buffer to make plasmid stocks. DNA yields were measured using a NanoDrop™ 3300 Fluorospectrometer (Thermo Scientific™).

2.2.7 Immunofluorescence Microscopy

$1x10^5$ cells were plated onto Matrigel Matrix coated 13 mm round sterile coverslips (No. 1.5; Scientific Laboratory Supplies) in a 12 well plate in DMEM/F12 0.2 % FBS. Cells were serum starved for 48 hr before fixing.

Immunostaining conditions including fixation, block and antibody concentrations were optimised for each antibody or stain individually (Table 2.3, Table 2.4, Table 2.5). Cells were fixed with chilled methanol (MeOH) for 5 mins at -20 °C or in 10 % formalin for 15 mins followed by 5 mins permeabilization with 0.05 % Triton X-100 in phosphate buffered saline (PBS). Coverslips were then blocked for 10 mins in 1 % [w/v] Marvel/PBS or 1 % [w/v] BSA/PBS. Coverslips were incubated with primary antibodies (diluted in 1 % [w/v] Marvel/PBS, or 1 % [w/v] BSA/TBS) in a humidified chamber for 1 hr, washed 3 times in 1X PBS and then incubated in secondary antibodies and cell stains diluted in 1 % [w/v] Marvel/PBS for 1 hr in a humidified chamber. Coverslips were then washed 5 times with PBS and mounted onto glass slides with ProLong™ Gold Antifade Mountant (Invitrogen™). Slides were left to cure overnight at RT. Slides were then stored in the dark at 4 °C and imaged within 1 week.

2.2.7.1 Confocal Microscopy

Confocal images were captured as manually acquired z-stacks of the same size using a Nikon A1R Confocal Laser Scanning Microscope, controlled by the NIS-Elements C software. Image acquisition was optimised on wild-type negative control cells for each experiment. The same laser intensity and image gain settings were maintained when imaging each set of experimental coverslips, to ensure fluorescence intensity was comparable between cell lines or conditions. All fields of view (FOV) were chosen at random or based on DAPI staining alone to avoid bias that could occur from observing staining of ciliary proteins. Single planes and z-stacks were captured using a 63X oil objective as 1024x1024 pixel images.

2.2.7.2 Analysis of Immunofluorescence images

Summative and maximum intensity projections, 3D reconstructions, and merged images of z-stacks were reconstructed in FIJI image software or Columbus™ software

2.2.7.2.1 Cilia length and incidence

Confocal images were analysed for cilia length and incidence using FIJI image software (268). Regions of interest (ROI), the cilia, were then either manually highlighted or automatically detected using a macro (Appendix B). ROIs were analysed for quantitative measurements of total number of ROIs, cilia length, and measures of total fluorescence. Nuclei number were also counted so that cilia incidence could be calculated as a percentage of total cell number per FOV. This was also done by either manual counting or was integrated into the same macro as above for automated counting.

2.2.7.2.2 3D reconstruction

3D analysis was done using the “3D Object Counter” v2.0 plugin (269). Images were thresholded and rendered as individual 3D ROI to allow all dimensions to be quantified including cilia volume as used in Chapter 5.

2.2.7.2.3 Co-localisation

Regions of interest (ROI) where then either manually highlighted or thresholded for using the mask function throughout a stack on using the “3D Object Counter” v2.0 plugin (269). 3D ROI regions only were then analysed for co-localisation between two channels using the “Coloc 2” plugin (270) using Costes statistical significance test, PSF 3.0 for 10 iterations. Other images were loaded into Columbus™ software and were analysed using the co-localisation building block from Perkin Elmer to specifically analyse co-localisation in ciliary ROIs (Defined “spots”). Both methods presented data using Pearson's correlation.

2.2.7.2.4 Image Structure

High-throughput images of MLC and phosphorylated MLC staining were analysed in 2D using Columbus™ software. Cell boundaries were defined and image texture was measured specifically within these boundaries excluding the

nucleus. Image texture was calculated using the “Calculate Texture Properties” building block. The method applied a Gabor Filter at a scale of 2 pixels, wavelength 8 and normalisation was calculated by region intensity. Texture values were then multiplied by 1000 for ease of interpretation when graphically displayed.

2.2.8 Whole Cell Protein Extraction

Cells were grown to confluence in a single well of a 6-well plate, with or without siRNA knock-down, plasmid over-expression or drug treatment, then washed 3 times in cold PBS. Cells were re-suspended in 50 µl of lysis buffer for western blotting (Section 2.1.3.1) using a cell scraper and pipette mixing. The lysed suspension was then added to an chilled 1.5 ml microfuge tube and underwent a freeze-thaw cycle at -80 °C. The lysis suspension was then clarified by centrifugation at 12000 x rcf for 15 mins at 4 °C. The supernatant was then transferred into a new ice-cold microfuge tube and the pellet discarded.

Protein concentrations of whole cell extracts (WCE) were measured using Quick Start™ Bradford Protein Assay. 2 µl of WCE or 1 µl of BSA standards (0.5, 1, 5, 7.5, 10, 1 5µg/µl) were added to 1 ml of 1X Dye Reagent in microfuge tubes and vortexed. Samples were incubated for 5 mins at RT, transferred to cuvettes and absorbance of standards and samples was read at 595 nm in a spectrophotometer. Sample absorbance was then compared to the BSA standard curve and divided by 2 to give the WCE protein concentration in µg/µl.

2.2.9 SDS PAGE and Western Blotting

15 µg of diluted WCE was mixed with LDS Sample Buffer (4X), freshly prepared with 2.5 % [v/w] β-mercaptoethanol, to final 1X concentration. Samples were loaded in separate wells alongside one lane containing 15 µl of Precision Plus Protein™ Standards ladder into 4-12 % Bis-Tris gels and run at 120 V for 90mins in MES SDS Running Buffer containing 15 % methanol.

Proteins were then transferred from the gel to an PVDF membrane that had been activated for 20 sec in 100 % MeOH. The transfer was run at 30 V for 90 mins in 1X Transfer Buffer (10 % MeOH) in an electrophoresis tank packed with ice. After transfer, membranes were blocked in 10 % [w/v] blocking solution

(blocking solution was optimised for each antibody individually, either Marvel or BSA was diluted in PBST or TBST) for 30 mins at RT. Primary antibodies were diluted in 5 % [w/v] blocking solution and incubated with the membrane in a falcon tube on a rolling shaker for 1 hr at RT or overnight at 4 °C.

Membranes were washed 6 times in PBST or TBST for 2 mins before being incubated in secondary antibody (in 5 % [w/v] blocking solution) for 1 hr at RT. Membranes were washed 6 times in PBST or TBST for 3 mins. Femto Maximum Sensitivity Substrate (Diluted Luminol/Enhancer:Stable Peroxide Buffer 1:1) was added to membranes and used for visualizing immuno-stained proteins. Blots were imaging using a ChemiDoc™ MP Imaging System (BIO-RAD) and exposure time was optimised for each blot individually. If membranes required re-blotting, they were either cut to remove the region of the membrane that had already been probed or chemically stripped for 10mins in Restore™ PLUS Western Blot Stripping Buffer and then washed in before blocking and re-staining.

Bands were identified and when required protein levels were quantified to a control reference band using Image Lab software (Version 5.2.1 Build 11) (BIO-RAD). Protein measurements were then normalised to the loading control quantifications.

2.2.10 Co-immunoprecipitation

WCE were prepared as in section 2.2.8. Immunoprecipitation of GFP-fusion-proteins was done using GFP-TRAP magnetic beads (ChromoTek). 1 µg of each WCE was diluted to a final volume of 500 µl with Dilution Buffer. Per immunoprecipitation, 20 µl of GFP-Trap® magnetic bead slurry was equilibrated in ice-cold 500 µl dilution buffer, magnetically separated and washed a further 2 times in 500 µl ice-cold dilution buffer. Diluted cell lysate was added to equilibrated beads and incubated for 2 hr 4 °C on a rotating shaker.

Supernatant was cleared by magnetically separating the beads and was then discarded. The beads were washed three times with 500 µl of ice-cold wash buffer. The beads were re-suspended in 50 µl 4X LDS Sample buffer (2.5 % β-mercaptoethanol) and boiled 10 mins at 95 °C. The beads were then

magnetically separated and 20 µl of supernatant was analysed by SDS-PAGE as described in section 2.2.9.

2.2.11 Cell Culture

Wild-type hTERT RPE-1 and mIMCD3 cultures, including all derived cell lines, were grown in DMEM/F12 – GlutaMAX™ with 10 % Foetal Bovine Serum (FBS). HEK293T cells were grown in DMEM with 10 % FBS. Cells were cultured under standard conditions (37 °C, 5 % CO_2) and passaged twice a week at a 1:12 ratio.

2.2.12 Fluorescent Activated Cell Sorting (FACS)

Cells expressing GFP from a transient transfection or stable viral transduction were grown to confluence in a T25 flask. Cells were washed in PBS and trypsinised in 0.05 % Trypsin/PBS for 5 mins, or until a single cell suspension was reached. Cells were re-suspended in DMEM F12 10 % FBS and spun at 200 x rcf for 5 mins. The supernatant was discarded and the cells were suspended in 1 ml of FACS buffer (Section 2.1.3.6).

2.2.12.1 Cell Counts

10µl of cell suspension was added to 10 µl of 0.4 % Trypan Blue Stain and transferred to a Countess® Cell Counting Chamber Slides for cell counts and viability. The cell suspension was then passed through a 70 µm filter into an FBS coated polypropylene 5 ml sterile FACS tube. Cells were then stored on ice before sorting.

2.2.12.2 FACS

A single cell index sort was used to isolate single GFP-expressing cells. Cell sorts were gated to removed doublets, debris and to select for the top 10 % of GFP expressing cells. Sorting was done on an Influx 6 Way Digital Fluorescence Activated Cell Sorter (BD Biosciences) by staff of the St James's Campus Infrastructure and Facilities (SCIF**)** into 100 µl of FACS Collection Media (DMEM F12, 50 % Conditioned Media, 20 % FBS, 1 % penicillin/streptomycin)**.** Plates containing single cells were then left between 2-3 weeks to clonal growth and to establish cell lines.

2.2.13 Generation of RPE-1 Derived Cell-Lines

2.2.13.1 CRISPR/Cas9 Genome Editing

All CRISPR/Cas9 edited cells used in this project were generated before the start date of this project by myself in my role as a Research Assistant.

gRNAs were designed using an online tool CRISPR Design provided by the Zhang Lab, MIT 2015 (No longer available) to the first coding exon of targeted genes (Appendix C, Table C.1). The highest ranked guide sequence, with added overhangs for cloning, were bought as forward and reverse HPLC-purified oligos from Sigma-Aldrich. Oligos were annealed and subsequently cloned into the pX458 CRISPR/Cas9 expression vector using the *Bbs*I restriction site and enzymatic ligation assisted by nucleases (ELAN) technique (271).

2.5 µg of cloned vectors were forward transfected into $1x10^6$ hTERT RPE-1 cells with 7.5 µl of Lipofectamine 2000 (Invitrogen™) following the manufacturer's protocol. Transfected single cells were sorted by FACS into 96-well plates 24 hrs post-transfection (as in section 2.2.12). Single cell colonies were cultured to confluence and the CRISPR targeted region, in genomic DNA extracted from colonies, was amplified by PCR (Section 2.2.1) and sequenced (Section 2.2.3 and 2.2.4) for analysis.

2.2.13.2 Viral Transduction for stably expressing cell lines

2.2.13.2.1 Lentiviral Transduction

LifeAct-GFP Lentiviral particles were made by Dr. Chiara Gallioni using 2nd generation lentiviral protocols. HEK293T cells were transfected with LifeAct-GFP lentiviral vector, pMD2.G (VSV-G envelope expressing plasmid, a gift from Didier Trono; Addgene plasmid # 12259) and psPAX2 (packaging plasmid, a gift from Didier Trono; Addgene plasmid # 12260). Media was changed after 24 hrs and DMEM 10 % FBS was added. A further 48 hrs post transfection the viral supernatant was collected and filtered through a 0.22 µm filter, then stored at -80 °C in aliquots until use.

RPE-1 cells were grown to 50 % confluency in a T75 flask. 8 µg/ml of polybrene was added to 3 ml of lentiviral supernatant (viral particles in DMEM Media 10 %

FBS) to make a transduction mix. The cells were washed in PBS and 3 ml of transduction mix was added drop wise to cells, then left to incubate overnight. 16 hrs later the cells were washed in PBS and 12 ml of fresh DMEM F12, 10 % FBS media was added. The cells were left to grow and passaged 3 times as in section 2.2.11. before running though FACS selection (as in section 2.2.12) to establish a clonal cell line.

2.2.13.2.2 Retroviral Transduction

Retroviral particles of pBABE GFP-ROCK2-ER (Ximbio #152723), pBABE GFP-ROCK2.KD-ER (Ximbio #152724), pBABE GFP-ER (Ximbio #152725) (Gifts from Prof. Mike Olson, University of Glasgow), were made by transfecting 12 µg of pBABE plasmids into Phoenix Ampho cells at 50 % confluence in a T75 flask. 24 hrs post transfection media was changed for fresh DMEM 10% FBS. 48 hs post transfection retroviral particles were collected and filtered through a 0.45 µm filter. 1 ml aliquots of virus were stored at -80 °C until use.

RPE-1 cells were transduced with retrovirus us described above in section 2.2.13.1.

2.2.14 siRNA knock-down

All knock-downs were performed with SMARTpool: ON-TARGETplus siRNAs (Dharmacon) (Appendix A.1) and were species specific. Cells plated for whole cell extracts were plated in 6-well plates and reverse transfected with 5µl of 20 µM siRNA and 3 µl of Lipofectamine® RNAiMAX. Cells plated for immunofluorescence microscopy were plated in 12-well plates on coverslips and transfected with 2.5 µl of 20 µM siRNA and 1.5 µl of Lipofectamine® RNAiMAX.

RPE-1 or mIMCD3 cells were trypsinised and re-suspended in DMEMF12, 0.2 % FBS. Cells were counted as in 2.2.12.1 and diluted to a final concentration of $1x10^5$ cells/ml. siRNA and Lipofectamine® RNAiMAX was added separately to 250 µl of Opti-MEM, reagents were incubated for 5 mins at RT before combining and incubating for a further 20 mins at RT. After the incubation transfection regents were added to each well of the culture plate the diluted cell suspension was added on top of the regents to give final cell counts of $2x10^5$

cells/well in 6-well plates and $1x10^5$ cells/well in 12-well plates. Cells were then incubated for 72 hrs before being used to prepare WCEs or for immunofluorescence microscopy.

2.2.15 Inhibitor Treatment of RPE-1 Cells

2.2.15.1 Chemical Inhibitors

Table 2.6 List of chemical inhibitors

Chemical inhibitors and their molecular targets. All chemicals were tested in dose response curves to show their effects on ciliogenesis and so an optimised concentration is not listed. All the chemicals listed were stored at stock concentrations in DMSO.

Inhibitor	Target	Conc. (μM)	Treatment Time	Vendor	Catalogue #
KD025	ROCK2 Kinase domain	0-5	48hrs	Cayman Chemical	17055
Cytochalasin D	(+) end of microfilaments, inhibiting F-Actin polymerisation	0-1	16hrs	Sigma-Aldrich	C8273
Blebbistatin	Myosin ATPase activity	0-10	16hrs	Calbiochem	203390

Different components of the ROCK2 actin regulation pathway were targeted with specific inhibitors listed in Table 2.6. RPE-1 or mIMCD3 cells were plated in DMEM F12 ,10 % FBS for either confocal microscopy ($1x10^5$ cells per well in a 12-well plate, on coverslips) or for high-throughput staining ($2x10^3$ RPE-1 cells or $1.6x10^3$ mIMCD3 cells per well in a 96-well plate). After the cells had settled and fully adhered the media was changed to DMEM F12, 0.2 % FBS with varying concentrations of each inhibitor or DMSO for a dose response curve. Cells were incubated in each inhibitor for varying lengths of time to determine the time frame of action of each inhibitor. For longer treatments the media and inhibitor was changed every 24 hrs. After treatment, cells were prepared for imaging as in section 2.2.7.

2.2.16 siRNA Screening

2.2.16.1 Primary genome screen filtering to generate datasets

The primary whole genome dataset was downloaded as an Microsoft Excel file from https://doi.org/10.1038/ncb3201, Supplementary Table 1. Excel filtering of z-scores was used to determine hits based on phenotype quantifications. siRNA sequences were provided by Dharmacon and then transcript specificity was tested using Basic Local Alignment Search Tool (BLAST).

2.2.16.1.1 Enrichment Analysis

Enrichment analysis was carried out using STRING online analysis tool (272) (https://string-db.org/). Hit lists were copied into the multiple proteins tool and interaction maps were then analysed. Enrichment of pathways, domains, protein function or biological processes within the hit list was analysed by comparing to the whole genome. Gene ontology (GO) terms, Kyoto Encyclopedia of genes and genomes (KEGG) pathways, and UniProt key words were then used to interpret the types of enrichment that were present in the hit lists. Enrichment and false discovery rate was calculated as described in Franceschini *et al*., 2013 (273).

2.2.16.2 Screen plates

Screens used 1 µM SMARTpool: ON-TARGETplus siRNAs for hTERT RPE-1, and derived, cell lines and 2µM SMARTpool: ON-TARGETplus siRNAs for mIMCD3 screens (Appendix A.1).

Plates in the second combinatorial screen were coated with Matrigel® Matrix basement membrane to minimise cell loss during washing steps, as seen in the first combinatorial screen, thus reducing plate-to-plate variation. 43.5 µl of Matrigel® (11.5 mg/ml) was defrosted on ice and diluted in 5ml of ice-cold Opti-MEM™ (final concentration 100 µg/ml). 50 µl of diluted Matrigel® was added to each well of the 96-well ViewPlate and incubated for 1 hr at RT in aseptic conditions. Wells were then washed twice in 100 µl of 37 °C Opti-MEM™. Any effect that the Matrigel® has on cilia incidence would be controlled for in the screen as each cell line was normalised to its own negative controls and compared only to the wild-type cells in that technical replicate.

2.2.16.3 siRNA transfection in 96-well plates

Confluent T75 flasks of cells were washed in PBS and then incubated in 1 ml of 0.05 % Trypsin at 37 °C for 5 mins. 5 ml of DMEM-F12 10 % FBS was added to the flask to re-suspend the trypsinized cells. The cell suspension was then transferred to a 15 ml Falcon tube and spun in a bench top centrifuge at 250 x rcf for 5 mins. The supernatant was discarded and cells were re-suspended in 3 ml Opti-MEM™.

5 µl of 1 µM (hTERT RPE-1 screens) or 2.5 µl of 2 µM (mIMCD3 screens) SMARTpool: ON-TARGETplus siRNA was added to each well of the 96-well ViewPlate. Negative control wells contained an equivalent volume of or 1X siRNA Buffer (Dharmacon™) A master mix was made of n+2 (number of wells) of 0.2 µl of Lipofectamine® RNAiMAX and 14.8 µl (hTERT RPE-1 Screens) or 17.3 µl (mIMCD3 Screens) of Opti-MEM™ per well and incubated for 5 mins at RT. Transfection reagent master mix was then added to each well on the 96-well plate. Plates were gently mixed on a rotary shaker for 5 mins before a further 20-60 mins incubation at RT (incubation time was consistent within individual biological replicates but may have varied between biological replicates).

Cell counts were analysed as in section 2.2.12.1 using the Countess®. Cell suspensions were then diluted to final concentration $2x10^5$ cells/ml (hTERT RPE-1 Screens) or $1x10^5$ cells/ml (mIMCD3 Screens) in Opti-MEM™. 80 µl of each diluted cell suspension was added to each well according to associated plate maps (Appendix D) to give final cell counts per well of 16000 cells/well (hTERT RPE-1 Screens) and 8000 cells/well (mIMCD3 Screens). Only mIMCD3 cells were plated using a XRD-384 Automated Reagent Dispenser (FluidX™ Ltd), hTERT RPE-1 cells and derived cell lines were manually plated using a multichannel pipette. Plates were then left for 1 hr at RT in aseptic conditions to allow cells to settle before incubation at 37 °C for 72 hrs, minimising edge effects and ensuring an even distribution of cells across each well.

2.2.16.4 Immunostaining of 96-well plates

72 hr post transfection plates were inverted to remove media and wells were washed for 10 mins in 100 µl PBS supplemented with $CaCl_2$ (0.49 mM) and

$MgCl_2$ (0.9 mM). Plates that were to be immune-stained with anti-acetylated alpha tubulin were incubated on ice for 30 mins prior to washing with PBS. Plates were inverted to remove PBS and blotted on tissue to remove excess and placed on blue ice blocks. 50 µl of chilled methanol was added to each well and plates were incubated at -20 °C for 5 mins followed by a 50 µl wash in PBS. Cells were then blocked with 50 µl of milk blocking solution (1 % w/v in PBS) for 5mins before primary antibody incubation.

All antibodies were diluted (section 2.1.7) in 1 % [w/v] in milk/PBS and spun at 13000 x rcf for 5 mins before use. Blocking solution was removed and 50 µl of primary antibody dilution was added to each well. Plates were incubated for 90 mins on an orbital shaker at 12 rpm. Wells were washed 3 times in PBS before being incubated in 50 µl of secondary antibody for 90 mins on an orbital shaker at 12 rpm. Wells were washed a further 6 times in PBS before being stored in 100 µl of PBS at 4 °C until imaging.

2.2.16.5 High-throughput imaging of screen plates

Plates were warmed to RT before imaging. Six fields of view were captured using an Operetta® High Content Imaging System and Harmony® software (Perkin Elmer) for each well. Image acquisition was optimised on wild-type negative controls. FOV were set in same pattern across every well (avoiding the centre of the well) for every plate that was imaged. All images were taken using a 20X air objective.

2.2.17 Analysis of Screen Plates

All screens were performed in triplicate (3 experimental replicates – the same cell lines but the whole experiment was repeated on separate days, stained with fresh dilutions etc.) which is standard for siRNA screening (274). Furthermore, hits must always be verified with downstream validation after screening conditions as high-throughput conditions may not be optimal for each siRNA/knock-down.

Combinatorial screens were also carried out with two technical replicates for each experimental replicate. Although three experimental replicates were performed for the combinatorial screen, loss of cells in some conditions meant

that data could only be collected for two experimental replicates. This was considered sufficient for a proof of concept screen. The combinatorial screen also contained some internal biological replicates as some CRISPR/Cas9 edited cell lines had mutations in the same genes.

2.2.17.1 Columbus Image Analysis

Image data was imported into Columbus™ Image Data Storage and Analysis System for high-throughput analysis. Recognition protocols were written with the provided software building blocks (Appendix E). Recognition protocols were optimised on wild-type negative controls to recognise nuclei, cytoplasm and cilia (Figure 2.2).

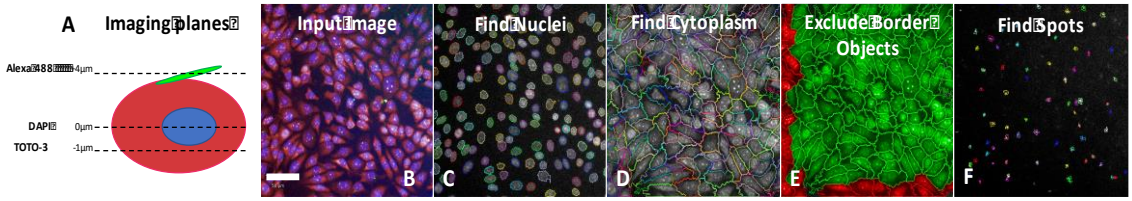

Figure 2.2 High-throughput Operetta Imaging and Columbus™ Recognition Protocol

Cells were imaged in 3 channels, each channel imaging at the optimal focal plane. B) Images were imported from Harmony® software to Columbus™ software C) 'Find nuclei' protocol recognition block was used in the DAPI channel to define nuclei. D) The cell body was defined using 'Find cytoplasm' by recognising TOTO-3 staining. E) Cells that were not completely within the field of view were removed from the analysis. F) 'Find spots' protocol was optimised to detect the maximum number of cilia without including background staining. Spot recognition was optimised based on spot radius, contrast, uncorrected spot to region intensity, distance between 2 spots and the spot peak radius. Spots were detected by ALR13B staining in the 488 nm channel. The population of cells with a single spot is then calculated from the calculated data and used to represent ciliary incidence. Cells with 2 or more spots were also calculated for comparison. Scale bar = 50 µM

Cell counts, ciliary incidence, cilia spot size and cilia spot intensity were then calculated as an average across all 6 FOV per well.

2.2.17.2 Preliminary Analysis

Heat maps of cell number are assessed for seeding errors or for loss of cells during washing steps. Any wells with >50 % cell loss were excluded from the

analysis as these outliers skewed the data. Further qualitative analysis removed data points based on the quality of immunostaining and image focus for each well (Figure 2.3).

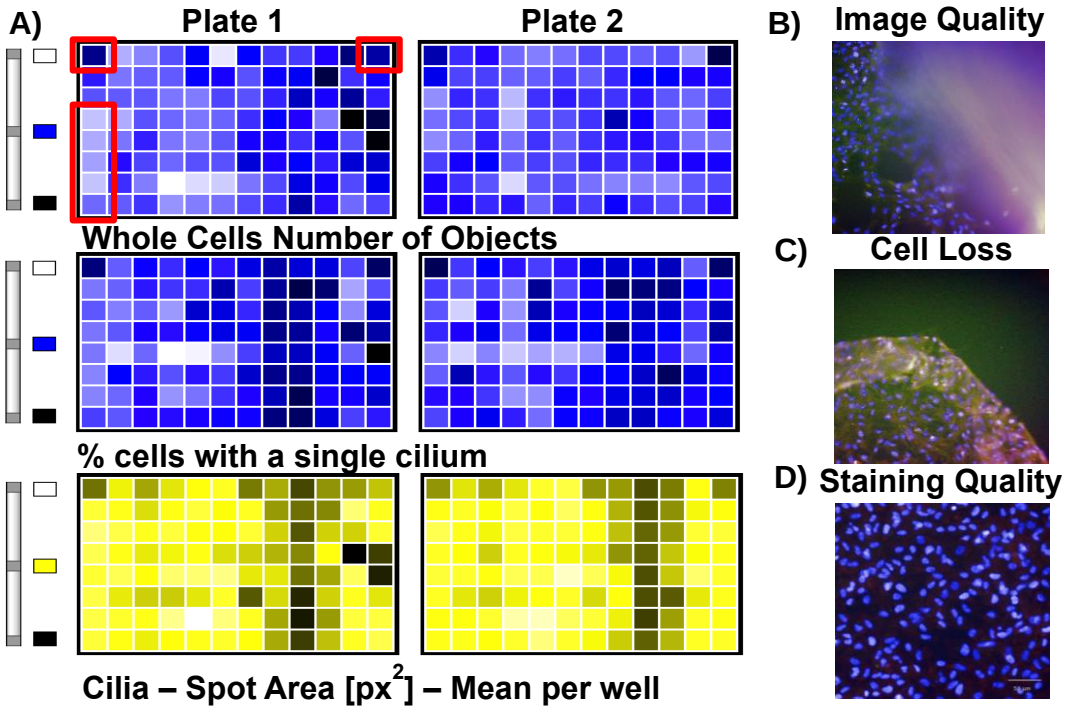

Figure 2.3 Qualitative assessment of combinatorial screen plates

A) Example heat maps shows a series of 5 control wells (highlighted in red rectangle) that have very high cell number compared to the corresponding controls in plate 2 or column 12. These wells were then examined for seeding errors or processing errors. si*Plk1* controls are also highlighted for cell number (red boxes) as these should have a very low cell number, the medium blue colour suggests a low transfection efficiency and would result in the entire plate being removed from analysis. **B)** Field of view (FOV) taken from a combinatorial screen plate that shows cell loss in a well. The high-throughput washing protocol caused lifting of the monolayer of cells. Lifted cells would then be aspirated and lost before imaging. **C)** Imaging artefact or possible piece of dust that is obscuring the FOV. **D)** Staining for cytoplasm with TOTO-3 failed and so cell boundaries could not be set by the automated recognition protocol. For any well if more than 50 % of cells were lost due to washing or unable to be analysed this well was excluded from the analysis to prevent outliers

Finalised data sets were then assessed for reproducibility between technical replicates by calculating the coefficient of determination (R^2), plates with R^2 >0.5 were considered reproducible. Positive and negative controls in each plate were then tested to be significantly different using a z-score comparison. If

calculated means of positive and negative controls were more than 1.5 standard deviations apart, then the plate was taken forward for full analysis.

2.2.17.3 Statistical Analysis

Wells that did not pass preliminary analysis were excluded from further analyses and robust z-scores were calculated from the remaining data. Robust z-scores were used in place of a standard z-score as this statistical normalisation takes into account experimental variation. The robust z-score represents the number of median absolute deviations data point x is away from the median of the negative controls.

$$\text{Robust } Z = \frac{x - m}{\mathcal{M}}$$

Where m = median values of the measured phenotype of the negative controls

M= median absolute deviation of the measured phenotype of the negative controls

And therefore on a normal distribution curve, of data point x compared to the negative controls

$-1.96 \geq Robust\ Z\ of\ x \leq +1.96$ is equivalent to $p = 0.05$

2.2.17.3.1 Secondary siRNA screens

Negative controls were pooled, (siScrambled pooled with RNAiMax transfection reagent only wells). These pooled negative controls were used to calculate robust z-scores for each quantified phenotype within each biological replicate of the screen. Transfection control (si*Plk1*) and ciliary controls (si*Ift88* and si*Rpgrip1l*) were then confirmed to be significantly different from negative controls on each screen plate (robust z-scores ≤ -1.96). Once each plate was validated for analysis, average robust z-scores were for experimental wells were calculated (n=2). Average robust z-scores for 3 phenotypes were assessed: cell number (z_{cell}), cilia incidence (z_{cilia}) and percentage of cells with 2 or more cilia ($z_{2MCilia}$). Hits were then filtered based on robust z-score values to identify validated hits.

2.2.17.2 Combinatorial screens

Robust z-scores were calculated for each cell line within in biological replicate of a screen and averaged across 2 technical replicates. The mean robust z-score across all biological replicates (n=3, n=2 for some conditions) was then calculated with standard error of the mean and presented graphically for analysis. The average robust z-score provides evidence the knock-down causes a significant change in phenotype compared to the negative controls in that cell line alone. The difference between two z-scores (ΔZ) was used to assess the type of genetic interactions inferred from the screens. The ΔZ then provides evidence that the change seen is significantly different to the knock-down of gene *x* in the wild-type mother cell line.

$$\Delta Z = Z_x - Z_{xy}$$

WhereZ_x= Robust Z of wild-type RPE-1 that has been treated with an siRNA against gene x

Z_{xy} = Robust Z of a cell line, with mutation in gene y that has been treated with an siRNA against gene x

The synthetic genetic interactions inferred from the screen were defined as:

Additive = $-1.96 \geq Robust\ Z \geq 1.96$ and $1.96 \geq \Delta Z \geq -1.96$.

Synergistic = $-1.96 \geq Robust\ Z \geq 1.96$ and $\Delta Z \leq -1.96$

Antagonistic = $-1.96 \geq Robust\ Z \geq 1.96$ and $\Delta Z \geq 1.96$.

2.2.17.4 Prioritising hits for validation

In all screens, only the strongest hits were taken forward for further validation. This was partially due to the time constraints of investigating each hit individually. Many hits were instantly discounted for follow up investigation due to a lack of validated reagents. Specific literature searching to find a potential ciliogenesis role would introduce a bias into the screening system, therefore just the top hits/interactions from each screen were taken forward and all literature searching was used to further justify each hit during validation and help develop a hypothesis for their role in ciliogenesis.

Chapter 3

Results: ROCK2 regulates ciliogenesis in RPE-1 cells through actin remodelling and acto-myosin contractions

3.1 Introduction

A whole genome, cell-based, high-content small interfering RNA (siRNA) screen and secondary validation screens were performed in ciliated cell lines to identify potential new ciliopathy genes and functional modules associated with ciliogenesis (266). The screens measured cilia incidence, cilia intensity and nuclear morphology, taking forward hits that reduced cilia incidence for further validation (Figure 3.1A). Primary morphological and numerical data from the whole genome screen allowed 4 further hit lists for different phenotypes to be identified. The 3 hit lists included genes that: **(i)** increased cilia incidence; **(ii)** increased the percentage of cells with 2 or more cilia; and **(iii)** significantly changed average cilia staining intensity (Figure 3.1B).

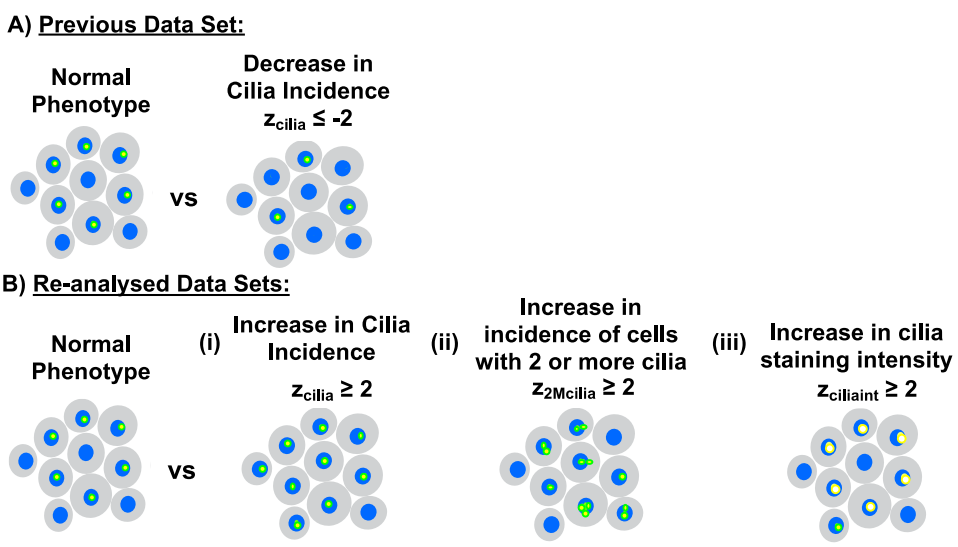

Figure 3.1 Quantifiable phenotypes that can be analysed from the whole genome screen data set

Schematic diagram comparing the phenotypes assessed in the original whole genome screen **(A)** and then subsequent phenotypes that could be analysed from the quantified data. **(B)** Cilia counts could be used to identify hits that increase cilia incidence or increase the percentage of cells with more than one cilium. Spot intensity measurements were also used as a proxy measurement of cilia length. Cell counts with associated cilia counts could identify possible cell cycle controls that decrease cell number and cilia number.

These hit lists provided candidate gene lists for secondary screening to identify components implicated in ciliary structure and function, the regulation of ciliogenesis, or links between ciliogenesis and the cell cycle. By repurposing the whole genome screen data in this way, there was potential to identify novel pathways and genes that contributed to the molecular control of cilia, without the bias inherent when selecting specific libraries or gene subsets.

The majority of the research that seeks to understand ciliary biology and the molecular pathology of ciliopathies has focused on patient mutations and experimental gene disruption that ablates, or impairs ciliogenesis. Positive regulators of ciliogenesis such as transition zone (TZ) or intraflagellar transport proteins (IFT), which cause ciliopathies such as Joubert Syndrome or skeletal dysplasias, have therefore been the research area for many groups because mutations in these genes cause ciliary loss. However, few recent studies have noted the importance of identifying mechanisms or pathways that increase ciliogenesis through functional loss of negative regulators as these could present potential therapeutic targets for ciliopathies (96, 260, 275). Across ciliary research generally a growing number of cellular pathways have been shown to contribute to the complex maintenance and regulation of ciliogenesis and disassembly, including the ubiquitin-proteasome (276) and actin remodelling systems (Reviewed in (54, 277, 278)). Thus, an unbiased approach using siRNA screening could identify novel genes and pathways that contribute to the molecular control and maintenance of cilia formation.

3.1.1 Chapter Aims and Objectives

Aim: To improve ciliopathy patient quality of life through greater understanding of their genetic disease and though identifying potential therapeutic pathways. Specifically, this chapter aims to identify novel negative regulatory pathways of ciliogenesis as these have the potential to be therapeutic targets in ciliopathies.

Hypothesis: Ciliogenesis and the cell cycle are intrinsically linked in both timing and role in progression of a cell towards division. If the cell cycle has several positive and negative regulatory pathways for the timely and precise progression though each stage of the cycle, which have been well defined, ciliogenesis would also require strict positive and negative regulatory pathways.

Most research has highlighted positive regulatory pathways in ciliogenesis, therefore there are key negative regulators that are still to be identified.

Experimental Objectives:

- To generate a data set from existing whole genome reverse genetic screening data of potential hits that increase cilia incidence
- To carry out secondary screening to validate hits and identify candidates to take forward for further investigation
- Further validation of hits in human cell line models
- Elucidate the mechanistic links between validated hits and regulation of ciliogenesis

3.2 Primary whole genome siRNA screen hits that increase cilia incidence

Three stringent filtering steps were used to identify hits that increased cilia incidence from the whole genome data set (Figure 3.2). Firstly, the data set was filtered to identify hits that reproducibly increased cilia incidence: in other words, the siRNA knockdown had a z_{cilia} score ≥ 1.96 in both biological replicates of the screen.

The second filter was used to remove any hits that significantly increased or decreased cell number ($-1.96 < z_{cell} < 1.96$). The final filtering step controlled for siRNA quality by removing siRNA pools that has published off-target effects. Enrichment analysis showed that the final hit list was significantly enriched for genes associated with “Intracellular non-membrane bound organelle” (GO: 0043232 Cellular Component) (Table 3.1). This Gene Ontology (GO) term is defined as: “Organized structure of distinctive morphology and function, not bounded by a lipid bilayer membrane and occurring within the cell. Includes ribosomes, the cytoskeleton and chromosomes” (279). However the 83 hits did not highlight any obvious pathways or gene networks in a STRING analysis (Figure 3.3) (280).

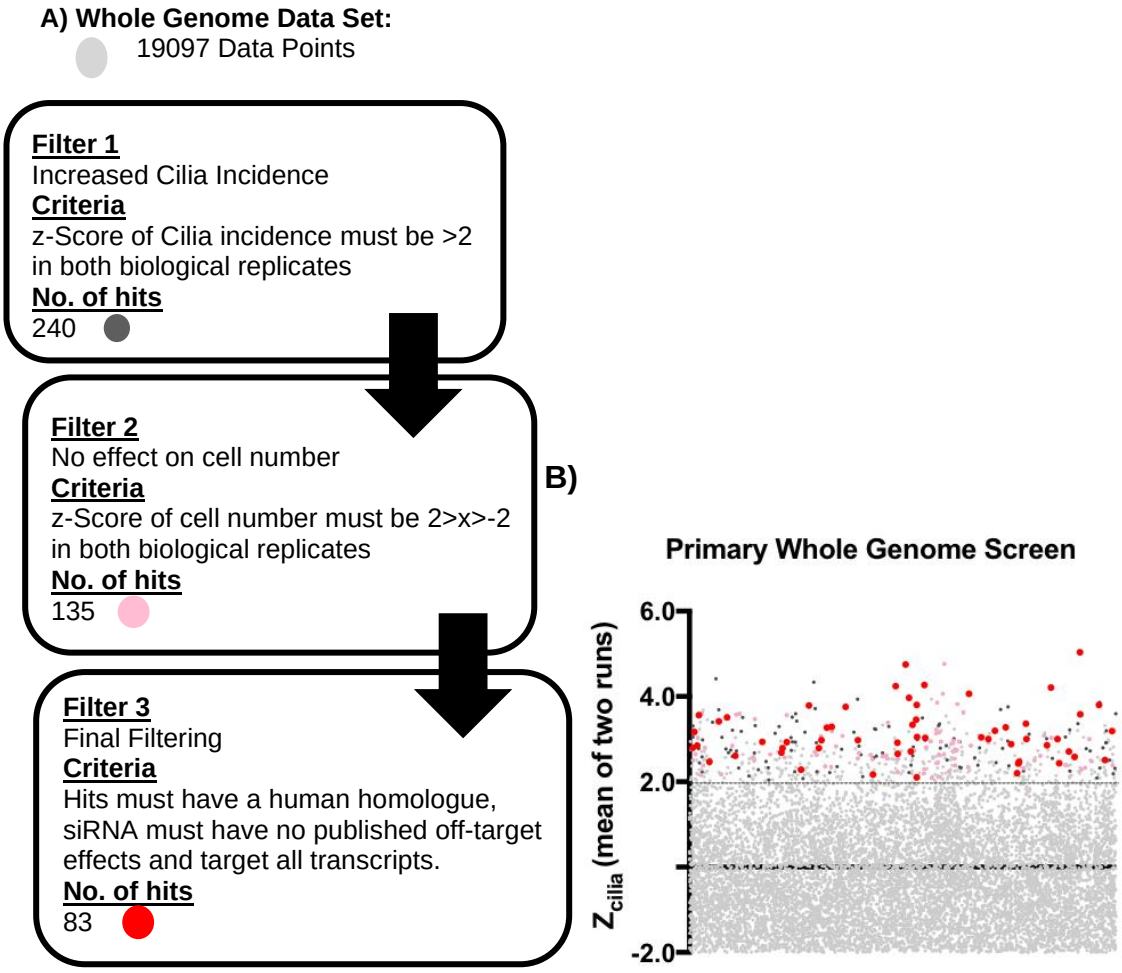

Figure 3.2 Filtering steps used to identify hits that increase cilia incidence from whole genome screen data.

A) The workflow of filtering steps that were used to create the increasing cilia hit list. Three filtering steps were used that were to ensure high specificity over sensitivity. Therefore hits could be taken forward for validation in human cell lines. **B**) Scatter graph shows average robust z-score for cilia incidence of each siRNA knock-down across the whole genome screen. Dark grey points indicates hits that passed Filter 1, pink points that passed Filter 2, and red points highlight the final 83 hits to be taken forward for secondary screening. (8907 data points are outside y-axis limit of -2). Statistical significance calculated using robust z-scores.

Table 3.1 Gene enrichment during filtering steps to identify hits that increase cilia incidence

Filter 1 returned hits that significantly increased cilia incidence in both runs of the whole genome screen. This gene list was significantly enriched for olfactory transduction and rhodopsin-like G protein-coupled receptor (GPCR) protein domains. The same pathways were more significantly enriched after Filter 2, with additional enrichment of GPCRs. The final enrichment step (Filter 3) removed significant enrichment in the previously identified pathways and the final hit list was only enriched in the Gene Ontology Cellular Component: “Intracellular non-membrane-bound organelle”.

FILTER 1 **PPI enrichment p-value: 1.57e-11**			
Pathway ID	**Pathway**	**No. of Hits**	**False Discovery Rate**
KEGG Pathways			
04740	Olfactory Transduction	30/240	0.000184
INTERPRO Protein Domains and Features			
IPR000725	Olfactory Receptor	29/240	0.00984
IPR000276	G protein-coupled receptor, rhodopsin-like	30/240	0.014
FILTER 2 **PPI enrichment p-value: 6.85e-12**			
Pathway ID	**Pathway**	**No. of Hits**	**False Discovery Rate**
KEGG Pathways			
04740	Olfactory Transduction	22/135	5.85e-05
INTERPRO Protein Domains and Features			
IPR000725	Olfactory Receptor	21/135	0.00441
IPR000276	G protein-coupled receptor, rhodopsin-like	21/135	0.012
IPR017452	GPCR, rhodopsin-like, 7TM	22/135	0.0379
FILTER 3 **PPI enrichment p-value: 0.0429**			
Pathway ID	**Pathway**	**No. of Hits**	**False Discovery Rate**
GENE ONTOLOGY (GO) - Cellular Component			
GO:0043232	Intracellular non-membrane-bounded organelle	26/83	0.0227

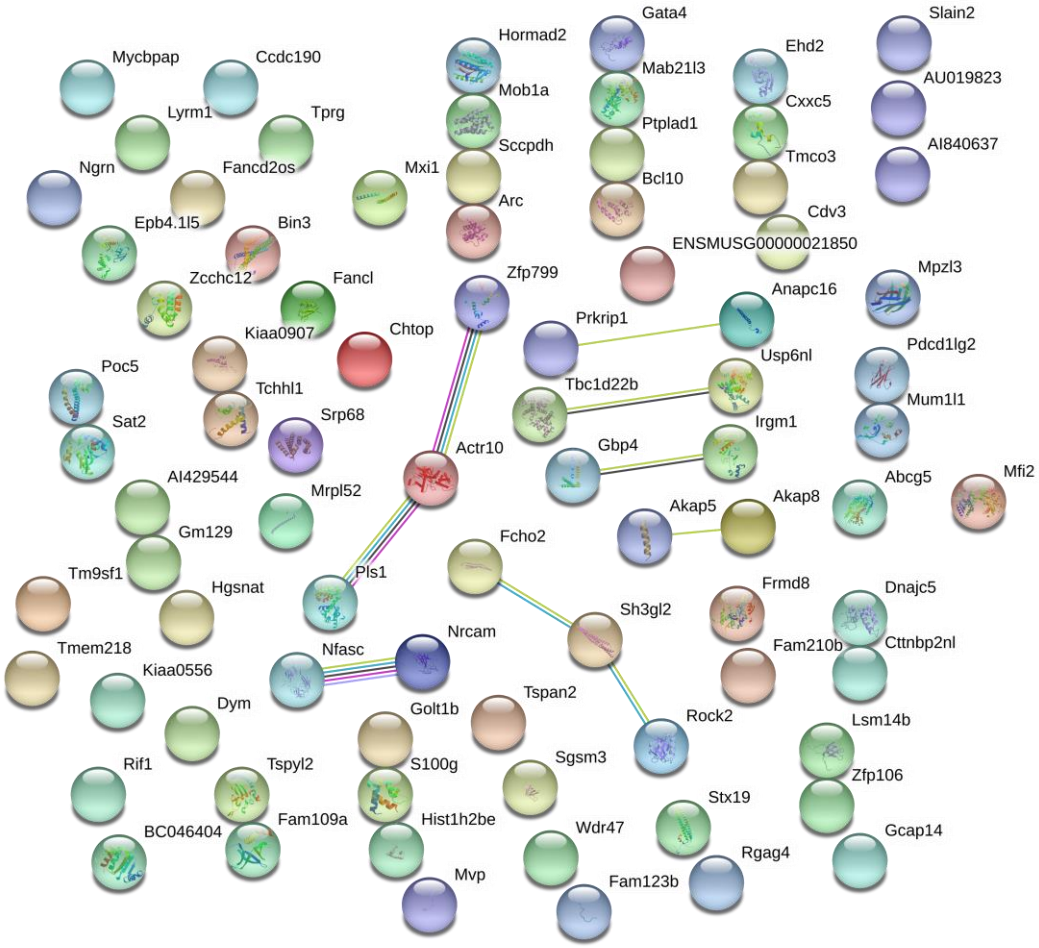

Figure 3.3 STRING analysis of the final 83 hits for secondary screening

STRING analysis (https://string-db.org/) (272) did not identify any significantly enriched pathways amongst the filtered final 83 hits taken forward for secondary siRNA screening. This does not reflect the potential of the data set to identify valuable hits and is more likely a reflection on the lack of sensitivity in the filtering steps used. Pink lines represent experimentally determined interactions, light blue lines represent interactions found in curated databases, black lines represent genes that are co-expressed, yellow lines represent genes that are co-mentioned in published abstracts.

This was likely due to the stringent filtering. This stringency comes from ensuring that z_{cilia} values were >2 in both runs of the primary whole genome screen rather than just analysing the average z_{cilia} of the runs. If only average z_{cilia} was used, this would have provided 596 hits, whereas the more stringent filter returned 240 hits. Likewise, if average z-scores were used for not only filtering step 1 but also filtering step 2, this would have returned 445 hits rather than the 135 returned with more stringent filtering. Thus the filters employed here ensured specificity over sensitivity.

3.3 Increasing cilia incidence secondary screen

The secondary screen followed the same optimised protocol as the whole genome screen in mouse inner medullary collecting duct cells (mIMCD-3) (266) but used a different chemistry of siRNAs that have reduced off-target effects (281) and used a different batch of anti-Ac-α-tubulin antibody. Cell seeding density, fixation and antibody concentration were validated and re-optimised for secondary screening.

The 83 hits to be validated (Appendix A.1.1, Table A.1) were plated across two 96-well plates with re-tested and validated controls (Figure 3.4). Although there were no positive controls for increased cilia incidence across the screen, the use of robust z-scores allowed all hits to be normalized and compared to negative controls. Furthermore, the recognition protocol for primary cilia was re-optimized and validated within this screen, ensuring that positive control siRNAs (that decreased cilia incidence) were significantly different to negative controls (Figure 3.4).

Heat maps of the raw screen data were used for initial qualitative analysis to assess any obvious seeding, staining, or processing errors (Figure 3.5). Wells treated with si*Plk1* (A1, A12) showed very low cell counts and cilia incidence, a qualitative indication of the transfection efficiency on each plate. The heat map for run one, plate two, showed very high cell numbers in parts of row A and row H (Figure 3.5, red highlight). This could reflect a mechanical seeding error in which more cells were plated in these wells, or be an edge effect that arose during incubation of the plates. These wells were all negative controls (treated with RNAiMAX transfection reagent only) and so were removed from the analysis pipeline to prevent skewing the statistical analysis. Once removed, the quantified data of the 2 biological replicates was compared. The correlation between runs showed evidence of good reproducibility in the screen set up and data for both cell counts and cilia incidence (Figure 3.6).

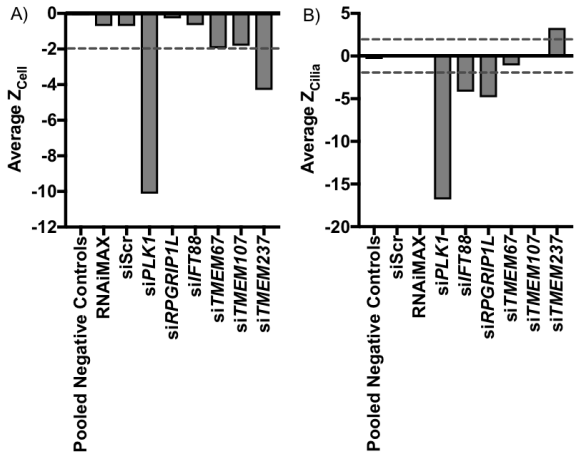

Figure 3.4 Control siRNAs are robust in the increase cilia incidence secondary screen

A) Transfection efficiency in the screen was assessed with si*Plk1*, as knock-down of Polo-like kinase 1 (*Plk1*) inhibits cell proliferation. Mean robust z-score for cell number (Z_{cell}) across the 2 runs of the screen was -10.758, indicating that transfection efficiency of siRNAs across the screen was high. **B)** Positive control siRNAs for loss of cilia, si*Rpgrip1l* and si*Ift88*, were used to validate the accuracy of the cilia recognition protocol. Mean robust z-scores for cilia incidence were -2.605 and -5.523, respectively, indicating that the recognition protocol allowed accurate cilia identification and differentiation between hits of different strengths. Statistical significance was calculated using robust z-scores to compare negative with positive control siRNAs.

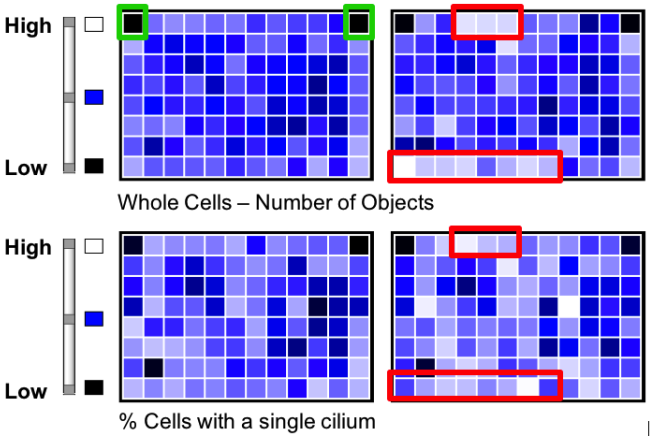

Figure 3.5 Heat Maps from the increased cilia incidence secondary screen

Heat maps for cell number and cilia incidence from screen run one. The heat maps were assessed for cell seeding errors, staining or recognition protocol errors. Low total cell numbers associated with the si*Plk1* control can be seen in wells A1 and A12 (examples highlighted in green). Wells excluded from the analysis for possible seeding errors (examples highlighted in red) with significantly higher cell count. The wells chosen to be removed from analysed screen plates were all negative controls, treated with RNAiMAX transfection reagent only, so did not affect identification of validated hits.

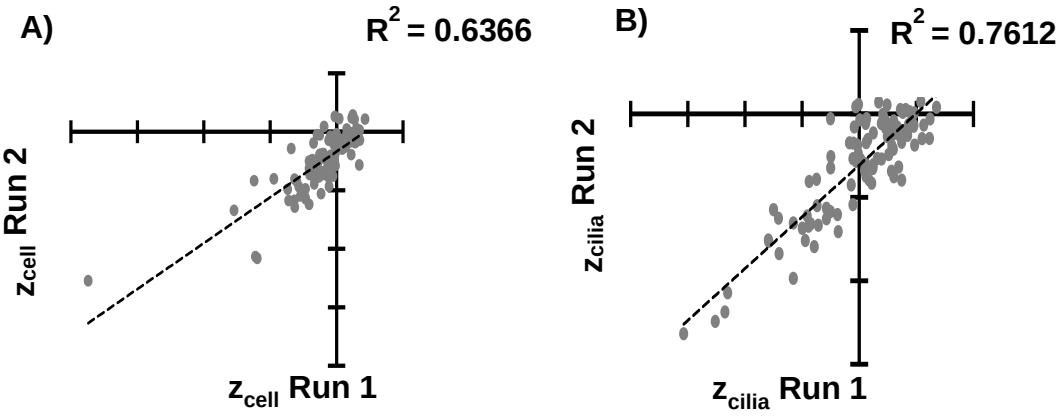

Figure 3.6 Correlation between runs of the increased cilia incidence secondary screen

Scatter graphs showing the correlation between the 2 biological replicates of the Increased Cilia Secondary Screen. **A)** z_{cell} of biological replicates 1 and 2 of the secondary screen were plotted to show correlation between runs. Pearson's correlation coefficient (R^2) between runs was 0.6366. **B)** Pearson's correlation coefficient for z_{cilia} was 0.7156, indicating that the screen was highly reproducible.

3.3.1 Hits from the secondary screen

Pooled negative controls were used to calculate robust z-scores within each plate of the screen. The average z_{cilia} was used to select hits that significantly increased cilia incidence. Hits were defined by a cut-off of average $z_{cilia} \geq 1.96$. Eight of the 83 screened siRNAs were validated as hits (Table 3.2 & Figure 3.7). There was a clear qualitative increase in cilia staining intensity and cilia incidence seen across each field of view captured for the top 4 hits when compared to negative controls (Figure 3.8). The total of 8 hits meant the screen had a validation rate of 9.6%. The final data set had 2/176 negative controls with an average $z_{cilia} \geq 1.96$ and the screen therefore had a false positive rate of 1.1%. The false negative rate could not be calculated, but hits in both the whole genome and secondary screens may have been missed due to false negatives. The top hit from the screen was *Rock2,* with an average z_{cilia} of 3.796, equivalent to $p<0.001$ when compared to negative controls.

Table 3.2 Validated hits from the increase cilia incidence secondary screen

Validated hits from the increase supernumerary cilia secondary screen. The average z-scores (rounded to 3 decimal places) from 2 biological replicates are shown for cilia incidence (z_{cilia}) and cell number (z_{cell}). Hits are ordered from highest to lowest based on the z_{cilia} score.

Gene	Accession No.	z_{cell}	z_{cilia}
Rock2	NM_009072	-0.300	3.796
Stx19	NM_026588	1.213	3.458
Fancd2os	NM_027633	-1.487	2.819
Bcl10	NM_021328	0.901	2.490
Rif1	NM_175238	0.228	2.360
Ngrn	NM_031375	-0.280	2.314
Irgm1	NM_008326	0.947	2.169
Dnajc5	NM_016775	0.750	2.022

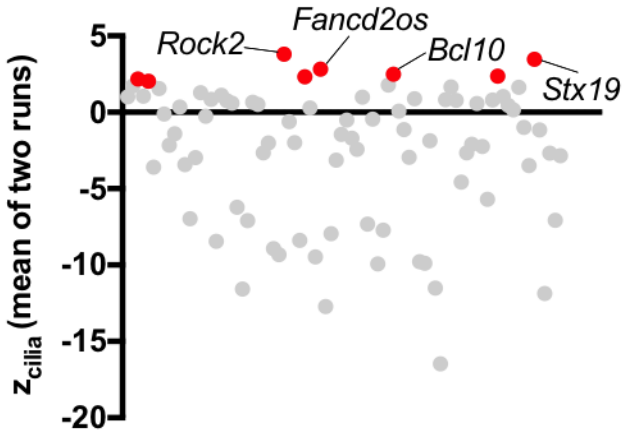

Figure 3.7 Scatter graph of z_{cilia} scores from the increase cilia incidence secondary screen

The average robust z-score for cilia incidence (z_{cilia}) of both biological replicates of the screen was plotted. 8/83 hits (red points) were validated with average z_{cilia} >1.96. The top 4 hits from the screen are labelled, each with z_{cilia} values as follows: *Rock2* (3.796), *Stx19* (3.458), *Fancd2os* (2.819), Bcl10 (2.490). These hits were then considered for tertiary validation in a human ciliated cell line. Statistical significance of hits calculated with robust z-scores normalising to pooled negative controls.

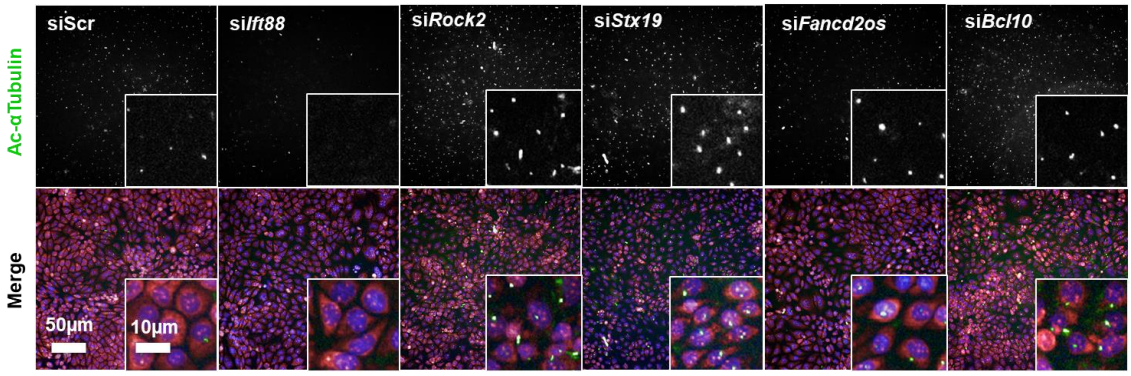

Figure 3.8 Immunofluorescence high content imaging of the top hits from the increased cilia incidence secondary screen

Single fields of view were taken from the screen plates of the second biological replicate of the screen to compare control siRNAs to the top 4 hits from the screen. There is a clear qualitative increase in cilia incidence seen in si*Rock2*, si*Stx19*, si*Fancd2os* and si*Bcl10* knock-down cells compared to the siScr negative control. The positive control for cilia loss (si*Ift88*) is also shown for comparison. Merge images show DAPI (blue), TOTO-3 (pink) and Ac-α-tubulin (green) staining.

The limitations of available reagents and time encouraged the tertiary validation of only the top hit from the screen. The current literature and databases were reviewed in order to assess the potential role of each gene in ciliogenesis and to ensure justification for the validation of the top hit, RhoA-Associated Protein Kinase 2 (ROCK2).

3.4 ROCK2

ROCK2 has not been directly shown to be a negative regulator of ciliogenesis in previous studies, but downstream actin remodelling pathways activated by ROCK have provided indirect evidence for the importance of actin remodelling in controlling cilia incidence and length (92-94) Thus, the current published evidence suggests that a highly complex network of pathways and regulators control the actin cytoskeleton's role during ciliogenesis. Further investigation into these mechanisms could give further clarity and insight into this process during ciliogenesis.

3.4.1 Validation of knock-down and phenotype

The SMARTpool siRNAs used in secondary screening and for tertiary investigation were validated to cause a significant decrease of ROCK2 protein levels in 2 ciliated cell models, on average giving an 80% knock-down as shown by western blot (Figure 3.9).

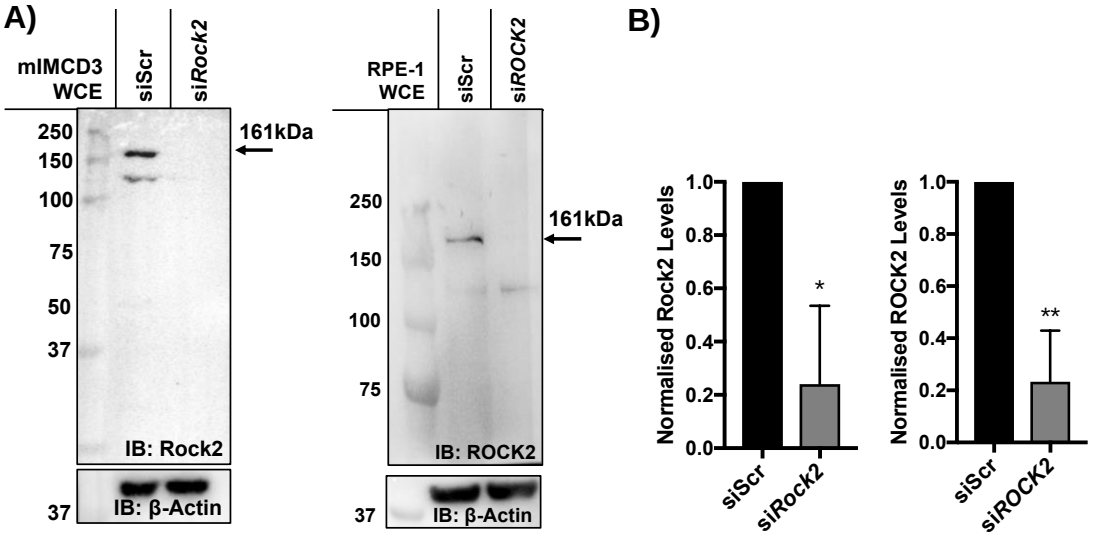

Figure 3.9 Western Blots validate loss of protein by siRNA knock-down of *ROCK2*

A) Western blots validated loss of both mouse and human ROCK2 following siRNA knockdowns in mIMCD3 and RPE-1 cells respectively. **B)** Quantification of western blot densitometry measures for technical replicates of knock-downs for each cell line. Quantifications of ROCK2 levels were normalised to β-actin. Statistical significance of pairwise comparisons was calculated with an unpaired, two-tailed, Student's t-test. * =p<0.05, ** =p<0.01. Error bars represent S.D and WCE stands for whole cell extract.

Tertiary screening of *ROCK2* knock-downs was done in a human cell model to confirm the phenotype across different model organisms. Knock-down of *ROCK2* in human retinal pigment epithelial cells (RPE-1) showed a marginal increase in cilia incidence across 3 averaged biological replicates. This did not reproduce the strong increase in cilia incidence seen in secondary screening for the mIMCD3 mouse cell line (Figure 3.10). RPE-1 cells treated with si*ROCK2* did, however, show a large and significant increase in cilia length, increasing on average by 30%. The longest cilium measured was 9.6μm (Figure 3.10).

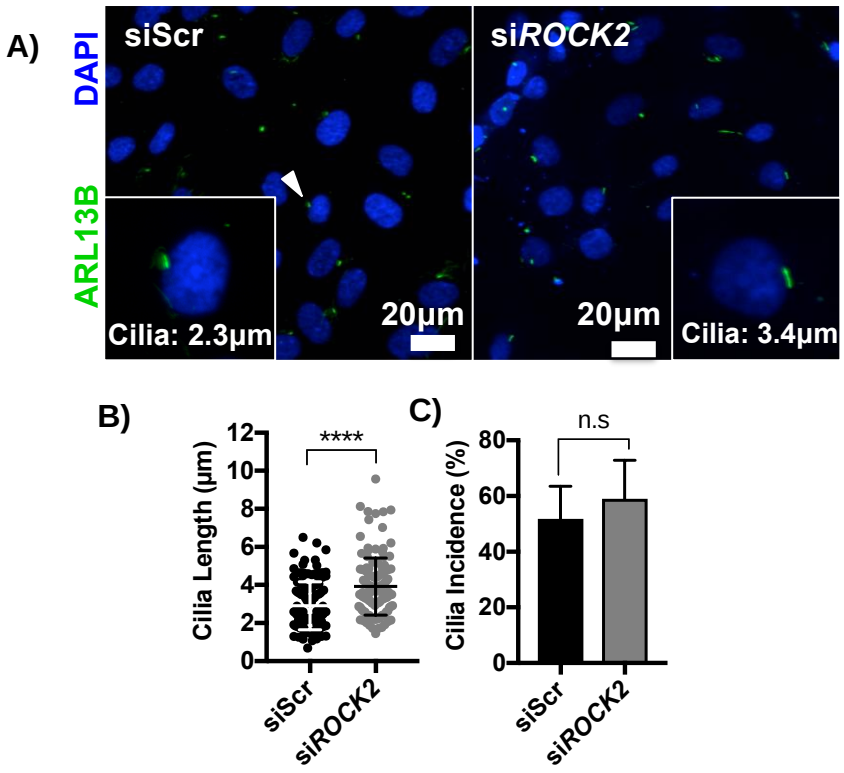

Figure 3.10 *ROCK2* knock-down in human hTERT-RPE-1 cells increases cilia length

A) Immunofluorescence confocal microscopy of RPE-1 cells following knockdown of si*ROCK2* shows increased cilia length across the cell population, compared to cells treated with siRNA scrambled (siScr) negative control. An example cell is highlighted in each condition, with the length of cilia indicated. **B)** Average cilia length for negative controls was 2.91µm and in si*ROCK2* treated cells was 3.92µm (n=3 biological replicates, minimum of 40 cilia measured per replicate).**C)** Quantified data shows there is no significant difference in cilia incidence between negative control cells and cells treated with si*ROCK2* (n=3, p=0.5310). Data was confirmed to be normally distributed using D'Agostino-Pearson omnibus K2 test. Significance was then calculated for **B)** and **C)** with an unpaired two-tailed Student's t-tests. **** = p<0.0001. Error bars represent S.D.

3.4.2 Overexpression of m*Rock2* inhibits ciliogenesis

A GFP-m*Rock2* construct validated by western blot (Figure 3.11A) was transfected into RPE-1 cells to assess if over-expression of *Rock2* caused a loss in cilia incidence or length. Cells expressing GFP-m*Rock2* were compared to cells expressing untagged GFP or un-transfected cells. There was a significant decrease in cilia incidence in cells expressing GFP-m*Rock2*, compared to the cells expressing only GFP or the un-transfected populations. Cells expressing GFP-m*Rock2* also had significantly shorter cilia than cells expressing untagged GFP or un-transfected RPE-1 cells (Figure 3.11).

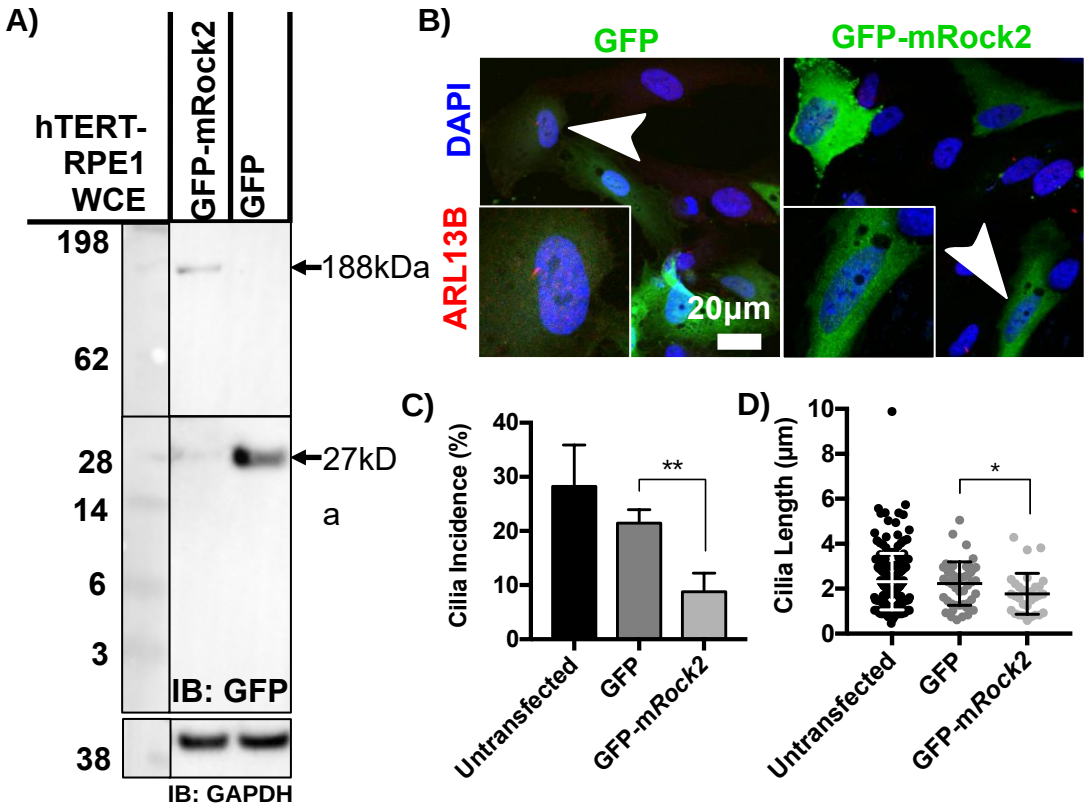

Figure 3.11 Cilia incidence in RPE-1 cells expressing GFP-m*Rock2*

A) Western blot to confirm overexpression of GFP-mRock2. Membrane immunoblotted against GFP. A band at 27kDa, likely to be GFP cleaved from Rock2, can also be detected. **B)** Cilia incidence and cilia length were determined for RPE-1 cells transiently transfected with either GFP-m*Rock2* or an untagged GFP construct. N=3 experimental replicates with at least 100 cells counted per condition in each replicate **C)** RPE-1 cells expressing GFP-m*Rock2* had a significantly lower cilia incidence compared to cells expressing GFP only. **D)** Cells expressing GFP-m*Rock2* also had significantly shorter cilia compared to controls, suggesting a dominant negative effect of protein over-expression. Data in **C)** was confirmed to be normally distributed using D'Agostino-Pearson omnibus K2 test and not normally distributed in **D)**. Significance was then was calculated with an unpaired, two-tailed Student's t-test (cilia incidence) and a Mann-Whitney U test (cilia length). * = $p<0.05$, ** = $p<0.01$. Error bars represent S.D.

3.4.3 *Rock2*$^{-/-}$ mouse has ciliary defects

As both cell lines tested showed a significant ciliogenesis phenotype with a transient *Rock2* knock-down, it was of interest to confirm if a full animal knock-out model of *Rock2* would also show a ciliogenesis phenotype since transient knock-downs and constitutive, global knock-out models frequently manifest different phenotypes. For example, in some knock-out models compensatory mechanisms and genetic interactions can rescue phenotypes that are not

observed in the transient knock-down cell models (reviewed and summarised in (238, 282)).

The *Rock2*$^{-/-}$ knock-out mouse has a more severe phenotype than the *Rock1*$^{-/-}$ mouse. Most embryos only survived to E13.5 due to placental failure but surviving mice, although smaller than wild type controls, did not show any histological differences (283). Follow-on work investigating cilia formation during angiogenesis in the *Rock2*$^{-/-}$ mice also noted some ciliary defects including longer cilia in embryonic fibroblasts (Figure 3.12), a different distribution of cilia across cell types in blood vessel lumens, and an overall reduced cilia number in tissues (265).

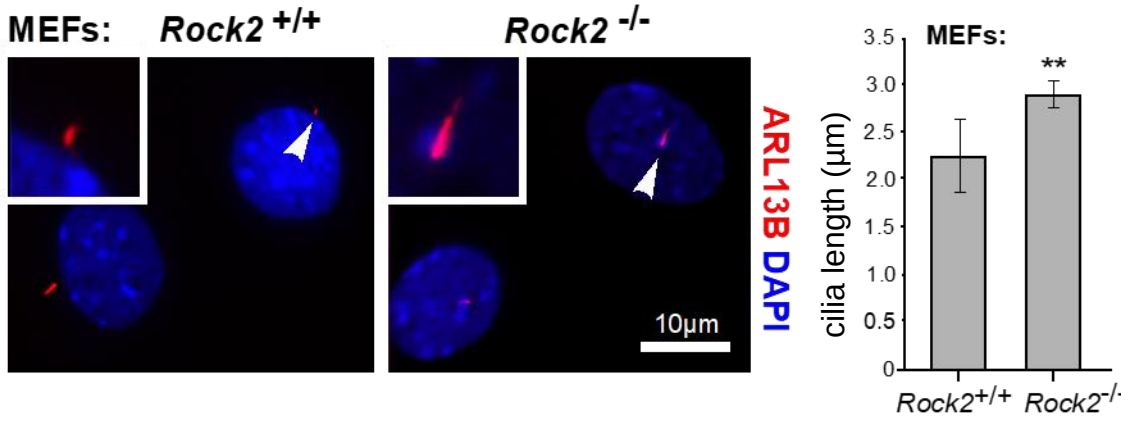

Figure 3.12 The *Rock2*$^{-/-}$ mouse has longer cilia than wild-type controls

Embryonic fibroblasts (MEFs) taken from mutant and wild-type mice were serum starved and then stained for cilia using ARL13B as a marker. Cells from the Rock2$^{-/-}$ mice had significantly longer cilia compared to the wild-type controls. Significance calculated with an unpaired, two-tailed Student's t-test.** = $p<0.01$. Error bars represent S.D. This figure was provided by Dr. Gary Grant and partly presented in his thesis (265).

3.4.4 ROCK1 does not have the same role as ROCK2 in ciliogenesis

The whole genome siRNA screen data suggested that *Rock2* but not *Rock1* was involved in the negative regulation of ciliogenesis in mIMCD3 cells (average z_{cilia} for si*Rock1* from the primary screen data set = 0.863863). Previously published work gave evidence that ROCK1 knock-down increases cilia incidence in RPE-1 cells (98). However, in previous experiments presented in this thesis, ROCK1 activity was not able to compensate for loss of ROCK2. However, it is possible that ROCK1 plays a redundant role in ciliogenesis.

These different roles for the ROCKs have been described in other molecular mechanisms, despite the 93% homology in their kinase domains (284). Therefore, to test if Rock1 was a true false negative hit from the whole genome screen, validated knock-downs (Figure 3.13) were carried out in both mIMCD3 and RPE-1 cells.

IMCD3 cells treated with si*Rock1* showed a ciliogenesis phenotype, with a moderate decrease in cilia incidence and a significant increase in average cilia length, from 2.7μm in negative controls to 3.7μm (Figure 3.14 A). RPE-1 cells showed no significant changes in cilia incidence or cilia length between negative controls and cells treated with si*ROCK1* (Figure 3.14 B). Since residual ROCK2 cannot compensate for ROCK1 knock-down, and *vice versa*, this highlights the distinct roles of these proteins in ciliogenesis, confirming findings in other cellular pathways. Thus, the hypothesis going forward, was that only the kinase activity of ROCK2 was a negative regulator of ciliogenesis.

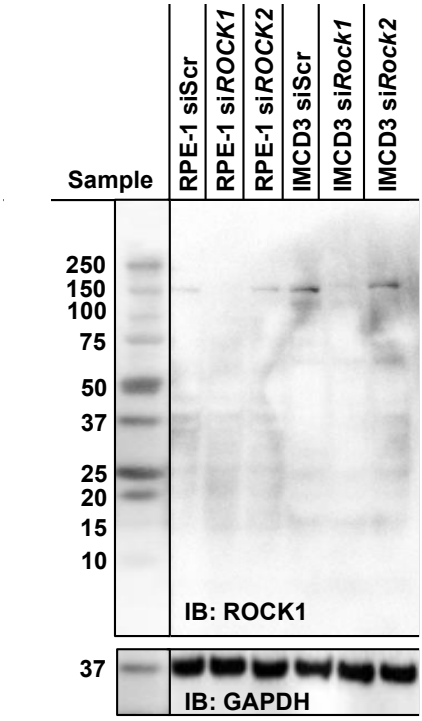

Figure 3.13 Validation and specificity of ROCK siRNAs

A) siRNAs targeting both human and mouse *ROCK1* are efficient and specific. There is no non-specific knock-down of ROCK2 with the si*ROCK1* siRNAs.

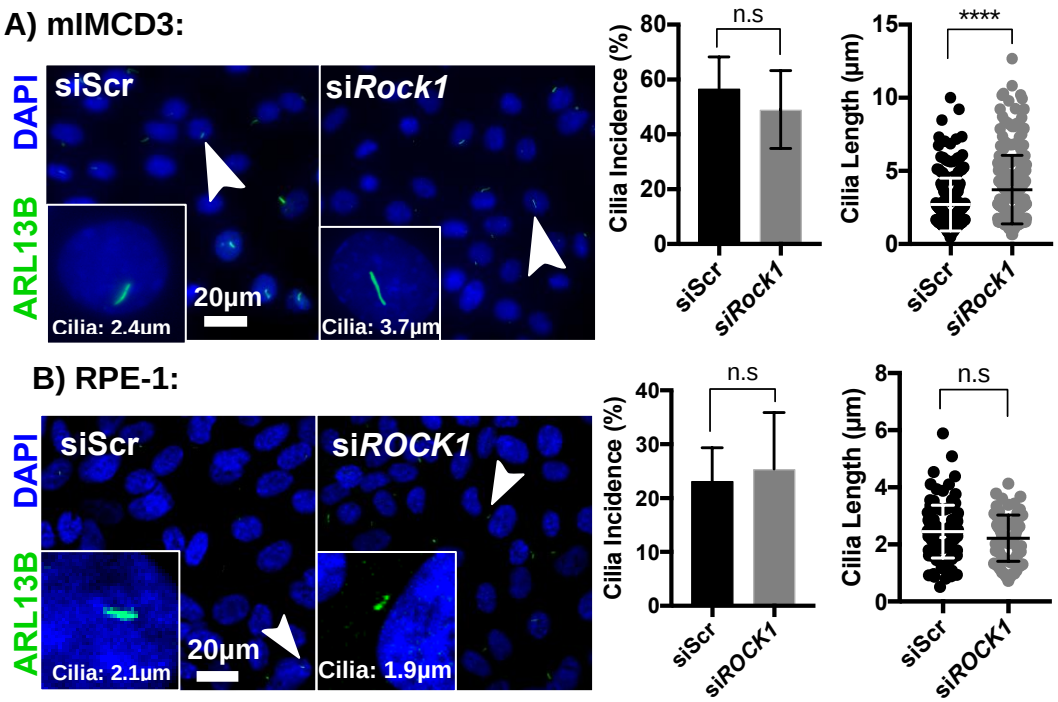

Figure 3.14 Loss of ROCK1 does not phenocopy loss of ROCK2

A) IMCD3 cells treated with si*Rock1* or a scrambled negative control siRNA. A moderate decrease in cilia incidence was seen across cell populations (n=3 technical replicates, p=0.3724). A significant increase in average cilia length from 2.7µm to 3.7µm was noted (n=3, at least 50 cilia measured per technical replicate). **B)** RPE-1 cells showed no significant changes in ciliary phenotypes compared to negative controls when treated with si*ROCK1*. Data for cilia incidence was confirmed to be normally distributed using D'Agostino-Pearson omnibus K2 test whereas cilia length data was not normally distributed. Statistical significance of pairwise comparisons was then calculated with Student's two-tailed t-test (for cilia incidence) and the Mann-Whitney U-test (for cilia length) ****=p<0.0001. Error bars represent S.D.

3.4.5 ROCK2 kinase activity negatively regulates ciliogenesis

Evidence presented thus far from an *in vivo* mouse and 2 *in vitro* cell models indicated that ROCK2 was a negative regulator of ciliogenesis. To decipher the functional role that ROCK2 played in ciliogenesis, the known kinase activity of the protein was specifically tested for a functional role in this process.

Previous work with ROCK inhibitors in ciliary research have used non-specific inhibitors such as Y27632 (119, 285), noted more commonly for cilia elongation, or GSK 429286 (286), which was able to rescue loss of cilia in a Rho GTP Activating Protein (*Arhgap35*) mutant mouse embryonic fibroblast (MEFs) model (286). These studies did not aim to dissect the specific functional roles of ROCK1 and ROCK2 in ciliogenesis but still showed the significance of ROCK

inhibition in restoring cilia in ciliopathy cell models. Despite its use in previous ciliary studies, because Y27632 chemically inhibits both ROCK1 and ROCK2 in addition to other kinases (287) it was judged to be unsuitable for this project. In contrast, KD025 is a relatively new drug that selectively binds and inhibits ROCK2 with a minimal effect on ROCK1 in a cell-free system (IC_{50}= 105 nM and IC_{50} = 24 µM, respectively). Since KD025 is a competitive ATP inhibitor, when used *in cellulo* KD025 is expected to be between IC_{50} = 1-10µM for ROCK2 and greater than 200µM for ROCK1 (288), allowing the reasonable assumption that only ROCK2 is selectively inhibited in the experiments described below.

RPE-1 cells were treated with KD025 for either 2 or 48 hours to confirm the efficacy of the drug. ROCK2 kinase activity was assessed by quantifying changes in phosphorylated MLC. Initially, western blots were used analyse phosphorylated MLC. Unfortunately, despite optimisation of all antibodies, biological replicates were not reproducible with some blots not showing consistent patterns or, indeed, any bands during imaging (Appendix F). Instead, an immunofluorescence staining and high content imaging method was therefore developed. Due to the previous antibody variability observed for western blotting, total fluorescence measurements were avoided. Instead, the presence of active acto-myosin (myosin is active when MLC is phosphorylated), which can be seen as thin fibre like structures in immunofluorescence microscopy, were assessed using and automated image structure analysis. Inactive, unphosphorylated myosin staining appears speckled cytoplasmic staining. These staining patterns were consistent in both the human and mouse cell lines (Appendix G.2). The image structure analysis was used to quantify the presence of regular structures, such acto-myosin fibres made from phosphorylated MLC. This quantification, in arbitrary units, was then used as an indirect measure of ROCK2 kinase activity on MLC (Figure 3.15).

KD025 treatments led to a decrease in visible acto-myosin fibres and specific staining of phosphorylated MLC in both RPE-1 (Figure 3.15 and Appendix G.1) and mIMCD3 cells (Appendix G.2). 48 hours KD025 treatment caused a trend that showed reduced image structure with increasing concentrations of KD025, with a significant loss of image structure (visualized by the presence of acto-myosin fibres with bi-phosphorylated (Thr18, Se19) MLC (pp-MLC)) following

5μm KD025 treatment. 2 hour treatment also showed a trend of fewer fibre structures with increasing concentration of KD025. Similar results were observed in miMCD3 cells, but there were significant decreases in image structure across all antibody stains tested (Appendix G.2).

The specific ROCK2 phosphorylation site in MLC is unclear. It is known that MLC is preferentially phosphorylated by ROCK at Ser19 before Thr18 (289). However, the literature remains unclear if ROCK1 and ROCK2 both phosphorylate these sites in all cell types and if preferential phosphorylation is initiation or pathway-specific.

The specificity of the chemical inhibitor KD025 towards ROCK2 was confirmed in this thesis by showing that it caused a dose-dependent response in acto-myosin fibre structure. Treatment of cells with KD025 indicated that the kinase activity of ROCK1 cannot compensate the loss of ROCK2 activity. However, ROCK1 knock-downs in previous publications (98) and in IMCD3 cells (Figure 3.14) still had a ciliogenesis phenotype when assessing ciliary length. This therefore questions the true contribution of each kinase to ciliogenesis in the mouse and human model systems.

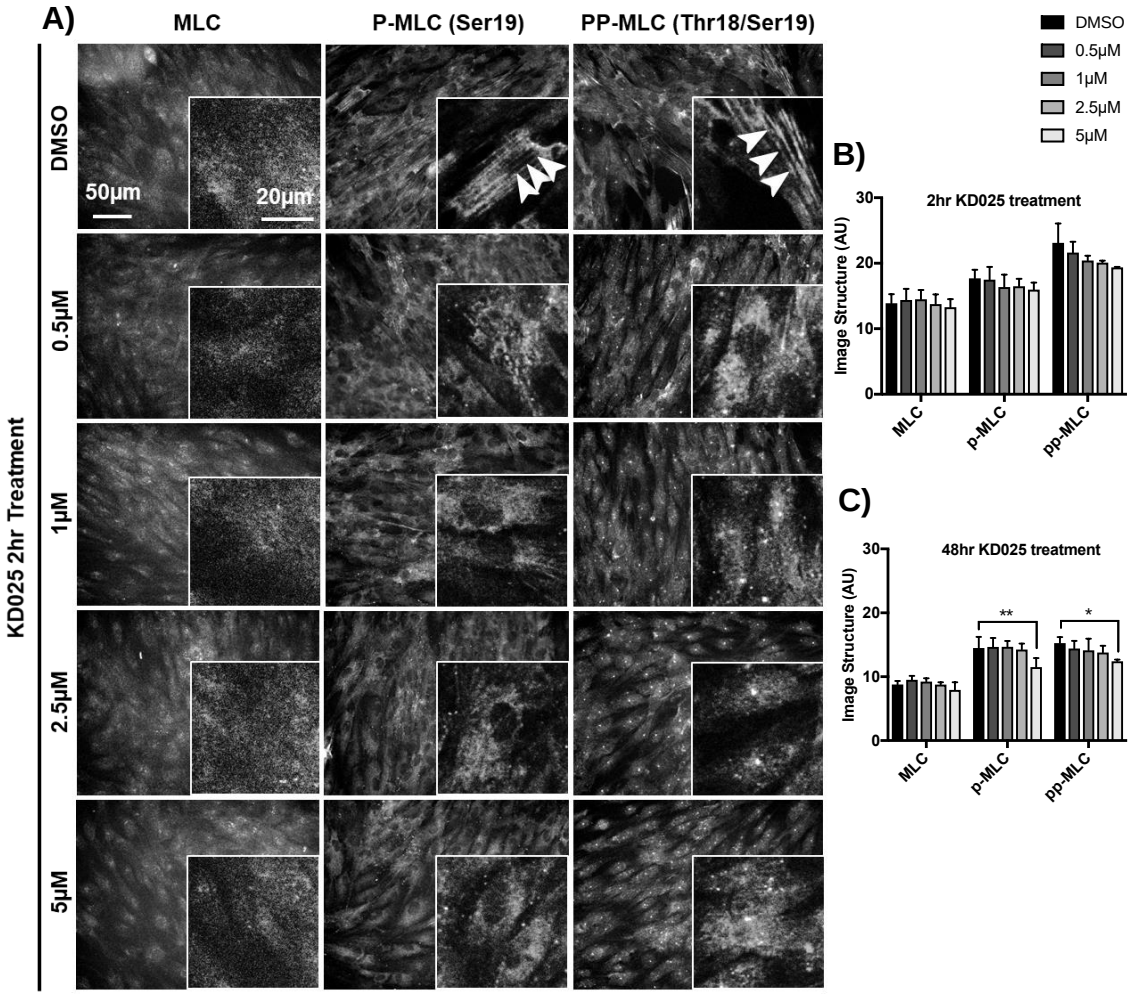

Figure 3.15 KD025 inhibits the kinase activity of ROCK2 and reduces the presence of acto-myosin fibres in RPE-1 cells

A) Representative high-throughput images of RPE-1 cells treated for 2hrs with KD025. Single cells are shown in magnified high contrast insets to highlight the presence or absence of fibre structures (indicated by arrowheads). No fibre structures can be seen in the negative control myosin light chain II (MLC) staining across all concentrations of KD025 treatment. There is a qualitative reduction in specific staining of fibre-like structures as the concentration of KD025 increases for both mono-phosphorylated (Ser19) MLC (p-MLC) and bi-phosphorylated (Thr18, Ser19) MLC (pp-MLC) stained cells. **B)** When quantified, the 2hr treatment showed a gradual loss of image structure. **C)** The 48hr KD025 treatment also showed a decrease of image structure with increasing concentrations of inhibitor, and significant changes at 5µM. Differences in baseline control MLC structure likely due to experiments being carried out independently with different batches of antibody. Data in **B)** and **C)** was confirmed to be normally distributed using D'Agostino-Pearson omnibus K2 test. Significance was then calculated with a two-way ANOVA with Dunnett's multiple comparisons test. * = $p<0.05$, ** = $p<0.01$. Error bars represent S.D.

KD025 was tested on RPE-1 cells that had been transduced with lentivirus constructs expressing GFP-LifeAct and maintained as a polyclonal cell line (henceforth referred to as RPE-1:LifeAct).

These cells were used to observe changes in cilia phenotypes and actin morphology as artefacts were noted when using other actin stains such as phallodin (Puncate background staining as seen in Figure 3.20A and Figure 3.21B). In RPE-1:LifeAct cells serum-starved and treated with KD025 for 48 hours, cilia incidence was significantly increased at all concentrations tested and cilia length was significantly increased at concentrations ≥2.5μM (Figure 3.16). RPE-1 cells serum-starved for 24 hours and then treated with KD025 for a further 2 hours in serum starvation media showed no significant changes in cilia incidence or length. However, average cilia incidence in DMSO (vehicle)-treated cells was 45% whereas cells treated with 0.5μM KD025 had an average cilia incidence of 60%. mIMCD3 cells treated with KD025 also showed significant increases in cilia incidence and length following 48hrs 0.5μM KD025 treatment, but showed no significant changes to cilia incidence after 2hrs KD025 treatment. As seen in the RPE-1 cells, the IMCD3 cells treated for 2hrs had average cilia incidence following DMSO (vehicle) treatment of 50%, whereas cells treated with 0.5μM KD025 had average cilia incidence of 61%. (Appendix G.3). This data suggests that the serine/threonine kinase activity of ROCK2 is directly implicated in modulating ciliogenesis and is not compensated for by residual ROCK1 activity. This also gives insight into the timeline of ciliogenesis, suggesting that cilia formation does not occur within 2 hours of disruption of the cytoskeleton and axoneme elongation must also take over 2 hours treatment to be significantly impacted.

48hr 5μM KD025 treatment caused a 22% increase in average cilia length (from 2.47 to 3.01) which was comparable although not as large an increase as seen by siRNA knock-down of *ROCK2* (Figure 3.10) which caused a 26.5% increase in average cilia length from negative siScr controls (from 3.12 to 3.95).

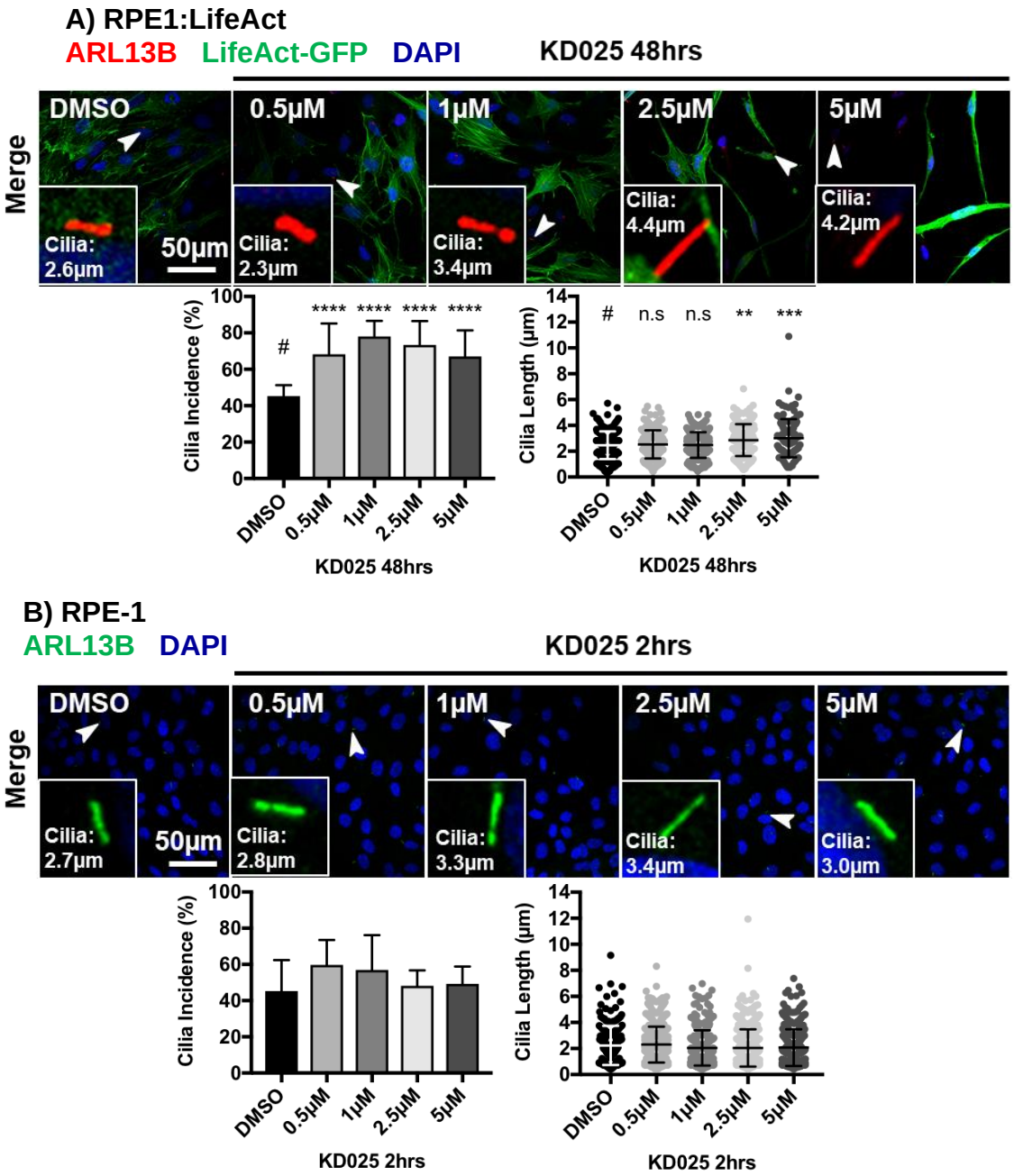

Figure 3.16 KD025 treatment increased cilia incidence and length in RPE-1

A) RPE-1:LifeAct cells treated with KD025 in serum starvation media for 48 hrs had increased cilia incidence compared to DMSO-treated negative control cells. There was also a significant increase in cilia length in cells treated with 2.5 μM or 5 μM KD025 over 48 hrs compared to the DMSO control. However, there was a clear reduction in cell number and change in cell morphology. **B)** 2 hr treatment with KD025 after 24 hrs serum starvation did not cause significant changes to either cilia incidence or cilia length in RPE-1 cells. Data for cilia incidence was confirmed to be normally distributed using D'Agostino-Pearson omnibus K2 test whereas cilia length data was not normally distributed. Significance was then calculated using one-way ANOVAs with Dunnett's test for multiple corrections (cilia incidence) and Kruskal-Wallis tests with Dunn's multiple comparisons test (cilia length). *=p<0.05. **=p<0.01, ***=p<0.001, ****=p<0.0001. # Is the control all data sets were compared to. Error bars represent S.D.

KD025 showed that it is specific loss of kinase activity that affects ciliogenesis. The siRNAs used previously were therefore also tested to show if the same mechanistic changes could be linked to the ciliary phenotype. siRNA knock-down of ROCK2 in both RPE-1 and mIMCD3 cell lines showed decreased acto-myosin structures when staining for bi-phosphorylated MLC (pp-MLC) (Figure 3.17), an indirect measure of ROCK activity.

A) mIMCD3:

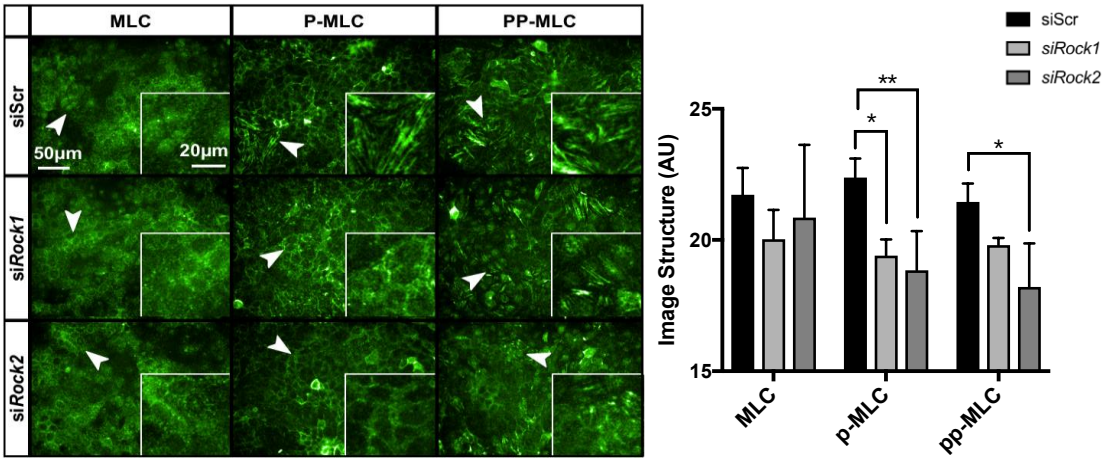

B) RPE-1:

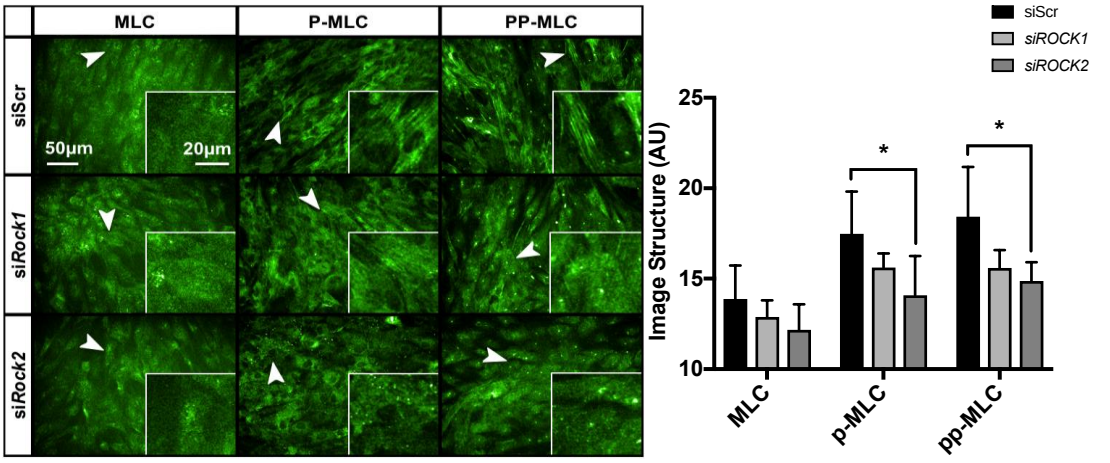

Figure 3.17 Knock-down of ROCK2 by siRNA inhibits the kinase activity of ROCK2 and reduces the presence of acto-myosin fibres

siRNAs for *Rock1* and *Rock2* were tested in both IMCD3 **(A)** and RPE-1 **(B)** cells. There was a significant loss of image structure seen in both knock-down conditions when assessing bi-phosphorylated (Thr18,Ser19) myosin light chain II (pp-MLC). However, there was only a significant change in mono-phosphorylated MLC (p-MLC) in mIMCD3s with *Rock1* knock-down. This represents a decrease in MLC activation and loss of acto-myosin fibres in siRNA knock-downs of *Rock1* and *Rock2*. Overall there was a trend of decreased structure in both cell types under both knock-down conditions. Data was confirmed to be normally distributed using D'Agostino-Pearson omnibus K2 tests. Significance was the calculated using two-way ANOVAs with Dunnett's multiple comparisons tests. * = $p<0.05$, ** = $p<0.01$. Error bars represent S.D.

A complementary experiment was designed to validate the role of ROCK2 kinase activity in the observed ciliary phenotypes and rule out any possible novel or structural role of ROCK2 that we had not yet identified. This used a time-course of ciliogenesis with conditionally-activated form of ROCK2. A fusion construct comprising the ROCK2 KD fused to an N-terminal green fluorescent protein (GFP) and a C-terminal oestrogen receptor (ER) domain was used (GFP-ROCK2-ER). Negative controls included a validated kinase-dead (k/d) ROCK2 KD ($ROCK2^{k/d}$) and a GFP-only construct, each fused to an ER domain (GFP-$ROCK2^{k/d}$-ER, GFP-ER). The ROCK2 fusion proteins (kindly gifted by Prof. Mike Olson, Ryerson University, Canada) are expressed but the KD is inactive until treatment with 4-hydroxytamoxifen (4-HT) which binds the ER domain, releasing it from the KD, thus providing controlled activation of ROCK2 (290). RPE-1 cells were retro-virally transduced to stably express the fusion constructs and single cell clones were selected. Eight GFP-ER, 8 GFP-$ROCK2^{k/d}$-ER and 6 GFP-ROCK2-ER expressing clones had stable growth in culture and were tested for GFP expression and cilia incidence (Figure 3.18). From this data, 2 GFP-ER, 3 GFP-$ROCK2^{k/d}$-ER and all the GFP-ROCK2-ER clones were taken forward for further validation. As the GFP-ROCK2-ER clones all had very low cilia incidence it was decided to base clone selection on the ROCK2 activity, assessed by phosphorylation of myosin light chain (MLC). The ROCK2 antibody used for western blotting was not suitable for immunofluorescence (IF) and so cells expressing the fusion constructs could not be co-stained for ROCK2 to look for increased expression. Only the GFP within the fusion constructs could be detected by IF.

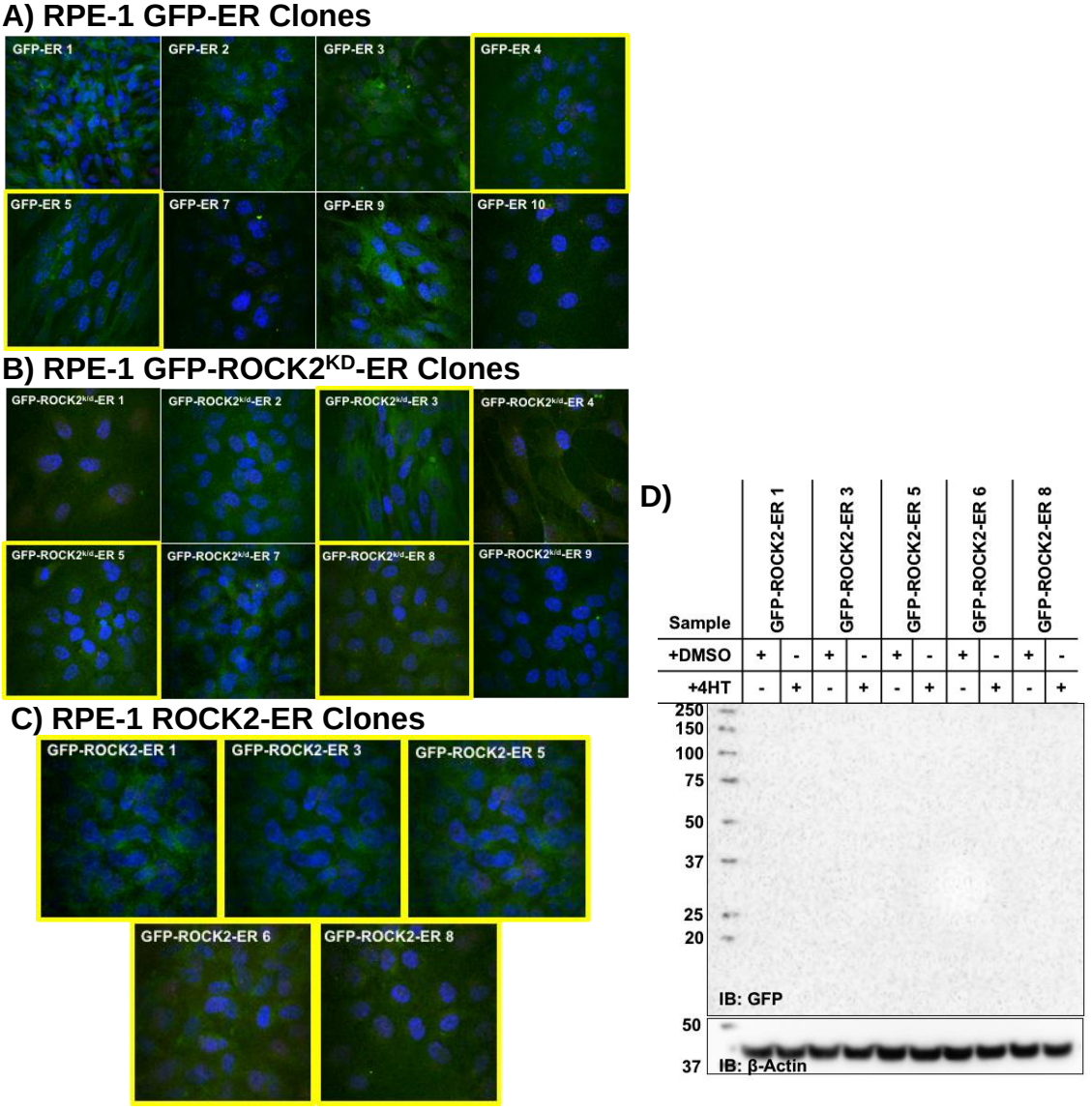

Figure 3.18 Expression and cilia incidence of RPE-1 cells stably transfected with ROCK2 kinase domain fusion proteins

A) RPE-1 clones expressing GFP-ER. Clone 7 and 10 did not have detectable cilia incidence. Clones 4 and 5 had the highest cilia incidence and so were taken forward for further validation. **B)** RPE-1 clones expressing GFP-ROCK2$^{k/d}$-ER. Clones 1 and 4, despite previously stable cell growth, did not continue to grow in culture and were not considered for further validation. Clone 9 was disregarded due to low GFP expression. Clones 3, 5, and 8 had the highest cilia incidence and were taken forward for further validation. **C)** RPE-1 clones expressing GFP-ROCK2-ER had low levels of cilia incidence and so all were taken forward to identify the clone with the highest ROCK2 kinase activity. Images were all taken at equivalent laser power and presented as maximum intensity projections (MIPs) of equal size z-stacks. Cilia incidence and GFP expression was assessed qualitatively. All merge images show the fusion construct GFP in green, cilia in red and nucleus (DAPI) in blue. **D)** Western blots showed no detectable GFP expression with 30μg whole cell extract (WCE) loaded on to an SDS-PAGE gel.

The chosen clones were then tested for their kinase activity to confirm increased activity in GFP-ROCK2-ER cells and lack of activity in the negative control cell lines (GFP-ROCK2$^{k/d}$-ER & GFP-ER). GFP was only detectable in the GFP-ROCK2-ER clones by confocal microscopy (Figure 3.18). As there were no detectable levels of the fusion proteins following western blotting, it was assumed that any changes in MLC phosphorylation would also be undetectable or quantifiable. Therefore, due to time constraints and the commitment required for cell line validation, this experiment was not taken forward.

3.4.6 Loss of ROCK2 does not cause cilia disassembly defects

As the population of cells had an increase in cilia incidence it was important to rule out the possibility ROCK2 was affecting ciliary disassembly or ciliary retention rather than impacting ciliogenesis, or to clarify whether it had a role in both processes.

To test this, RPE-1 cells were plated in a high-throughput format and treated for 72 hrs with si*ROCK2* in serum starvation conditions. Half of the experimental wells were then treated with 10 % serum for the final 24 hrs to induce ciliary resorption and cell cycling. Cells with *ROCK2* knock-down had a significant decrease in cilia incidence when treated with serum compared to those that were serum starved. In both conditions, cells treated with si*ROCK2* had comparable cilia incidence to the scrambled siRNA treated controls. This data suggests that loss of ROCK2 does not affect ciliary resorption and that ROCK2 is likely acting in the initiation of and/or initial stages of ciliogenesis.

The confluency of the RPE-1 cells in the 96-well plate set up used in this experiment likely limited the effect of serum addition for the final 24hrs of the siRNA knock-down. As the RPE-1 cells reach confluency contact inhibition causes the cells to slow or stop cycling, increasing the overall percentage of cells within the population that would have a primary cilium. Despite this, there was a 29% decrease in cilia incidence with the addition of serum.

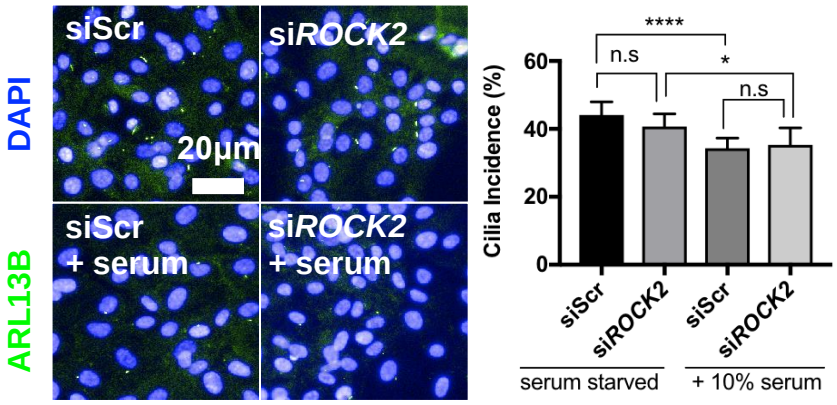

Figure 3.19 *ROCK2* siRNA knock-down does not cause ciliary disassembly defects

RPE-1 cells were transfected high-throughput with si*ROCK2* or negative control scrambled siRNA and serum starved for either 72 hrs or 48 hrs, followed 24 hrs with 10 % serum to induce cell cycling and cilia resorption. RPE-1 cells treated with si*ROCK2* had no significant change in cilia incidence compared to cells treated with siScr control. RPE-1 cells treated with si*ROCK2* or siScr had a significant decrease in cilia incidence with the addition of 10 % serum, compared to cells that were only serum starved. This suggested that there was not a ciliary disassembly defect in cells with depleted expression of *ROCK2*. Data was confirmed to be normally distributed using a D'Agostino-Pearson omnibus K2 test Significance was then calculated with a two-way ANOVA with Sidak's multiple comparisons test. * = $p<0.05$, **** = $p<0.0001$. Error bars represent S.D.

3.4.7 F-actin stability and acto-myosin contractions modulate ciliogenesis

The downstream pathways of ROCK2 phosphorylation required further investigation to elucidate their specific contributions to ciliogenesis. As discussed, LIMK2 is phosphorylated by ROCK2 and has been previously linked to ciliogenesis through F-actin stabilisation (96, 98). To validate this previously published work, RPE-1 cells were treated with cytochalasin D, a chemical inhibitor that binds actin monomers and causes destabilisation of F-actin (291), mimicking the molecular effect of LIMK2 inactivation. It has also been shown to reduce ROCK activity though a cytoskeletal tension feedback loop (292). Cytochalasin D treatment of RPE-1 cells for 16 hrs significantly increased both cilia incidence and cilia length when compared to DMSO (vehicle) negative controls (Figure 3.20). 2 hr treatment followed the same trend, but did not show significant differences, as has been reported previously where cilia were only seen to appear exponentially after 6 hr treatment with cytochalasin D (98).

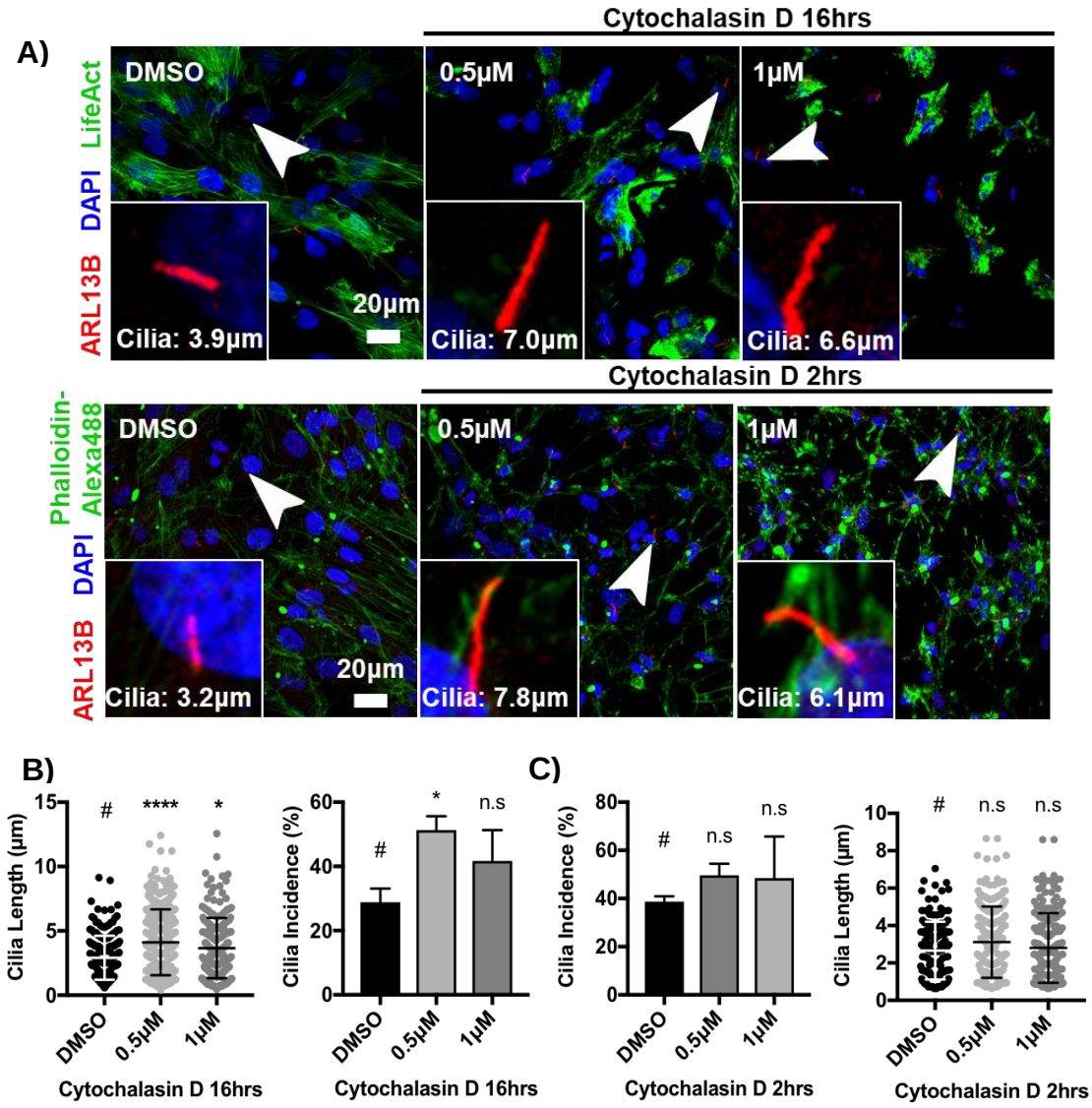

Figure 3.20 Chemical destabilisation of F-Actin increases cilia incidence

A) RPE-1:LifeAct cells were treated for 16 hrs with cytochalasin D or DMSO as a vehicle negative control in serum starvation media (0.2 % FBS), or RPE-1 cells were treated with cytochalasin D for 2 hrs after 24 hr serum starvation. Effects on cilia incidence and length were assessed by confocal microscopy and quantified. **B)** Cells treated with ≥0.5 μM cytochalasin D for 16 hrs had a significant increase in cilia incidence and cilia length. **C)** RPE-1 cells were treated with cytochalasin D for 2 hr and showed a marginal increase in cilia incidence and average cilia length. Phalloidin staining in these images showed a large punctate artefact across all biological replicates and fields of view (Marked with * in DMSO condition). This was not considered biologically relevant and actin staining was not quantified. Data for cilia incidence was confirmed to be normally distributed using D'Agostino-Pearson omnibus K2 test whereas cilia length data was not normally distributed. Significance was calculated using one-way ANOVAs with a Dunnett's multiple comparisons tests (cilia incidence) and Kruskal-Wallis tests with Dunn's multiple comparisons tests (cilia length). *=p<0.05, ****=p<0.0001. # indicates the control to which all data sets were compared. Error bars represent S.D.

Cytochalasin D induced significant changes to cilia length after just 2 hrs of treatment. This has not been tested before and reiterates the conclusion drawn from KD025 treatment (Figure 3.16) of a fast and dynamic process that overrides other regulatory pathways in the cell to allow increased ciliogenesis in an unsynchronised population of cells.

The second ROCK2 activated pathway that was tested was induction of acto-myosin contraction, which was selectively inhibited with blebbistatin. Blebbistatin selectively targets an ATPase intermediate of myosin II, blocking the myosin heads and resulting in low actin affinity, thus reducing acto-myosin contraction (293). Myosin heavy chains have also previously been implicated in ciliogenesis. Evidence has shown that non-muscle Myosin IIB (Myh10) increases actin dynamics through an antagonistic interaction with Myh9 and a direct interaction with microtubule acetyltransferase Mec17 (101). Myh10 siRNA knock-downs have also been shown to impair ciliogenesis and reduce the apical localisation of ezrin (which is required for centriole docking in multi-ciliated cells (294)). MYH10 has also been implicated in reduced apical migration of centrioles. RPE-1 cells with *MYH10* siRNA knock-down had a significant decrease in cilia incidence and centrioles in these cells were shown to have a more basal localisation than controls which could be rescued with expression of siRNA resistant *MYH10* (100).

RPE-1:LifeAct cells treated with up to 2.5 μM blebbistatin for 16 hrs had a significant increase in cilia incidence compared to cells treated with DMSO. Blebbistatin concentrations ≥5 μM induced apoptosis or mitotic failure, thus presumably any changes in cilia incidence were masked by this cytotoxicity. However, cilia length increased in a dose-dependent manner and was significant in cells treated with 5 μM blebbistatin when compared to DMSO (Figure 3.21). As blebbistatin showed cytotoxic effects after 16 hr treatment, the experiment was repeated with a 2 hr incubation. Cells were initially serum starved for 24 hrs and then fixed following 2 hrs further serum starvation with varying concentrations of blebbistatin. This work showed no significant changes to cilia incidence but there were significant increases to cilia length in cells treated with ≥2.5 μM blebbistatin compared to DMSO (Figure 3.21).

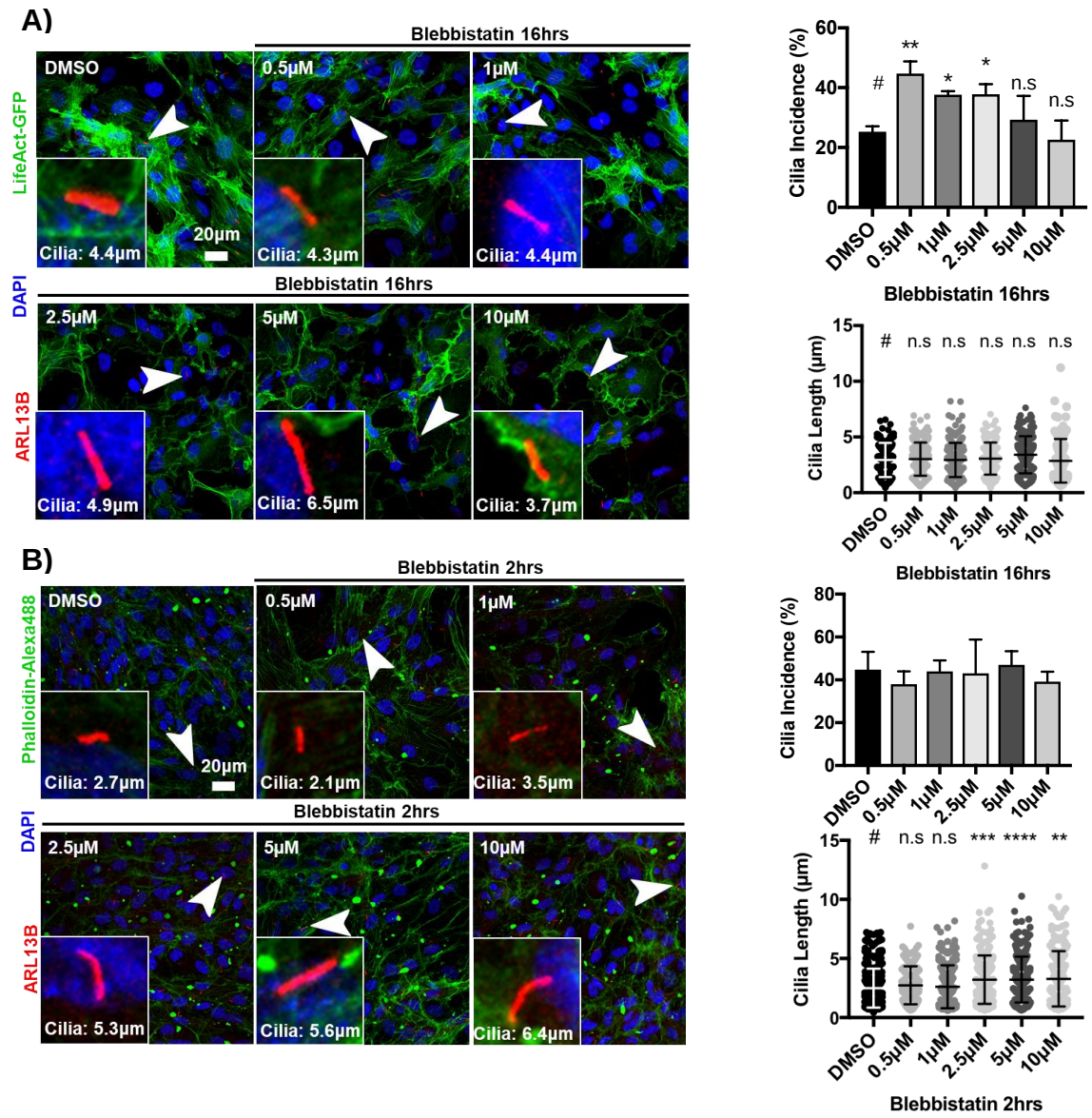

Figure 3.21 Chemical inhibition of acto-myosin contraction increases cilia incidence and length

A) RPE-1:LifeAct cells were treated for 16 hrs with blebbistatin or DMSO vehicle negative control in serum starvation media (0.2 % FBS). Cells treated with blebbistatin between 0.5 μM and 2.5 μM for 16 hrs had a significant increase in cilia incidence. Across all concentrations, there was no significant increase in cilia length. **B)** Wild-type RPE-1 cells were treated with blebbistatin for 2 hr after 24 hr serum starvation. Treated cells did not show any changes in cilia incidence across all drug concentrations. However, there was a significant increase in average cilia length in cells treated with ≥2.5 μM blebbistatin. Phalloidin staining showed large punctate artefacts across all biological replicates (marked with * in DMSO condition). This was not considered biologically relevant and actin staining was not quantified. Data for cilia incidence was confirmed to be normally distributed using D'Agostino-Pearson omnibus K2 test whereas cilia length data was not normally distributed. Significance was tested using one-way ANOVAs with Dunnet's multiple comparisons tests (cilia incidence) or Kruskal-Wallis tests with Dunn's multiple comparisons tests (cilia length). **= p<0.01, ***= p<0.001, ****= p<0.0001. # Is the control to which all data sets were compared. Error bars represent S.D.

The differences in ciliary phenotypes at the 2 time points was not further investigated thus no individual time point exactly phenocopied the *ROCK2* siRNA knock-down (Figure 3.10). Individually only one downstream pathway of ROCK2 is being targeted with the inhibitor treatments, whereas ROCK2 knock-down would affect all downstream pathways. Hence, when the data for both time points for blebbistatin and cytochalasin D treatments are collated, this provides a satisfactory reflection of the ROCK2 knock-down phenotype, showing both an increase in cilia incidence and length over the timescale measured.

3.4.8 Overexpression of a constitutively inactive MLC increases cilia incidence

MLC fusion constructs of rat myosin light chain 9 (*Myl9*) with an N-terminal GFP tag were used to further test the role of MLC and acto-myosin contractions in ciliogenesis. A double-mutant construct with alanine replacements at Thr18 and Ser19 (MLC^{TASA}) was used as a non-phosphorylatable MLC mutant. This mutant had been previously characterised, and expression of the mutant was shown to reduce actin filament bundles or stress fibres which are required for contractility (295). The non-phosphorylatable mutant is a constitutively inactive form of MLC. ROCK2 directly activates MLC by phosphorylation. So it was predicted that overexpression of this MLC mutant would phenocopy a ROCK2 knock-down by replacing the majority of endogenous MLC through a dominant negative mechanism.

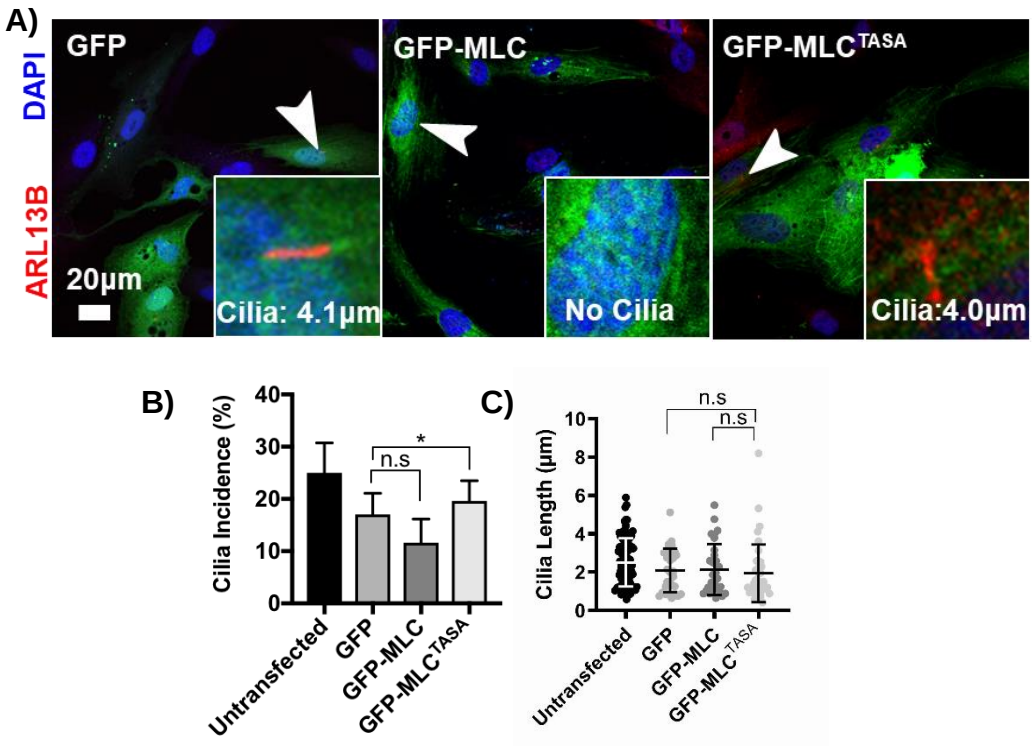

Figure 3.22 Constitutively inactive MLC increased cilia incidence

A) RPE-1 cells were transfected with wild-type or non-phosphorylatable (MLC^{TASA}), GFP-tagged Myosin Light Chain (MLC). These were compared to RPE-1 cells transfected with an un-tagged GFP construct. **B)** Cells that over-expressed active MLC had a moderate decrease in cilia incidence (n=3, p=0.0866) whereas cells expressing MLC^{TASA} had a significant increase in cilia incidence compared to the negative control (n=3, p=0.0174). **C)** There were no significant changes to cilia length in any of the cell populations tested. Data for cilia incidence was confirmed to be normally distributed using D'Agostino-Pearson omnibus K2 test whereas cilia length data was not normally distributed. Significance calculated with unpaired, two-tailed Student's t-tests (cilia incidence) and Mann-Whitney U tests (cilia length). * $p<0.05$. Error bars represent S.D.

3.4.9 Inhibition of ROCK2 can rescue loss of cilia in RPE-1 cells with IFT88 knock-down.

As evidence thus far showed ROCK2 to be a negative regulator of ciliogenesis, it was tested if it could be a potential therapeutic target for rescuing cilia incidence in ciliopathy cell models. *IFT88* and *RPGRIP1L* knock-downs gave robust loss of cilia phenotypes (Figure 3.4) through 2 different mechanisms: loss of intraflagellar transport and disruption of the transition zone, respectively. These knock-downs were used to model a ciliopathy-like phenotype in both mIMCD3 and RPE-1 cells in a high content imaging experiment. mIMCD3 cells

only responded with a significant increase in cilia incidence to KD025 treatment in the negative control cells treated with scrambled (siScr) siRNA. Remarkably however, *IFT88* knock-down in RPE-1 cells saw a complete recovery of cilia incidence after KD025 treatment. Cells with *RPGRIP1L* knock-down did not show any recovery of ciliary incidence (Figure 3.23).

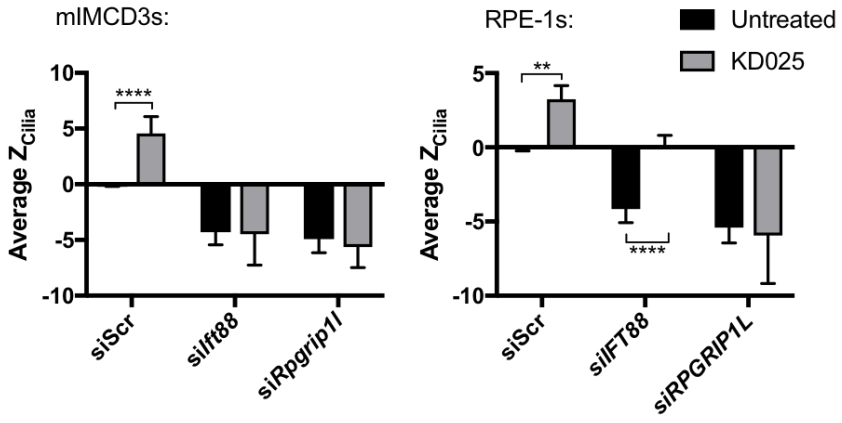

Figure 3.23 KD025 treatment rescues cilia incidence in ciliopathy gene knock-downs

Cells were treated in a high content imaging format with siRNAs to induce cilia loss over 72 hrs. Cells were then left untreated or treated with 1 μM KD025 for the final 48 hrs. **A)** mIMCD3 cells with si*Ift88* and si*Rpgrip1l* knock-downs had significant loss of cilia compared to siScrambled (siScr) controls: average robust z-score for cilia incidence (z_{cilia}) was -4.30 and -4.91, respectively (equivalent to $p<0.0001$). There was a significant increase in cilia incidence, in siScr controls treated with KD025 (z_{cilia}= 4.56). However, there were no changes in cilia incidence in cells with either *Ift88* or *Rpgrip1l* knock-down when treated with KD025. **B)** RPE-1 cells also showed significant loss of cilia in cells with *IFT88* or *RPGRIP1L* knock-down compared to negative controls, with z_{cilia} of -4.15 and -5.40, respectively. There was also a significant increase in cilia in the negative controls treated with KD025 (z_{cilia}= 3.25) and a complete rescue of cilia in the *IFT88* knock-down cells treated with KD025 (z_{cilia}= 0.0016). There was no rescue of cilia incidence in *RPGRIP1L* knock-down cells treated with KD025. Experimental work by Dr. Claire E. L. Smith. Significance calculated by change in average z-score. Where difference between two compared averages is >2.58 **= $p<0.01$, or >3.89 ****= $p<0.0001$. Error bars represent S.E.M.

3.5 Discussion

The 4 main objectives of this part of the project were met; a new data set of potential genes involved in the negative regulation of cilia incidence was generated from a primary whole genome siRNA screen data set. A secondary screen was completed in mIMCD3 cells to identify hits that increased the incidence of cilia across cell populations. The top hit of this screen, *Rock2*, was validated in the human RPE-1 cell line and further investigation into its mechanistic function was carried out.

3.5.1 The secondary screen

3.5.1.1 Generating a list of hits that increased cilia incidence

The filtering method used to generate the final hit list was designed to remove as many false positive hits as possible. However, this inevitably meant some true hits were filtered out. There is inherent variability across cell-based screening and many siRNAs caused a significant increase in one run of the primary whole genome screen but did not have a substantial effect on run 2 of the screen, or *vice versa*. This could be due to the normalisation used for each batch of experimental plates in the screen, or due to due to other technical factors such as plating or transfection efficiency of individual wells or plates.

This is therefore not a definitive list of hits that increase cilia incidence. This can be stated with some certainty since independently identified and validated hits such as *LIMK2*, *GSN* and *ACT3*, were not supported by the primary whole genome screen data and therefore did not pass the filtering used to select hits for secondary screening (Table 3.3). However, the independently identified hits were identified in human cell lines, whereas the primary genome screen data used in this thesis was from a mouse cell line. This highlights the possible differences between the 2 models, or the relative evolutionary importance of ROCK2 between species.

Table 3.3 Previously identified actin regulators of ciliogenesis did not increase cilia incidence in primary whole genome screen data

The 7 genes listed were identified and validated in independent laboratories using RPE-1 cells. However, all the listed actin regulation components decreased or did not affect cilia incidence when knocked-down with siRNA. Over half of the knock-downs caused significant loss of cilia in at least one run of the primary whole genome screen (red text). 2/8 of the hits robustly and significantly decreased cilia incidence with $z_{cilia} \leq -1.96$ in both runs of the screen. From this data set, none of these hits would have been detected as negative ciliogenesis regulators. However, *Cfl1* which codes for Cofilin, an actin severing protein did significant decrease cilia incidence and fits with the model of actin remodelling regulation of ciliogenesis presented in this thesis.

		Wheway et al., 2015 screen data		
Reference	**Gene**	**Run 1**	**Run 2**	**Average z_{cilia}**
Kim et al., 2010	*Actr2*	-5.08567	-1.20536	-3.14552
Kim et al., 2010	*Actr3*	1.551726	-0.94016	0.305783
Kim et al., 2015	*Cfl1*	-4.13656	-1.54851	-2.84254
Kim et al., 2010	*Gsn*	-4.95743	-4.26976	-4.6136
Kim et al., 2015	*Limk2*	-0.05609	-0.98986	-0.52297
Nagai et al., 2017	*Limk1*	-1.90408	-0.82221	-1.36315
Kim et al., 2015	*Tesk1*	-2.59938	-3.09470	-2.84704

3.5.1.2 B-cell Lymphoma Leukemia 10's (*Bcl10*) potential role in ciliogenesis

The average robust Z_{cilia} for B-cell Lymphoma Leukemia 10 (*Bcl10)* knock-down was 2.490, equivalent to p=0.013. There were no previously published studies identifying *Bcl10* as a ciliogenesis modulator, although there is a possible link between *Bcl10* and motile multi-ciliogenesis. Bcl10 activates nuclear factor κB (NFκB), a family of stimuli-induced transcription factors (296). Separately, NFκB has been linked to increased cilia incidence in nasal epithelium through regulation of p63. Inhibition of NFκB or siRNA knock-down of p63 increased microvilli and cilia incidence on human nasal epithelial cells (297). Therefore, it is not unreasonable to predict that loss of *Bcl10* by siRNA knock-down could cause inactivation or lower activation levels of NFκB and, downstream, cause an increase in cilia incidence through reduced p63 expression. However, multi-ciliated cells are known to have very different ciliogenesis pathways compared

to primary ciliogenesis. Without a clear hypothesis for primary ciliogenesis, *Bcl10* was not taken forward for further investigation.

3.5.1.3 Fanconi Anemia Opposite Strand Transcript Protein's (*Fancd2os*) potential role in ciliogenesis

The average robust z_{cilia} for Fanconi anemia opposite strand transcript protein (*Fancd2os*) knock-down was 2.819, equivalent to p=0.0048. *Facnd2os* is highly expressed in the testis and also expressed in the kidney (298). However, very little is known about the function of any encoded protein and it has not been the focus of any published investigation. Some descriptions have been published about its localisation and possible role in the testis (299, 300) but the molecular structure of the protein or localisation within other cell types is still unknown. Without any information, a hypothesis about its role in ciliogenesis could not be made and so it was not taken forward for further validation and investigation.

3.5.1.4 Syntaxin 19's (*Stx19)* potential role in ciliogenesis

Syntaxin 19 (Stx19) is a poorly characterised glutamine-donating soluble NSF attachment proteins receptor (Q-SNARE) that is homologous to syntaxin 11 (38% homology) (301). Syntaxins are involved in protein trafficking and membrane dynamics. Syntaxin 19 localises to the plasma membrane and recycling endosomes in HeLa cells, and although Stx19's exact function remains unknown it has been shown to co-localise with and regulate Rab8-positive vesicles (302). Rab8 is a small GTPase that is involved in intracellular membrane trafficking and is essential for ciliogenesis. Rab8 is activated by co-ordination with Rab11 and Rabin8, both enriched at the base of the primary cilium (303). Rab8 activation leads to cilia elongation and it recruits ciliary-specific membrane proteins such as Smoothened to the cilium, with fusion of Rab8-positive vesicles with the periciliary membrane (304).

Overexpression of GPF-STX19 prevented Rab8 vesicles from fusing with the plasma membrane, suggesting STX19 regulates trafficking and fusion of these vesicles in a dominant negative fashion (302). Current evidence suggests that STX19 works in opposition to the v-SNARE VAMP3 to negatively regulate the fusion of Rab8 vesicles with the periciliary region (304). Therefore, it could be hypothesised that loss of STX19 would allow more Rab8 vesicle fusion during

ciliogenesis, allowing for cilia to be more readily formed and perhaps also likely to be longer.

However, *Stx19* is still reasonably uncharacterised and so further investigation of this hit was considered to be out of the scope of this project, but would be of interest to take forward for further investigation at a later date.

3.1.1.1 ROCK2 is a top hit and not ROCK1

ROCK2 had not been directly shown to be a negative regulator of ciliogenesis in previous studies, but downstream actin remodelling pathways activated by ROCK have provided indirect evidence for the importance of actin remodelling in controlling cilia incidence and length (92-94) Thus, the current published evidence suggests that a highly complex network of pathways and regulators control the actin cytoskeleton's role during ciliogenesis. However, the isozyme of ROCK2, ROCK1 was not shown in the secondary screen or downstream work to have a significant role in ciliogenesis.

RhoA-associated protein kinases (ROCK) are part of the AGC serine/threonine kinase family. ROCK2 is a homologue of ROCK1 and these proteins display 67% homology across the full length of their amino acid sequences (284). They have an N-terminal kinase domain (KD) for which they share 92% homology (284), a central coiled-coiled region including a RhoA binding domain (RBD), and a C-terminal plekstrin homology domain and cysteine rich C1-domain (114). Both ROCK1 and ROCK2 form and act as homodimers (305-307) through interaction from the N-terminal extension of the KDs to the coiled-coiled domains. The homodimers therefore have dimerised KDs which are able to phosphorylate monovalent and possibly dimerised substrates (305). ROCK1 and ROCK2 homodimers have an auto-inhibitory structure that blocks their kinase activity, keeping them in an inactive conformation. They act as a molecular switch and upon binding of RhoA-GTP to the RBD, a conformational change releases the C-terminal region from blocking the KD and thus activates the proteins (308) (Figure 3.24).

A)

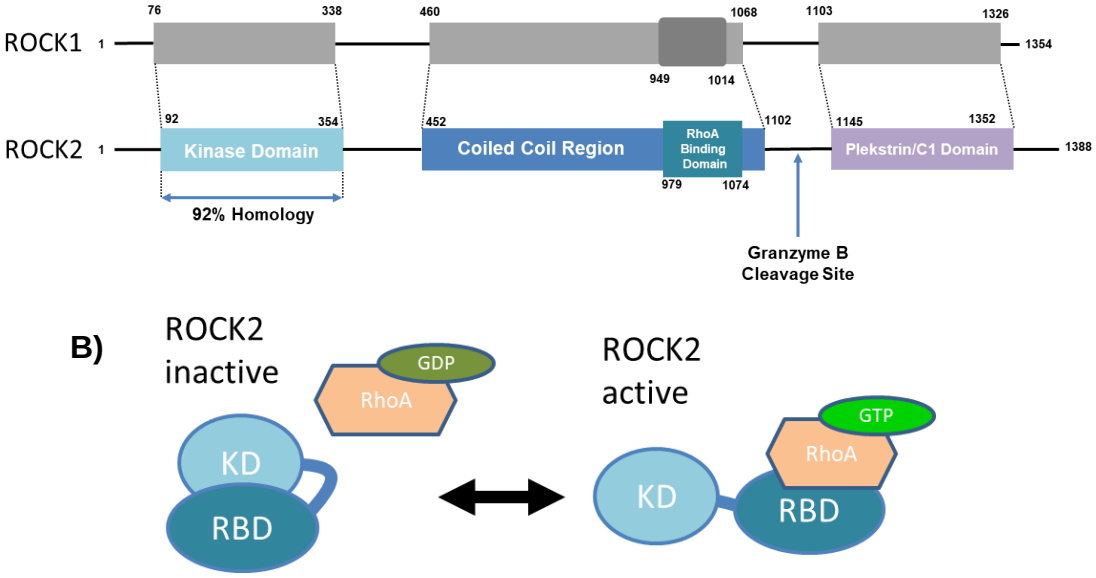

Figure 3.24 ROCK2 protein domains and activation

A) Schematic diagram of mouse ROCK1 and ROCK2 protein domains, modified from (309) Figure 1 with copyright permissions. ROCK structure and modes of regulation. Use licensed under the Creative Commons Attribution 4.0 International License. **B)** Schematic diagram of the activation and conformational changes of ROCK2. ROCK2 has an auto-inhibitory structure where the kinase domain (KD) activity is blocked by the RhoA-binding domain (RBD). ROCK2 is activated by RhoA-GTP which binds to the RBD. Once bound, there is a conformational change that releases the kinase domain to allow phosphorylation of targets.

When activated by RhoA-GTP, ROCKs (both ROCK1 and ROCK2) phosphorylate a large number of proteins and activate several downstream pathways to regulate actin remodelling and dynamics. They have therefore been highly investigated for their role in cell adhesion (292, 310), stress fibre and focal adhesion formation (311, 312), and cell motility/migration (reviewed in (313)). ROCK controls these cellular mechanisms by directly phosphorylating key actin regulators. ROCK phosphorylates LIMK2 (314), which in turn phosphorylates cofilin to modulate F-actin stabilisation (315). ROCK also phosphorylates MLC (289) and MYPT1 (316), to control acto-myosin contraction and the formation of stress fibres (317). Further to this ROCK also phosphorylates EZR regulating the linking of the actin cytoskeleton to the plasma membrane (318).

These apparent differences between the isozymes in other molecular mechanisms highlights several ways in which the specificity of ROCK2 can exist

over ROCK1 in the negative regulation of ciliogenesis. However, more clarity into the differing roles in ciliogenesis could be tested with ROCK1 specific inhibitors and with the development of the cell lines described in Figure 3.18.

3.1.2 Limitations

3.1.2.1 Screening

The primary whole genome screen was carried out in mIMCD3 cells. Upon reflection, given the inconsistencies between cell types and the data from the primary whole genome screen not correlating with independently-verified hits (Section 3.5.1), a genome screen data set from RPE-1 cells may have been more relevant. Previous ciliary whole genome screen data sets from RPE-1 cells (93, 96) could have also been re-tasked separately, or correlated with the primary genome screen data used throughput this thesis. Including several screening datasets would have increased statistical power when identifying true positive hits that are conserved between both mouse and human, or across different tissue types. This strategy could highlight more clinically-relevant therapeutic targets for ciliopathy patients.

There was a reasonably low validation rate in the secondary screen. This could be due to a high number of false negatives in the whole genome screen data or the stringent filtering steps used to generate the secondary screen hit list. However, as previously noted this stringent filtering ensured a robust methodology and data set to test, with the downside of likely missing other hits. It should be noted that the whole genome screen data (Section 3.5.1) does not identify the same hits as independently published data, so it is possible that the whole genome screen had a high false negative rate.

3.1.2.2 Drug specificity and potency

The specificity of the inhibitor KD025, although previously tested and verified (288), was not confirmed as part of this thesis. Therefore the statements made are based on an assumption that KD025 is truly specific to ROCK2 since it does not exactly reiterate the siRNA knock-down phenotype. The siRNA knock-down did not cause a significant increase in ciliary incidence 72 hrs post siRNA transfection (Figure 3.10), whereas 48 hrs KD025 treatment did show a significant increase in cilia incidence at all concentrations (Figure 3.16). It is

possible that these differences in time points are influencing the phenotypes measured. siRNA treatments were for 72 hrs and although an approximately 80% total protein reduction was confirmed by western blots over this time, it may require longer for the knock-down to have the same level of inhibition as KD025 which acts instantly (Figure 3.9). Indeed, given the catalytic nature of kinase activities complete blockade of ROCK2 activity by siRNA treatment seems unlikely, a major reason for identifying small molecule inhibitors of this kinase to facilitate the mechanistic work presented here.

The potency of both cytochalasin D and blebbistatin were also only qualitatively assessed by observing changes in the actin cytoskeleton and overall cell morphology. There was no quantified measure to show the inhibition of either actin polymerisation or acto-myosin contraction, respectively.

3.1.2.3 Live actin imaging and actin stains

The polyclonal RPE-1 cell line expressing GFP-LifeAct was used to qualitatively assess the potency of drug treatments through changes to the actin cytoskeleton. What was not initially taken into account was that LifeAct expression alone can change actin dynamics, so requires optimisation, and it does not bind to specific actin structures (reviewed in (319)). Phalloidin was therefore also used on fixed cells to confirm this data, despite the non-specific staining and imaging artefacts occasionally seen with this stain (Figure 3.20A and Figure 3.21B)

3.1.2.4 ROCK2 over-expression

The data presented in Figure 3.11 showed the opposite phenotype to that noted with the siRNA knock-down of ROCK, providing evidence that the phenotype observed with siRNA knock-down was specific to *ROCK2* and not an off-target effect. However a dominant negative effect on ciliogenesis with GFP over-expression alone was noted in RPE-1 cells. Thus, it must be considered that GFP-mROCK could also be acting through a separate dominant negative effect to decrease ciliogenesis, rather than the proposed mechanism of actin remodelling. It is also possible that over-expressed mROCK was affecting overall cell viability through global sequestering of RhoA.

3.1.2.5 Phospho-Myosin Light Chain Antibodies

The antibodies used to confirm the inhibition of ROCK2 did not give reproducible results by western blot (Appendix F) and instead were used for high-content image analysis. The raw image analysis was based on the presence of acto-myosin fibre-like structures, but unfortunately co-staining with phalloidin to visualise actin had interfering background staining. This staining was not considered to be biologically relevant but it meant that actin co-localisation with the phospho-MLC staining could not be quantified. A clear and strong qualitative change in both staining intensity and the presence of fibres could be seen across the raw image data, but quantified data only showed marginal changes. This may be due to the lower image quality that is generated by high content imaging, or it could indicate that the analysis method needs further optimisation.

3.1.2.6 Cell confluency affects ciliogenesis

It is well documented that confluence of cells in culture affects their ability to ciliate. Thus all experiments were plated with the same cell number to minimise any effect of cell confluence on ciliogenesis. 48 hrs and 16 hrs drug treatments affected cell number due to cell death or inhibition of cell cycle progression, but nevertheless were able to induce significant increases in ciliogenesis. However, the role of acto-myosin contraction in ciliogenesis has been shown to be greatly affected by cell shape and therefore also confluency (320).

RPE-1 cells grown on a micro-pattern of different sizes enable different levels of cell spreading. Cells grown in smaller micro-patterns ciliated more readily than cells that were more spread and flat. These flatter cells were treated with blebbistatin, causing a significant increase in cilia incidence (321), in agreement with the data presented in Figure 3.21. However, a second study has shown that RPE-1 cells grown on smaller micro-patterns had a much rounder shape, and that centrosome migration and presumably ciliogenesis was reduced by blebbistatin treatment (322). This is consistent with the hypothesis that acto-myosin contraction is required for the assembly of microtubule bundles that provide the driving force for centrosome migration (322). This was not tightly controlled for in this work as although cells were consistently seeded at the same density, blebbistatin treatment was not tested at variable cell densities.

Therefore, this observation may be specific to RPE-1 cells grown in a thin monolayer and may be different for other cell types that have a rounder shape and greater height.

3.1.2.7 Interpretation of drug treatment time points

A comparison between 2, 16 and 48hrs for drug treatment should be made with caution. Each experiment was completed with a different batch of RPE-1 cells as independent experiments. This would likely affect the baseline cilia incidence in each of the DMSO control conditions (as seen when comparing 2 and 16hrs DMSO treatment for blebbistatin (Figure 3.21)), As the time points were not collected as part of the same experiment the affect and timing on overall ciliogenesis is hard to interpret. A possible way to overcome this would be to look at average fold change, percentage change in cilia incidence and length or to normalise the data. However, the investigation into the timing of ciliogenesis and the effect of each drug was out of the scope of this project and so data was not analysed in this way.

3.1.3 Future Experiments

3.1.3.1 Rescue experiment

The specify of the ROCK2 siRNA could have been validated with an overexpression construct that is not targeted by the siRNA. This would then rescue cilia incidence down to WT levels. The same experiment could be completed with a construct for ROCK1. These are possible future experiments to provide further evidence in support of the specificity of ROCK2 to ciliogenesis.

3.1.3.2 ROCK2 localisation

As an antibody suitable for immunofluorescence detection was not available, it would be of interest to specifically track ROCK2 through the cell cycle and confirm it’s localisation in these cell types compared to ROCK1. It would be of particular interest to observe if and when ROCK2 localises with centrosomes as this may suggest localised changes to actin remodelling, rather than global remodelling, promote ciliogenesis. This could also be done through live cell imaging of ROCK2 if the cell lines presented in Figure 3.18 were remade and

validated. ROCK2 may be localised to the base of the cilium where it negatively regulates ciliary length by preventing vesicle trafficking of ciliary vesicles. Fluorescence recovery after photobleaching (FRAP) of ciliary vesicles could be used to determine if there is a change in the speed of trafficking to the cilium when ROCK2 is inhibited and the result would provide insights into the dynamics and timing of ciliogenesis. Experiments using the KD025 inhibitor on synchronised cells could also be used to more finely define the timing of signalling which causes the inactivation of ROCK2 and allows for dynamic actin and ciliogenesis to occur.

3.1.3.3 Ciliary function

Longer cilia have been shown to have diluted signalling and reduced functionality. As cilia length increased in both cell models tested with ROCK2 knock-down, ciliary function tests should be carried out. Further investigation could include testing the Shh pathway with a Gli reporter assay, or observing translocation of Smoothened into the cilium upon Shh activation following SAG treatment. It may be that, as there is increased vesicle trafficking as suggested by Kim *et al.* (98), that there is also an increased delivery of signalling receptors, so longer cilia may remain functional. Conversely, signalling may be slower as receptors and signals will have further to travel through a longer cilium and are diluted along the longer ciliary membrane. In turn it would also be of importance to confirm rescue of ciliary function and not just ciliary incidence in the RPE-1 cells after *IFT88* knock-down and KD025 treatment (Figure 3.23).

3.1.3.4 Acto-myosin contraction

As discussed in section 3.1.2.6, cell shape and confluency affects the impact of blebbistatin treatment on ciliogenesis. Future work should corroborate these results for RPE-1 cells grown on micropatterns, or assess the effect of blebbistatin on cell-line types relevant to disease manifestation in ciliopathies such as kidney, liver or bone cell-lines.

It should also be determined which signalling pathways are activated when acto-myosin contraction is inactive, and how these contribute to ciliogenesis. As has been shown previously for F-actin and the role of Hippo signalling on vesicle trafficking (92), the signalling pathways and mechanistic insights into

acto-myosin contractions during ciliogenesis could offer a new downstream therapeutic target of ROCK2 and potentially further our understanding of basal body migration and docking.

3.1.3.5 Other hits

Other hits in the secondary screen, such as syntaxin 19, could be followed up in a separate research project to further investigate its role in Rab8 vesicle trafficking and negative regulation of ciliogenesis. If data is re-analysed and compared to other whole genome siRNA screens, further hits could also be revealed for downstream analysis.

Chapter 4

Results: RACGAP1-mediated cytokinesis is not a prerequisite for centriole maturation and ciliogenesis

4.1 Introduction

The previous chapter presented evidence that repurposing and reanalysing a whole genome reverse genetics screen dataset can provide novel biological insights. Chapter 3 provided further support that actin regulation and acto-myosin contraction are fundamental negative modulators of ciliogenesis. In this chapter, the whole genome screen dataset was therefore reanalysed for possible negative regulators of number of cilia per cell. The primary screen counted individual cilia as spots (using a cilia recognition algorithm) within a defined cell boundary, enabling re-analysis to identify populations of cells with more than one cilium per cell (Figure 4.1). Therefore, the second main phenotype that was taken forward for secondary screening was a series of knock-downs that caused an increased incidence of cells with two or more cilia, referred to in this thesis as a supernumerary cilia phenotype.

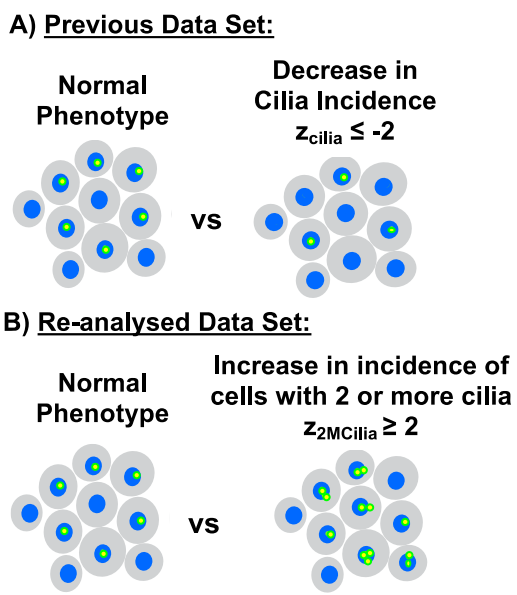

Figure 4.1 Re-analysis of whole genome screen data

Schematic diagram comparing the phenotypes assessed in the original whole genome screen, which was used to identify positive regulators of ciliogenesis **(A)** and the analysis of the proposed phenotypes of negative regulators of ciliogenesis **(B)** measured from the raw screen data. As cell boundaries and spots (cilia staining) are defined separately it is possible to calculate the number of spots per cell.

Multi-ciliated cells are cells with many cilia, which are most commonly found as motile ciliated cells, such as lung epithelium and ependymal cells. Exceptions to this include choroid plexus cilia. or olfactory sensory neuronal cilia that, despite having the 9+2 microtubule arrangement, lack the dynein arms required for motility and are present as multi primary ciliated cells (11). Most other cell types have a single primary, immotile cilium (323). Ciliogenesis is notably different between these cell types (54, 324, 325). Multi-ciliogenesis requires large multiplication of centrioles for the subsequent formation of multiple cilia, whereas primary ciliogenesis is a process tightly controlled for only a single duplication. It also requires extensive ciliary resources and machinery.

Unlike in primary ciliogenesis where centrosomes duplicate from the mother centriole, in multi-ciliogenesis of motile cilia the centrioles are either formed from the mother centriole, via a cytoplasmic structure called the deuterosome (a protein complex required for pro-centriole biogenesis that stem from existing centrioles) in the deuterosome-dependent pathway, or using a centriole-dependent assembly pathway (326, 327) (Figure 4.2). It has been shown in *Xenopus* embryos that production of centrioles from the deuterosome is mediated by Multicilin (328, 329), DEUP1 (a *Cep63* paralogue) (327) and CCDC78 (330), which in turn regulate the localisation of CEP152 (327), also a main regulator for centriole biogenesis in standard centriole duplication (331). The deuterosome is signalled to form when Notch signalling is downregulated. It has been shown in *Xenopus* multi-ciliated cells that reduction of Notch signalling causes transcription of Multicilin, which in turn causes increased expression of centriole assembly genes including DEUP1 when in complex with E2F4 (328). This allows biogenesis of new centrioles from the deuterosome structure, a poorly understood event.

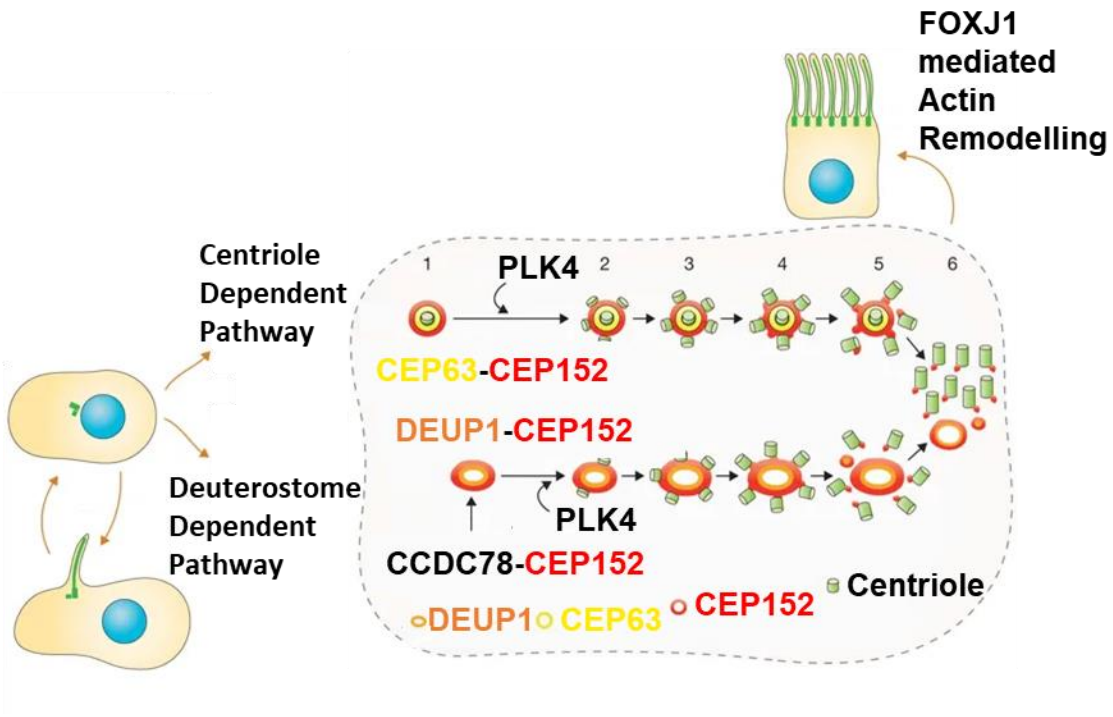

Figure 4.2 Schematic of multi-ciliogenesis of motile cilia pathways

Cycling cells that differentiate into multi-moitle-ciliated cells can do so one of via two pathways, the centriole-dependent pathway, or the deuterosome-dependent pathway. The centriole dependent pathway has similarities to normal centriole duplication and involves many of the same proteins including CEP63 and CEP152 to initiate amplification. This occurs through PLK4 activation, causing centriole biogenesis in a rosette formation around the mother centriole. The deuterosome-dependent pathway relies heavily on its main protein DEUP1 which is expressed through multicilin-mediated transcriptional regulation. CEP152 is recruited by CCDC78 and together they mediate centriole biogenesis from the deuterosome structure. After biogenesis the centrioles migrate to become basal bodies and form cilia. Schematic modified from Figure 2 of Reference (326) with copyright permissions.

Once formed the centrioles migrate to the apical cell surface to form basal bodies as in primary ciliogenesis. The migration and docking of this mass of centrioles requires support and stabilisation from the actin cytoskeleton. This dynamic actin polymerisation is regulated by FOXJI via Ezrin and RhoA. The actin web that supports the multiple basal bodies is not present for primary cilia, but primary cilia have been shown to rely on dynamic actin remodelling for migration and basal body docking (103, 332).

It has also been shown that U2OS cells, which normally form primary cilia, can be forced to produce supernumerary centrosomes if regulators of multi-

ciliogenesis such as DEUP1 (327) are overexpressed. This demonstrates that the deuterosome-dependent pathway can over-ride normal centriole regulation.

There are some documented ciliopathy phenotypes with supernumerary cilia in affected tissues, allowing us to gain possible new insight into ciliopathy disease mechanisms. Meckel-Gruber syndrome patients with *MKS1* or *TMEM67* (also known as *MKS3*) mutations have supernumerary centrosomes, spindle poles and primary cilia in foetal kidney cysts in addition to significantly increased ciliary length (333). Polycystic kidney disease is another ciliopathy caused by mutations in *PKD1* (334). Patient primary renal epithelial cells display supernumerary cilia as a downstream consequence of supernumerary centrosomes that is associated with aneuploidy and genomic instability (334). Supernumerary cilia dilute ciliary signalling receptors and signalling responses and this dysregulated signalling is thought to be the mechanism behind cyst formation, however it is not fully described (335). Targeted resorption of supernumerary cilia has been suggested as a possible therapeutic intervention for autosomal dominant polycystic kidney disease in order to reduce cyst formation and slow disease progression (336), although this approach first requires a suitable drug target to be identified.

The presence of two or more cilia in both kidney and retinal cell types would be of interest to gain further insight into disease pathology. Negative regulators of ciliogenesis or centriole maturation could give insight into ciliopathy disease mechanisms as supernumerary centrosomes are currently the only described disease mechanism seen in ciliopathies with supernumerary primary cilia. Overall, the details of the mechanisms that determine the formation of multiple primary cilia from these supernumerary centrosomes is only understood in the sense that supernumerary centrosomes are retained after failed cytokinesis and can form the supernumerary cilia (335).The authorisation pathway, or lack of a negative regulator, for the maturation of more than one mother centriole and production of excess ciliary proteins for assembly of the supernumerary cilia have yet to be defined.

It is therefore of interest to identify the molecular pathways or genes involved in the formation of supernumerary cilia, including any potentially independent of the cell cycle and processes that licence the maturation of over-duplication of

centrosomes. These are presumably independent pathways to centrosome biogenesis which has previously been screened for in an independent whole genome siRNA screen (261). This screen identified TRIM37 as a negative regulator of centriole duplication (261), therefore it would be of interest to see if this hit can also produce supernumerary cilia or if the pathways, as hypothesised are independent.

These mechanisms could also give insight into processes such as centrosome over duplication in cancer development, where a loss or suppression of primary cilia allows unregulated proliferation and migration. This has been specifically noted in pancreatic cancer (337, 338). Paradoxically however, supernumerary centrosomes can also cause cancer cell death due to abnormal mitosis when each centrosome forms individual spindle poles (339) and cilia have been noted to increase choroid plexus tumour growth through facilitation of Sonic hedgehog signalling (340).

The presence of two or more primary cilia or supernumerary centrosomes are often noted as a disease phenotype as most normal human cells do not have multiple primary cilia. However, there is one cell type that has supernumerary centrosomes and no cilia. Hepatocytes, as they age, become tetraploid and retain supernumerary centrosomes (341) yet are one of the 2 cell types alongside red blood cells that do not produce any primary cilia (although published data has only reported on the hepatocytes of rat models (342, 343)). If these cells did have the capacity and necessity, to form cilia, due to their multiple centrosomes they would likely produce multiple primary cilia. However, this may be the exact reason that ciliogenesis does not occur in these cells; since multiple cilia are associated with disease, they may have inhibited ciliogenesis altogether to prevent this occurring. Rather than having a specialised signalling hub and signalling responses, once terminally differentiated these cells would signal through receptors on the cell membrane. The production of multiple primary cilia would be deleterious to the cell, as it has been shown in previous studies that supernumerary cilia dilute signalling receptors and slow signalling responses (335).

In summary, hits that cause supernumerary cilia in an unbiased whole genome reverse genetics screening dataset have the potential to identify novel pathways or provide further insights into ciliopathy disease mechanisms.

4.1.1 Chapter Aims Objectives

Aim: To improve ciliopathy patient quality of life through greater understanding of their genetic disease and though identifying potential therapeutic pathways.

More specifically, this chapter aims to identify the novel regulatory pathways or mechanisms that control the formation of a single primary cilium rather than multiple primary cilia.

Hypothesis: Cells such as olfactory neurones have several primary cilia, and cells such as hepatocytes have multiple centrosomes but no cilia. This highlights that differentiated cells have the capacity to generate more than one primary cilium and to prevent ciliary formation entirely. Therefore there is likely a regulatory pathway or molecular switch that controls a cells ability to produce a single primary cilium or generate multiple primary cilia, that has yet to be identified.

Experimental Objectives:

- To generate a data set of potential hits that increase the incidence of cells with two or more cilia from existing whole genome reverse genetics screening data (a supernumerary cilia phenotype)
- To carry out secondary screening and identify candidates to take forward for further investigation
- To validate hits in human cell line models
- To examine mechanistic links between validated hits and the regulation of ciliogenesis for a single cilium in comparison to multiple primary cilia.

4.2 Whole genome screen hits that increased the incidence of supernumerary cilia

A primary whole genome cell-based reverse genetics visual screen data-set (266) was reanalysed to identify hits that significantly increased the incidence of supernumerary cilia, specifically measured through a high content imaging algorithm for “cells with two or more cilia” (Appendix E.2). Similar filtering steps to those used to generate the “increased cilia incidence” hit lists in Chapter 3, were used to remove hits that: (i) did not cause a significant phenotype in both biological replicates of the primary screen; (ii) affected cell number; (iii) did not have on-target siRNAs for all annotated transcripts; and those hits for which there was not a human orthologue for follow up experiments.

Initially these 3 filtering steps were designed to generate a hit list that could identify a novel pathway involved in licencing supernumerary cilia that was unlinked to the cell cycle. However, there were only 14 hits that passed through all 3 stringent filtering steps (Figure 4.3). Enrichment analysis also showed that there was no enrichment for any Gene Ontology (GO) terms, Kyoto Encyclopaedia of Genes and Genomes (KEGG) pathways, Protein Families Database (PFAM) protein domains or Integrative Protein Signature Database (InterPro) protein domains and features in these 14 hits. Therefore a 10% secondary validation rate would only highlight a single hit to investigate.

The largest loss of hits occurred after filtering step two, which was designed to exclude hits that had any significant changes to cell number, as centrosome duplication is known to be tightly linked to cell cycle regulation (344). Without this filtering step, a list of 91 hits was generated (Figure 4.4) (Appendix A.1.2, Table A.2). The risk of not including the cell number filter and taking forward a longer hit list, was that known cell cycle regulators could be false positive hits that have no direct link to ciliogenesis. However, less stringent filtering allowed for fewer false negative hits to be lost.

A) **Whole Genome Data Set:**
19097 Data Points

Filter 1
Increased Number of Cilia Per Cell
Criteria
Z-Score of "% of cells with ≥2 cilia" must be >2 in both biological replicates
No. of hits
96

Filter 2
No effect on cell number
Criteria
Z-Score of cell number must be 2>x>-2 in both biological replicates
No. of hits
18

Filter 3
Final Filtering
Criteria
Hits must have a human homologue; siRNA must have no off-target effects and target all transcripts.
No. of hits
14

B)

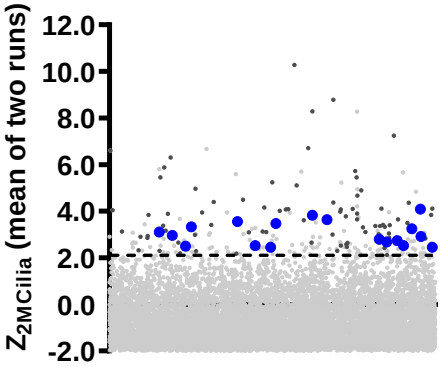

C)

Gene	Average z_{cell}	Average $z_{2Mcilia}$
Cnih3	0.798	2.965
Dcps	-0.683	2.498
Dnajc9	-0.074	3.332
Hectd2	0.030	3.548
Kif27	-1.174	2.527
Mapk8ip3	0.306	2.457
Mkl1	-0.818	3.475
Phox2a	-0.580	3.636
Sox2	-1.119	2.793
Supt7l	-0.554	2.677
Tmed6	-1.323	2.740
Ubn2	0.088	3.242
Vpreb3	0.952	4.088
Vps53	-1.276	2.912

Figure 4.3 Original filtering Steps used to identify hits that increase the incidence of two or more cilia per cell

A) The work flow of filtering steps that were used to identify hits that increased the incidence of cells with two or more cilia. Three filtering steps were initially used to select hits that were; unlikely to give false positive results, could be taken forward for validation in human cell lines and could potentially identify novel pathways that regulate or maintain cilia. However, as only 18 hits passed Filter 2, this step was removed and the hits that passed Filter 1 and Filter 3 only were taken forward for subsequent screening. All 96 hits from Filter 1 also passed Filter 3. **B)** Scatter graph shows average z-score for incidence of cells with two or more cilia across the whole genome screen. Dark grey indicates hits that passed Filter 1, all of thee hits were taken forward for secondary screening. Light blue hits passed Filter 2 and Dark blue highlights the 14 hits that passed all three filtering steps. (6872 data points are outside y-axis limits). **C)** List of the 14 final hits made with stringent filtering. Genes are listed with their average z_{cell} and average $z_{2Mcilia}$ numbers from the primary whole genome screen.

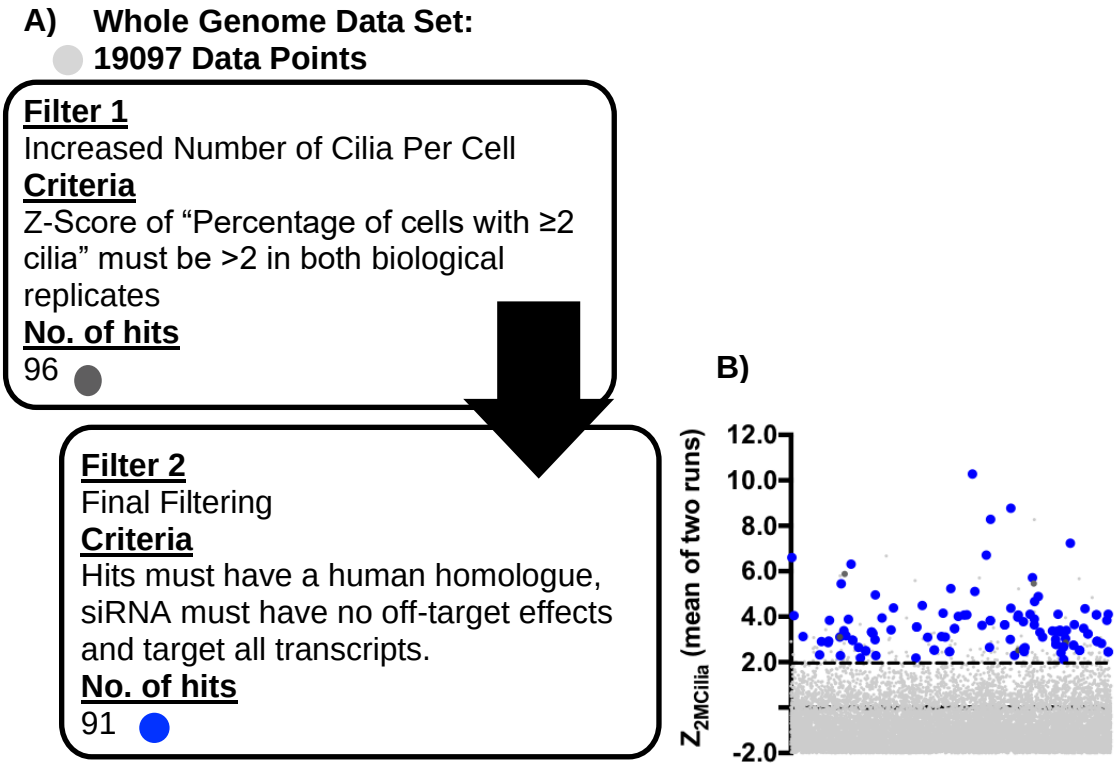

Figure 4.4 Adapted filtering steps to identify hits that increase the incidence of cells with two or more cilia

A) The flow chart to represent the filtering steps used to generate the final hit list of 91 hits that were taken forward for secondary screening. This filtering minimizes the potential for false negative hits and is also more likely to be biologically relevant since it is enriched for specific GO terms and KEGG pathways (Table 4.1). **B)** Scatter graph of whole genome screen data highlighting the final 91 hits taken forward for secondary screening in dark blue. (6872 data points are below the y-axis limit of -2)

As expected, the final data set was highly enriched in KEGG pathways for cell cycle genes. Search tool for recurring instances of neighbouring genes (STRING https://string-db.org/) (272) analysis identified a central network of G2/M transition genes and peripheral nodes involved in DNA replication (Table 4.1 and Figure 4.5). This dataset therefore has the potential to identify new links between cell cycle regulation and ciliogenesis.

Table 4.1 Gene Enrichment in the final hit list for the increase in incidence of cells with two or more cilia secondary screen

The 91 hits are enriched for genes encoding nuclear proteins (43/91). The data set is also significantly enriched for cell cycle genes, approximately 10% (9/91) when compared to the whole genome.

FINAL HIT LIST **PPI enrichment p-value: 0.00248**			
Pathway ID	**Pathway**	**No. of Hits**	**False Discovery Rate**
Gene Ontology (GO) – Cellular Component			
GO:0097125	Cyclin B1-CDK1 complex	2/91	0.0158
GO:0070013	Intracellular Organelle Lumen	31/91	0.0158
GO:0044446	Intracellular Organelle Part	47/91	0.0158
GO:0044428	Nuclear Part	31/91	0.0158
GO:0031981	Nuclear Lumen	29/91	0.0158
GO:0005634	Nucleus	43/91	0.0158
GO:0061695	Transferase Complex, Transferring Phosphorus-Containing Groups	6/91	0.0189
GO:0043231	Intracellular Membrane-Bounded Organelle	53/91	0.0216
GO:0005654	Nucleoplasm	22/91	0.0244
KEGG Pathways			
mmu04110	Cell Cycle	6/91	0.0011
mmu03030	DNA Replication	3/91	0.0191
UniProt Key Words			
KW-0539	Nucleus	36/91	0.0064
KW-0832	Ubl conjugation	19/91	0.0464
KW-0765	Sulfation	3/91	0.0464
KW-0131	Cell Cyle	9/91	0.0464
KW-0010	Activator	9/91	0.0464

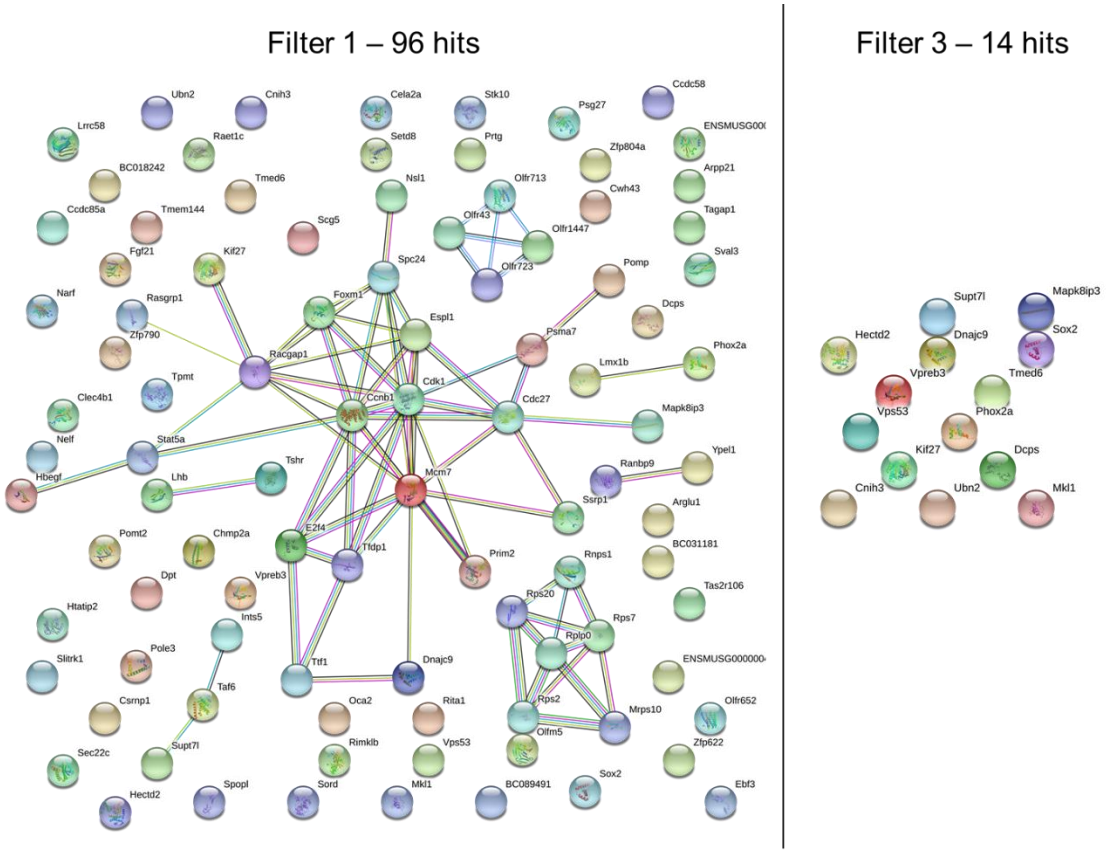

Figure 4.5 STRING analysis of the final 91 hits for the increase incidence of cells with two or more cilia secondary screen

A clear network of genes is present from the STRING analysis (https://string-db.org/) (272)of the final 91 hits. The central nodes (eg. *Ccnb1*, *Cdk1*) are involved in the G2-M transition of the cell cycle and the more peripheral nodes of the network (eg. *Prim2*, *Tfdp1*) are involved in DNA replication. The original, more stringent, hit list of 14 genes does not have any known interactions within the dataset when assessed using STRING analysis. Pink lines represent experimentally determined interactions, light blue lines represent interactions found in curated databases, black lines represent genes that are co-expressed, yellow lines represent genes that are co-mentioned in published abstracts.

4.3 Increased incidence of supernumerary cilia: secondary screen

A secondary validation screen of the 91 candidate hits was performed using smartpool siRNAs of a different chemistry (Dharmacon ON-Target Plus siRNA). This screen followed the same general methodology as described in Chapter 3. The screen did not include a positive control for supernumerary cilia, but the image analysis algorithm used for high content imaging of cilia was validated by controls that decreased cilia incidence. The same controls used in the increase of cilia incidence screen were retested and found to be suitable for this secondary screen (Figure 4.6).

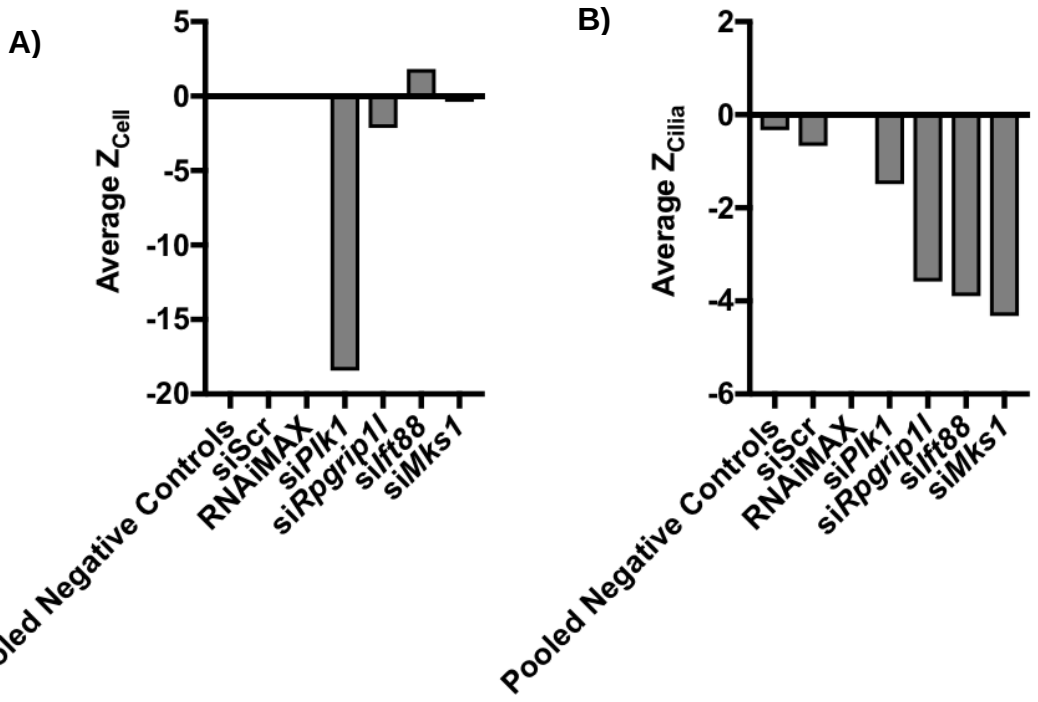

Figure 4.6 siRNA negative and positive controls in the supernumerary cilia (increased incidence of cells with two or more cilia) secondary screen

A) The average robust z-score of all the control siRNAs for cell number (z_{cell}). Average calculated across 2 biological replicates of the increased incidence of cells with 2 or more cilia secondary screen. The positive control for transfection, si*Plk1*, has average z_{cell} of -18.425 which indicates a very high transfection efficiency across the screen. **B)** Negative and positive controls for cilia incidence validated the image analysis algorithm used for high content imaging of cilia. Average robust z-scores for cilia incidence (z_{cilia}) for si*Rpgrip1l*, si*Ift88* and si*Mks1* were -3.580, -3.896 and -4.327 respectively.

This secondary screen had to be repeated 3 times as one biological replicate failed qualitative testing (as outlined in Chapter 2, Section 2.2.17.2). Correlation between the final 2 biological replicates taken forward for analysis was low, with a Pearson's correlation co-efficient of only 0.1716 when comparing the robust z-scores for incidence of cells with 2 or more cilia ($z_{2MCilia}$) between replicates (Figure 4.7).

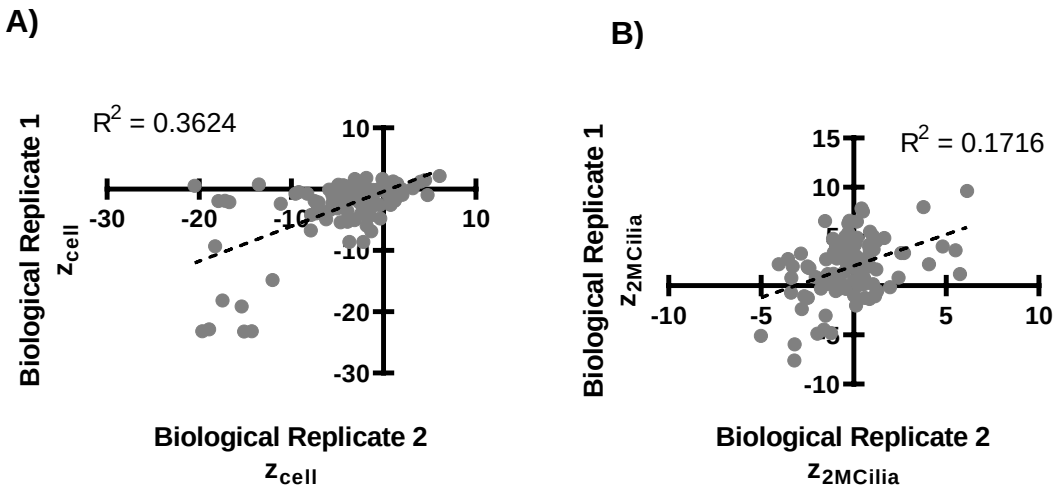

Figure 4.7 Correlation between separate biological replicates of secondary screens for cell number and supernumerary cilia

Scatter graphs showing the correlation between the 2 successful biological replicates of the supernumerary cilia secondary screen. **A)** Pearson's correlation co-efficient (R^2) is 0.3624 when comparing robust z-scores for cell number (z_{cell}). **B)** The R^2 for comparing robust z-scores for supernumerary cilia ($z_{2MCilia}$) is 0.1716. R^2 for both phenotypes are below 0.5, suggesting poor reproducibility of the results or large experimental variation between biological replicates.

4.3.1 Hits from the secondary Screen

After qualitative and statistical analysis, 10 hits (Table 4.2) were shown to significantly increase the incidence of supernumerary cilia, with average robust $z_{2MCilia}$ scores >1.96 (Figure 4.8). The total of 10 hits meant the screen had a validation rate of 11%. The final data set had 3/77 negative controls with an average $z_{2MCilia} \geq 1.96$ and the screen therefore had a false positive rate of 3.9%. The false negative rate could not be calculated, but hits in both the whole genome and secondary screens may have been missed due to false negatives.

Table 4.2 Validated hits from the increase supernumerary cilia secondary screen

Validated hits from the increase supernumerary cilia secondary screen. The average z-scores (rounded to 3 decimal places) from 2 biological replicates are shown for cilia incidence (z_{cilia}), incidence of cells with two or more cilia ($z_{2Mcilia}$) and cell number (z_{cell}). Hits are ordered from highest to lowest based on the $z_{2Mcilia}$ score.

Gene	*Accession No.*	z_{cilia}	$z_{2Mcilia}$	z_{cell}
Racgap1	*NM_012025*	*-9.764*	*10.141*	*-14.965*
Cdk1	*NM_007659*	*-8.713*	*7.769*	*-13.243*
Espl1	*NM_001014976*	*-3.625*	*7.455*	*-14.877*
BC089491	*NM_175033*	*-0.828*	*4.399*	*-4.101*
Tfdp1	*NM_009361*	*-0.947*	*3.086*	*-9.486*
Hectd2	*NM_172637*	*2.138*	*2.940*	*0.775*
Ssrp1	*NM_182990*	*-0.778*	*2.754*	*-4.041*
Lhb	*NM_008497*	*-0.474*	*2.233*	*-6.332*
Narf	*NM_026272*	*-0.714*	*2.195*	*-2.962*
Mcm7	*NM_008568*	*-2.646*	*1.988*	*-4.349*

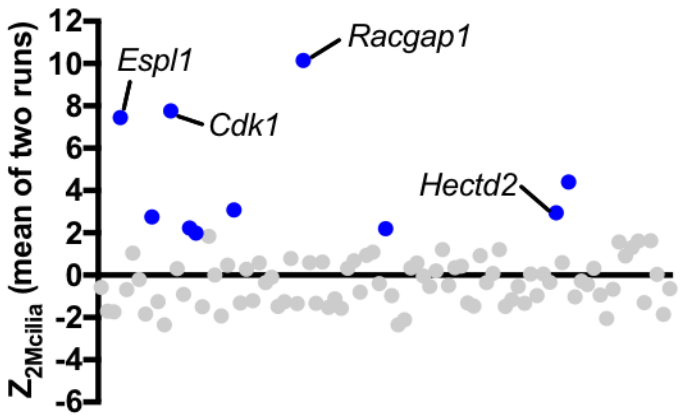

Figure 4.8 Scatter graph of mean $z_{2Mcilia}$ from the secondary screen.

The top 10% of hits are highlighted in blue. The four labelled hits reproducibly increase supernumerary cilia (incidence of cells with 2 or more cilia) with robust z-scores $z_{2Mcilia} \geq 2$ for both biological replicates of the secondary screen. The top 4 hits and their $z_{2Mcilia}$ values were: *Racgap1* (10.141), *Cdk1* (7.769), *Espl1* (7.455), and *Hectd2* (2.940). Significance calculated using robust z-scores to compare knock-downs to pooled negative controls.

There were 3 clear top hits that could be taken forward for further investigation, all with $z_{2MCilia}$ >7.45, equivalent to p< 0.00001. The top 3 hits also had a clear qualitative difference from the negative controls when assessing raw image data by eye. Cell numbers were significantly reduced and raw image data showed a high proportion of large, multinucleated cells, suggesting cell division defects in these knock-down conditions (Figure 4.9).

The 3 top hits (*Cdk1, Espl1* and *Racgap1*) encode proteins that interact. CDK1 phosphorylates both ESPL1 (345) and RACGAP1 (346), thus highlighting a functional network or pathway that, when perturbed, caused the increased incidence of supernumerary cilia.

The limitations of available reagents and time encouraged the tertiary validation of only the top hit from the screen. The current literature and databases were reviewed in order to assess the potential role of each gene in ciliogenesis and to ensure justification for the validation of the top hit *Racgap1*. Further literature searches were carried out to devise the simplest biological hypothesis for why *Racgap1* knock-down caused supernumerary cilia.

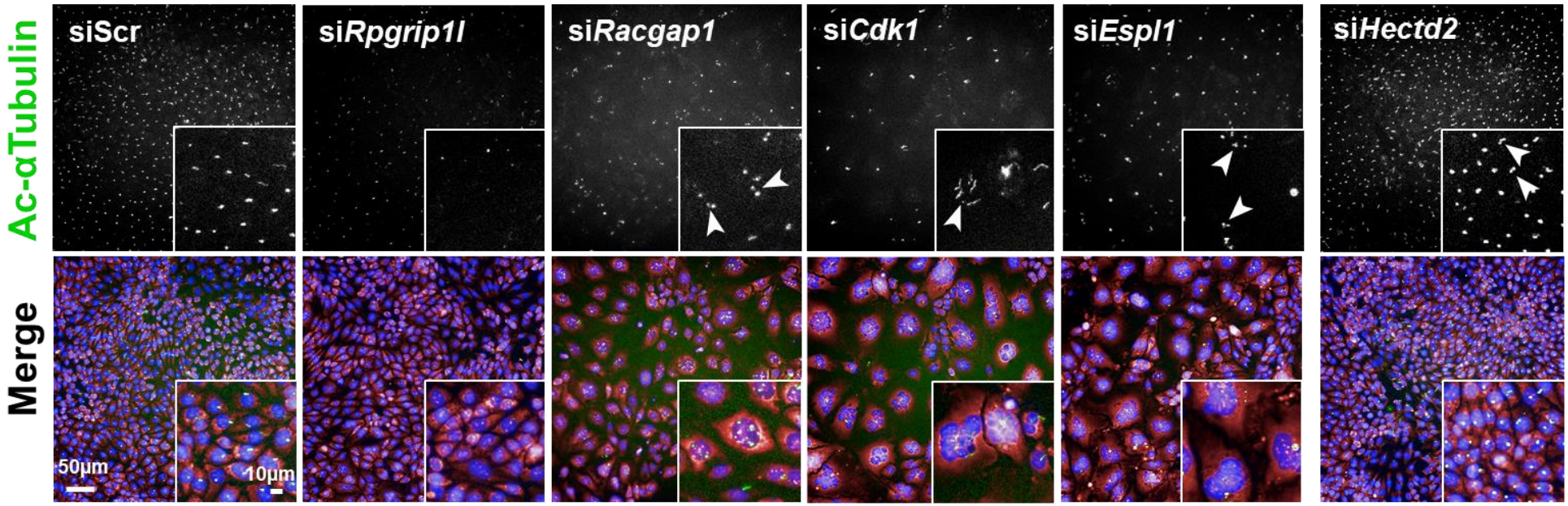

Figure 4.9 Raw image data of top hits from the increased supernumerary cilia (increased incidence of cells with two or more cilia) secondary screen

Raw image data taken from the increased incidence of 2 or more cilia secondary screen. Wild-type mIMCD3s have punctate cilia staining in the siScr control and there is a loss of cilia in the si*Rpgrip1l* positive control. The 3 top hits of the screen were *Racgap1*, *Cdk1* and *Espl1*. Cilia also appeared longer when cells were treated with si*Cdk1*. These cells were also multinucleated, with some cells having over 6 individual nuclei. All 3 top hits showed a significant decrease in overall cell number that was associated with an increase in cells with 2 or more cilia (examples indicated by white arrows). si*Hectd2* knockdown ($z_{2MCilia}$ = 2.94) was the only validated hit that did not show a significant change in cell number or the presence of multinucleated cells

4.3.2 Validation of siRNA knock-down

siRNAs for use in both mouse mIMCD3 and human RPE-1 cells to knock-down the orthologues of RACGAP1 were validated by reverse transcriptase-PCR (RT-PCR). Knock-down of the *RACGAP1* mRNA in both mIMCD3s and RPE-1 cells was observed when compared to cells transfected with the scrambled siRNA and normalised to GAPDH mRNA levels (Figure 4.10). This validates the efficacy of the siRNA reagents used both in the secondary screen and for downstream validation work.

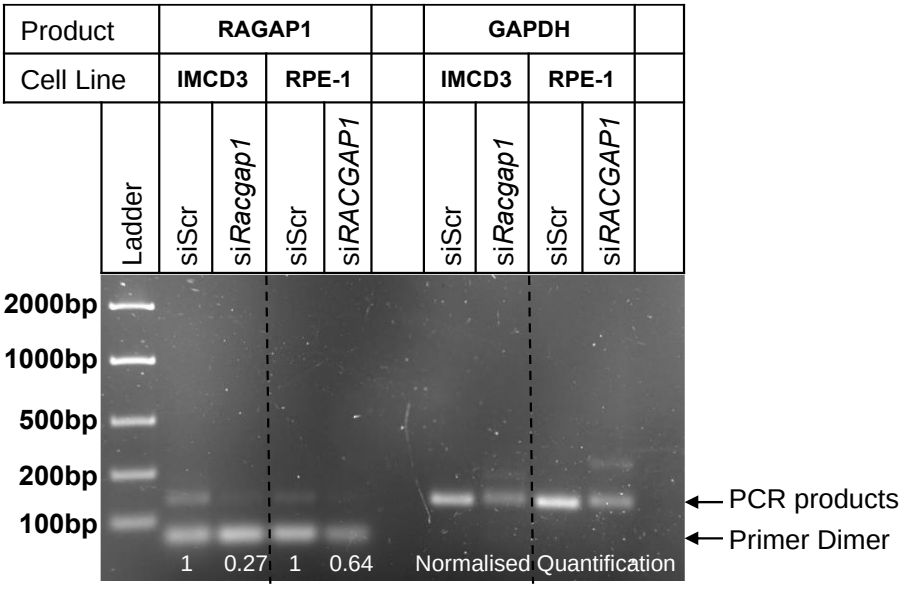

Figure 4.10 Racgap1 siRNA validation by RT-PCR

RT-PCR was used to validate siRNAs targeting both mouse and human *RACGAP1*. Cells were treated with siRNA for 72 hours before whole RNA was extracted, and cDNA generated. RT-PCR was run for 50 cycles and showed a decrease in *Racgap1* mRNA levels when densitometry was normalised to GAPDH mRNA levels in the same sample. N=1 technical replicate.

4.3.3 *RACGAP1* knock-down increases the incidence of supernumerary cilia in RPE-1 cells

To further investigate and validate Racgap1 as the top screen hit, an siRNA mediated *RACGAP1* knock-down was performed in human RPE-1 cells. This would also show if the cellular phenotype seen during secondary screening was consistent in a different cell model and species since, phenotypes can vary between different cell lines. When RPE-1 cells were treated with si*RACGAP1* there was a significant increase in the number of cells with supernumerary cilia

compared to cells treated with scrambled negative control siRNA (Figure 4.11). Cilia originated from separate centrosomes and there was no branching or splitting of the axonemes seen in the captured fields of view. Nuclei also appeared to be much larger than in cells treated with scrambled negative control siRNA (data not shown), implying a 4N DNA content consistent with the multinucleated large cells observed in the raw secondary screen data (Figure 4.9) arising from mitotic failure. As described for other ciliopathy disease mechanisms in Section 4.1, it was therefore assumed that the increase in supernumerary cilia following *RACGAP1* knock-down could be explained by an increase in centrosome number following exit from a failed mitosis. Thus, the observed increase in cilia incidence would be a secondary, indirect consequence of *RACGAP1* knock-down.

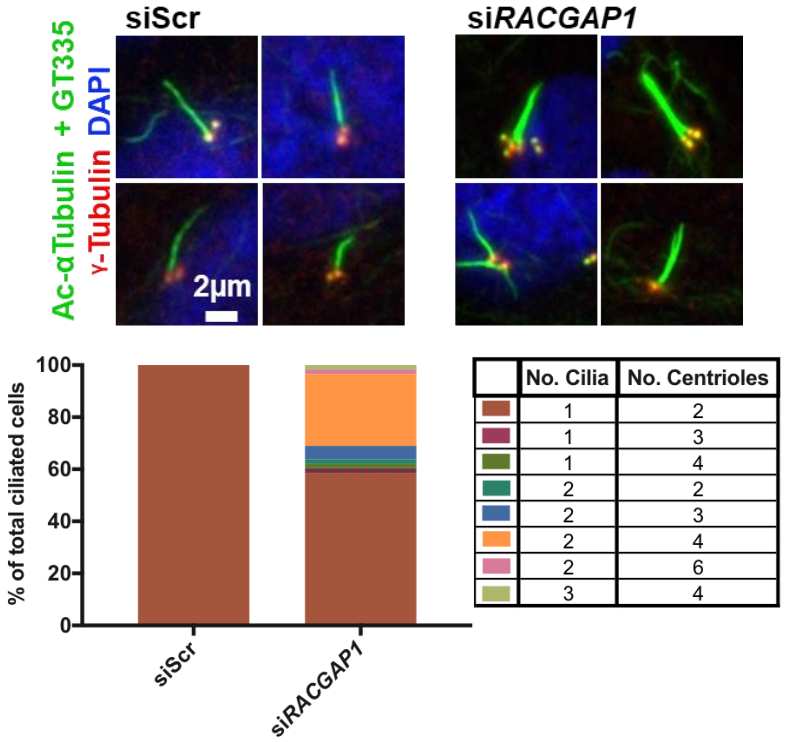

Figure 4.11 RACGAP1 knock-down increases the number of cilia and centrosomes per cell in RPE-1 cells.
A) Examples of primary cilia in RPE-1 cells treated with negative control scrambled siRNA (siScr) or siRNA targeting *RACGAP1* (si*RACGAP1*). Cells treated with si*RACGAP1* have more centrosomes compared to controls. Each cilium in these cells appears to originate from separate centrioles, and no cells were visualized that had either 2 cilia originating from a single centriole or branched/split cilia. **B)** The proportion of cells with different cilia:centriole ratios (normal ratio = 1:2). Over 40% of cells had either an increase in centriole number, increase in cilia number or both following *RACGAP1* knockdown. The most frequent aberrant ratio comprised of a duplication of both cilia and centrosomes (2:4). Other ratios (2:2 and 3:4) may indicate errors of centriole maturation. Figure provided by Dr. Basudha Basu. N=3 technical replicates.

Each cilium appeared to originate from individual centrioles within single and separate centrosomes (as distinguishable at this resolution of microscopy), suggesting that there were no aberrations in centriole maturation or incorrect ciliogenesis from daughter centrioles. To confirm that cilia only formed from the mother centriole in each centrosome, the experiment was repeated with immunostaining for CEP164, a mother centriole marker required for ciliogenesis (88) (Figure 4.12). Cilia always originated from the mother centrioles marked with CEP164 staining. Centrosomes not marked with CEP164, daughter centrioles, were not seen to produce cilia in any of the fields of view. This suggests that centrosome duplication and maturation is happening normally following *RACGAP1* knock-down.

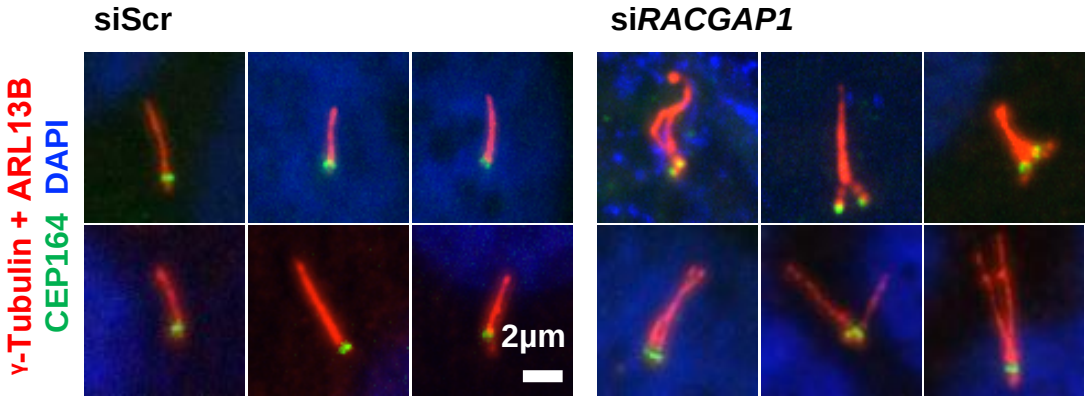

Figure 4.12 Supernumerary cilia originate from mother centrioles

RPE-1 cells with *RACGAP1* siRNA knock-down were stained for cilia (red), centrosomes (red) and CEP164 (green), a marker of the distal appendages in the mother centriole. This was to test if centriole maturation was correctly specified and that supernumerary cilia originated from mother centrioles marked by CEP164. All cilia in the fields of view captured appeared to stem from adjacent staining for CEP164. Figure provided by Dr. Basudha Basu.

4.3.4 *RACGAP1* knock-down in cycling cells

RACGAP1 has a well-defined role in cytokinesis as discussed in section 4.4.3. The presence of supernumerary centrosomes observed in RPE-1 cells following *RACGAP1* siRNA knockdown, and the prominent multi-nucleated phenotype observed in mIMCD3s during secondary screening, was likely due to a mitotic defect.

The data thus far, alongside the known role of RACGAP1, suggested that centrosome duplication and maturation is occurring normally under *RACGAP1* knock-down conditions. However, after failed cytokinesis cells would retain both duplicated centrosomes. These supernumerary centrosomes then correctly mature and mark their mother centriole with CEP164, allowing two cilia to form in the aneuploid cell. The signalling mechanisms for centrosome maturation therefore do not compensate for or are unable to identify the supernumerary centrosomes, allowing for maturation of the duplicated centrosomes as if they were in a new daughter cell.

As the supernumerary centrosomes are a downstream effect of mitotic failure, the supernumerary ciliated phenotype would presumably be more apparent in cycling cells. This would not have been tested in previous experiments which were performed under conditions of serum starvation in order to induce ciliogenesis. To test if supernumerary cilia were more frequent in cycling cells, RPE-1 cells were treated with either scrambled negative control siRNA or si*RACGAP1*. For the last 24 hours prior to fixation, medium supplemented with 10% serum medium was added to half of the technical replicates in order to observe any changes in the number of multinucleated cells in induced cycling conditions. This experiment would test for a possible ciliary resorption defect, where cilia were just retained on cycling cells, or prevented cell cycling.

RPE-1 cells treated with si*RACGAP1* showed a significant increase in the percentage of cells with supernumerary cilia after addition of serum (Figure 4.13). RPE-1 cells treated with either scrambled siRNA control or si*RACGAP1* resumed cycling after addition of serum, as shown by an increase in nuclei number (Figure 4.14A). Cell and nuclei numbers suggested that although cells were cycling, they were becoming multi-nucleated. This is consistent with the phenotype seen during secondary screening in mIMCD3s. However, raw image data of RPE-1 cells (Figure 4.14C) showed a more subtle phenotype, with fewer multinucleated cells when qualitatively compared to mIMCD3s. This was likely due to the difference in cell cycle duration between the 2 cell lines under serum starved conditions.

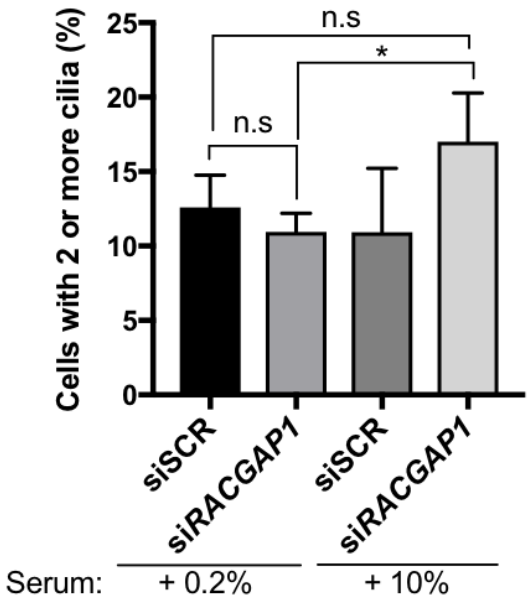

Figure 4.13 *RACGAP1* knock-down cells treated with serum have increased incidence of cells with supernumerary cilia

RPE-1 cells were treated with siRNAs and imaged, then analysed high-throughput to assess the incidence of cells with 2 or more cilia, with and without serum in the growth medium. There was no significant change in the percentage of cells with two or more cilia in the negative controls both with or without serum treatment. Cells with *RACGAP1* siRNA knock-down had a significant increase in the percentage of cells with 2 or more cilia after 24hr serum treatment, compared to serum starved cells with *RACGAP1* knock-down. By re-introducing serum and allowing the cells to re-initiate cycling, this further increased the incidence of supernumerary cilia. This suggests that the presence of cells with supernumerary cilia, observed following *RACGAP1* knock-down, is linked to an active cell cycle. Data was tested for normal distribution using a D'Agostino-Pearson omnibus K2 test and confirmed to be normally distributed. Statistical significance was then calculated using an unpaired, two-tailed Student's t-test. Experimental work performed by Dr. Basudha Basu analysis and figure prepared by myself. Error bars represent S.D.

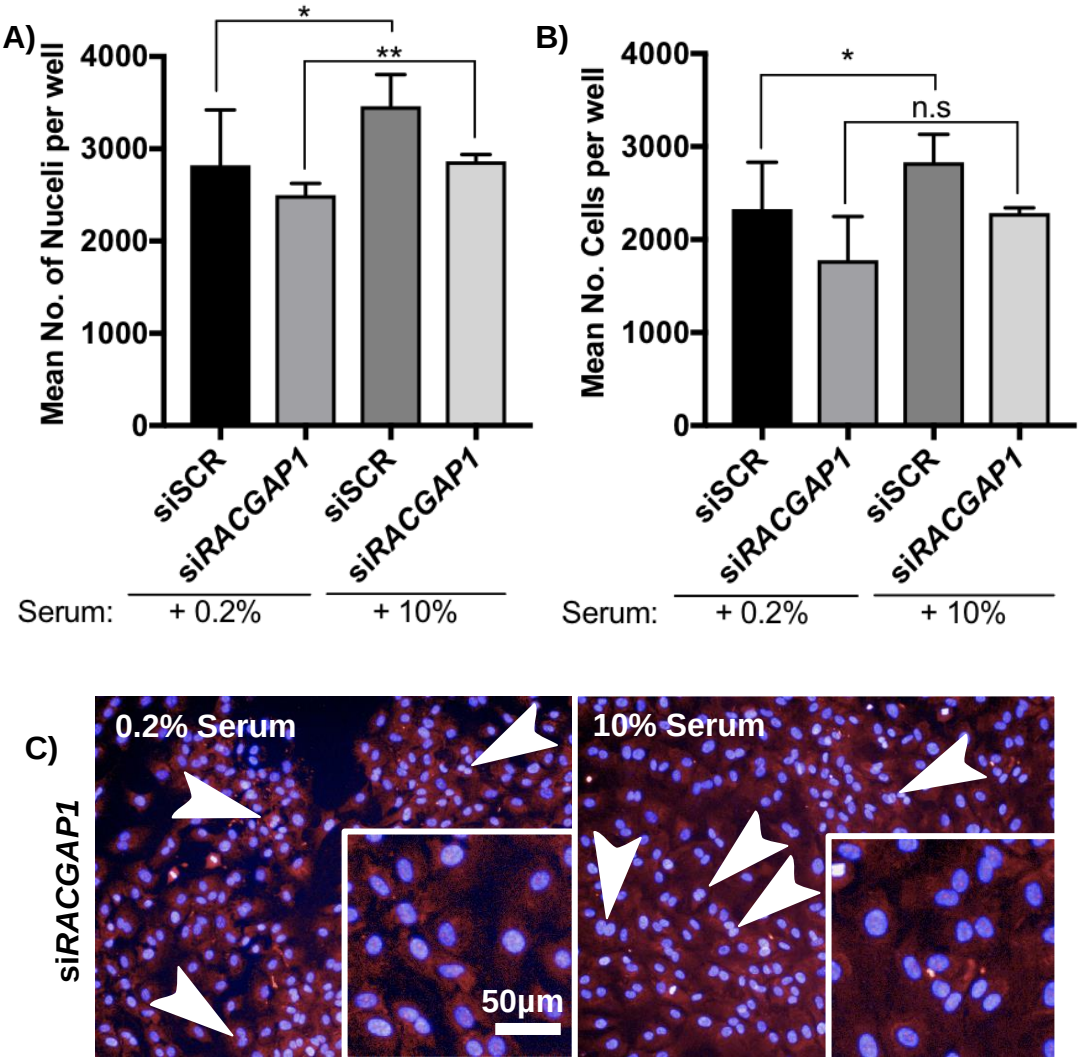

Figure 4.14 *RACGAP1* knock-down cells treated with serum have increased numbers of nuclei per cell

RPE-1 cells were treated in a 96 well plate with either scrambled siRNA negative control or si*RACPGAP1*. High-throughput imaging and quantification of cilia was used to determine the incidence of cells with 2 or more cilia. Technical replicates (n=2) of the knock-downs were serum starved for 72hours or had 10% serum added for the final 24hrs to induce cell cycling. **A)** Nuclei counts per well significantly increased in both knock-down treatments with the addition of 10% serum showing that cell cycling was resumed after serum starvation. **B)** Although there was an increase in nuclei counts per well there was not a significant change with or without serum in the total number of cells in wells with *RACGAP1* knock-down. As nuclei counts were also higher than cell counts, this indicates that a proportion of the cells in wells treated with si*RACGAP1* and serum were multinucleated. **C)** Raw image data shows increased incidence of multinucleated cells in 10% serum supplemented medium compared to 0.2% serum supplemented medium (indicated with white arrows). Data was tested for normal distribution using a D'Agostino-Pearson omnibus K2 test and confirmed to be normally distributed. Statistical significance was then calculated using unpaired, two-tailed Student's t-tests. Error bars represent S.D.

This work provided evidence that following *RACGAP1* knock-down, cells continued to cycle but failed to divide. In addition, there are no negative regulators or compensation mechanisms for retained supernumerary centrosomes and, consequently, supernumerary cilia in the cell lines examined.

4.3.5 *RACGAP1* knock-down causes supernumerary cilia as a consequence of mitotic failure

To confirm that a mitotic defect caused supernumerary cilia, cell cycle progression was assessed by live cell imaging experiments. mIMCD3 cells expressing GFP-LifeAct to visualise the actin cytoskeleton, or mIMCD3s stably expressing serotonin receptor 5HT6-GFP to visualise cilia, were used so that cell division and cilia formation could be tracked in real time. Live cell imaging of cells treated with *Racgap1* siRNA showed mitotic failure, causing multi-nucleation and formation of supernumerary cilia (Figure 4.15A). The cells appeared to still ingress in telophase (Figure 4.15A 180mins), a process that appears to be compensated for by the lack of RACGAP1, but failed to complete abscission. As cells continued to cycle and additional centrioles matured, the cells became over-ciliated with up to 4 cilia per cell after 2 failed mitotic divisions (Figure 4.15B).

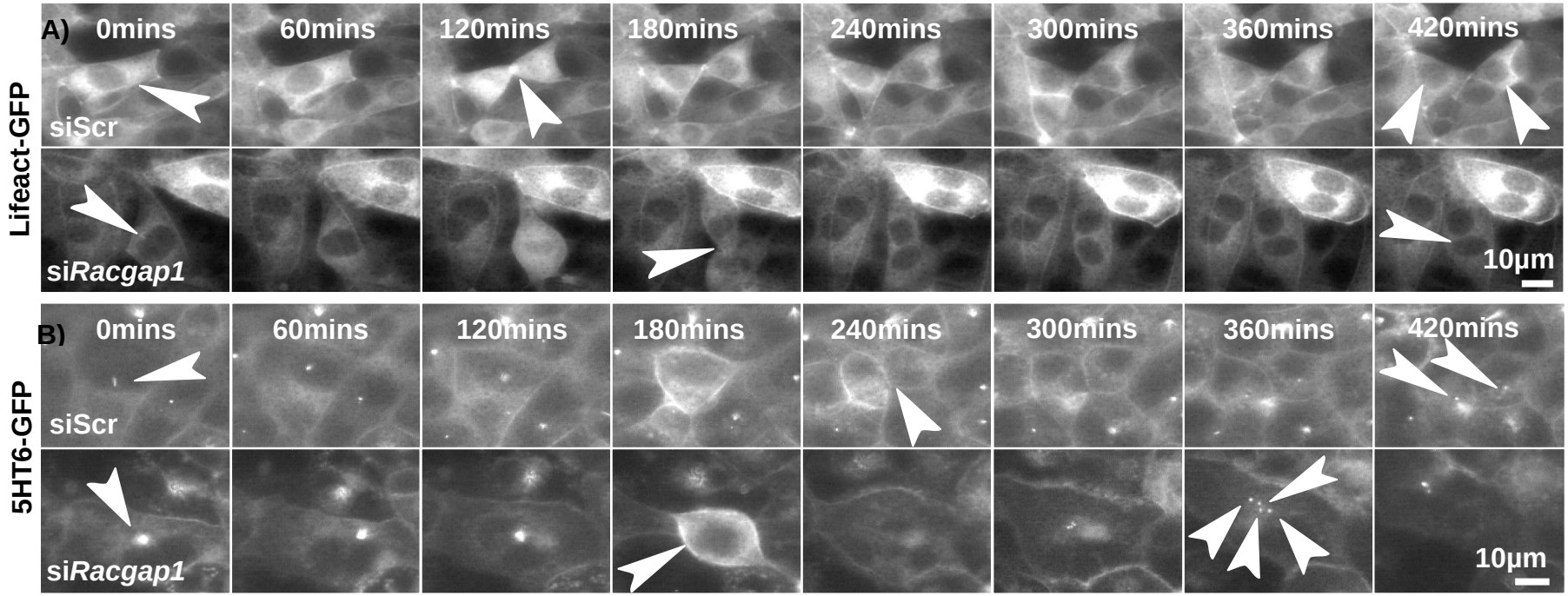

Figure 4.15 Live cell imaging of mIMCD3 cells treated with siRacgap1 shows mitotic abscission failure

A) mIMCD3 stably expressing *LifeAct-GFP*, to visualise actin, were treated with scrambled negative control or si*Racgap1*. Cells treated with scrambled siRNA undergo normal mitotic division. The midbody (highlighted at 120mins) forms, and the 2 daughter cells successfully undergo cytokinesis and are identifiable as separate cells from 240mins (indicated by white arrows at 420mins). Cells treated with si*Racgap1* show abscission failure after mitosis. At 180min the cells can be seen trying to separate and do not complete cytokinesis. The indicated cells within the field of view are polyploid, with at least 2 nuclei per cell due to the mitotic failure. **B)** mIMCD3 cells stably expressing 5HT6-GFP, to visualise cilia, were treated with scrambled negative control or si*Racgap1*. In negative control cells cilia form following normal cell division, with 1 cilium forming in each cell. In cells treated with si*Racgap1,* arrowheads indicate a polyploid cell that attempts to undergo mitosis and after abscission failure, 4 centrosomes each produce a cilium (indicated at 360mins). Arrows show exemplar cells that follow the description above. Live cell imaging was performed by Dr. Basudha Basu.

4.4 Discussion

The 4 main aims of this part of the project were met; a new data set of potential genes involved in the negative regulation of supernumerary cilia was generated from a primary whole genome siRNA screen data set. A secondary screen was completed in mIMCD3 cells to identify hits that increased the incidence of supernumerary cilia. The top hit of this screen, *Racgap1*, was validated in the human RPE-1 cell line and further investigation into the mechanism was carried out with immunofluorescence microscopy and live cell imaging.

4.4.1 The secondary screen for increased incidence of cells with 2 or more cilia

4.4.1.1 The Final Hit List

It was initially planned to generate a hit list that would identify hits that were unlinked to the cell cycle, in the hope that a novel pathway could be identified that regulates supernumerary cilia. Thus, the filter which removed hits affecting cell number was initially thought to be the most important filter. After removing this step, STRING and GO analysis highlighted that only 10% of hits were cell cycle regulators. It is possible that many of the other genes in the remaining 90% of the data set, although are not directly linked to cell cycle previously, when knocked down experimentally significantly affect cell number.

Interestingly there was no overlap between the final 96 hits for the two or more cilia incidence screen and the 32 candidate genes required for restricting centriole number that were identified in the whole genome screen carried out for centriole biogenesis in the Gonzcy lab (261). This highlights that the pathways between centriole duplication and centriole maturation are likely to be independent from one another.

4.4.2 Secondary screen hits

4.4.2.1 Cyclin Dependant Kinase 1 (*Cdk1*)

Cyclin Dependant Kinase 1 (CDK1) is a serine/threonine kinase that is a very highly conserved cell cycle regulator (347).It is known to interact with over 75 different proteins across many cellular pathways and has key roles at each

stage of the cell cycle (348). The most notable of these is its role at cell cycle checkpoints. CDK1 levels are lowest in G1. As they start to increase this activates transcription factors such as E2Fs to activate DNA replication genes and drive the transition into S phase. CDK1 is upregulated to its highest levels during the cell cycle in prometaphase, when it drives the initiation of mitosis (349).

Due to the clear phenotype of aneuploidy/large nuclei seen in mIMCD3 cells during secondary screening (Figure 4.9), it is suggested that these cells experienced cell cycle failure. High levels of cell loss were observed with this knock-down (average z_{cell} = -13.24

Global knock-down of CDk1 in these cells means that many stages of the cell cycle would be dysregulated and there would be high genome instability. It is unclear if one or all of these dysregulations would contribute to the supernumerary cilia phenotype seen. However, it is simplest to assume that retained centrioles from failed mitosis would produce the supernumerary cilia phenotype. As CDK1 has essential roles throughout the cell cycle and its knock-down is greatly detrimental to cell health, it would be almost impossible to accurately validate this phenotype, even in experiments using synced cell cultures.

4.4.2.2 Separin (*Espl1*)

Espl1 codes for a protease also known as Separin or Separase, because of its essential role in chromatid separation. ESPL1 cleaves a key protein in the final stages of sister chromatid separation during mitosis (350). Thus knock-down of *Espl1* will cause non-disjunction and metaphase arrest. Any surviving cells would then return to interphase. DNA breakage and random disjunction is the likeliest cause of the small micronuclei seen in Figure 4.9.

This failure of mitosis in *Espl1* knock-downs would also cause retention of duplicated centrosomes which, as discussed in the previous section, allows supernumerary cilia to form. This hit was not taken forward for further investigation.

4.4.2.3 HECT Domain E3 Ubiquitin Protein Ligase 2 (*Hectd2*)

HECT Domain E3 Ubiquitin Protein Ligase 2 (HECTD2) is a predicted E3 ubiquitin ligase but little is known about its function, molecular targets or regulation.

As an E3 ligase, HECTD2 would help an E2 ligase ubiquitinate its target protein. Therefore, knock-down of *Hectd2* by siRNA would lead to loss of ubiquitination on target proteins. If the ubiquitination of this target protein is required for it to be targeted for degradation, knocking-down the degradation of a positive regulator of ciliogenesis would lead to unregulated ciliogenesis. Ubiquitination of target proteins can also lead to changes in protein localisation. A *Hectd2* knock-down could therefore could potentially lead to a target protein being mis-localised. A negative regulator of ciliogenesis that is not correctly targeted could also lead to unregulated ciliogenesis.

Image data from the secondary screen may show longer cilia (Figure 4.9), but this is hard to assess qualitatively and cannot be accurately quantified in mIMCD3 cells because cilia are positioned vertically and thus are recognised as a single spot using the Columbus™ algorithms. However, it is possible that longer cilia in the mIMCD3 cells were angled or lying flat, thus were incorrectly detected by the recognition protocol and broken down into 2 separate “spots” (Figure 4.16), an artefact that had been noted in previous screens (personal communication with Dr. Katarzyna Szymanska, Univeristy of Leeds).

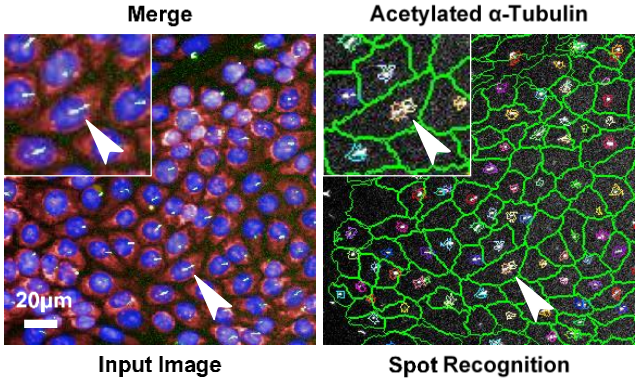

Figure 4.16 Limitations of the spot recognition protocol

Raw image data taken from the increase in the secondary screen for incidence of cells with two or more cilia. The optimised recognition protocol failed to recognise single longer cilia as a single spot and were instead segmented into two separate adjacent spots.

Therefore, as there was relatively little known about this gene and its function and without any available validated reagents, it was not taken forward for further investigation.

4.4.3 Rac GTPase activating protein 1 (*Racgap1*)

Rac GTPase activating protein 1 (RACGAP1) also known as MgcRacGAP or CYK4, is a component of the centralspindlin complex and is required for successful cytokinesis. Its localisation is cell cycle dependent, but it is localised at the mitotic spindle during metaphase, the cleavage furrow and central spindle during anaphase, and then in the midbody during cytokinesis (351).

RACGAP1 dimerises and auto-associates with a KIF23 dimer to make up a heterotetrameric centralspindlin complex (352). RACGAP1 and KIF23 are functionally interdependent, such that removal of one or the other causes central spindle defects (353, 354). RACGAP1 tethers microtubules to the plasma membrane for cleavage furrow formation (Figure 4.17A) but also has a role in the signalling required to form the acto-myosin contractile ring during anaphase though its direct interaction with ECT2 (355) (Figure 4.17B).

With *Cdk1, Espl1* and *Racgap1*, the logical hypothesis behind the incidence of supernumerary cilia was the induction of mitotic defects. Therefore, because both *Cdk1* and *Espl1* would have caused significant cell cycle defects and cell death, *Racgap1* was the only viable hit to take forward in tertiary screening because some knockdown cells can survive as binucleate, allowing time for observation of the ciliary phenotype. *Racgap1* was also the top hit in the secondary screen (Figure 4.8) and was a confirmed negative regulator in an independent whole genome siRNA screen. the previous screen (260).

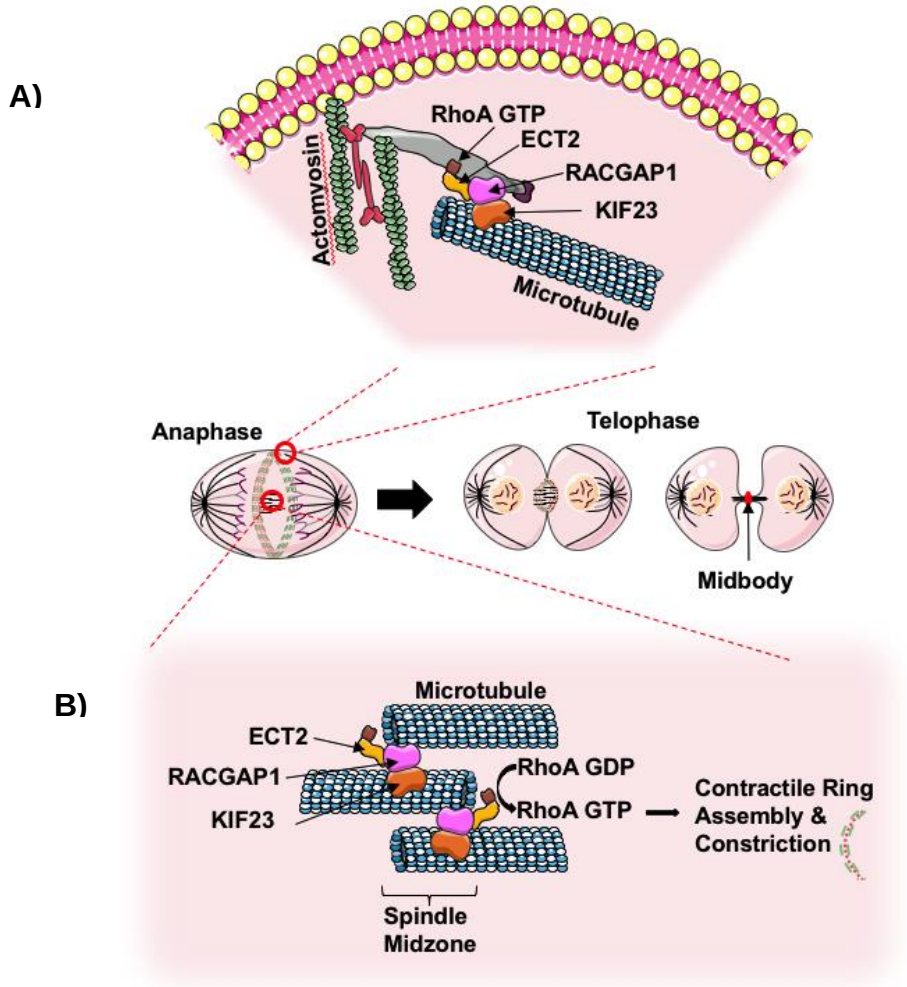

Figure 4.17 The localisation of RACGAP1 in the centralspindlin complex and mitosis

Schematic diagram shows the formation of the centralspindlin complex on peripheral microtubules (**A**) and at the central spindle (**B**). KIF23 binds to microtubules and has myosin like activity within the centralspindlin complex with RACGAP1. ECT2 interacts with RACGAP1 and is then able to activate RhoA bound to the GAP domain in RACGAP1. RhoA pathways initiate formation of the cleavage furrow and central actomyosin contractile ring. Modified from (351) Figures 1 and 4 with copyright permissions.

4.4.4 Limitations

4.4.4.1 Secondary screening

For both cell number and incidence of cell with two or more cilia there was a low Pearson's correlation ($R^2 < 0.5$) between the 2 biological replicates of the screen. This is despite re-optimisation of controls and recognition protocols. This increases the likelihood for both false positives and false negatives in the dataset. The low correlation and high variation between biological replicates of

the secondary screen could be due to the lack of a positive control to validate the recognition protocol. Without such a control, there is not a quantifiable way to determine the recognition protocols ability to detect cells with more than one cilium, or separate 2 very close cilia. Two adjacent cilia may not be separately resolved at the 20X magnification used for high content imaging leading to potential false negative results. This highlights the importance of tertiary validation of phenotypes.

The secondary screen was also limited by the stringent filtering steps used, which did not account for the lack of reproducibility between hits seen in the primary screen (Table 6.1 and Figure 4.7). Initial filtering produced only 14 hits of which none were known to be related or interact. It is likely that, because the whole genome screen data set and recognition protocols were not optimised to identify 2 separate cilia per cell, there was a high margin of error for both false positives (possibly caused by long cilia as discussed 4.4.2.3) or false negatives in the primary data. However, taking datasets like this forward and repurposing it has been shown throughout this thesis to be a useful strategy to identify new hits and regulatory pathways. There are, of course, inherent limitations when this repurposing is for a slightly different phenotype to that for which the screen was optimised because the detection protocols are likely to not precisely analyse the new phenotype of interest.

4.4.4.2 Imaging resolution

During tertiary validation of *RACGAP1* knock-down in RPE-1, cells with 2 centrosomes and 2 cilia, or 4 centrosomes and 3 cilia, were noted (Figure 4.11B). This implied that there was a defect of centriole maturation, but it could be argued that this was merely a technical artefact that arose from the limitations of resolution achievable with light microscopy. At the resolution of microscopy used in these experiments (Zeiss ApoTome with structured illumination, which has comparable or slightly improved axial resolution to confocal microscopy (356) which is 500nm at optimal conditions (357)), cells that were visualized with 2 centrioles and 2 cilia may not have had additional centrioles resolved due to their close proximity to punctate staining seen or because they were spatially obscured from imaging. This appears to be the simplest biological explanation for the odd ratios seen in Figure 4.11. In future

work, resolution could be improved by using Airyscan microscopy (400nm axial resolution (358)) or using a different cell model for imaging.

Furthermore, polyglutamylated tubulin was used as a marker for centrioles. This specifically marked post translational modifications, which are dynamic and often mark a nascent cilium. Other centrioles without these post-translational modifications may have been missed as they would not have been stained by the GT335 antibody.

4.4.4.3 Lack of HECTD2 Validated Reagents

Possibly the most interesting hit that could have been taken forward for further investigation was *Hectd2*, since it was the only secondary screen hit that did not have an apparent mitotic defect. The initial aim of this screen was to identify hits that did not cause changes in cell number, and hence likely to be independent of defects in mitosis or centrosome duplication, in order to identify a novel pathway that led to supernumerary cilia. *Hectd2* was the only hit that fit these initial criteria and was in the small dataset of 14 hits that passed all 3 filtering criteria. However, there is little known about this gene and protein and there are very few validated reagents available for experiments. Due to time constraints it would not have been feasible for new reagents to be produced and validated, and thus it was decided to discontinue this branch of the project.

4.4.5 Impact and Significance

A novel role for RACGAP1 was not identified in this work, but a secondary downstream phenotype of *RACGAP1* knock-down was identified. To our knowledge, this is the first described link between the centralspindlin complex and incidence of supernumerary primary cilia. Furthermore, HECTD2 may be a component of a novel regulatory mechanism that specifies cilia number.

4.4.6 Potential future work

4.5.6.1 Cilia function tests

It would be interesting to investigate any changes in cilia function in the multi-ciliated cells using signalling assays. Sonic Hedgehog (Shh) signalling has been shown to be depleted in “super-ciliated” cells caused by *Plk4* knock-down. Shh expression was not proportionally increased with incidence of supernumerary

cilia; instead, Shh receptors were proportionally diluted across the multiple cilia which dampened the cell's overall Shh signalling response (335).

Wingless-related integration site (Wnt) signalling has also been shown to be altered in MEFs induced to have supernumerary cilia by treatment with a DNA polymerase inhibitor. Single ciliated cells dampened Wnt signalling in comparison to non-ciliated cells, whereas bi-ciliated cells further reduced Wnt signalling response and caused decreased levels of nuclear β-catenin (158)

These signalling assays could be used to assess changes in signalling with *RACGAP1* knockdown, as the supernumerary cilia were induced using different techniques and targets in the previous studies. It would be beneficial to provide further evidence that ciliary signalling is diluted across supernumerary cilia or highlight if the phenotype described in this thesis does not correlate to previous functional data in supernumerary cilia.

4.5.6.3 The centralspindlin complex components

It would also be of interest to investigate *Kif23* and centralspindlin regulators to see if knock-downs phenocopy the phenotype of *Racgap1* knock-downs.

Alongside this it would be a priority to confirm that supernumerary cilia formation is a secondary phenotype arising from mitotic failure and not a novel direct function of RACGAP1 or the centralspindlin complex. Actin remodelling and RhoA activation was discussed in Chapter 3 as an important component of ciliogenesis and Racgap1 has a direct role in actin remodelling during cytokinesis. This alternative mechanism would have to be tested with specific RACGAP1 antibodies at different stages of ciliogenesis.

Chapter 5

Results: The transition zone genetically interacts with IFT88

5.1 Introduction

Genetic interactions between ciliary genes are already known to contribute to the spectrum of phenotypes observed for ciliopathies such as Bardet Biedl syndrome (359-362), as discussed in (Chapter 1, Section 1.5.2). As the cilium is highly regulated and has complex molecular signalling, it is likely that there are many more genetic interactions to be identified that contribute to the observed variability in ciliopathy phenotypes. A high-throughput methodology could therefore be a useful tool in screening for genetic interactions amongst ciliary genes to aid in our understanding of the molecular pathology behind these varying phenotypes. This chapter describes the development and a proof of concept experiment to show that the development of a large scale genetic interaction screen is possible if looking at ciliary phenotypes.

Knock-outs of ciliary genes often cause severely decreased cilia incidence or a reduction in ciliary length, as seen in mouse derived cultures (363-365). In this chapter, I have hypothesised that heterozygous mutant cell-lines, that have a residual protein level, would still have quantifiable ciliary phenotypes. These heterozygous cell lines were then further perturbed to detect genetic interactions with small interfering RNA (siRNA), generating “double perturbation” conditions to identify synthetic genetic interactions (366). These combinatorial screens of siRNA and Clustered Regularly Interspaced Short Palindromic Repeats/Cas9 (CRISPR/Cas9)-edited cells acted as a primary screen to provide potential follow-up projects for secondary validation, whereas previous chapters have used a secondary screen and tertiary validation to gain mechanistic insight. Any potential interactions that were identified could provide novel insights into the genetics of ciliogenesis, ciliary maintenance or disassembly.

Known ciliopathy genes coding for different structural and functional compartments of the cilium (Figure 5.1, Table 5.1 Genes targeted by CRISPR/Cas9

were targeted by CRISPR/Cas9 genome editing to generate a panel of heterozygote genome-edited cell lines. Targets included a ciliary membrane protein (ARL13B), intraflagellar anterograde transport protein (IFT88) and transition zone proteins (CEP290, TMEM67, RPGRIP1L and TMEM216). These uncharacterised cell lines were validated and used in combinatorial screening with siRNAs targeting a separate panel of genes. Both panels were selected based on available reagents in the lab and were focused on the transition zone, a ciliary compartment shown in previous studies to be tightly regulated and influenced by epistatic interactions (82, 360, 367).

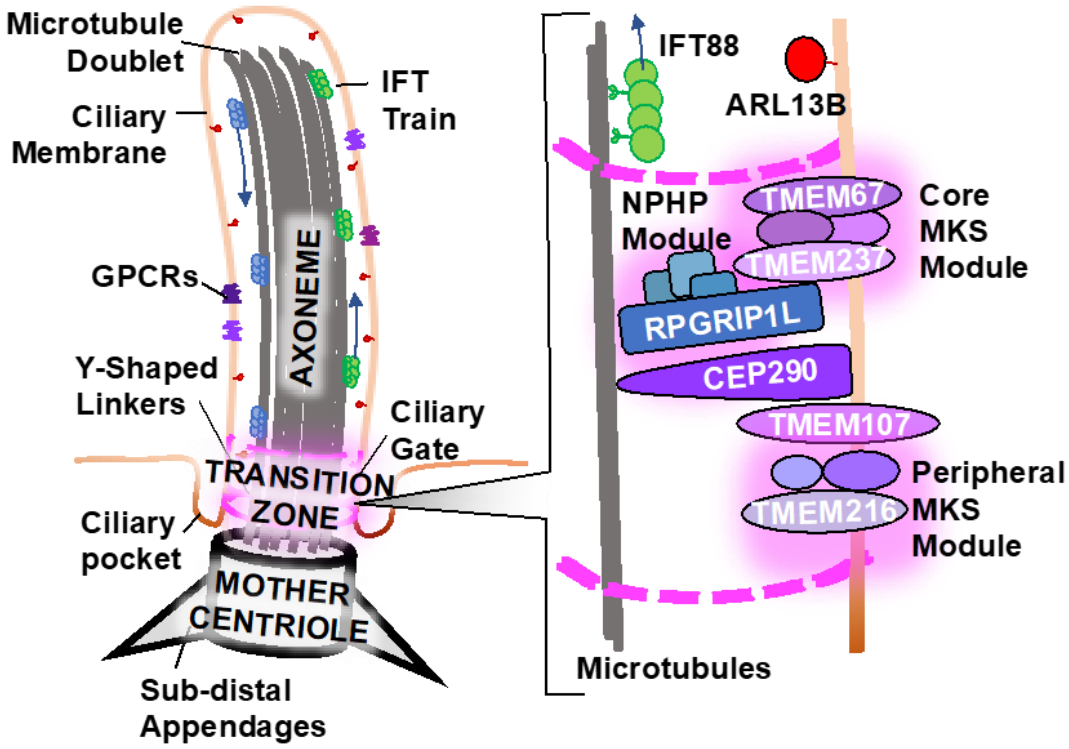

Figure 5.1 Schematic of the primary cilium and transition zone

The primary cilium has a complex ultrastructure with many different compartments. Genes that code for components of the ciliary membrane (*ARL13B*), intraflagellar trafficking (*IFT88*), and transition zone (*CEP290*, *RPGRIP1L, TMEM67, TMEM216*) were targeted with CRISPR/Cas9 genome editing to generate heterozygous mutations. Modified from (368) Figure 1. Clinical features of Meckel–Gruber syndrome (MKS) and schematic of primary cilia structure, use licensed under the Creative Commons Attribution 4.0 International License.

Table 5.1 Genes targeted by CRISPR/Cas9

This table summarises the genes and specific exons targeted by CRISPR/Cas9. Data is also provided on the known or predicted structural modules in the cilium and the published phenotypes for each gene. COACH = Cerebellar vermis aplasia, Oligophrenia, congenital Ataxia, Coloboma and Hepatic fibrosis. RHYNS = Retinitis pigmentosa, HYpopituitarism, Nephronophthisis, and mild Skeletal dysplasia. Data collected from Online Mendelian Inheritance in Man, OMIM® (369) and * IFT88 phenotype described in (370).

Gene	OMIM No.	Target Exon	Human Ciliopathy Phenotype	Phenotype MIM No.	Protein Localisation
ARL13B	608922	1	Joubert Syndrome 8	612291	Ciliary Membrane
CEP290	610142	2	Bardet-Biedl syndrome 14	615991	Y-Shaped Linkers of the Transition Zone, Centrioles, Centriolar satellites
			Joubert syndrome 5	610188	
			Leber congenital amaurosis 10	611755	
			Meckel syndrome 4	611134	
			Senior-Loken syndrome 6	610189	
IFT88	600595	7	Non-syndromic recessive retinal degeneration*	-	Ciliary Axoneme, Intraflagellar Transport Complex (IFT B)
RPGRIP1L		2	COACH syndrome	216360	Transition Zone: NPHP Module
			Joubert syndrome 7	611560	
			Meckel syndrome 5	611561	
TMEM67	609884	1	RHYNS syndrome	602152	Transition Zone : Core MKS module
			Bardet-Biedl syndrome 14, (modifier of)	615991	
			COACH syndrome	216360	
			Joubert syndrome 6	610688	
			Meckel syndrome 3	607361	
			Nephronophthisis 11	613550	
TMEM216		2	Joubert syndrome 2	608091	Transition Zone : Peripheral MKS module
			Meckel syndrome 2	603194	

5.1.1 Chapter Aims and Objectives

Aims: To understand the molecular mechanisms behind the spectrum of phenotypes seen in ciliopathy patients.

Hypothesis: The high variation in phenotypes seen across the ciliopathy disease group is due to epistatic genetic interactions between ciliary genes as has been identified in a few familial cases of Bardet Biedl Syndrome (371). The inheritance of a variety of alleles, that are unidentified in traditional clinical mutation screening, act in an epistatic manner to affect ciliogenesis and ciliary function. Thus providing a molecular explanation for the spectrum of phenotypes and diseases seen from mutations in the same gene.

A quick and high-throughput methodology could be used to screen ciliary genes and genes associated with ciliary function to identify potential epistatic interactions through the impact on simple ciliary phenotypes, such as ciliary incidence and length.

Experimental Objectives:

- To validate CRISPR/Cas9-edited cell lines for use in high-throughput screening.
- To design, optimise and develop a high-throughput technique which is able to identify epistatic genetic interactions.
- To carry out a proof of concept small scale screen, henceforward called a combinatorial screen, to show that the technique is feasible and has the potential to be developed
- To use screen test data to identify synthetic genetic interactions between knockout and knockdowns of ciliary genes
- To validate and determine the mechanistic basis for any potential genetic interactions inferred from the primary combinatorial screen data.

5.2 Validation of CRISPR/Cas9-edited cell lines

CRISP/Cas9-edited hTERT-RPE-1 cell lines were generated in Prof. Colin Johnson's group during my time as a research assistant prior to undertaking this thesis project. The cell lines were tested for heterozygous and compound heterozygous mutations by a T7 Endonuclease I Digestion Assay (T7 assay) (Figure 5.2). Due to the random mutation events from CRISPR/Cas9 editing, it was assumed that mutations on both alleles would be different. Therefore, both single allele and double allele mutations would give a positive result in a T7 assay. Across all genes targeted 59 clones were identified by T7 assay to as having mutations in target exons. The frequency of positive results in the T7 assay was also used to predict the overall efficacy of each of the guide RNAs (gRNAs) used to initially generate these cell lines (Table 5.2).

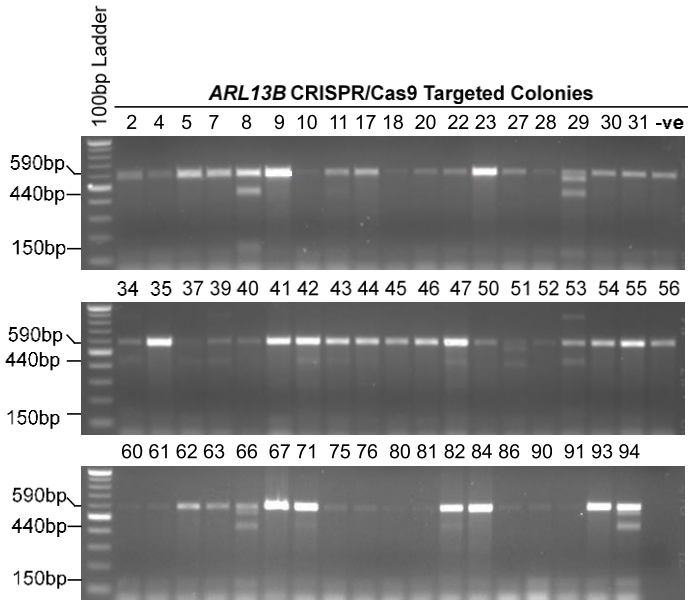

Figure 5.2 T7 assay of *ARL13B* CRISPR/Cas9 targeted colonies

T7 assay using re-annealed polymerase chain reaction (PCR) products of *ARL13B* exon 1 from CRISPR/Cas9 treated colonies (PCR product 590bp, expected cut bands approx. 440bp and 150bp). This assay was used to identify heterozygous and compound heterozygous mutated colonies to take forward for validation, examples seen for colonies 8 and 29.

Table 5.2 Predicted gRNA efficacies

For each gene targeted only one gRNA was used. T7 assays were used to predict the efficacy of each gRNA's ability to induce indel mutations. This was based on the number of positive results from the T7 assay which indicates either a heterozygote or compound heterozygote mutation in the targeted exon. The predicted gRNA efficacy is calculated using an equation described in (372).

% gene modification = 100 × (1 − (1 − fraction cleaved)1/2)

Gene	No. Colonies Tested	No. T7 Positive Results	% Gene Modification
ARL13B	55	15	14.7
CEP290	48	7	7.6
IFT88	59	9	7.9
RPGRIP1L	88	20	12.1
TMEM67	95	4	2.1
TMEM216	83	4	2.4

5.2.1 Mutation analysis of CRISPR/Cas9-edited cell lines

CRISPR/Cas9 induced mutation positive colonies identified by T7 assay were taken forward for Sanger sequencing. Both Sanger sequencing (Appendix H) and Mutation Taster online tool (http://www.mutationtaster.org/) (373) were used to define heterozygous mutations and predict their pathogenicity. Mutations ranged from a single base-pair insertion to a 361bp deletion. Polyclonal cell lines were assessed using TA cloning so that all individual alleles within the cell population could be sequence verified. Both monoclonal and polyclonal cell lines that were shown to have mutations with predicted deleterious pathogenicity were taken forward for further validation (Table 5.3). Throughout this thesis these cell lines will be referred to by their gene, clone number, and mutation abbreviations.

The top 20 potential off-target sites of these 10 chosen cell lines were also sequenced to verify the specificity of editing and to ensure that any validated phenotype was due only to the mutation in the targeted gene. There were no off-target mutations detected by Sanger sequencing in the clones taken forward for phenotype validation (data not shown). However, this does not comprehensively confirm that the clones are free of off-target mutations.

Table 5.3 Sequence Validated heterozygous CRISPR/Cas9-edited cell lines

Validated mutations for the cell lines used throughout this project. The targeted gene, clone number and mono or polyclonal genetic status of each cell line are listed. Coding sequence and protein mutations are listed alongside abbreviations to represent the overall predicted pathogenicity (+ = wild type allele, - = pathogenic allele, if.del = deleterious allele, if.indel = possibly deleterious). **TMEM67* inversion was not fully characterised and the inversion starts before, and covers exon 1.

Gene Target	Clone	Clon-ality	Genotype	Predicted Protein Change	Abv. of genetic status
ARL13B	8	Poly	NM_144996.4:c.[323_324insG];[314_320delGGTTCAA];[323_329delGGTGGCG];[314_329=]	- p.W15Vfs*10 p.W11Cfs*19 p.W15Sfs*15	+/-
ARL13B	71	Mono	NM_144996.4:c.[325_326insT];[325_326=]	- p.W15Lfs*10	+/-
CEP290	53	Poly	NM_025114.4:c[400_401ins159];[400_401ins361];[400_401=]	- p.R20Pfs*50 p.R20Wfs*4	+/-
IFT88	29	Mono	NM_001318493.2:c.[1489_1526delinsAAGAAAAAAG];[1489_1526=]	- p.P124Qfs*4	+/-
IFT88	31	Mono	NM_001318493.2:c.[1491_1496delinsTGCAAG];[1491_1496=]	- p.[L125C, S126K]	+/if.indel
RPGRIP1L	19	Mono	NM_001127897.4:c.[109_131delTGATGAGACTGCAGGAGACTTGC];[109_131=]	- p.D6Cfs*35	+/-
RPGRIP1L	49	Mono	NM_001127897.4:c.[111_119delATGAGACTG];[118_127delTGCAGGAGAC]	p.24_33del p.A9Cfs*3	if.del/-
*TMEM67**	47	Mono	NC_000008.11:g.93754818_?ins?_93755370inv	- ??	+/-
TMEM216	42	Mono	NM_001173990.3:c.[1213_1264delAGTATTAGCGTGGCCTTGACCTTCCCATCTGCCATGATGGCCTCCTATTACC];[1213_1264=]	- p.S90Cfs*14	+/-
TMEM216	89	Mono	NM_001173990.3:c.[1213_1218delAGTATT];[1213_1264delAGTATTAGCGTGGCCTTGACCTTCCCATCTGCCATGATGGCCTCCTATTACC]	p.268_319del p.S90Cfs*14	if.del/-

5.2.1.1 *TMEM67* C47 Mutation Analysis

TMEM67 C47 was the only colony for which the mutation could not be accurately defined. Initial colony sequencing data showed an uninterpretable electropherogram that did not align to any *TMEM67* wild-type sequence. The PCR products used for this sequencing were checked and shown to be clean single bands at the expected size. Other PCR products from colonies in the same run were also sequenced and showed the expected amplified region across exon 1 of *TMEM67*. After repeated polymerase chain reactions (PCR) and Sanger sequencing of C47 with either failed or further uninterpretable results, the cell line required further analysis. New primers spanning a larger amplification region were designed in case primer sites were mutated or a larger deletion had deleted primer sites altogether. Primers of increasing further distance from the predicted mutation site were used. By using these primers, a potential inversion across exon 1 (Figure 5.3) was detected alongside a full wild-type sequence, although this was only detected in the forward primer Sanger sequencing results. Thus it was possible that the reverse primer sequence was being missed for this allele or was deleted entirely, so only the wild-type allele was sequenced. Further primers were designed to amplify a 1.1kb region over exon 1, but Sanger sequencing of these PCR products only produced wild-type sequence. The cell line was taken forward to look for loss of protein and any robust phenotype that would allow the cell-line to be kept in the CRISPR/Cas9 panel, but all results were interpreted with the consideration that this may simply be a wild-type clone that had under gone clonal selection making it differ from normal wild-type controls. The possibility that this was a polyclonal cell line with a high proportion of wild-type cells compared to mutant cells, which meant sequencing was inconsistent, was also considered.

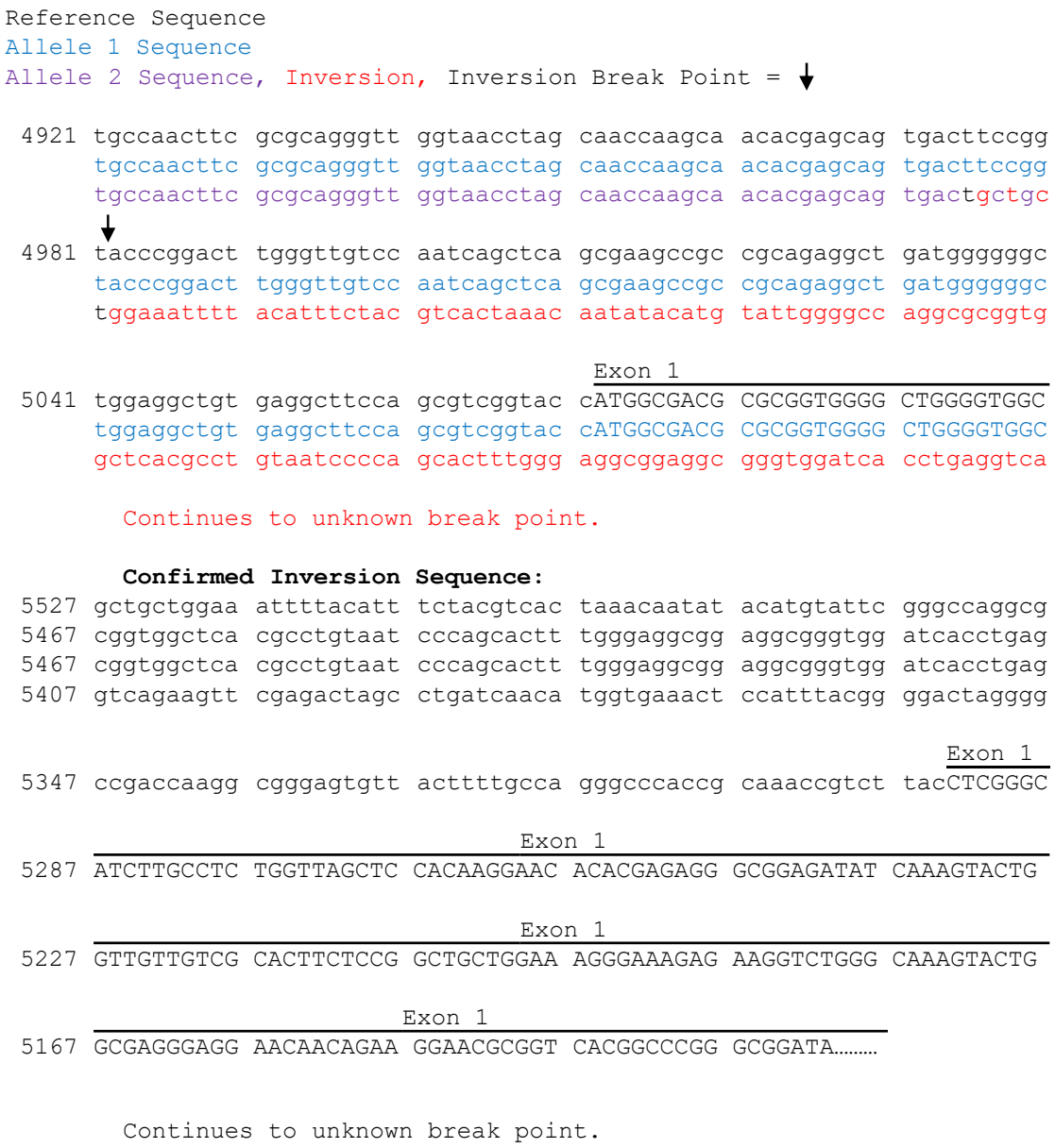

Figure 5.3 *TMEM67* C47 +/- mutation analysis

Using primers that extended into the intron region before Exon 1 of *TMEM67*, an inversion (red) was detected in the second allele of *TMEM67* C47 (purple) was detected. The inversion starts at base 4982 when reading the second allele 5' to 3'. The inversion sequence refers to the sequence starting at 5527 in the reference sequence and matching the reference sequence when read 3' to 5'. This inversion spanned over exon 1 but the second break point was not covered in the Sanger sequencing data of the reverse primers. Further primers into the intron sequence after exon 1 failed to generate readable electropherograms after Sanger sequencing and so this mutation was not fully characterised.

5.2.2 CRISPR/Cas9-edited cell lines have reduced levels of target proteins

Western blot and reverse transcriptase-polymerase chain reaction (RT-PCR) showed loss of protein or gene expression in all cell lines compared to negative controls (Figure 5.4). Protein levels in cells were compared to wild-type, passage matched, retinal pigment epithelial (RPE-1) cells treated with either siScr negative control or with siRNA against the CRISPR/Cas9 targeted gene (positive control). Quantifications were normalised to loading controls to estimate the protein levels in the mutant cell lines relative to the negative wild-type control (Figure 5.4). *ARL13B*, *CEP290* and *IFT88* mutant cell lines all showed reduced protein levels compared to negative controls. Despite the lack of characterised mutation *TMEM67* C47$^{+/-}$ also showed reduced protein levels relative to controls. Normalised protein or RT-PCR results matched the predicted pathogenicity and mutant allele frequency in all cell lines tested.

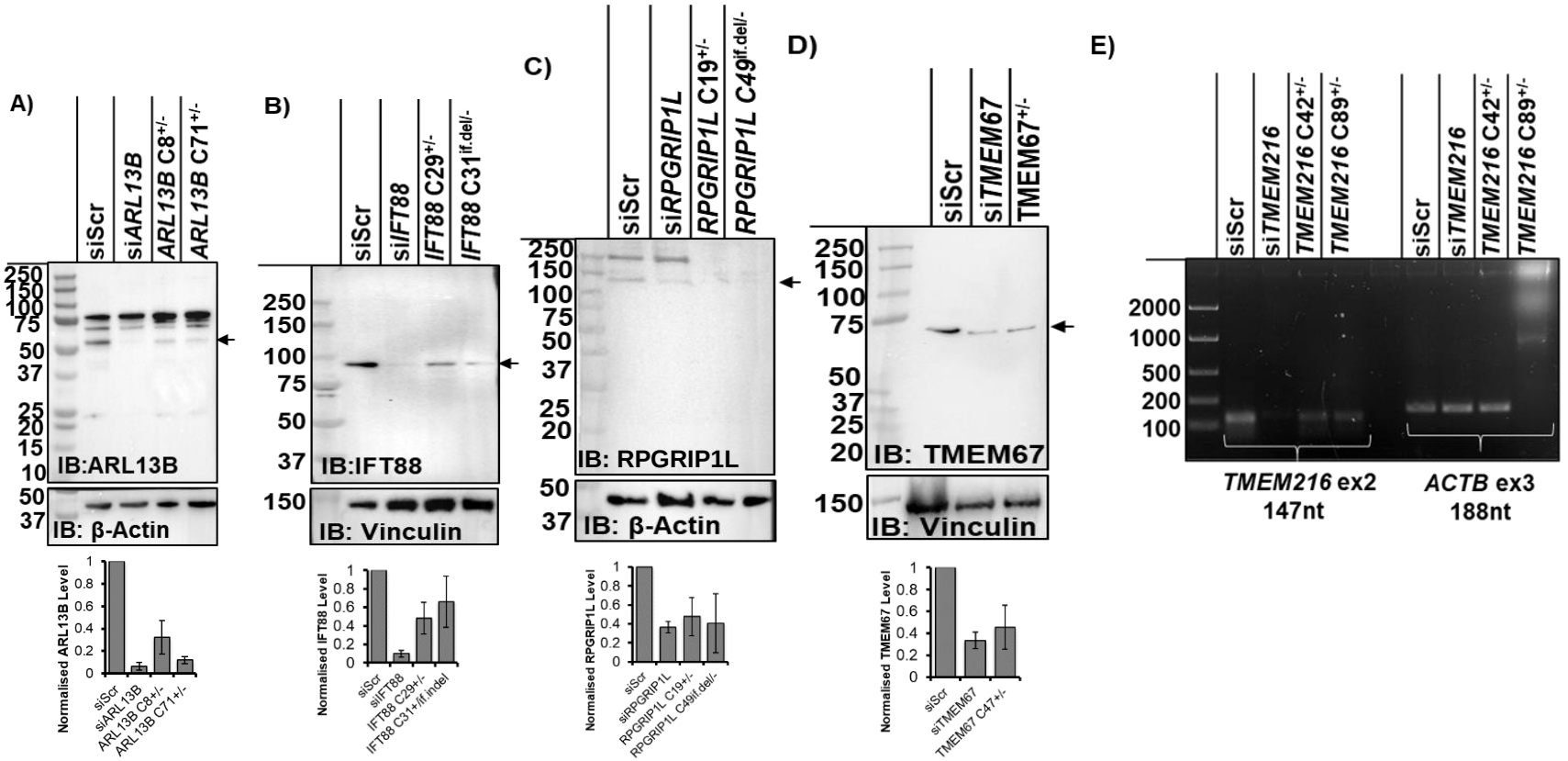

Figure 5.4 CRISPR/Cas9-edited cell lines have loss of targeted protein or mRNA

A) Western blot shows loss of ARL13B protein levels in C19$^{+/-}$ and C71$^{+/-}$ cell lines compared to negative control when densitometry is normalised to β-Actin levels. ARL13B has predicted molecular weight 49kDa, the siRNA positive control allows correct identification of the band at approx. 55kDa. **B)** Western blot shows loss of IFT88 protein levels in *IFT88* C29$^{+/-}$ and C31$^{if.del/-}$ cell lines compared to negative control when normalised to Vinculin loading control. **C)** RPGRIP1L protein levels reduced in both cell lines and siRNA knock-down compared to siScr negative control. Expected bad size 150kDa but bands appeared at approx. 40kDa. **D)** TMEM67 protein levels were reduced in both the si*TMEM67* and *TMEM67* C47$^{+/-}$ samples when normalised to vinculin and compared to siScr control **E)** *TMEM216* mRNA levels were reduced in siRNA and edited cell line samples when normalised to *ACTB* mRNA levels and compared to siScr control. Results were interpreted across n=3 experimental replicates for western blots and n=1 for RT-PCT. Quantifications were therefore applicable to TMEM216 cell lines. Average protein levels presented in graphs, normalised to loading controls. All westerns were loaded with RPE-1 whole cell extracts. Error bars represent Standard Deviation.

5.2.3 Ciliary Phenotypes

9/10 of the CRISPR/Cas9-edited cell lines that were phenotyped and validated by high-throughput high content imaging had significant changes to either cilia length or cilia incidence compared to pooled wild-type (WT) control cells that had also been clonally selected (Figure 5.5 & Figure 5.6). *CEP290 C53*$^{+/-}$ did not show any significant change in the ciliary phenotypes measured across the polyclonal cell population (Figure 5.5). This is despite 2 alleles across the polyclonal cell population with frame-shift mutations (Table 5.3).

IFT88 C31$^{if.del/-}$ was also a deleterious mutation, despite an in-frame deletion on one allele. Protein levels were also higher in this cell line compared to *IFT88* C29$^{+/-}$ but the cilia incidence and length defects were more significantly different when compared to wild-type controls (Figure 5.5 & Figure 5.6).

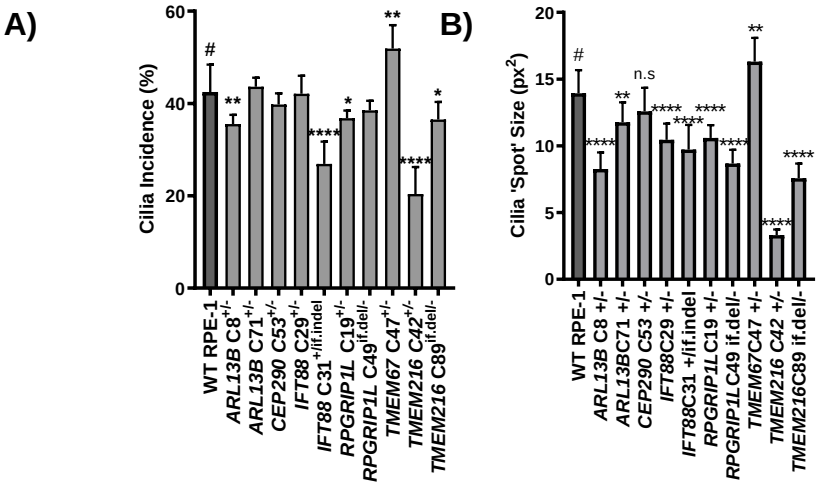

Figure 5.5 High-throughput quantification of cilia incidence and cilia spot size in CRIPSR/Cas9-edited cell lines

A) 6/10 cell lines showed a significant change in ciliary incidence. *ARL13B* C71$^{+/-}$, *CEP290* C53$^{+/-}$, *IFT88* C29$^{+/-}$, and *RPGRIP1L* C49$^{if.del/-}$showed no significant change in ciliary incidence. *TMEM67* C47$^{+/-}$ however showed a significant increase in ciliary incidence. **B)** 9/10 cell lines showed a significant decrease in cilia membrane area (measured as spot size in pixels squared (px^2)). *TMEM67* C47$^{+/-}$ was the only clone to show a significant increase in cilia size compared to wild-type controls. *CEP290* C53$^{+/-}$ did not have any significant change in either cilia incidence or cilia length. Data was confirmed to be normally distributed using a D'Agostino & Pearson omnibus K2 test. Significance was calculated with One-Way ANOVA with Dunnets test for multiple corrections. where # indicates the control each data set was compared to. * = p<0.05, ** = p<0.01, ***= p<0.001, **** = p<0.0001. Error bars represent S.D.

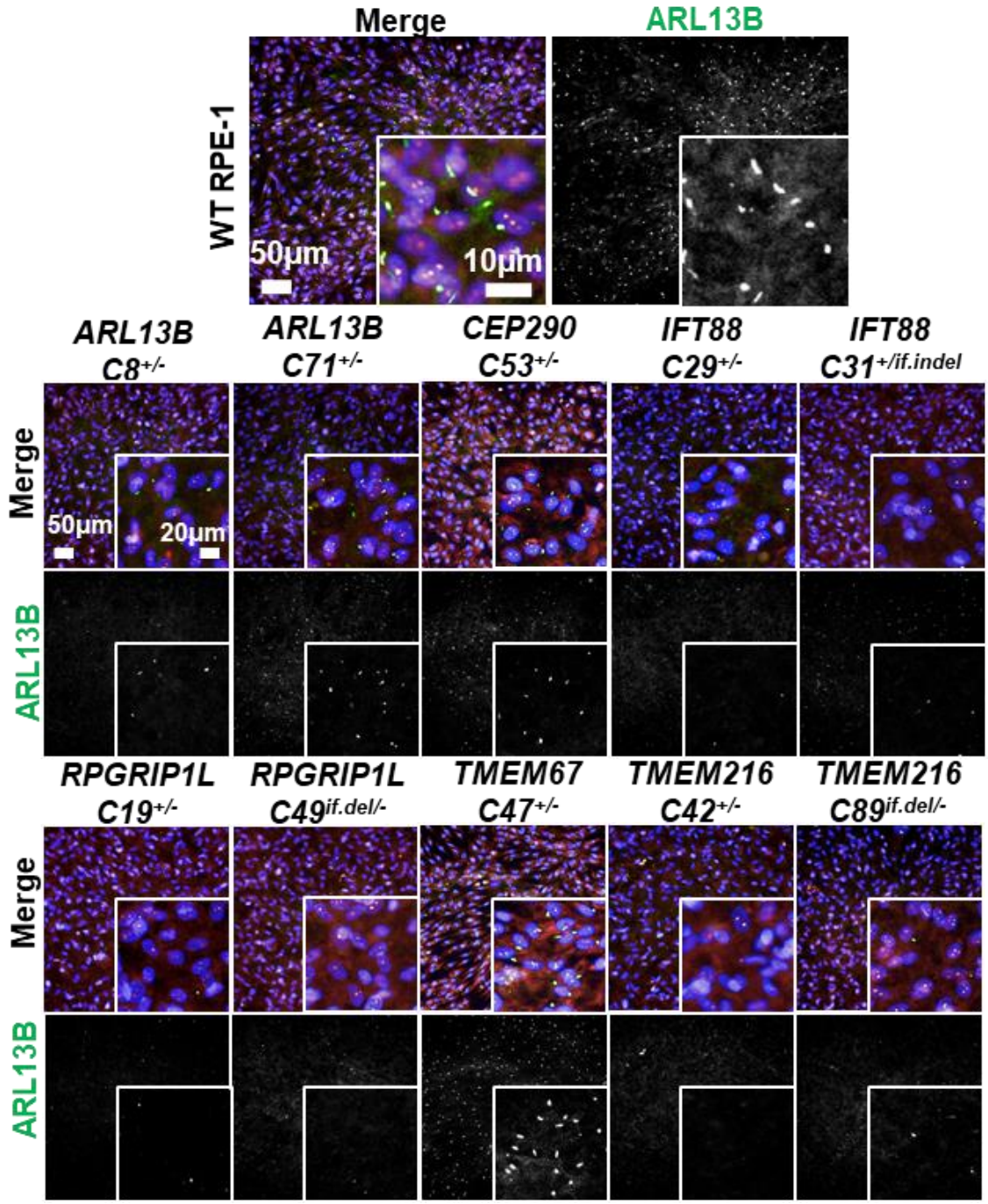

Figure 5.6 High-throughput high content imaging of CRISPR/Cas9 mutant cell-lines shows qualitative changes in cilia incidence and size

Raw image data from Operetta high-throughput imaging shows qualitative differences in cilia incidence and spot size. Cilia incidence appears to be lowest in the *RPGRIP1L* and *TMEM216* mutant cell lines. *ARL13B* C71$^{+/-}$ and *CEP290* C53$^{+/-}$ have similar ciliary staining patterns to wild-type (WT) RPE-1. *TMEM67* C47$^{+/-}$ cilia appear brighter than WT RPE-1 cells, which could reflect increased cilia length or ARL13B expression. Confluency is consistent across all cell lines imaged and so changes in cilia incidence could not be influenced by cell density.

5.2.4 *CEP290* C53$^{+/-}$ polyclonal cell line validation

Despite sequencing suggesting deleterious mutations and western blot showing a significant loss of protein across the polyclonal population in the *CEP290* C53$^{+/-}$ cell line, high-throughput imaging showed no significant phenotype for cilia incidence or spot size when compared to wild-type controls. This cell line was shared with a collaborator, Dr. Elisa Molinari at Newcastle University, so that their validated CEP290 antibody could be used for western blot (Figure 5.7B).

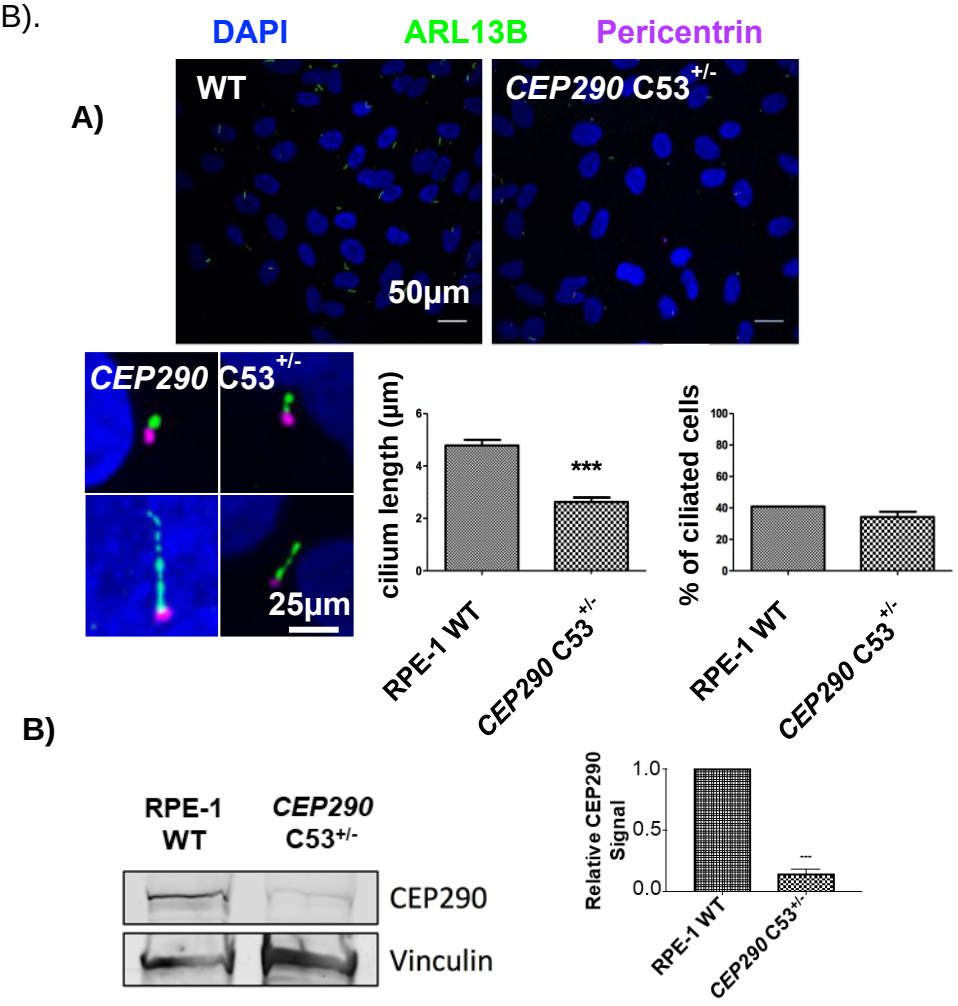

Figure 5.7 *CEP290* C53+/- cell line has significantly smaller cilia compared to wild-type controls

No significant change in cilia incidence was seen in the C53$^{+/-}$ cell line compared to WT controls. However, changes in cilia size leading to a significant decrease in average length across the population were observed. The presence of bulbous cilia and discontinuous ARL13B staining was also noted. Experimental work, analysis and figures were provided by Dr. Elisa Molinari, Newcastle University. Significance was tested with a two-tailed Student's T-test. *** = p<0.001 **B)** Western blot shows significant loss of CEP290 in the *CEP90* C53 +/- polyclonal cell line relative to wild-type (WT) RPE-1 controls, down to approximately 15% n=3. Full figure provided by Dr. Elisa Molinari, Newcastle University. Error bars represent S.D.

After the lack of quantifiable phenotype that was seen in high-throughput imaging, the cell line was tested again in Newcastle. Their work showed that although there was no significant difference in cilia incidence, there was a significant change to cilia size in the *CEP290* C53$^{+/-}$ cell line, including the presence of some bulbous cilia and discontinuous ARL13B staining (Figure 5.7). This meant that the *CEP290* polyclonal mutant cell line was suitable to take forward for combinatorial screening, as it showed a significant ciliary phenotype without complete loss of cilia incidence.

5.2.5 Polyclonal Colonies

Two of the 10 chosen cell lines were confirmed to be polyclonal, but were still taken forward for phenotype validation (*ARL13B* C8$^{+/-}$, *CEP290* C53$^{+/-}$). This was justified because the mutant allele frequency and protein levels remained consistent after 5 passages of the cell line. Cilia incidence and length in the cell populations were also consistent across 3 biological replicates of phenotyping (Figure 5.5, Figure 5.6, Figure 5.7)This suggests a stable population ratio of the different mutant cells during routine passaging. However, polyclonal populations may not have maintained a stable population across further passaging and experimental work, which was not tested for, but was considered during interpretation of all downstream work.

5.3 Combinatorial Screen

5.3.1 Set up of the Combinatorial Screen

The panel of siRNAs used in the combinatorial screen were confirmed to knock-down protein or mRNA levels in WT RPE-1 cells compared to a scrambled siRNA negative control (siScr) (Figure 5.8). Once both the heterozygous cell lines and siRNAs were validated, the combinatorial screen was optimised for seeding density, transfection efficiency and immunofluorescent staining of the cilia marker ARL13B.

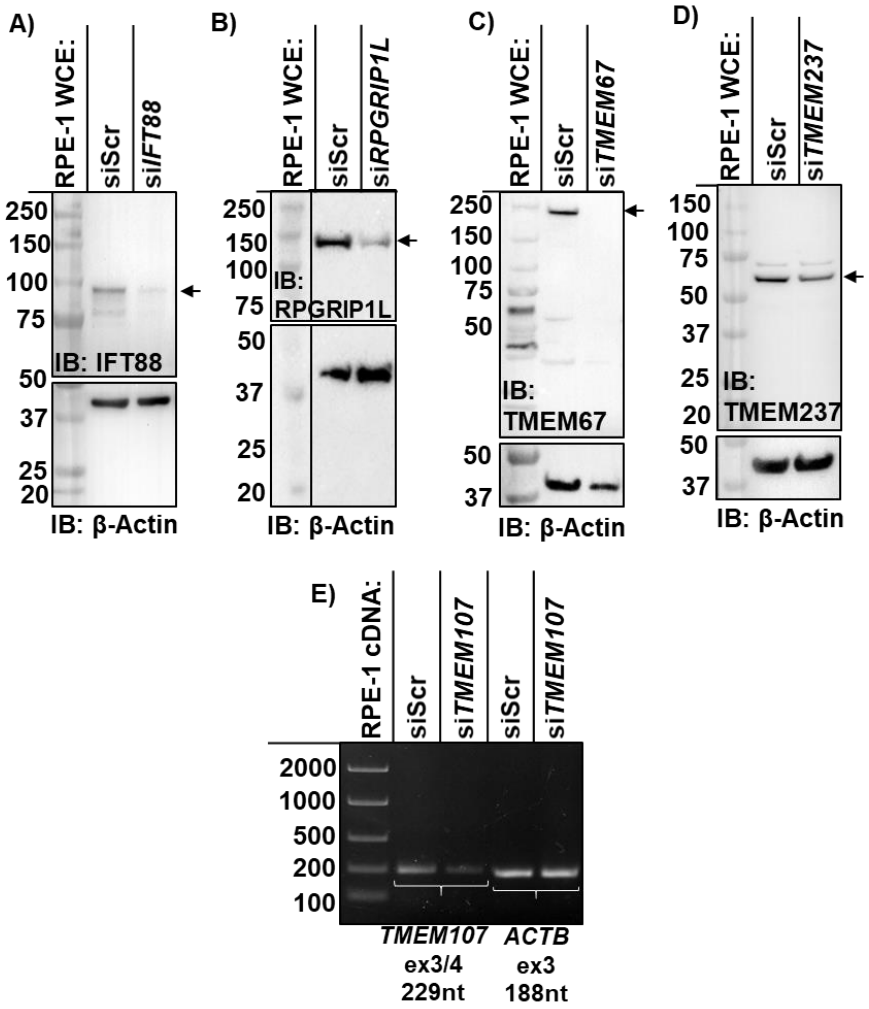

Figure 5.8 Validation of the siRNA panel used in the combinatorial screen

Validation of the *IFT88* **(A)**, *RPGRIP1L* **(B)**, *TMEM67* **(C)**, *TMEM237* **(D)**, and *TMEM107* **(E)** siRNAs used as the siRNA panel in the combinatorial screen by western blot or RT-PCR. There are reduced protein levels in all RPE-1 cells treated with siRNA versus the negative scrambled control (A, B, C, D). Equal loading can be seen in blots when comparing β-actin levels, except in blot C), when quantified and normalised to the loading control there was a reduction in TMEM67 levels compared to the scrambled control. E) *TMEM107* mRNA levels were reduced in the sample treated with siRNA when normalised to *ACTB* mRNA. WCE stands for whole cell extract.

High cell loss was seen in the first combinatorial screen which was not present during optimisation experiments. Therefore during the second round of the combinatorial screening, which screened the *CEP290* and *TMEM67* mutant cell lines, Matrigel® was added to plates prior to seeding and transfection to minimise cell loss.

5.3.2 Primary Analysis of the Combinatorial Screen

Heat maps were used to qualitatively assess transfection efficiency, plate seeding and controls. This initial primary analysis acted as a quality control which excluded any potentially failed screen plates, which could then be repeated. Heat maps also highlighted wells that had high (>50%) loss of cells which were therefore removed from statistical analyses. This was likely due to high-throughput washing steps in the protocol that disturbed the cell monolayer. The addition of Matrigel® coating in the second combinatorial screen reduced the number of wells excluded from the analysis due to cell loss, and any consistent cell loss was mostly confined to a single field of view within a well. Primary analysis also excluded wells on the basis of immunostaining quality. In some wells the staining quality was poor or the field of view was obscured by a dust fragment (Materials and Methods Figure 2.3). Once these individual wells were excluded from the data set, all conditions were covered by a minimum of 2 biological replicates. The screen data was also shown to have strong correlation between experimental replicates, suggesting that the screen is likely to be reproducible (Figure 5.9).

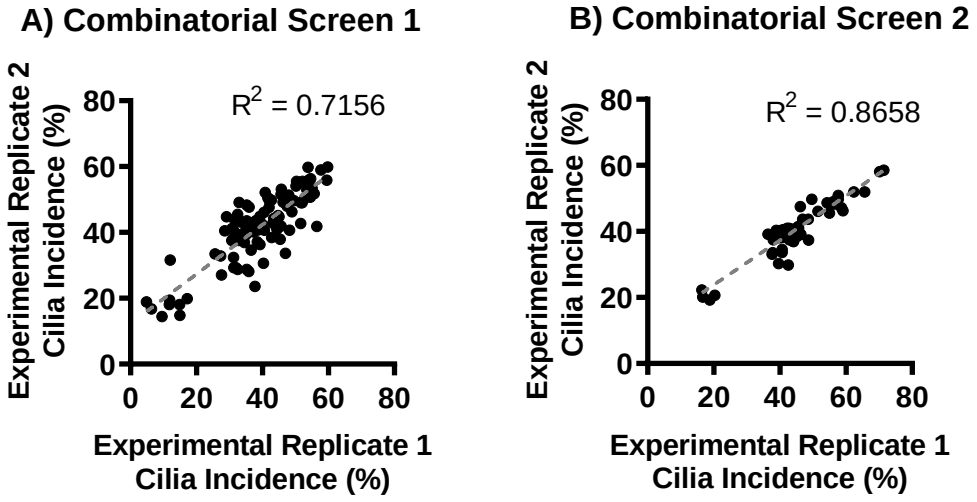

Figure 5.9 Correlation between biological replicates of the combinatorial screen

A) Screen one had a Pearson's Coefficient (R^2) value of 0.7156 between experimental replicate 1 and 2. Despite the inherent variability expected in this screen set up the data could still be considered reproducible as it has a R^2 value >0.5. **B)** The second combinatorial screen only screened 2 CRISPR/Cas9-edited cell lines, *CEP290* C53$^{+/-}$ and *TMEM67* C47$^{+/-}$. When comparing experimental replicate 1 and 2 the screen had an R^2 value of 0.8658, providing evidence that this screen was also reproducible.

After primary analysis was assessed to ensure the quality of screen data, the siRNA controls were assessed using average robust z-scores to determine the transfection efficiency for each screen plate and ensure the accuracy of the automated cilia recognition protocol (Figure 5.10).

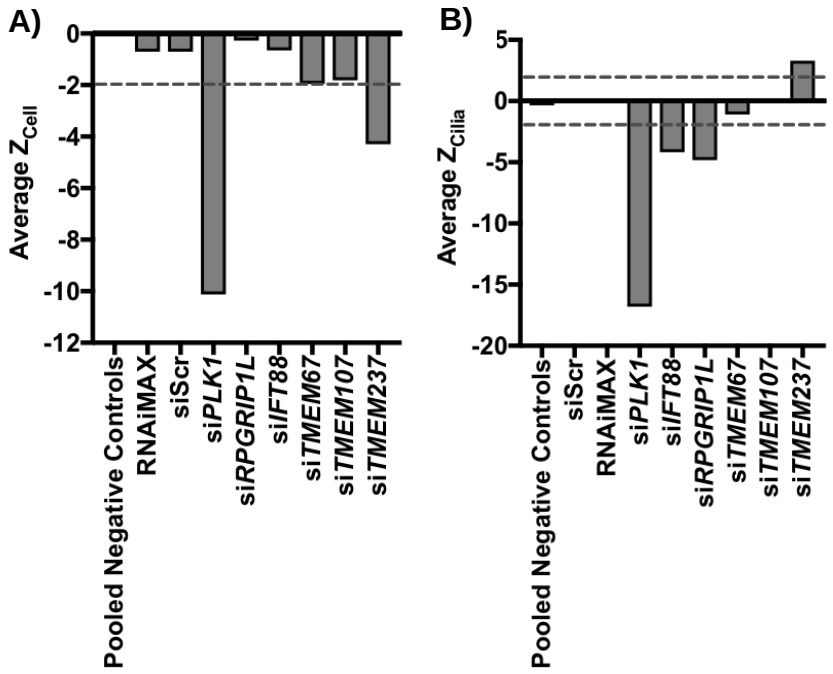

Figure 5.10 siRNA controls were robust in the combinatorial screen

A) Average robust z-scores of siRNA controls in wild-type RPE-1 cells showed that si*PLK1* and si*TMEM237* significantly decreased cell number (z_{cell} <-1.96) compared to negative controls. Loss of *PLK1* causes cell death which is a reproducible and easily quantified phenotype used as the transfection control. The transfection efficiency was therefore estimated from the amount of cell death seen in wells treated with si*PLK1*. **B)** si*IFT88* and si*RPGRIP1L* were used as controls for cilia incidence as these genes are essential for ciliogenesis. Treatment of cells with these siRNAs causes a reproducible and significant decrease in the average robust z-scores for cilia incidence (z_{cilia} <-1.96). These controls were used to validate the cilia recognition protocol but were also included in the analysis for identifying genetic interactions. Grey dotted lines mark cut-offs for significance equivalent to p = 0.05 (1.96< z <-1.96). Significance calculated using robust z-scores.

To minimalize the impact of experimental variation that is inherent when using several cell lines in a single plate high-throughput format, robust z-scores were calculated for each cell line separately throughout the screen. The robust z-scores for CRISPR/Cas9-edited RPE-1 cell lines were then compared to WT RPE-1 for each siRNA condition. Data for each cell line was normalised, so that

irrespective of any genetic background or defined ciliary phenotypes, the negative controls (siScr) in each cell line would have an average robust z-scores for cilia incidence (z_{cilia}) of 0. Therefore, z-scores would represent the change in phenotype due to the siRNA knock-down for each cell line only. Any significant differences between z_{cilia} of the knock-downs in the mutant cell lines and WT RPE-1 could be then attributed to the different genetic backgrounds of those cell lines. This difference is henceforth referred to as Δz_{cilia}. Significant Δz_{cilia} were used to identify genetic interactions between the CRISPR/Cas9-edited genes and the genes targeted with siRNA. The same analysis was used to assess changes in spot size (z_{size}), assumed to represent cilia size. The statistical method is outlined in (Chapter 2, Section 2.2.17.3).

5.4 Genetic interactions of Cilia Incidence

The combinatorial screen provided evidence for 14 potential synergistic interactions, of which 2 present as a reciprocal pair. There is also evidence for 8 additive interactions and one antagonistic interaction inferred from the screen.

5.4.1 Additive Genetic Interactions

Eight additive genetic interactions were identified from the cilia incidence data. These interactions had a significant change in cilia incidence but the change was not significantly greater than that seen in the WT RPE-1 cells treated with the same siRNA:

$$1.96 \leq Average\ z_{cilia} \leq -1.96 \text{ and } 1.96 > \Delta z_{cilia} > -1.96$$

The genetic background of the CRISPR/Cas9-edited cell line did not significantly change the loss of cilia caused by the siRNA knock-down, so each genetic background had the same proportional cilia loss. However if raw data were to be compared it would show a more severe phenotype than the WT cells treated with the same siRNA.

ARL13B cell-lines only presented with additive genetic interactions (Figure 5.11) and no synergistic or antagonistic interactions were inferred from the combinatorial screen data. This was also the cell line that showed the highest variation in z-scores across biological and technical replicates of the screen.

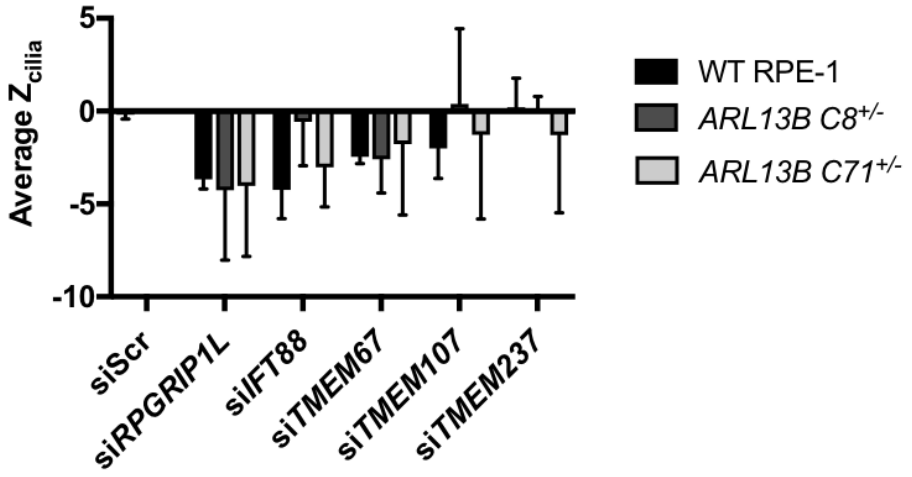

Figure 5.11 Additive synthetic genetic interactions identified in *ARL13B* CRISPR/Cas9-edited cell lines.

ARL13B mutant cell lines showed very high variability between biological replicates. Reducing the ability to accurately identify any potential genetic interactions using the combinatorial screening methodology. However, additive genetic interactions were suggested between *ARL13B* and *RPGRIP1L*. Significance calculated using Δz (described in Section 2.2.17.3) Error bars represent S.E.M.

5.4.2 Synergistic Genetic Interactions

Twelve synergistic genetic interactions were identified from the cilia incidence data. These interactions had a significant change in cilia incidence that was significantly greater than that seen in WT RPE-1 cells treated with the same siRNA:

$1.96 \leq Average\ z_{cilia} \leq -1.96$ and $1.96 < \Delta z_{cilia} < -1.96$

Thus the genetic background of the mutant cell line meant that proportionally, when normalised to base levels of cilia incidence, there was a greater effect on the cilia incidence phenotype in the mutant cell lines compared to WT RPE-1 cells. This suggested a synthetic synergistic interaction between the CRISPR/Cas9-edited gene and the gene targeted for knock-down by siRNA.

5.4.2.1 *IFT88* and Transition Zone Genes

IFT88 is well known to be a central regulator of ciliogenesis and ciliary maintenance (13, 38) as part of the IFT B complex (57, 374), therefore it was not unexpected that it was part of many of the genetic interactions identified

(5/12 total synergistic interactions for cilia incidence). All of the synthetic synergistic interactions involving *IFT88* were with transition zone genes (Figure 5.12A). A clear triad of interactions was noted between *IFT88, RPGRIP1L* and *TMEM67* as these showed partial reciprocal interactions (Figure 5.12B, C).

IFT88 C29$^{+/-}$ and *C31*$^{+/if.del}$ treated with si*RPGRIP1L* had a z_{cilia} of -8.32 and -7.50 respectively, showing a significant loss in cilia incidence. In contrast, the z_{cilia} for WT cells treated with si*RPGRIP1L* was -3.68, significantly lower than the loss of cilia seen in the *IFT88* cell lines ($\Delta z_{cilia} = 4.64$ and 3.82 respectively, equivalent to $p<0.00001$ and $p=0.000233$) (Figure 5.12A). As the sum loss of cilia was higher than that seen in either gene individually, this was taken forward as a synthetic synergistic interaction between *IFT88* and *RPGRIP1L*.

The reciprocal interaction between *IFT88* and *RPGRIP1L* was tested in *RPGRIP1L C19*$^{+/-}$ and *RPGRIP1L C49*$^{if.del/-}$ cells treated with si*IFT88.* The z_{cilia} were -0.75 and -6.21, with Δz_{cilia} of -3.50 and 1.96 respectively (Figure 5.12B). Therefore the *RPGRIP1L C49*$^{if.del/-}$ also showed a synergistic interaction with *IFT88* ($p=0.05$), but this was not replicated in the *RPGRIP1L C19*$^{+/-}$ cell line.

IFT88 C29$^{+/-}$ and *C31*$^{+/if.del}$ treated with si*TMEM67* had z_{cilia} of -12.71 and -6.74 and Δz_{cilia} of 10.26 and 4.29 respectively (Figure 5.12A). These suggested a strong synthetic synergistic interaction. However, an interaction between *IFT88* and *TMEM67* was only partially supported by the reciprocal experiment. *TMEM67* C47$^{+/-}$ treated with si*IFT88* had a significant loss of cilia ($z_{cilia} = -2.39$), but this was seen only as an additive interaction as the loss of cilia seen in WT cells treated with si*TMEM67* was larger ($z_{clia} = -3.74$) (Figure 5.12C).

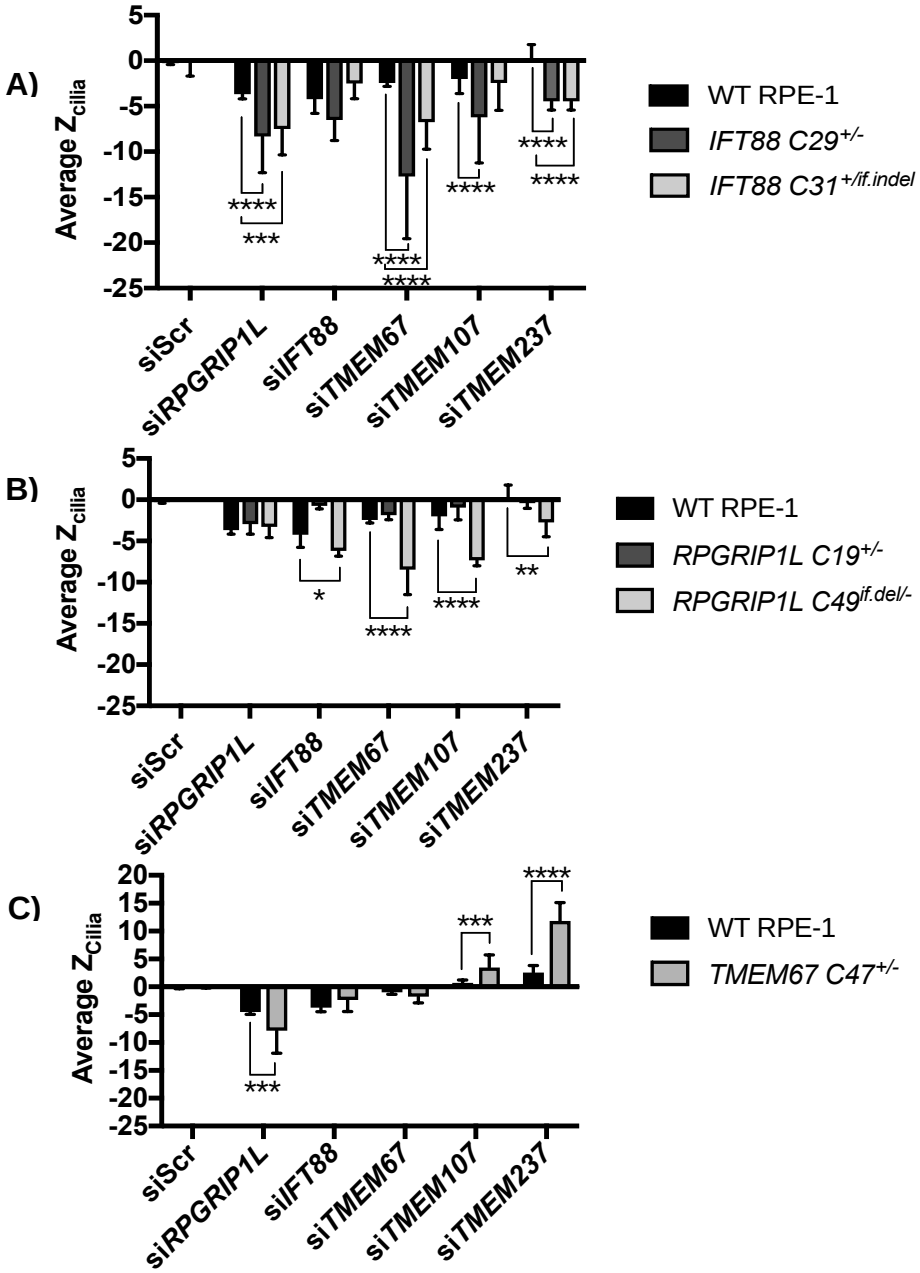

Figure 5.12 Genetic interactions between *IFT88* and transition zone genes

A) *IFT88* mutant cell lines had significantly greater loss of cilia when treated with si*RPGRIP1L*, si*TMEM67* and si*TMEM237* compared to WT cells treated with the same siRNAs. This suggested a synthetic genetic interaction between *IFT88* and each of these genes. **B)** *RPGRIP1L* mutant cell lines only showed potential genetic interactions for the *RPGRIP1L* C49$^{if.del/-}$ cell line, none of which were replicated in the C19$^{+/-}$ cell line. *RPGRIP1L* C49$^{if.del/-}$ showed a reciprocal synthetic synergistic interaction with *IFT88*. Synergistic interactions were also suggested with *TMEM67*, *TMEM107* and *TMEM237*. **C)** The *TMEM67* mutant cell line showed a reciprocal interaction with *RPGRIP1L*, an additive interaction with *IFT88* and synergistic interactions with *TMEM107* and *TMEM237*. Significance was calculated using Δz scores, representing the number of standard deviations between each experimental value and the comparison value (described in Section 2.2.17.3) * = $1.96<\Delta z<-1.96$, ** = $2.58<\Delta z<-2.58$, *** = $3.3<\Delta z<-3.3$, **** = $3.89<\Delta z<-3.89$. Error bars represent S.E.M.

RPGRIP1L C19$^{+/-}$ and *C49*$^{if.de/-}$ treated with si*TMEM67* had z_{cilia} of -1.88 and -8.50 with Δz_{cilia} of -0.58 and 6.04 respectively (Figure 5.12B). As seen with si*IFT88*, there was no discernible genetic interaction for the *RPGRIP1L C19*$^{+/-}$ cell line. However, the large Δz_{cilia} value observed for *C49*$^{if.de/-}$ suggested a strong synergistic interaction between *RPGRIP1L* and *TMEM67.* This was supported by the reciprocal interaction when *TMEM67 C47*$^{+/-}$ was treated with si*RPGRIP1L*, which had a z_{cilia} of -7.87 and a Δz_{cilia} of 3.35 Figure 5.12C).

5.4.2.2 Synergistic interactions that increased cilia incidence

The second combinatorial screen consistently showed that si*TMEM237* increased cilia incidence (z_{cilia} = 2.58). However, this phenotype was not significant in the first combinatorial screen (z_{cilia} = 0.20), possibly due to higher variation across the first screen. Three synergistic interactions that increased cilia incidence were suggested from the second combinatorial screen data, one of which was the only synergistic interaction inferred for *CEP290*. The increased cilia incidence phenotype was further significantly increased in *CEP290* C53$^{+/-}$ polyclonal cells treated with si*TMEM237* (Figure 5.13) and *TMEM67* C47$^{+/-}$ cells treated with si*TMEM237* or si*TMEM107* (Figure 5.12C). The increase in cilia incidence was greater than that seen in WT cells treated with the same siRNA.

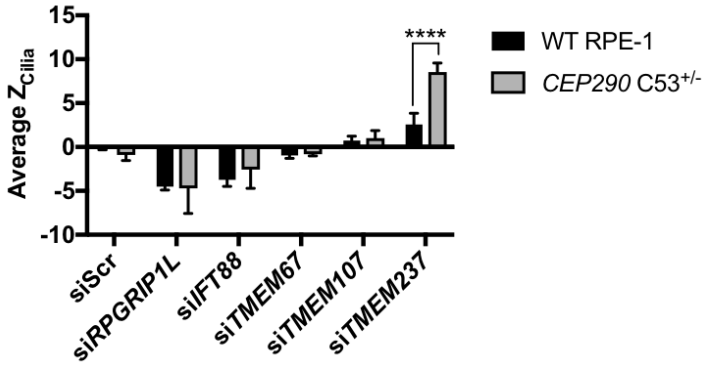

Figure 5.13 *TMEM237* knock-down increases cilia incidence

CEP290 edited cells did not show any significant ciliary phenotype compared to WT RPE-1. However, when treated with si*TMEM237* there was a significantly greater increase in cilia incidence (z_{cilia} for WT RPE-1 = 2.578 and for *CEP290* C53$^{+/-}$ = 8.553). This would suggest a potential synergistic interaction between *CEP290* and *TMEM237.* This was also the only synthetic genetic interaction suggested for *CEP290* that affected cilia incidence. Significance was calculated using Δz scores, representing the number of standard deviations between each experimental value and the comparison value (described in Section 2.2.17.3). **** = 3.89<Δz. Error bars represent S.E.M.

5.4.3 Antagonistic Genetic Interactions

In addition to the above genetic interactions which further perturbed or increased ciliary incidence, an antagonistic interaction was also inferred for ciliary incidence between *TMEM216* and *RPGRIP1L*. In both *TMEM216* CRISPR/Cas9-edited cell lines there was a significantly lower cilia incidence compared to WT controls. When these cells lines were treated with si*RPGRIP1L* cilia incidence increased, whereas WT RPE-1 cells had a significant decrease in cilia incidence in response to si*RPGRIP1L* (Figure 5.14). This suggests an antagonistic interaction between *TMEM216* and *RPGRIP1L*.

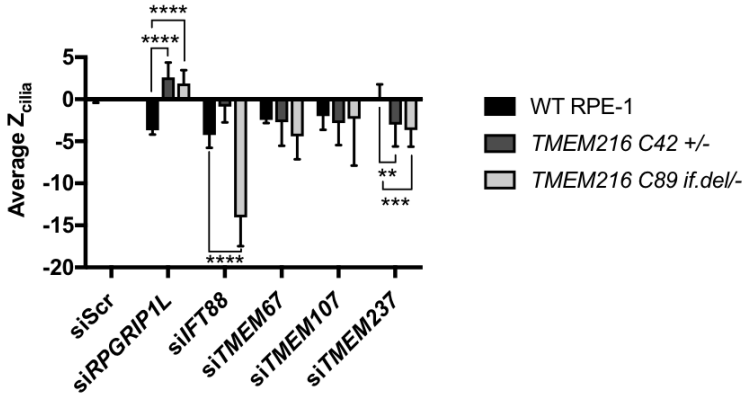

Figure 5.14 A potential antagonistic interaction between *RPGRIP1L* and *TMEM216* affecting cilia incidence

TMEM216 heterozygous cell lines showed a significant loss of cilia compared to wild-type (WT) RPE-1 cells. Each cell line was normalised to siScr control in order to quantitate the differences in response to each siRNA treatment. There was a significant increase in cilia incidence for both *TMEM216* edited cell lines following knock-down of *RPGRIP1L*, whereas WT RPE-1 showed a significant decrease. This suggests an antagonistic synthetic genetic interaction between *TMEM216* and *RPGRIP1L.* Significance calculated using Δz scores, representing the number of standard deviations between each experimental value and the comparison value (described in Section 2.2.17.3). ** = $2.58<\Delta z<-2.58$, *** = $3.3<\Delta z<-3.3$, **** = $3.89<\Delta z<-3.89$. Error bars represent S.E.M.

Raw data from the combinatorial screen was used to assess the extent of the rescue of cilia incidence in this synthetic antagonistic interaction. This showed that cilia incidence increased in the *TMEM216* mutant cell lines with *RPGRIP1L* knock-down compared to negative controls. However, this was not a significant increase and under these conditions cilia incidence was still significantly lower than in WT RPE1 controls (Figure 5.15). Although the raw data did not support

a statistically significant difference, the trend of the data suggested an antagonistic interaction.

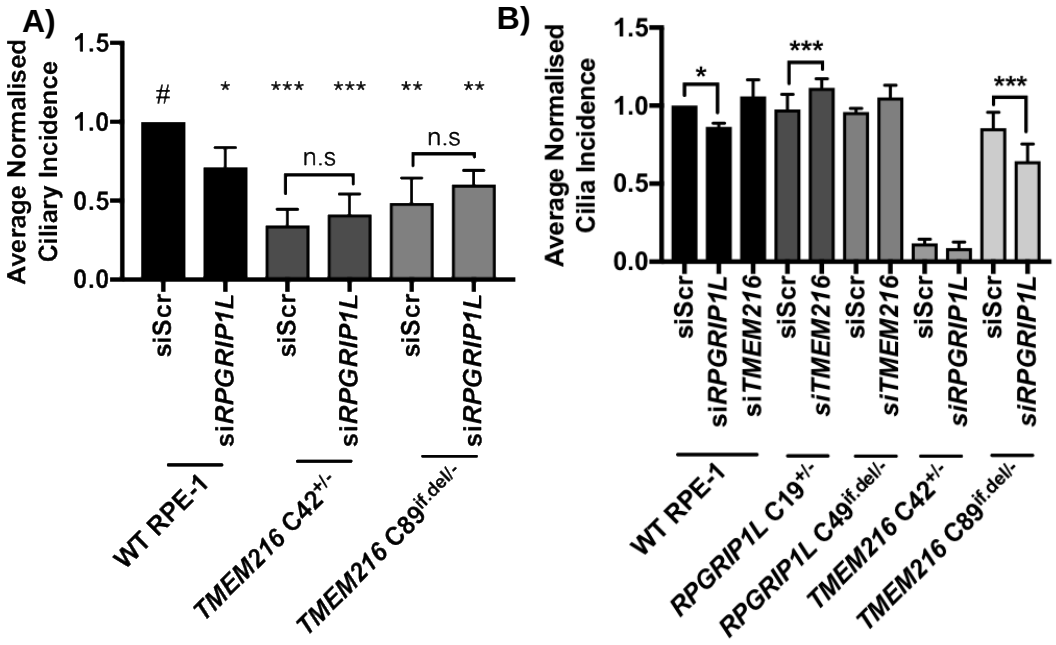

Figure 5.15 Validating a synthetic antagonistic interaction between *RPGRIP1L* and *TMEM216*

A) Normalised raw data from the combinatorial screen showed an increase in cilia incidence in both *TMEM216* mutant cell lines treated with si*RPGRIP1L*, but was not significant and did not rescue cilia incidence to WT levels. **B)** A secondary screen with both *RPGRIP1L* and *TMEM216* mutant cell lines contradicted the primary screen and indicated reduced cilia incidence in *TMEM216* mutant cell lines treated with si*RPGRIP1L*. However, *RPGRIP1L* C19$^{+/-}$ showed a significant increase in cilia incidence with *TMEM216* knock-down. There was also an increase in cilia incidence in WT RPE-1 cells treated with si*TMEM216*. This suggested *TMEM216* knock-down alone increased cilia incidence and *TMEM216* does not have an antagonistic relationship with *RPGRIP1L.* Data was confirmed to be normally distributed using a D'Agostino & Pearson omnibus K2 test. Statistical significance was then calculated using two-way ANOVAs with Dunnet's multiple comparisons tests. # indicates the control each data set was compared to. * = p<0.05, ** = p<0.01, *** = p<0.001. Error bars represent S.D.

A secondary validation experiment, with reciprocal experiments in the *RPGRIP1L* cell lines, was therefore carried out in order to test the presence of a synthetic antagonistic interaction. In contrast to the combinatorial screen data, *TMEM216* mutant cell lines treated with si*RPGRIP1L* had a further decrease in cilia incidence that did not support an antagonistic interaction. However, *RPGRIP1L* mutant cell lines treated with si*TMEM216* did have an increase in cilia incidence and were rescued to WT levels (Figure 5.15). In WT cells,

TMEM216 knock-down also had a trend of increased cilia incidence. Therefore, it is unlikely that the mutations in *RPGRIP1L* have an antagonistic affect and that *TMEM216* knock-downs alone can increase cilia incidence in this screen (Figure 5.15). This data also highlighted the difference between transient knock-downs with siRNA and stable CRISPR/Cas9 knock-outs: *TMEM216* siRNA knock-down in WT cells increased cilia incidence whereas the heterozygote *TMEM216* mutant cell lines had significantly fewer cells when compared to WT RPE1.

5.5 Further investigation of synthetic synergistic interactions between *IFT88*, *RPGRIP1L* and *TMEM67*

When all the inferred interactions from the combinatorial screen were summarised, a triad of partially reciprocal genetic interactions between *IFT88*, *RPGRIP1L* and *TMEM67* was prominent.

Previous research in *C. elegans* has also genetically linked the separate structural modules of the transition zone containing RPGRIP1L and TMEM67. The *RPGRIP1L* orthologue *mks-5*, which is part of the NPHP module (Figure 5.1), was shown to functionally and genetically interact with the MKS module which includes *TMEM67* (*mks-3*) (Figure 5.1) (375). Although a genetic interaction between *RPGRIP1L* and *TMEM67* was not directly tested, the *RPGRIP1L* (*mks-5*) mutants failed to localise TMEM67 (mks-3) and all other MKS module components to the transition zone, suggesting a functional link between the 2 modules (375). To determine if this interaction was conserved in mammalian cilia, *RPGRIP1L* heterozygote mutant RPE-1 cells were assessed to identify if any other proteins within the *IFT88-RPGRIP1L-TMEM67* triad were mis-localised in each of the CRISPR/Cas9-edited cell lines.

5.5.1 Mislocalisation of TMEM67 in *IFT88* and *RPGRIP1L* heterozygous mutants

To test if the observed genetic interactions also mediated a functional link between these modules in the transition zone (NPHP and MKS modules) and IFT, the localisation of each protein for each of the heterozygous mutants within the *IFT88-RPGRIP1L-TMEM67* interaction triad was determined.

IFT88 co-localisation with either acetylated α-tubulin or γ-tubulin did not significantly change in *IFT88*, *RPGRIP1L* or *TMEM67* CRISPR/Cas9 edited cell-lines when compared to WT RPE-1 controls (data not shown). This suggested that there was no functional link between maintaining the integrity of the transition zone and the correct localisation of IFT88. Localisation of RPGRIP1L also did not show any changes in localisation in the *IFT88* heterozygous mutant cell lines, however RPGRIP1L did show a greater increase in co-localisation with the basal body marker γ-tubulin in the *TMEM67* C47$^{+/-}$ cell line (Figure 5.16). This could suggest that in *TMEM67* C47$^{+/-}$ cells, RPGRIP1L and the transition zone had extended more proximally towards the basal body, as the co-localisation with the ciliary axonemal marker acetylated α-tubulin did not significantly change.

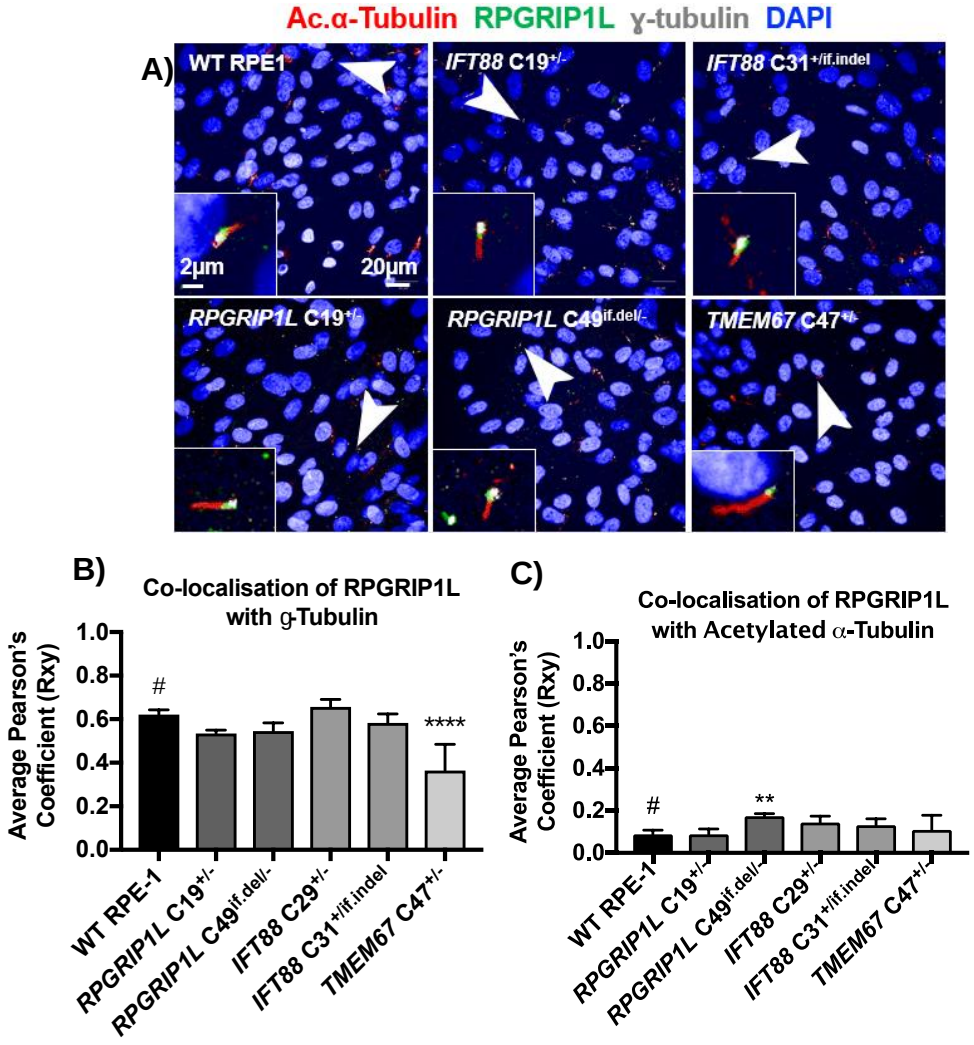

Figure 5.16 RPGRIP1L was mis-localised in *TMEM67* C47+/- cell line

A) Image data from each cell line stained for acetylated α-tubulin (ciliary axonemal marker), RPGRIP1L and γ-tubulin (basal body marker). Examples of cilia for each cell line are highlighted (white boxes and marked by white arrowheads). In the *TMEM67* C47$^{+/-}$ cell line; RPGRIP1L did not co-localise with the basal body to the same extent as other cell lines. **B)** When quantified this shows a significant shift in RPGRIP1L distally from the basal body. **C)** Although there is a slight increase, there is no significant change to co-localisation of RPGRIP1L with acetylated α-tubulin. Data was confirmed to be normally distributed using a D'Agostino & Pearson omnibus K2 test. Statistical significance was then calculated using one-way ANOVAs with Dunnet's multiple comparisons tests, where # indicates the control each data set was compared to. ** = p<0.01 and **** = p<0.0001. Error bars represent S.D. N=3 technical replicates with over 1000 cells over 300 cilia analysed per replicate high-throughput

TMEM67 localisation however was significantly affected in all of the cell lines tested. Wild-type cells showed TMEM67 in the transition zone with some distal localization along the ciliary membrane as previously reported (60, 376).

However, TMEM67 showed significantly reduced co-localisation with acetylated α-tubulin and significantly greater co-localisation with γ-tubulin (Figure 5.17). This suggested that TMEM67 was restricted to the transition zone in both *RPGRIP1L* and *IFT88* CRISPR/Cas9-edited cell lines.

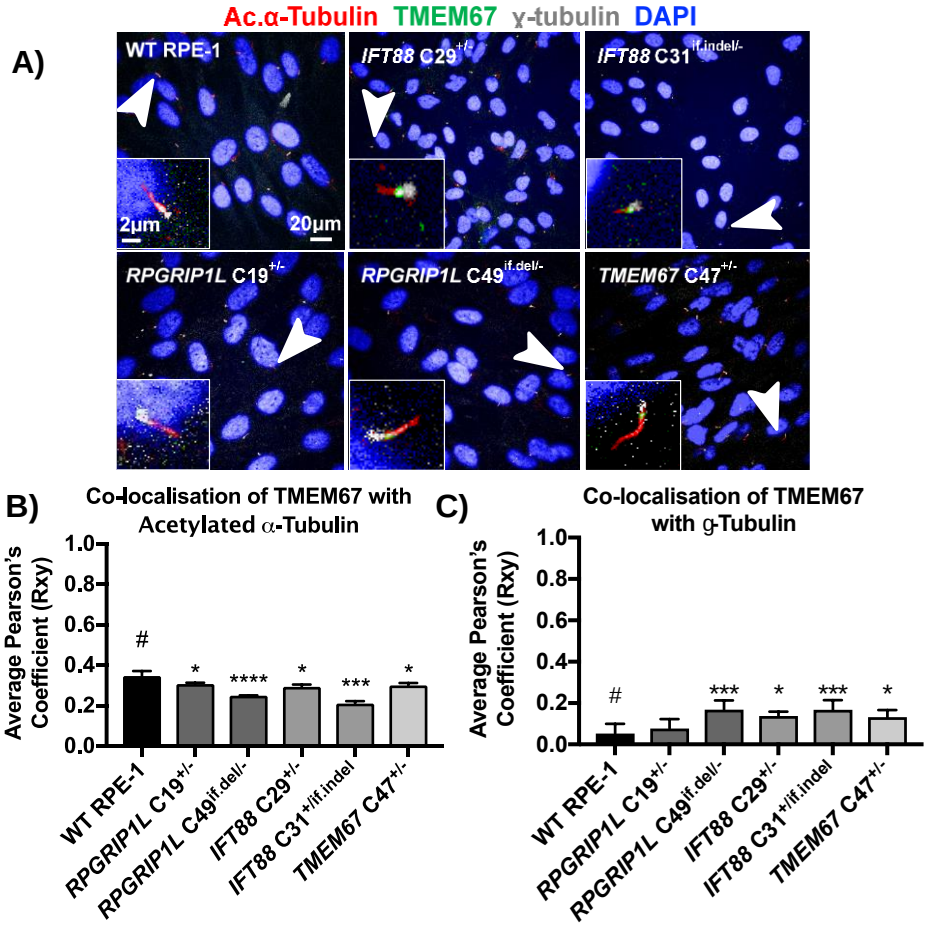

Figure 5.17 TMEM67 mis-localises in *RPGRIP1L* and *IFT88* heterozygote mutant cell lines

A) TMEM67 extends distally from the transition zone the ciliary membrane in wild-type cells. In *IFT88, RPGRIP1L* and *TMEM67* heterozygous mutant cells; TMEM67 appeared as a distinct spot at the base of the cilium, with no distal extension **B)** There was a statistically significant reduction in co-localisation of TMEM67 with the axonemal marker acetylated α-tubulin, despite an associated decrease in cilia length. **C)** TMEM67 staining showed an associated increased co-localisation with γ-tubulin in *RPGRIP1L*, *IFT88* and *TMEM67* CRIPSR/Cas9 edited cell lines. Data was confirmed to be normally distributed using a D'Agostino & Pearson omnibus K2 test. Statistical significance was then calculated using one-way ANOVAs with Dunnet's multiple comparisons tests, where # indicates the control each data set was compared to. * = p<0.05, *** = p<0.001 and **** = p<0.0001. Error bars represent S.D. N=3 technical replicates with over 1000 cells over 300 cilia analysed per replicate (high-throughput).

It is likely that the changes in localisation of TMEM67 in these cell lines was driven through different pathways because different ciliary modules (the IFT and the NPHP transition zone modules) were affected. It was also interesting to note that in the *TMEM67* C47$^{+/-}$ cell line, TMEM67 localisation was significantly altered. There was reduced distal localization along the ciliary membrane and an increase in co-localisation with the basal body, indicating a shift in the position of the transition zone. The reduced co-localisation with the ciliary axoneme could be due to reduced protein levels in this cell line (Figure 5.4) or that overall the cilium is longer, affecting the quantified ratio of TMEM67 localisation.

5.5.2 Biochemical interactions between IFT88, TMEM67 and RPGRIP1L

Co-immunoprecipitations were used to test if the synthetic genetic interactions were mediated by biochemical associations. IFT88, TMEM67 and RPGRIP1lL fused to epitope or protein tags in expression constructs were made using Gateway cloning technology (described in Chapter 2, Section 2.2.6.2). The constructs were validated by western blot and Sanger sequencing to demonstrate expression of each protein with the correct tag. Co-immunoprecipitation experiments were initially inconclusive or uninterpretable due to issues with control antibodies, agarose beads or antibody specificity.

GFP-TRAP was then used (described in Chapter 2, Section 2.2.10) as an alternative pull-down reagent to demonstrate a potential biochemical association between IFT88 and RPGRIP1L. IFT88-eYFP fusion protein interacted with 3xFLAG-RPGRIP1L (Figure 5.18). However, a GFP-*RPGRIP1L* construct could not be made and the reciprocal pull-down was not tested. Pull-downs indicated that *C*-terminal tagged TMEM67-TAP was aberrantly small, suggesting that TMEM67 was cleaved from both of its C-terminal fusion tags. However, TMEM67-GFP pulled down 3XFLAG-RPGRIP1L and, separately, IFT88-eYFP pulled down TMEM67-TAP. Taken together these data suggest that there is a potential biochemical interaction between RPGRIP1L, TMEM67 and IFT88, but this requires further investigation because the aberrant size of TMEM67 fusion proteins put into question the reliability of the data. It is possible, for example, that any tag cleavage from TMEM67 only occurred when

WCE or GFP-TRAP samples were prepared for SDS-PAGE. Alternatively, a small amount of full-length tagged TMEM67 may have been present, below the threshold of detection for the antibodies used in blotting, but sufficient to permit the pull down of interacting species.

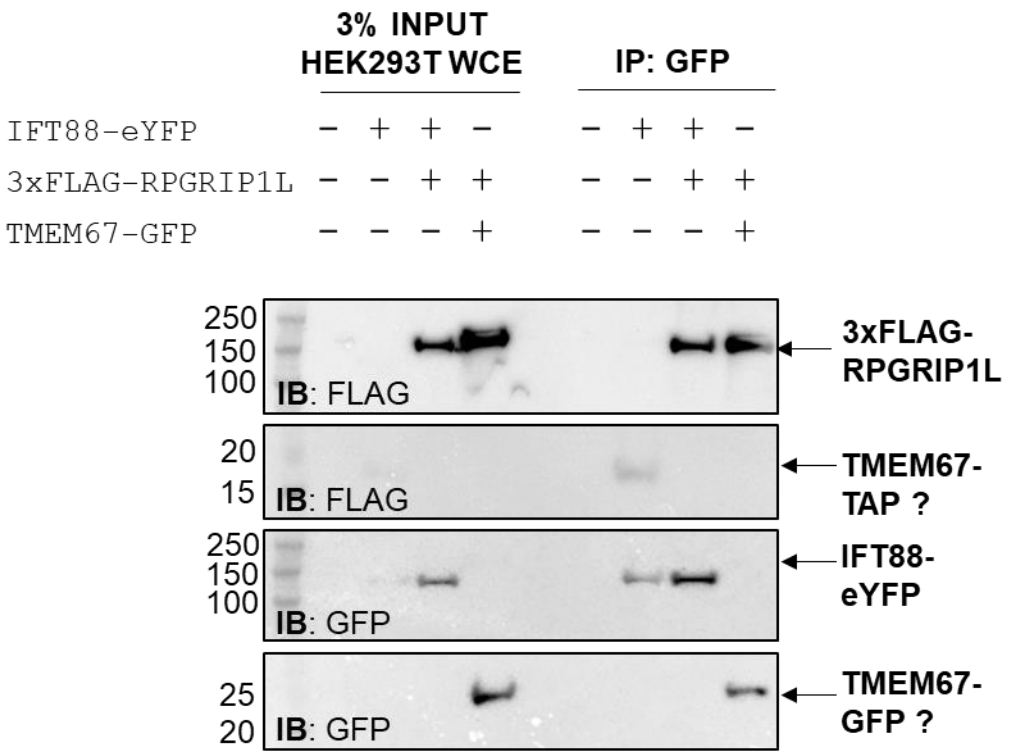

Figure 5.18 IFT88, RPGRIP1L and TMEM67 may biochemically interact

Co-immunoprecipitation of GFP or eYFP tagged fusion proteins from whole cell extract (WCE) of HEK293T cells expressing combinations of the above constructs. A potential biochemical interaction was seen between IFT88 and RPGRIP1L because IFT88-eYFP pulled-down 3XFLAG-RPGRIP1L, although the reciprocal pull down could not be tested. TMEM67 fusion proteins were aberrantly sized when analysed by western blot, migrating in the gel at the approximate molecular weights of the tags only (GFP 27kDa, TAP 20kDa).

5.6 Genetic Interactions of Cilia Size

The second phenotype assessed in the combinatorial screen was cilia size. This was measured indirectly by quantification of the spot size of ARL13B staining. It was suggested that spot size would be a proxy measurement of cilium length as RPE-1 cilia are known to be both partially intracytoplasmic and to lie flat in close association with the apical cell surface (33). Cilia could

therefore be imaged within one imaging plane and lengths measured from a single image plane or maximum intensity projection (37). The aim of this work was to identify interactions that were involved in controlling cilia length, but due to high experimental variation fewer genetic interaction were inferred from this data. This was likely due to the parameters of the recognition protocol (Appendix E.3) or an increase in intrinsic variation in cilia size under “double perturbation” conditions. The screen provided evidence for 3 synergistic interactions, 7 additive interactions and 2 antagonistic interactions.

5.6.1 Antagonistic Interactions

Across the combinatorial screen data for cilia size, 2 antagonistic interactions were inferred. The strongest of all these was between *RPGRIP1L* and *TMEM107* (Figure 5.19). *RPGRIP1L* C49$^{if.del/-}$ had cilia spots with an average z_{size} of 2.70 when treated with siTMEM107 and Δz_{size} of -3.92. *RPGRIP1L* C19$^{+/-}$ cells treated with si*TMEM107* had z_{size} of 1.47, so although not significantly different to *RPGRIP1L C19*$^{+/-}$ treated with siScr control, the Δz_{size} was -2.69 showing it was significantly different to WT RPE-1 cells treated with si*TMEM107*. WT cells treated with si*TMEM107* had an average z_{size} of -1.22, a reduction in cilia size. Therefore the positive z-scores seen in CRISPR/Cas9-edited *RPGRIP1L* cell lines suggested an antagonistic interaction between *RPGRIP1L* and *TMEM107*.

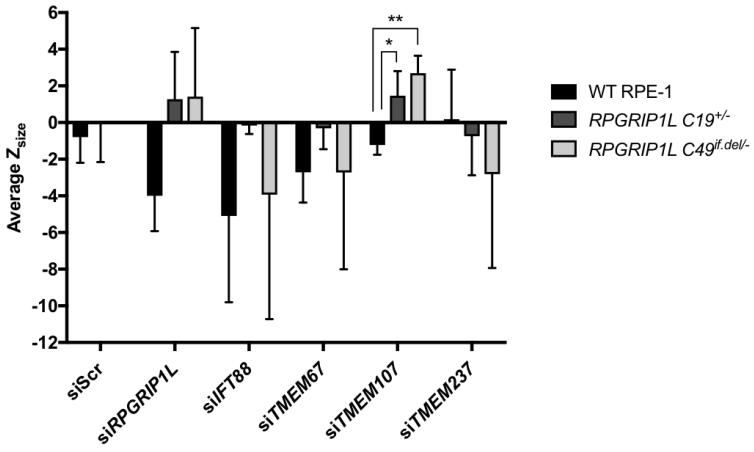

Figure 5.19 A synthetic antagonistic genetic interaction between *RPGRIP1L* and *TMEM107*

RPGRIP1L heterozygous cell lines showed a significant increase in the average robust z-score for cilia spot size (z_{size}) when treated with si*TMEM107* (z_{size} for *RPGRIP1L* C19$^{+/-}$ = 1.47, z_{size} *RPGRIP1L* C49$^{if.del/-}$ = 2.70). In contrast, wild-type RPE-1 cells showed a decrease in cilia spot size when treated with si*TMEM107* (z_{size} = -1.22). This suggested a synthetic antagonistic interaction between *RPGRIP1L* and *TMEM107*. This interaction was seen for both *RPGRIP1L* CRISPR/Cas9-edited cell lines and no other genetic interactions were inferred that affected cilia size in these cell lines. Significance calculated using Δz scores, representing the number of standard deviations between each experimental value and the comparison value (described in Section 2.2.17.3). * = $1.96<\Delta z<-1.96$, ** = $2.58<\Delta z<-2.58$. Error bars represent S.E.M

The raw data from the combinatorial screen was then assessed to determine if the “double perturbation” conditions showed a complete rescue in cilia size (Figure 5.20). There was a complete rescue of cilia size in *RPGRIP1L C19$^{+/-}$* and partial rescue in *RPGRIP1L C49$^{if.del/-}$*. This interaction was therefore chosen to be taken forward for further validation by confocal microscopy.

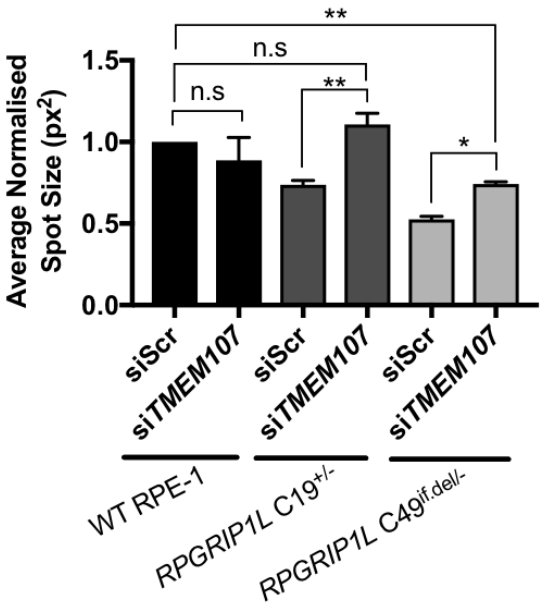

Figure 5.20 Raw data show si*TMEM107* treatment rescues cilia size in *RPGRIP1L* CRISPR/Cas9-edited-cell lines.

Normalised data from the screen indicated that wild-type RPE-1 cells showed no significant change in average cilia size with si*TMEM107* treatment. The loss of cilia membrane area seen in *RPGRIP1L* C19$^{+/-}$ was rescued by si*TMEM107* treatment. The same phenotype in *RPGRIP1L* C49$^{if.del/-}$ was not completely rescued by si*TMEM107* treatment, but a significant increase in average cilia membrane area was seen. Data was confirmed to be normally distributed using a D'Agostino & Pearson omnibus K2 test. Statistical significance was then calculated using a one-way ANOVA with Dunnet's multiple comparisons test. * = p<0.05, ** = p<0.01. Error bars represent S.D

5.7 Further investigation of a synthetic antagonistic interaction between *RPGRIP1L* and *TMEM107*

The interaction between *RPGRIP1L* and *TMEM107* was of interest because it worked antagonistically, could potentially rescue cilia size and could have a

direct downstream effect on ciliary function. This was also the only interaction in which both CRISPR/Cas9-edited cell lines showed corroborating results supporting an antagonistic interaction. All other interactions for cilia size were inferred from a single heterozygous cell line for each mutant gene.

As the screen used high content imaging with a x40 air objective, a lack of resolution prevented accurate measurement of cilia size. Therefore the

interaction was tested again and imaged using confocal microscopy. As seen in the combinatorial screen *TMEM107* knock-down in *RPGRIP1L* heterozygous mutant cells did not significantly change cilia incidence (Figure 5.21). However, this imaging did not confirm an effect on cilia length, suggesting that the original result was a false positive finding and that high content imaging of cilia spot size is a poor proxy measurement for ciliary length. In this confocal image data *TMEM107* knock-down did not rescue ciliary length and, in fact, for *RPGRIP1L* $C19^{+/-}$ cells average ciliary length decreased from 2.9μm to 2.6μm.

Further qualitative inspection of the image data showed a ball-like phenotype in the *RPGRIP1L* heterozygote cells lines with *TMEM107* knock-down. Total ciliary volume was then quantified, which was consistent with the primary combinatorial screen data by showing a significant increase. It is highly likely that this increased ciliary volume and bulbous ball-like phenotype was detected by high content imaging as an increase in ciliary spot size.

To ensure that the bulbous phenotype was not a structural defect of the ciliary axoneme, the total volume of acetylated α-tubulin staining was quantified (data not shown) which showed no significant changes. Qualitatively, staining of acetylated α-tubulin also appeared as expected. This new bulbous phenotype therefore could suggest an IFT-A defect as seen in *Chlamydomonas* (377) and mice (70). Alternatively, it could reflect total disruption of the ciliary gate, allowing diffusion of cytosolic proteins into the cilium causing the ciliary membrane to appear bulbous.

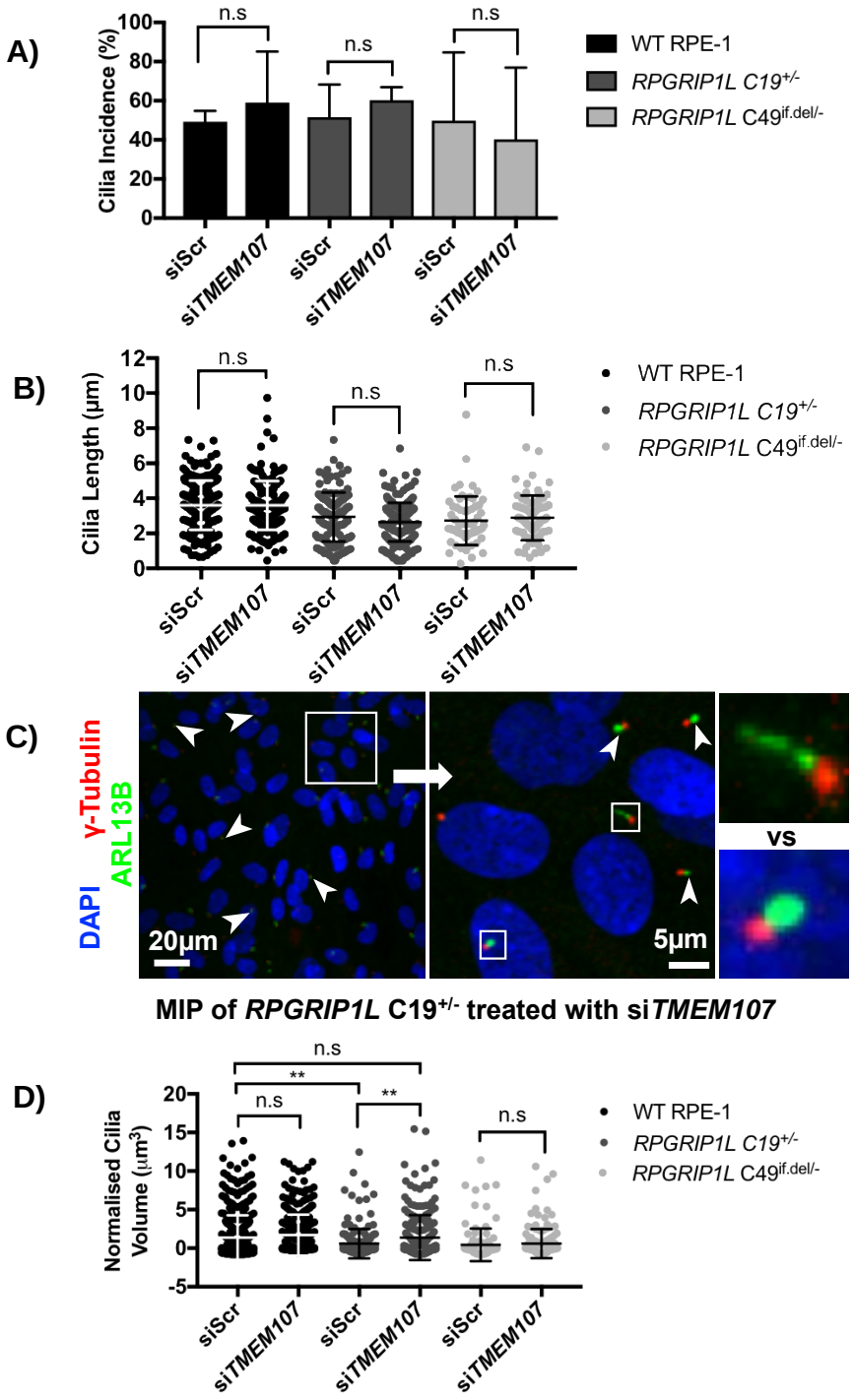

Figure 5.21 Confocal microscopy reveals a cilia volume increase in *RPGRIP1L* heterozygous mutant cell-lines with *TMEM107* knock-down

A) Cilia incidence and **B)** cilia length were not significantly affected by *TMEM107* knock-down in wild-type (WT) or *RPGRIP1L* mutant cell lines. **C)** Qualitative assessment of images showed a bulbous phenotype in *RPGRIP1L* homozygous mutant cell lines. **D)** The volume of *RPGRIP1L* C19$^{+/-}$ cilia was rescued to WT levels following *TMEM107* knock-down. . All data was confirmed to be normally distributed using a D'Agostino & Pearson omnibus K2 test. Statistical significance was then calculated using one-way ANOVAs with Dunnet's multiple comparisons tests, ** = p<0.01 and error bars represent S.D. **** = p<0.0001. Error bars represent S.D.

5.8 Discussion

The 4 main aims of this part of the project were met; CRISPR/Cas9 mutant cells were validated to have a loss of protein but still presented with a quantifiable ciliary phenotype, a combinatorial screen was designed, tested and completed and was shown to be reproducible and able to identify novel genetic interactions. Since the work presented here was completed, it has also been shown that *IFT88* knock-out RPE-1 cells show complete loss of cilia (378). Therefore showing that when assessing ciliogenesis, any genetic interactions with other genes would not have been quantifiable or detectable in complete knock-out cell lines. A triad of interactions for ciliary incidence were further investigated to determine the mechanistic basis for any potential genetic interactions inferred from the primary combinatorial screen data, and a potential biochemical interaction was identified. A second interaction was also followed up for ciliary size which identified a novel phenotype.

5.8.1 CRISPR/Cas9-edited Cell lines

Although significant when compared to cultured wild-type controls, the detected phenotypes in the CRISPR/Cas9-edited cell lines must be assumed to be sub-clinical, as heterozygous parents of ciliopathy patients or unaffected carriers mostly do not manifest any discernible clinical phenotypes. However, there are some reports of heterozygous manifestations of Meckel syndrome presenting with isolated features such as polydactyly and this may be reflected in the more severe cellular phenotypes seen in the *RPGRIP1L* and *TMEM216* CRISPR/Cas9 edited cell lines (Figure 5.5). Mutations in both of these genes cause Meckel Syndrome.

The phenotypes may also be tissue specific, or comprise endophenotypes that manifest under artificial cell culture conditions. The exception to this are *RPGRIP1L* C49$^{if.del/-}$ and *TMEM216* C89$^{if.del/-}$, which are biallelic mutations and could therefore manifest clinically relevant phenotypes.

5.8.1.1 *ARL13B* edited cell lines

The two heterozygous mutants for *ARL13B* showed approximately 50% of the protein seen in WT cells, consistent with the heterozygous null alleles both lines

carried. However, the phenotypes varied slightly: the *ARL13B* $C8^{+/-}$ polyclonal cell line showed a significant decrease in cilia incidence while in $C71^{+/-}$ incidence was highly variable and was therefore not considered to be significant. Conversely, both cell lines did show a significant decrease in cilia size when measured by high content imaging. This could be due to a technical measurement artefact, as discussed in Section 5.7 when validating the genetic interaction between *RPGRIP1L* and *TMEM107*. The overall reduced ARL13B protein levels in these cell lines could reduce apparent spot size either by decreasing total staining, or mis-localising along the ciliary membrane.

Arl13b -/- mice are embryonic lethal but conditional adult knock-outs showed destabilised axonemes and transition zones in the specialised photoreceptor cilium (379). This highlights the severe phenotypes associated with *ARL13B* mutations. As the phenotypes for the *ARL13B* mutant cells used in the project were comparatively mild, it seems likely that the residual protein in the these cell lines was sufficient for adequate ciliogenesis and cilia function.

5.8.1.2 *CEP290* mutant cell line

The only *CEP290* mutant cell line successfully created and investigated was the polyclonal $C53^{+/-}$ cell line. This was shown to have approximately 20% less protein across the cell population and significantly shorter cilia when compared to WT cells (Figure 5.7). This is contrary to the knock-out mouse model, which showed reduced cilia numbers and highly elongated cilia (380). Therefore, as there was no significant change to cilia incidence, this could suggest that the polyclonal population is made up of 2 individual heterozygote cell linages.

It may be of interest to separate this cell line into 2 monoclonal cell lines, to allow transition zone integrity and ciliary function to be more accurately investigated. It is possible that the cell line is 2 separate heterozygote lines and the WT alleles in both cell types are sufficient to maintain a normal ciliary phenotype (Figure 5.5). The *CEP290* orthologue in *Chlamydomonas* shows evidence of being a key structural component of the Y-shaped linkers in the transition zone (381) and likely acts as a scaffold for other transition zone proteins to correctly localise. Therefore, monoclonal mutant cells may present genetic interactions with the ciliary siRNA panel used in the combinatorial

screen and help to decipher the hierarchy of CEP290 in transition zone organisation in this cell line.

5.8.1.3 *IFT88* mutant cell lines

IFT88 is part of the IFT-B module (382), which is responsible for anterograde trafficking from the base to the tip of the cilium. Commonly, IFT-B mutations are associated with complete loss of cilia, as without anterograde transport the cilium is unable to recruit new protein and extend its axoneme.

The heterozygous *IFT88* mutants both presented with significantly shorter cilia than WT controls (Figure 5.5). However, it was interesting to note that *IFT88* C31$^{+/if.indel}$ had a more severe phenotype than C29$^{+/-}$, as it also presented with a significant reduction in cilia incidence. This could indicate that the in-frame deletion of 2 amino acids in *IFT88* was a dominant negative mutation.

IFT88 C31$^{+/if.indel}$ cell line had a loss of total IFT88 protein despite no change being predicted from genotyping and pathogenicity analysis (Table 5.3). The 2 amino acid change NP_001340497.1:p.(Leu125_Ser126delinsCysLys) occurs in an undefined domain of the protein but is close to the predicted start of a TPR-like helical domain (383), which therefore may affect domain or protein stability.

5.8.1.4 *RPGRIP1L* mutant cell lines

Both *RPGRIP1L* heterozygotes had a significant decrease in cilia incidence and a decrease in cilia length compared to WT cells (Figure 5.5), reflecting a similar phenotype seen in embryonic fibroblasts taken from the *Rpgrip1l*$^{-/-}$ mouse (364). However, the *Rpgrip1l* -/- mouse was also independently been shown to have elongated cilia compared to WT embryos, in embryonic fibroblasts and across other cell types (384). The data presented here supports the former study by suggesting that RPGRIP1L has a positive effect on cilia length.

Regardless of observations from mouse phenotypes, *RPGRIP1L* C49$^{if.del/-}$ was predicted to have a more severe phenotype due to the biallelic mutations and predicted pathogenicity of the p.24_33del mutation. As this cell line had both fewer and shorter cilia than C19$^{+/-}$ it provides evidence that this uncharacterized region of RPGRIP1L has importance in the correct function of this protein. Also

of note was that genetic interactions were only inferred in the *RPGRIP1L* C49$^{if.del/-}$ cell line, possibly highlighting the important role of residual RPGRIP1L in the C19$^{+/-}$ cell line in organising and maintaining a functional transition zone; this protein is considered to act near the top of the hierarchical organisation of the transition zone.

5.8.1.5 *TMEM67* mutant cell line

The *TMEM67* heterozygote cell line had greater cilia incidence and longer cilia than WT cells (Figure 5.5). *Tmem67*$^{-/-}$ mice have been shown to have significantly fewer and shorter cilia in lung tissue (365), but longer cilia in the distal nephron of the kidney when compared to WT RPE-1 and heterozygous controls (202). Thus different cell types will likely present varying ciliary phenotypes. Accordingly, the increased cilia incidence and length phenotype seen in *TMEM67* C47$^{+/-}$ could be a retinal-specific phenotype, which could be tested for in the current mouse models as retinal phenotypes have not been previously studied.

However, the mutation in the *TMEM67* C47$^{+/-}$ cell line could not be fully characterised, and it may therefore not be a true heterozygous monoclonal cell line. The phenotype quantified (Figure 5.5) may simply be due to the clonal selection of the cell line and not due to a mutation in *TMEM67*. This is a possibility following work independent of this thesis that generated a second *TMEM67* heterozygote cell line in RPE-1. This new heterozygote cell line showed the opposite phenotype to the one presented in this chapter, with shorter and fewer cilia than WT controls. (Personal communication with Dr. Sunayna Best, University of Leeds).

5.8.1.6 *TMEM216* mutant cell lines

The *TMEM216* heterozygous cell lines had the greatest decrease in cilia incidence compared to WT cells of all the cell lines phenotyped in this project (Figure 5.5). *TMEM216* is a Joubert syndrome gene and the encoded transmembrane protein is thought to be located in the peripheral MKS module of the transition zone (385) (Figure 5.1).

It was surprising to see that heterozygotes of other ciliopathy genes had reasonably mild but significant phenotypes whereas the *TMEM216* C42$^{+/-}$ cell

line lost more than 60% of its cilia. Furthermore, human carriers of *TMEM216* mutations do not present with any clinically relevant ciliopathy phenotypes. This again could highlight the limitations of cell models and how much they may vary from actual disease states.

5.8.2 The combinatorial screen

Although the primary screen presented with high variability, it was also shown to be reproducible with a significant correlation between biological replicates (Figure 5.9). The screen has also been independently validated by the fact that many of the genetic interactions inferred have been identified and published as part of other work since it was completed. This supports the value of this experimental set up and its ability to accurately identify genetic interactions.

For example, TMEM107 was found to biochemically interact with other MKS module proteins in the transition zone (TMEM237 and TMEM216) (81). This biochemical interaction was reflected in the combinatorial screen data, as the *TMEM216* mutant cell lines showed an additive interaction with *TMEM107.*

As a preliminary reverse genetics screening technique this could be very useful for finding primary hits or interactions aimed at follow up work by screening with a larger panel of siRNAs. Initially, the main limiting factor for this technique was the generation and validation of the CRISPR/Cas9-edited cell panel. With the huge advances in genome editing efficiency with CRISPR (386-388) alongside new technological advances, targeting capacity and improved technologies for specific genomic changes, repeating the screen set-up would now be quicker. A larger panel of genes could therefore be targeted with CRISPR/Cas9. A panel modelling patient-specific alleles, for example, could be adopted and used in this technique. This would test for genetic interactions that directly affect the severity of patient phenotypes, thus giving a greater understanding of ciliopathy phenotype variations. However, the non-patient mutations used in this thesis are still relevant to understanding underlying ciliary biology.

It could also be up-scaled to test for more reciprocal interactions and across an increased panel of CRISPR/Cas9-edited genes, making this a useful future technique towards understanding the many genetic and functional interactions seen across ciliary genes.

5.8.3 Additive vs Synergistic interactions

Additive interactions from the screen could suggest that these genes, or their resultant proteins are working in the same functional component, protein complex or functional pathway; thus the difference between a single genetic perturbation and a double is small (eg TMEM107 and TMEM216, Figure 5.14). A synergistic interaction would suggest that these genes or proteins are from distinct modules, components or pathways that are interacting and contributing to ciliogenesis individually. Synergistic interactions discussed previously (Sections 6.5.2 and 6.5.3) have helped researchers to define different functional modules of the transition zone and determine their hierarchy in ciliogenesis. The main synergistic interactions identified in in this screen were between *IFT88* (IFTB, anterograde intraflagellar transport), *RPGRIP1L* (NPHP module of the transition zone) and *TMEM67* (MKS module of the transition zone).

5.8.4 Genetic Redundancy

Genetic redundancy would have been indicated by a significant change in phenotype observed after the genetic perturbation of 2 genes, such as a CRISPR/Cas9 bi-allelic null treated with siRNA, but no significant change in phenotype when each of the 2 genes were knocked out individually. There were no gene combinations that displayed genetic redundancy. It is important to consider that true genetic redundancy cannot be assumed from the combinatorial screen data because there was not a complete knock-out in any of the CRISPR/Cas9 edited cell lines and siRNAs do not provide complete experimental knock-out as there are usually residual protein levels.

5.8.5 Limitations

5.8.5.1 Validation of Interactions

Many of the interactions presented in this chapter require further validation, particularly for interactions with either *TMEM67* or *CEP290* because these genes were represented by only one validated mutant cell line. The cell lines available for this project were greatly limited by the quality of the technology at the time they were made. Since this work CRISPR/Cas9 technology has greatly improved in both specificity and efficiency. These cell lines were also all generated from the same gRNA for each gene, targeting the same exon. A

more robust approach would have used cell lines that were mutated with different gRNAs targeting different exons. This would then further support the hypothesis that the genetic interactions are specific to the gene targeted, and not an unidentified off-target effect of using CRISPR/Cas9.

5.8.5.2 Scale of the screen

The developed combinatorial screen technique would benefit from being up-scaled to reduce both the technical issues in plating each cell line and the overall variability that was seen throughout screening. Due to the technical challenges in setting up the screen, it only covers a very small panel of potential genetic interactions, reducing the potential number of validated interactions and overall impact. Despite this, the high-throughput set up was shown to be reasonably robust and independently validated.

5.8.5.3 Technical Limitations

Using ARL13B as a ciliary marker could have affected the detection of interactions across the screen. It is well documented that mutations in transition zone genes cause mis-localisation of ciliary membrane proteins (389), including ARL13B (390). As the siRNA panel mostly focused on genes in the transition zone, it is possible this led to variable staining of ARL13B and thus increased variability across the technical and biological replicates of the screen. This could be mitigated by using a ciliary axonemal marker such as acetylated alpha-tubulin, which was initially not selected as the staining was less suited for high content imaging than ARL13B.

5.8.6 Potential Future Work

Some interactions were taken forward for further validation and presented in this thesis but time constraints limited validation or further investigation of several of the potential genetic interactions. Reciprocal testing for each of the interacting pairs should be taken forward for further validation. It is also important to retest and validate the data generated with the *TMEM67* C47$^{+/-}$ cell line. A second mutant clone could be used to verify the interactions inferred from the combinatorial screen and also be used for further validation work or

other investigations as the mutation in *TMEM67* C47$^{+/-}$ was unable to be fully characterised.

Ciliary function and signalling defects should be tested for in the CRISPR/Cas9-edited cell lines. Initial testing in a Gli reporter assay using a luciferase reporter construct (data not shown) was highly variable and inconclusive. This could be re-tested using immunofluorescence microscopy to assess the translocation of Smoothened into the cilium upon Shh stimulation. Other ciliary function tests could include measurement of changes in non-canonical Wnt signalling in the *IFT88* and *RPGRIP1L* mutant cell lines as an assessment of functional consequences from TMEM67 mis-localisation.

As mentioned previously, the combinatorial screen may be less variable if a different ciliary marker was used, for example acetylated α-tubulin. This would hopefully validate the data presented here and highlight any false negative results due to variable ARL13B localisation. Furthermore, scaling up of the combinatorial screen could include internal repeats and reciprocal testing for each of the potential interacting pairs and should include ARL13B siRNA to see if previously published interactions can be validated using this technique.

A test for biochemical interactions between RPGRIP1L and TMEM107 should be carried out to see if the genetic interaction reflects a biochemical one. This was initially attempted but *TMEM107* constructs failed to express.

From the follow-up investigations presented in this thesis there were also several new questions and lines of study. Follow up immunofluorescence investigations, signalling assays and possible fluorescence recovery after photo-bleaching (FRAP) to look at dynamics for the transition zone or membrane proteins, would give further insight into transition zone organisation and function in relation to the genetic interactions presented in this chapter.

Chapter 6
Final Discussion

6.1 Reverse genetic screening

Although forward genetics and identification of patient mutations remains at the forefront of basic and clinical research into ciliopathies, reverse genetics is an increasingly important strategy for effective molecular research into ciliary biology and for biomedical research.

As a growing number of studies identify novel roles for cilia across cellular mechanisms and disease pathology, the interest and impact of ciliary research has increased. This necessitates an unbiased approach to collate data at the genomic level, for all genes in a genome, in order to define their contribution to ciliary phenotypes. This strategy has the potential benefit in allowing surprising and novel functions to be identified. It may also provide further evidence to support previously identified pathways or ciliary gene functions. Further defining each gene's role in ciliary biology would not only increase our understanding, but also allow us to more precisely manipulate cellular systems and to generate more focused hypotheses to test in further research.

Several whole-genome siRNA screens have now been published, for at least two different cell models, with a range of protocols for imaging and quantification of different ciliary phenotypes (96, 266, 391). These data sets have the potential to be repurposed, as in Chapter 3 and 4 of this thesis, and lead to significant or novel screen hits that can provide unexpected insights into ciliary biology. The value of the original whole genome siRNA screen data used throughout this thesis was the availability of raw image data and the quantification of a full range of phenotypes, both ciliary and cellular. This made it suitable for reanalysis from the start of the project, allowing for quick identification of hits and increasing the time available for downstream investigation work to be carried out. This methodology generated two independent and coherent pieces of work that provide insights into molecular mechanisms that would otherwise have been impossible within the time frame of this thesis.

A correlated, freely available database of all previous ciliary-related siRNA screen datasets would be a highly valuable resource for researchers, including screens that have been published to assess cellular phenotypes linked to ciliary biology. Data from whole genome reverse genetic screens, for example assessing DNA damage responses (392, 393) or ciliary signalling (264), could all be correlated with structural ciliary phenotype screens such as the one used in this thesis. All published datasets have already been optimised and validated extensively for high-throughput screening, providing both precise and accurate data points that will be invaluable for future research.

The database would have to provide evidence of the quality of image staining and correlate data based on each cell line being screened. This would provide stronger biological evidence of true positive results if data is replicated independently. Images could also be available so that the raw image data could be downloaded and reanalysed using different scripts so that immunofluorescent staining could be reused to assess similar but different phenotypes from the data.

Other microscopy-based phenogenomic data repositories include the “Image Data Repository” https://idr-demo.openmicroscopy.org/, or “Mineotaur” http://www.mineotaur.org/. These are interactive visual analytics tools and repositories for imaging and microscopy datasets but do not have the advantage of an unbiased whole genome siRNA screen.

6.2 ROCK2 is a key regulator of ciliogenesis and not ROCK1

6.2.1 The different roles of ROCK1 and ROCK2

In Chapter 3, it was confirmed that ROCK1 does not compensate for the loss of ROCK2 kinase activity (Figure 3.16) and that siRNA knock-downs of *ROCK1* do not phenocopy *ROCK2* knock-downs (Figure 3.14). Due to their extensive homology, these 2 genes were initially thought to be functionally redundant, but over the last 15 years increasing evidence has shown that they play distinct roles in regulating many cellular mechanisms.

The ROCKs have different expression profiles across tissues and some differences in sub cellular localisations (reviewed in (309)), however both have

a cytosolic localisation and a centrosomal association (394, 395). They have also both been shown to localise to the plasma membrane; ROCK1 in mouse intestinal epithelial cells (396) where ROCK2 was undetectable by immunostaining; and ROCK2 in HeLa cells (397). The published localisations of the ROCKs were not confirmed in either RPE-1 or mIMCD3 cells for this thesis. Overexpression constructs used in Figure 3.11 had non-specific localisation of GFP signal, A better test of localisation would have been to use published polyclonal antibodies against both ROCK2 and ROCK1, however the antibodies used for western blot were tested in immunofluorescence experiments and shown to not be suitable (data not shown).

Based on previous studies describing localisation (398); logic would suggest ROCK1 would have a more prominent role in ciliogenesis because of its stronger localisation to the plasma membrane and involvement in vesicle trafficking. However, this notion was not supported by the work presented in this chapter.

Differences in the C-terminal regions of ROCK1 and ROCK2 may explain their different cellular localisations and functions. The plekstrin-like and C1 domains bind to membranes. ROCK2 was found to have high affinity for the lipids phosphatidylinositol (3,4,5)-trisphosphate (PIP_3) and phosphatidylinositol (4,5)-bisphosphate (PIP_2). ROCK2 activity was sensitive to the levels of these lipids *in vitro*. ROCK2 kinase activity increased in the presence of overexpressed phosphoinositide-3 kinase, which would increase the cell's pool of PIP_2 and PIP_3. However, ROCK1 was shown to not strongly bind to either lipid type (399). PIP_2 is known to localise to the base of cilia in *C. elegans* (400) and has been shown to translocate through the ciliary membrane upon Inositol Polyphosphate-5-Phosphatase E (INPP5E) inactivation in mouse neural stem cells (401). If localisation of PIP_2 is similar in human cells, this suggests that ROCK2 could have a higher affinity for the base of the cilium, allowing for localised regulation and stabilisation of actin remodelling that would prevent excessive extension of the ciliary axoneme.

Furthermore, there are several differences that have been identified in the regulation and activation of the ROCKs. ROCK2 activity, unlike ROCK1, is increased by phosphorylation of Ther967, Ser1099, Ser1133 and Ser1374 by

Plk1 (402). In contrast, work on focal adhesion dynamics has shown that phosphorylation of Tyr722 decreases ROCK2's affinity for RhoA, which could be used as a fine tuning regulatory mechanism of ROCK2 activation (403). These phosphorylation events have not been identified in ROCK1.

Although both isoforms of ROCK are able to bind RhoA, only ROCK1 is able to bind RhoE. Binding of RhoE inhibits ROCK1 activity, but RhoE is also a phosphorylation target of ROCK1. When RhoE is phosphorylated by ROCK1 it is stabilised, increasing its binding to ROCK1, thus suggesting the existence of a ROCK1-specific negative feedback loop (404). The differences in regulation allow independent activation of ROCKs and, potentially, localised fine tuning of ROCK2 activation to negatively regulate ciliogenesis.

It should also be noted that ROCK1 and ROCK2 differentially phosphorylate the same targets. In rat embryonic fibroblasts it was shown that when ROCK1 was knocked down by siRNA, MLC phosphorylation at Ser19 was reduced, but this was not noted in ROCK2 knock-downs (399). This can be seen in Figure 3.17A where siRNA knock-down of *Rock1* in mIMCD3 cells reduced both mono (Ser19) and bi-phosphorylated (Thr18/Ser19) MLC, whereas *Rock2* knock-downs only significantly reduced bi-phosphorylated MLC structure. These findings provide evidence of distinct roles for ROCK1 and ROCK2, supporting the data presented in this thesis that the regulation of ciliogenesis is primarily regulated by ROCK2.

An independent secondary screen of actin remodelling factors in RPE-1 cells identified LIMK2 as a negative ciliogenesis regulator (92). ROCK1 and ROCK2 were also included in this screen, which demonstrated that ROCK1 knock-down caused a greater increase in cilia incidence than ROCK2 knock-down, although both had a smaller effect on ciliogenesis than knock-down of LIMK2 and TESK1. Myosin light chain kinase (MLCK) was also tested in this small screen and its knock-down marginally increased cilia incidence. However, this was not investigated further as the study focused on F-actin dynamics and phenotypes other than cilia incidence, such as cilia morphology or length, were not analysed (98).

RhoA-GTP, is the activator of ROCK2. RhoA knock-down in the primary whole genome screen gave an average z_{cilia} of -3.28 and also significantly reduced cell

number (average $z_{cell} = -5.97$). This is likely due to the global knock-down of RhoA, which is essential across many cellular pathways, greatly reducing cell viability causing significant cell and cilia loss. It therefore did not phenocopy *Rock2* knock-down.

6.2.2 Acto-myosin contractions and actin dynamics contribute to ciliogenesis

Acto-myosin contraction is controlled by the phosphorylation of MLC which causes the myosin complex to adopt an active confirmation. MLC is directly phosphorylated by ROCK and indirectly regulated by ROCK phosphorylation of MLCK, suggesting an important role for acto-myosin contraction during ciliogenesis. It should be noted that previous studies have only investigated different myosin heavy chains (100, 101). Activation of myosin occurs on the light chains, thus upstream regulation of molecular function of these heavy chains would still involve ROCK phosphorylation, providing further evidence in support of ROCK2-mediated actin remodelling regulating ciliogenesis.

Evidence presented in this chapter adds to previous publications highlighting the essential role of actin regulation in ciliogenesis. The pathway is summarised in Figure 6.1. The data presented in Figure 3.21 and Figure 3.22 provide evidence for an important role in acto-myosin contraction in the negative regulation of ciliogenesis. Thus, upon inhibition of contraction or constitutive inactivation of MLC, ciliogenesis was significantly increased. Over-expression of GFP-tagged constitutively-inactive $MLC^{(TASA)}$ could substitute for endogenous MLC and thus the cellular population of MLC was inactive and prevented from ROCK2 phosphorylation, functionally phenocopying ROCK2 knock-down. This data indicated that inhibiting acto-myosin contraction caused an increase in cilia incidence compared to the GFP-only control. Acto-myosin contraction has previously been implicated in ciliogenesis. Blebbistatin rescued cilia incidence in RPE-1 cells following myosin heavy chain 10 (*Myh10*) siRNA knock-down (101), supporting the hypothesis that acto-myosin contraction negatively regulates ciliogenesis and could rescue a loss-of-cilia phenotype.

Contradictory results have shown that blebbistatin treatment reduced microtubule stability and bundles in RPE-1 cells grown on micro-patterns, which were used to improve spatial resolution in *z* as it forced cells grow with a

rounded shape. It was reported that microtubule bundles were the driving force in centrosome migration from the basal membrane and that their formation was inhibited with blebbistatin. However, the overall effect of blebbistation on was not determined in this study (95).

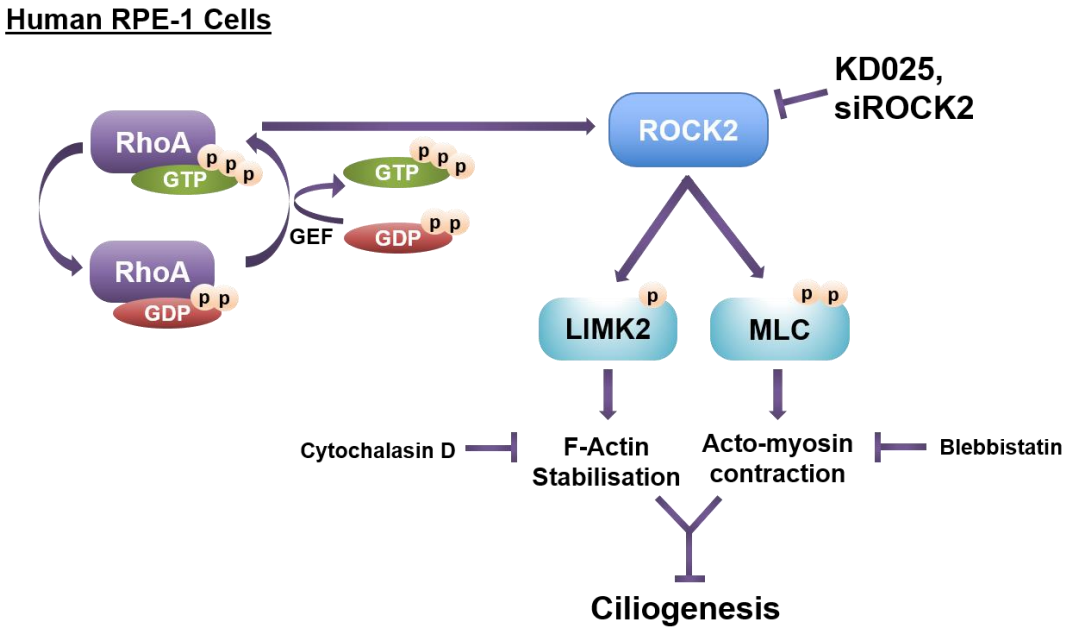

Figure 6.1 ROCK2 regulation of ciliogenesis through actin remodelling and acto-myosin contraction.

RhoA is activated by GTP which can then bind to ROCK2. This causes a conformational change that activates ROCK2 so it can phosphorylate downstream targets such as LIMK2 and myosin light chain (MLC). Phosphorylated LIMK2 stabilises F-actin through cofilin and phosphorylated MLC allows contractile acto-myosin fibres to form which repress ciliogenesis. If ROCK2 is inhibited by KD025 or siRNA knock-down, LIMK2 and MLC are not activated. This leads to the destabilisation of F-actin and deactivation of MLC which reduces acto-myosin contraction. These cytoskeletal changes promote ciliogenesis.

Throughout the experiments presented in Chapter 3, blebbistatin and cytochalasin D treatments gave slightly different phenotypes. Blebbistatin only significantly changed ciliary incidence and not ciliary length after 48hrs, but did increase cilia length at higher concentrations after 2hrs. The individual phenotypes noted with inhibitor treatments raises the question of the relative contributions of actin remodelling and acto-myosin contractility to each process in ciliogenesis; when does F-actin remodelling occur during ciliogenesis? And is acto-myosin contraction required for both centrosome migration and axoneme elongation?

It could be hypothesised that the 2 stages of ciliogenesis have different contributions from the localised regulation of actin dynamics that facilitate each process. The first process inhibits acto-myosin contraction in parallel with dynamic remodelling of actin, which allows centrosome migration but without cellular contraction restricting the movement of the centrosome or preventing centriole docking due to a lack in membrane flexibility. Once docked, F-actin stability allows for efficient trafficking of ciliary vesicles needed to continue elongation of the cilium and hence also contribute to the increase in ciliary length that was observed following cytochalasin D treatment. These results corroborate previous studies that also show specific accumulation of ciliary vesicles with cytochalasin D treatment (98) and inhibition of centriole migration when expression of myosin heavy chains are disrupted through siRNA knock-down (100). This could be tested for in live cell imaging and visualisation of both actin remodelling and centrosome migration. If stress fibre formation is reduced around the centrosome prior and during its migration to the apical membrane this could be evidence for the localised remodelling of actin to reduce acto-myosin contraction. Visualisation of ciliary vesicles (for example with a fluorescently tagged Rab8 marker) in a similar experiment could then highlight dynamic actin remodelling and vesicle trafficking after docking of the basal body. A super resolution microscope with live cell imaging set up would be required for accurate and fast imaging of these cellular processes.

Despite the current evidence presented, it is counter intuitive to think that vesicle trafficking increases when actin is disrupted, because it relies on correctly oriented F-actin filaments for the motor proteins to transport the vesicles along. It is possible that during normal ciliogenesis actin remodelling is tightly controlled and the removal of stress fibres but not branched F-actin facilitates vesicle trafficking. It is also likely that the fine tuning of this actin remodelling occurs in association with remodelling of other cytoskeletal components such as microtubules and septins, which have been shown to contribute to ciliogenesis (405, 406). It has also been shown in RPE-1 cells that ciliary elongation due to cytochalasin D treatment can be reduced by taxol mediated stabilisation of microtubules (407). However, how these interactions between cytoskeletal components contribute to ciliogenesis would need to be further investigated.

6.3 Cell cycle defects cause supernumerary cilia

The work in Chapter 4 is the first description mention of a supernumerary cilia phenotype due to disruption of the centralspindlin complex. This shows that although the screen did not identify a novel pathway, the methodology was robust in identifying hits that can be validated for the incidence of supernumerary cilia. These results, in addition to the results shown in Chapter 3 give even more value to the large data-sets from whole genome siRNA screens and the unexpected biological insights that can be gained from their re-analysis.

6.3.1 Top hits caused cell cycle defects

After filtering, the 3 top hits appeared to show some variation of cell cycle defects in raw secondary screen image data (Figure 4.9), as cells appeared enlarged or multinucleated. However, the multinucleated phenotype was more apparent in mIMCD3s, since these cells continue to divide even under serum starvation conditions, whereas RPE-1 cells significantly slow cell cycle progression and become quiescent under the same conditions.

Previous reports of supernumerary cilia in ciliopathies have mostly been reported in foetal kidney tissue (333, 334). It may be that this tissue is more sensitive to these knock-downs or have compensatory mechanisms that allow them to avoid apoptosis under these otherwise stressful conditions.

The top hit, *Racgap1*, has not been previously associated with ciliogenesis or ciliary biology, however the phenotype was consistent with previous studies on the highly conserved role of *Racgap1* in cytokinesis in eukaryotes (408, 409). Supernumerary cilia in *Racgap1* knockdowns can be concluded to be a secondary phenotype downstream of mitotic failure and the retention of duplicated centrosomes. These mitotic failures are likely due to a failure to assemble a centralspindlin complex, as published previously in *C.elegans*, *Xenopus* and zebrafish embryos with mutations in *Racgap1* orthologues (353, 410, 411). Signalling allows the older retained centrioles to develop into basal bodies and subsequently produce cilia. In *C. elegans,* mutations in the *Racgap1* orthologue allowed a cleavage furrow to form but prevented the formation of a central spindle, causing a subsequent failure of cytokinesis (353). This is likely the reason that mitosis failed in the mIMCD3 cell model following *Racgap1*

knock-down, consistent with observations made during live cell imaging (Figure 4.15).

What is particularly of interest is that there is no compensatory mechanism to prevent retained mother centrioles from maturing after mitosis failure. As cells return to G1 after exiting a failed mitosis, the signalling to mature mother centrioles does not have a checkpoint or regulatory mechanism to recognise the retained supernumerary centrosomes. Thus, the signalling allows for both mother centrioles to mature. Further to this unlicensed maturation of retained centrioles, the cells examined in this work also do not have any active regulation that prevented the formation of more than one primary cilium.

6.3.2 The central spindlin complex is implicated in cilia regulation

The centralspindlin complex is made up of RACGAP1 and KIF23, a kinesin family member that is the microtubule binding component of the centralspindlin complex. KIF23 is also responsible for recruitment of the guanine exchange factor, Ect2. The centralspindlin complex binds to microtubules during anaphase. Its accumulation is dependent on Aurora B, which is then able to phosphorylate centralspindlin and stabilise its accumulation at the spindle mid-zone. Centralspindlin also forms on peripheral microtubules towards the cell membrane in order to mediate cleavage furrow formation. Once accumulated and stabilised, RACGAP1 interacts with phosphorylated ECT2, which in turn activates RhoA to initiate formation of the acto-myosin contractile ring and cleavage furrow for telophase.

Although only *Racgap1* was taken forward for secondary screening in this thesis, data from the primary whole genome screen for many of the centralspindlin regulators and components support the data presented for *Racgap1*. ECT2 and RhoA are essential for correct localisation and local activation of cleavage furrow formation and the acto-myosin contractile ring (355). However, siRNA knock-downs of either of the genes encoding these proteins do not phenocopy *Racgap1* knock-down (Table 6.1). This could be due to RhoA's roles across many other cellular mechanisms and actin regulation, and acute global knock-down is deleterious to overall cell health. Aurora B, however, is essential for the accumulation of the centralspindlin complex and is upstream of this pathway. siRNA knock-down of *Aurkb* therefore appears to

phenocopy *Racgap1* knock-down by causing an increase in supernumerary cilia (Table 6.1). Retrospectively, *Kif23* and *Aurkb* were good candidates for secondary screening as they have highly significant $Z_{2MCilia}$ values (equivalent to $p<0.001$). However, they did not show consistent results in the primary whole genome screen and were excluded because of low z-score values in biological replicate 2 (Table 6.1). These are likely to be false negative results and again highlight the importance of sufficiently stringent filtering steps used to generate the secondary screening hit list.

Table 6.1 Whole genome screen data of centralspindlin components and regulators

The 2 components of the centralspindlin complex (*Kif23* & *Racgap1*) when knocked down by siRNA cause a significant increase in supernumerary cilia, as shown by the average robust z-score for incidence of cells with 2 or more cilia ($Z_{2MCilia}$). Both *Kif23* and *Aurkb* were not taken forward for secondary screening because in the second run of the whole genome screen they did not show a significant increase in cells with supernumerary cilia. Green represents numbers greater $Z_{2MCilia}$ >1.96 and red represents numbers <1.96.

	Run 1 z-score	**Run 2 z-score**	**$z_{2MCilia}$**
Kif23	5.556383	1.014768	3.285575
Racgap1	3.637513	3.931008	3.784261
Ect2	-0.76198	-1.15997	-0.96097
RhoA	-1.13110	-0.58016	-0.85563
Aurkb	4.975328	1.896057	3.435692

Kif23 has also been noted as a potential ciliary gene by high-throughput computational prediction analysis (412). It is also known to localise to the base of the cilium in RPE-1 cells and with a ciliary rootlet marker in multi-ciliated *Xenopus* epithelium (413). To our knowledge, the centralspindlin complex has not been localized to any ciliary or associated structures, and this thesis ascribes the supernumerary cilia phenotype as a secondary downstream consequence of mitosis failure. However, since mitotic progression was not directly tested, it is possible that there is another uncharacterised, direct role of the centralspindlin complex in primary ciliogenesis.

6.4 *Hectd2*'s potential role in ciliogenesis

Interestingly, only 1 of the 10 hits from the supernumerary cilia screen did not have a statistically significant decrease in cell number: si*Hectd2* treatment had an average $z_{2Mcilia}$ of 2.94 and average z_{cell} of 0.775 (Table 4.2).

Hectd2 is an obvious hit to take forward for further investigation as it does not significantly change cell number and has no obvious mitotic defect. Thus, initial experiments would need to validate the phenotype in RPE-1 cells and identify if the cilia stem from single or multiple centrioles. However, as it is an undescribed E3 ubiquitin ligase, the substrates and activating E2 ubiquitin conjugating enzyme would also need to be identified in order to fully understand its mechanism of action. From the 35 known active E2 ligases (414), the only E2 identified as a hit from the whole genome primary screen of ciliogenesis with an average $z_{2MCilia}$ >1.96 was *Ube2b*. The similarities in phenotypes suggest that *Ube2b* is a candidate E2 for *Hectd2*. However, it is much harder to predict the target(s) of Hectd2 (reviewed in (415)) and to define whether any subsequent ubiquitination mediated by it would be to mark the target for protein degradation, localisation or change in function, each dependant on which lysine residues are ubiquitinated.

The ubiquitin/proteasome system (UPS) has recently come to light as an important regulator of ciliogenesis with many components specifically localising to the base of the cilium (416, 417). E3 ligases have been shown to be involved in several stages and mechanisms of ciliogenesis and ciliary signalling. For example, UBR5, a HECT Domain containing E3 ubiquitin ligase, was identified as a positive regulator of ciliogenesis. siRNA knock-down of UBR5 completely ablated cilia in RPE-1 cells and UBR5 interacted with CSPP1, a centriolar satellite protein. The ubiquitination of CSPP1 was required for the correct localisation and stabilisation of centriolar satellites for ciliogenesis (418). By contrast, the CUL3-KCTD10 complex acts as an E3 ubiquitin ligase, with KCTD10 localising to the mother centriole and targeting CEP97 for degradation. Once CEP97 was removed this allowed CP110 to also be removed from the mother centriole to signal the timely initiation of ciliogenesis in G1 (419).

Hectd2 knock-downs, in the whole genome screen used in this project, only had a significant effect on the incidence of supernumerary cilia and had no

significant effect on overall cilia incidence or cell number. However, data from a separate whole genome reverse genetics screen (260), designed to identify modulators of ciliogenesis and cilium length, identified *HECTD2* as a putative negative regulator of ciliogenesis. Knock-down of *HECTD2* in their study caused a marginal increase in cilia incidence, albeit with only one of 4 siRNAs used against *HECTD2. HECTD2* was considered as a putative regulator in this screen because it fulfilled their arbitrary cut off criteria of showing more than 10 cells with cilia greater than 6μm in length across the image data captured. The screen did not specify or have any data to show the incidence of supernumerary cilia, but it does support the result of the secondary screen performed here which suggests that *HECTD2* is a negative regulator of ciliogenesis. However, this was not a hit in the increase cilia incidence screen data presented in Chapter 3 as it had an average of -0.595, showing no significant change to cilia incidence compared to controls. Unfortunately ciliary length was not quantified due to the set-up of the primary screen and as discussed in Chapter 4 it may be that the increase in cilia length was incorrectly measured as two or more cilia due to recognition protocol errors.

Possible interactors of HECTD2 were identified from literature searches and databases (420-423) but none had clear roles in ciliogenesis, centrosome duplication or the cell cycle. The interactors PIAS1 (424) and PPARγ (425) are linked to Hedgehog signalling regulation but not ciliogenesis, while many of the suggested interactors were less well characterised than HECTD2.

If validated antibodies were available, then immunofluorescence could be used to identify the subcellular location of Hectd2 throughout the cell cycle and stages of ciliogenesis. Its localisation could also suggest possible ubiquitination targets of Hectd2. Western blotting of cell cycle halted cell cultures could clarify whether Hectd2 levels vary in a cell-cycle dependent manner. Furthermore, immunohistochemistry could be used alongside mRNA studies to define the tissue distribution of *Hectd2* expression. Thus, although there are many avenues that can be taken to explore and define the function of Hectd2, reagents such as antibodies would need to be validated making this a large and extensive research project.

6.5 Genetic epistasis from transition zone genes contribute to the regulation of ciliogenesis

The combinatorial screen proved to be an effective technique to identify genetic interactions that affect ciliary incidence. Some further optimisation and use of new CRISPR/Cas9 techniques introduced in 1.6.7 provide the opportunity to scale up the screen and improve the high variability seen across the preliminary data. Despite that variability, the screen was able to highlight several potential genetic interactions for both ciliary incidence, summarised in Figure 6.2 and a few interactions for ciliary size, summarised in Figure 6.3

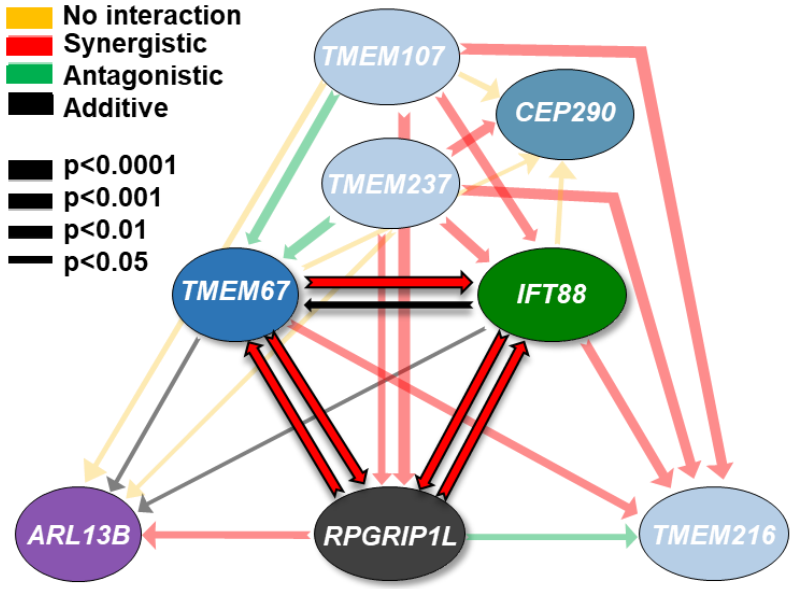

Figure 6.2 Summary of genetic interactions for cilia incidence

Diagram that summarises all of the genetic interactions for cilia incidence that were identified from combinatorial screen data. The arrow direction shows the siRNA knock-down and points to the CRIPSR/Cas9 edited cell line in which the knock-down was performed. The thickness of each arrow represents the strength of the interaction inferred from robust z-scores (and expressed as *p*-values). Synergistic interactions are represented by red arrows, antagonistic by green and additive by black. There is a clear triad of reciprocal interactions that is highlighted between *IFT88*, *RPGRIP1L* and *TMEM67.*

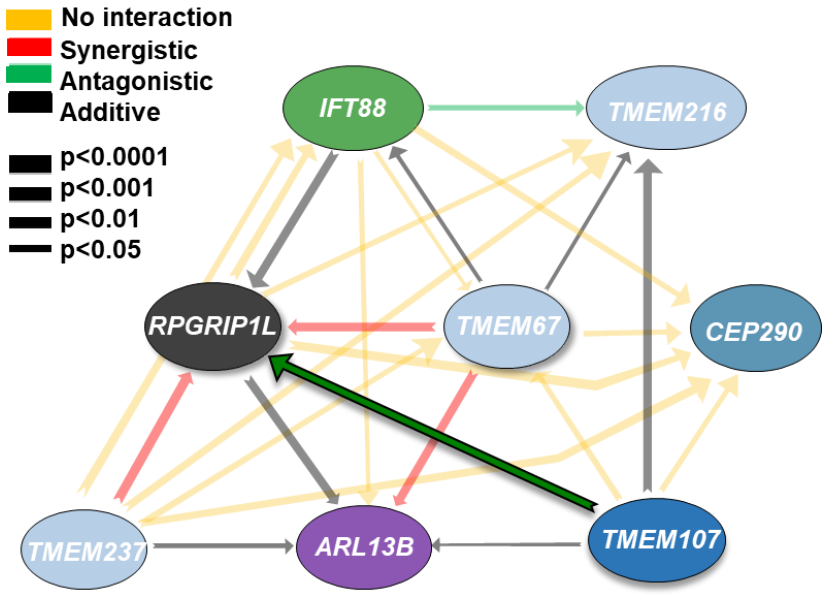

Figure 6.3 Summary of genetic interactions of cilia size

This diagram summarises all of the genetic interactions impacting on cilia size that were inferred from combinatorial screen data. The direction of the arrow shows the siRNA acting on the different genetic backgrounds of each cell line. The thickness of each arrow represents the strength/significance of the interaction. Synergistic interactions are represented by red arrows, antagonistic by green and additive by black. Highlighted in bold is the antagonistic interaction between *RPGRIP1L* and *TMEM107*.

6.5.1 Lack of synergistic interactions identified with *ARL13B* identified through combinatorial screen test data

It was surprising that data from the *ARL13B* mutant cell lines only inferred potential additive genetic interactions rather than synergistic interactions. Several synergistic interactions have been presented for *ARL13B* in past studies. Previous work in *C. elegans* has suggested that the *ARL13B* orthologue (*arl-13*) genetically interacts with both ciliary transport and transition zone proteins. Double mutants of *arl-13* and *nph-4* or *bbs-8* (orthologues to human transition zone genes *NPHP4* and *BBS8*, respectively) and double mutants of *arl-13* with *osm-3* or *che-11* (orthologues to human ciliary transport genes *KIF17* and *IFT140*, respectively) showed more severe ciliary morphology defects compared to single mutants. Double mutants of arl-13::*bbs-8* also showed reduced numbers of IFT particles, linking the transition zone and IFT which will be separately discussed. The data suggests *arl-13* genetically interacts with these genes to maintain cilia and IFT function (426). However, the

above interactions were associated with anterograde transport, whereas the combinatorial screen included *IFT88,* which is involved in anterograde transport.

In a separate study, *arl-13* was also shown to be involved in not just anterograde transport, but the docking of both IFT-A (anterograde) and IFT-B (retrograde) particles (427). In *Arl13b*$^{-/-}$ mutant mice it has also been suggested that IFT is generally mis-localised and impaired (379). This only presented as an additive interaction in the *ARL13B* heterozygote cell lines with *IFT88* knock-down. This suggests that IFT88 is higher up in the hierarchy of ciliary formation, as the knock-down was proportionally equivalent in both cell lines and was unaffected by a reduction in ARL13B protein levels. It is therefore possible that an *ARL13B* knock-down in the *IFT88* CRISPR/Cas9-edited cell lines may show a synergistic interaction, destabilizing the residual levels of IFT88.

It may be that other genetic interactions that are present with *ARL13B* would only be observed if CRISPR/Cas9-edited cell lines were treated with *ALR13B* siRNA, which was not part of the screen panel. It is therefore likely that some false negatives were missed in the screen.

6.5.2 Interactions between IFT88 and the Transition Zone

A clear triad of interactions was inferred between *IFT88, RPGRIP1L* and *TMEM67* because these were supported by reciprocal experiments (Figure 5.12). IFT proteins are already well known to interact with the BBSome for loading cargo for ciliary transport (428-430) and in the Hedgehog signalling pathway for changes in ciliary localisation (65, 431).

The *RPGRIP1L* orthologue in *C. elegans* has also been shown to genetically interact with IFT-A protein IFT-139 (432). This study suggests that core IFT-A proteins promote entry of the MKS module into the cilium and are therefore required for ciliogenesis. This work also describes a role for IFT-A in maintaining the correct MKS module localisation in the transition zone (432), a notion independently supported by work that shows IFT-A dynein has interactions with the transition zone (72). In comparison, little evidence has been published for a genetic or functional link between the transition zone and proteins in the IFT-B module, specifically IFT88.

However, recent evidence supports a functional interaction between IFT-B and the transition zone in maintaining the ciliary gate. In *Chlamydomonas rpg1-l* (*RPGRIP1L*) mutants, a dysfunctional ciliary gate is seen that allows flooding of cytoplasmic/non-ciliary proteins into the cilium. In contrast *fla11-1* (IFT172) mutants had significantly reduced levels of IFT and ciliary membrane proteins, suggesting that it has a role in retention of proteins that pass the ciliary gate. Consequently, both IFT-B and RPGRIP1L have to work together to maintain a functional ciliary gate (433). Nevertheless, the present study is the first work to suggest a synthetic synergistic interaction between IFT-B and 2 transition zone proteins, RPGRIP1L and TMEM67.

Interactions between *IFT88* and *TMEM67* were not shown to be reciprocal, as a synergistic interaction was shown in the *IFT88* cell line but an additive interaction was seen in the *TMEM67* cell line. This may be partly explained by the base-line level of cilia incidence in the *TMEM67* mutant cell line, which is significantly greater than WT cells (Figure 5.5). Consequently, the knock-down of *IFT88* would have to overcome the phenotype of increased cilia seen in this cell line, masking the synergistic interaction.

Reciprocal interactions were also inconsistent with *RPGRIP1L*. This may be due to the important role of *RPGRIP1L* in ciliogenesis and its role higher up in the hierarchy of transition zone organisation (79, 375, 434). C*19*$^{+/-}$ likely has enough functional *RPGRIP1L* to compensate and maintain a level of cilium formation, despite the *IFT88* knock-down, whereas residual protein levels in the *C49*$^{if.del/-}$ cell line (Figure 5.4) may not be functional or able to maintain cilia due to the p.24_33del mutation. This suggests that the interaction is not detectable in heterozygotes and would only be inferred in knock-outs or conditions with no functional *RPGRIP1L* protein. The functionality of *RPGRIP1L* in these cell lines would have to be tested by observing any mis-localisation of other transition zone proteins to support this hypothesis.

6.5.2.1 TMEM67 mis-localises in *IFT88* and *RPGRIP1L* heterozygous mutants

Many transition zone proteins mis-localise in *RPGRIP1L* mutants, as has been shown in *C. elegans* (435) and human fibroblasts (389). The mis-localisation and proximal restriction of TMEM67 in *RPGRIP1L* heterozygote cell lines

suggests that WT RPGRIP1L may licence the entry of TMEM67 into the ciliary membrane. In contradiction to this, previous work in *C. elegans* suggest that mks-5 (RPGRIP1L) restricts mks-3 (TMEM67) localisation to the transition zone, because *mks-5* mutants showed mks-3 dispersed along the ciliary axoneme (375). This may however a phenotypic difference between a heterozygote and a complete knock-out, or a species specific difference. This could be tested for in RPGRIP1L$^{-/-}$ RPE-1 cells.

If RPGRIP1L is licencing distal TMEM67 localization into the ciliary membrane, possibly as a role of the diffusion barrier at the transition zone (435), this may have a functional consequence as TMEM67 has been shown to contribute to non-canonical Wnt signalling (436). Complete knock-outs of TMEM67 have also previously been shown to affect the localisation of membrane proteins such as Arl13b and Smo in mouse embryonic fibroblasts (385), so it would be of interest to see if mis-localisation of TMEM67 alone would show similar functional consequences.

Separately, TMEM67 restriction to the basal body in the *IFT88* heterozygotes could be due to loss of an active transport of TMEM67 along the membrane. It has previously been discussed that transition zone proteins that mis-localise or are mis-assembled are actively recovered and returned to the transition zone by IFT-A (72). Independently it has been hypothesised, from data in *C. elegans,* that transition zone proteins are actively trafficked into cilia by anterograde IFT-B alongside evidence for IFT-A regulation of MKS module localisation (432). This independently supports the data in the *IFT88* heterozygous mutants presented here and suggests that there is active anterograde transport of TMEM67 along the membrane, thus the localisation seen in WT cells along the length of the ciliary membrane would not be due to passive diffusion. This could be the case for many other ciliary membrane proteins and therefore be a key part of correct signalling through cilia. This phenotype could potentially be tested for with an optimised fluorescence recovery after photo bleaching (FRAP) experiment to look at the recovery rates of these membrane proteins after bleaching the transition zone, where rapid recovery would suggest diffusion rather than active transport as hypothesised from the data presented here.

6.5.3 Antagonistic interaction between *RPGRIP1L* and *TMEM107*

Follow-up experiments from the combinatorial screen did not validate the antagonistic interaction between *RPGRIP1L* and *TMEM107*. It is likely that the ball-like phenotype described in Figure 5.21 increased the overall spot size detected in the primary combinatorial screen, thus making this hit a false positive antagonistic interaction. However, this novel phenotype suggests a synergistic interaction, and a possible functional interaction between *RPGRIP1L* and *TMEM107* since *TMEM107* knock-down alone does not significantly change ciliary phenotypes in WT cells (Figure 5.20). The ball like-phenotype that was noted could be a possible retrograde IFT defect or un restricted entry of cytosolic proteins that were able to diffuse across a faulty ciliary gate. RPGRIP1L has been genetically and functional linked to anterograde IFT (72, 432), therefore it is possible this interaction may, in part, be mediated by TMEM107.

This synergistic interaction has also been reproduced in *C. elegans*, with *mks5*::*tmem107* double mutant showing a far more severe phenotype than either single mutant. This interaction is specific to *mks-5* (*RPGRIP1L*), as the same phenotype was not noted in the control double mutant, *cep290::tmem107* (Personal communication with Professor Oliver Blacque, University College Dublin). However, it remains unclear why there is a synergistic interaction when transition zone proteins fail to be correctly localised or recruited in *mks-5* mutant worms.

It has been noted previously in mouse IMCD3 cells with *TMEM107* knock-down that there is no change in localisation of RPGRIP1L relative to the basal body (81). However, TMEM107 localisation has not been tested in the *RPGRIP1L* mutant cell lines. TMEM107 has been shown in *C. elegans* to be located in an intermediate layer of the transition zone (81), suggesting a unique function independent of other TMEM proteins. This is also reflected in the combinatorial screen data, as both TMEM67 and TMEM237 do not have a similar functional interaction with RPGRIP1L and there were no significant changes to ciliary size in these “double perturbations”.

RPGRIP1L CRISPR/Cas9 edited cell lines showed mis-localisation of TMEM67, and since RPGRIP1L is a master organiser of the transition zone there are

likely to be other mis-localised transition zone proteins in these cells. A disorganised transition zone may not be correctly tethered to the ciliary membrane, allowing the cytosolic proteins to diffuse in and cause the ball-like phenotype. Which could be tested with expression of a GFP construct, observing any diffusion of free GFP into the cilium or possibly using FRAP to assess the dynamics of GFP diffusion into the cilium. It may also be that excess membrane is produced due to a dysregulated ciliary gate, allowing flooding of other ciliary signalling and membrane proteins to increase the ciliary membrane size. This leads to the hypothesis that TMEM107 has key roles in tethering the ciliary membrane or in the control of the ciliary gate.

6.6 Future tools for ciliary research

Huge advances have been made in microscopy techniques with the development of super resolution and high-throughput microscopy. The molecular architecture and organisation of the cilium is still to be accurately defined despite initial work with super-resolution microscopy starting to elucidate this complex structure (60), it is likely that these techniques will lead to a far greater understanding of protein localisation and organisation in the primary cilia in the coming years.

Another exciting technology that could benefit ciliary research is biotin ligase (BioID) and ascorbate peroxidase (APEX) proximity biotinylation labelling techniques. These techniques are being used to build an interaction landscape of the ciliome by tagging key proteins with either BioID or APEX to then biotinylate all proteins within proximity to the tagged protein of interest. These biotinylated proteins are then purified and characterised to identify potential interactors or proteins structurally close to the tagged protein (40, 41). Rapid (so-called “turbo”) BioID over short (<1hr) time-scales is also being used to identify interactions involved in the different stages of ciliogenesis and how interactions change with mutant proteins (personal communication with Dr. Katarzyna Szymanska).

6.7 Future work

6.7.1 Drug repurposing

As there are no clear guidelines on the treatment of ciliopathies, management prioritises alleviation of symptoms as the underlying genetic disorder cannot be treated. The work in Chapter 3 of this thesis highlights ROCK2 as a potential therapeutic target for ciliopathies. For example, KD025 treatment was able to rescue cilia incidence in si*IFT88* knock-down conditions. As discussed in Chapter 3, KD025 is currently still undergoing safety and efficacy testing in phase 2 clinical trials for several skin diseases: chronic Graft Versus Host Disease (cGVHD) (ClinicalTrials.gov Identifier: NCT02841995), Idiopathic Pulmonary Fibrosis (ClinicalTrials.gov Identifier: NCT02688647), Diffuse Cutaneous Systemic Sclerosis (ClinicalTrials.gov Identifier: NCT03919799) and previous Phase II testing for Severe Psoriasis Vulgaris (437). Initial results from all trials are promising. It will, however, require several more years of clinical testing and additional Phase III clinical trials before it could be potentially delivered as a therapeutic for patients. Once approved the drug could be repurposed for ciliopathy patients.

Drug discovery is not only expensive and time-consuming but has high attrition rates, particularly at the safety stages of clinical testing, despite extensive pre-clinical research (438). Repurposed drugs such as KD025 or other ROCK2-specific inhibitors could be tested in pre-clinical organoid models of retina or kidney in order to confirm a potential therapeutic effect, before taking them forward for clinical safety testing in humans. Hence repurposing drugs offers a chance of much lower attrition rates and faster approval for use in rare diseases in addition to lower development costs. However, drug repurposing still has many challenges such as patent rights. This can impact a pharmaceutical company’s incentive to repurpose drugs, particularly for those that are generic and “off patent”. This is especially important if there is already publicly accessible research that investigates the novel uses of the drug, or it’s novel use has already been unofficially adopted in clinical practice as this impacts the ability to get a patent for the newly-proposed use (439, 440). However, with novel intellectual property, a method of use patent can easily be applied for repurposing “off patent” drugs.

Drug repurposing is an ideal approach for ciliopathies, as it is not financially viable to target each disease type individually. A drug developed to target a single ciliopathy would be classed as an “orphan” drug because of its very limited clinical use. Orphan drugs are not profitable to produce and so usually require government funding to assist production. Drug repurposing however avoids this issue as the drug is already in production for, with a known drug target and mechanism of action.

However, although drug repurposing could provide an easier route to a therapeutic for ciliopathies targeted drug design is still valuable. Ciliopathies as a group of diseases, are relatively common and present a large clinical burden. Therefore, a drug targeting ciliary function rather ciliopathy symptoms, as those currently in clinical trial, has the potential to have greater clinical impact and be profitable to produce.

6.7.1.1 Drug repurposing of ROCK inhibitors

There are few ROCK inhibitors in current clinical use, and none that have been approved for use by the European Medicines Agency (EMA) and U.S. Food & Drug Administration (FDA). Non-specific ROCK inhibitors include hydroxyfasudil (currently only approved for use in China and Japan) and the fasudil derivative ripasudil (currently only approved for use in Japan) which are potential drugs that could be repurposed for ciliopathy patients. Fasudil is of interest as it was initially approved for use in China and Japan to treat cerebral vasospasm. It has also been repurposed once before and went through a phase 2 clinical trial in China for use in amyotrophic lateral sclerosis (ALS) in 2013. However, the trial has yet to be published or completed (ClinicalTrials.gov Identifier: NCT01935518). As a previously approved drug this makes it an ideal candidate to fast-track through clinical trial and approval for use in ciliopathies.

ROCK2-specific inhibitors are also currently being developed for conditions involving fibrosis and have undergone successful pre-clinical testing. Fibrosis is a complication of diabetic neuropathy, idiopathic pulmonary fibrosis, Crohn’s disease and non-alcoholic steatohepatitis and thus these diseases are a major target for the commercial development of new ROCK2-specific inhibitors. RedX Pharmaceuticals have recently developed two new ROCK2 inhibitors, REDX10178 and REDX10325. Both inhibitors have been shown to be highly

selective for ROCK2 with minimal off-target effects across 468 kinases tested. They have IC50s of 1.4nM and 0.65nM respectively (when measuring phosphorylation of MYPT1), whereas the IC50 of KD025 is 70nM (441). Therefore, these clinical development compounds could also be taken forward for potential repurposing and clinical testing in ciliopathy patients. However, since these compounds are yet to be approved for any clinical use, they are unlikely to be an attractive choice for initial repurposing. However, if current clinical trials of KD025, REDX10178 and REDX10325 are successful and these drugs are approved for their original indications, these are better candidates to take forward for repurposing as data in this thesis shows that ROCK2-specific inhibition can rescue ciliogenesis. Other less specific drugs may have significant side-effects through off-target inhibition of other kinases. For example, fasudil dihydrochloride at 10uM inhibits ROCK2 to only 12% remaining kinase activity. However, it also significantly inhibits many off targets such as RSK1, ERK8, PRK2 and MSK1 to ≤20% kinase activity. Kinase profiling studies are important in defining the specificity of the potential drugs taken forward for ROCK2 inhibition to identify off-target effects and can be downloaded from the Medical research council (MRC) protein phosphorylation and ubiquitination unit (PPU) international centre for kinase profiling, Kinase Profiling Inhibitor database (http://www.kinase-screen.mrc.ac.uk/kinase-inhibitors).

KD025 and other ROCK inhibitors could be tested in additional human cell models and ciliopathy model organisms such as iPSC organoids or mice, to build on work in this thesis and examine potential therapeutic benefit at an organism level. Work should also include other ROCK inhibitors and include testing a specific ROCK1 inhibitor such as GSK 429286 (442) in cell models to further confirm that ROCK2 is the main therapeutic target. However, a full clinical trial into ROCK inhibitors such as KD025 would be the obvious future project stemming from the work in Chapter 3 after pre-clinical testing confirmed its value.

6.7.2 Current clinical trials of potential therapeutics for ciliopathies

At the time of writing, current therapeutic clinical trials for primary ciliopathies are limited to targeting obesity or visual acuity in Bardet Biedl Syndrome and Alström syndrome, or are using drugs to specifically target polycystic kidney

disease. BBS and Alström syndrome patients with moderate or severe obesity are currently in a phase 3 randomised double-blind clinical trial since December 2018 (ClinicalTrials.gov Identifier: NCT03746522). The trial is testing the effects of Setmelanotide on weight loss in the participants. Setmelanotide is a Melanocortin-4 Receptor (MC4R) Agonist, a receptor previously shown to regulate metabolism and body weight regulation in mice (443), and certain alleles have also been found in genome-wide association studies (GWAS) to be associated with high BMI (444). Patients with hyperphagia are included in the trial targeting MC4R to limit their food cravings and aid in weight loss. Setmelanotide is also being tested in a separate trial including a wider range of genetic disorders of obesity (ClinicalTrials.gov Identifier: NCT03013543). These trials are good examples of drugs being used to manage symptoms rather than target the underlying ciliary dysfunction.

There are several clinical trials aiming to improve visual acuity in ciliopathy patients but with limited success. The trials also only target BBS and LCA patients. A phase 2 trial using Metformin to improve visual acuity in BBS patients has been withdrawn in April 2019 due to “unrealizable wishes of national authorities” (ClinicalTrials.gov Identifier: NCT03490019) and no further information has been provided as to why the clinical trial was withdrawn.

Two other current drug trials are specifically targeting LCA patients with either a specific CEP290 p.Cys998X mutation (ClinicalTrials.gov Identifier: NCT03140969), or with mutations in GUCY2D (retinal guanylate cyclase) (ClinicalTrials.gov Identifier: NCT03920007). Both of these trials are early phase, but initial results from former have shown promising results (445).Therefore, there is potential of great impact in the clinical management and for patient outcomes in a drug that could be used across a broader range of ciliopathies, in particular a drug that targets the underlying ciliary dysfunction directly such as a specific ROCK2 inhibitor.

KD025 is an experimental drug currently in Phase 2 clinical trials for systemic sclerosis (ClinicalTrials.gov Identifier: NCT03919799), idiopathic pulmonary fibrosis (ClinicalTrials.gov Identifier: NCT02688647) and chronic graft-versus-host disease (ClinicalTrials.gov Identifier: NCT03640481) (446). Initial testing has reported promising safety results in patients from preclinical studies and

earlier Phase 1 clinical trials. It remains possible that this more specific ROCK2 inhibitor could be repurposed and re-trialed for ciliopathy patients. The impact of a treatment that specifically targets the underlying molecular pathology of disease rather than treats symptoms would have an and presents an exciting opportunity to make an immeasurable difference to ciliopathy patients and their families.

6.7.3 Developing a large scale combinatorial screen

Since the work presented in this thesis was carried out, CRISPR/Cas9 and genome editing technology has greatly improved in both efficiency and specificity as discussed in 1.6.7. It would be valuable to up-scale the combinatorial screen with more gene-edited cell lines following these advances. During the development of the screen presented in Chapter 5, the most time-consuming phase was the validation of the gene-edited cell lines. With improved editing efficiency, fewer cell lines would need to be screened to find deleterious mutations.

At the present time, the best evidence for genetic interactions in ciliopathies was identified in genes that cause of Bardet-Biedl syndrome. It would therefore also be beneficial to develop a panel of positive controls for genetic interactions using this data. These control interactions would be in addition to the usual screening controls for transfection and image analysis, and would represent positive controls for synergistic, additive and antagonistic interactions. Inclusion of these controls would greatly increase the reliability and precision of this screening methodology.

Alongside a larger panel of cell lines, a broader panel of siRNAs would also increase the scope of this validated and reliable methodology. This could include internal repeats and reciprocal testing for each of the potential interacting pairs and should include *ARL13B* siRNAs to ascertain whether previously published interactions can be confirmed by using this technique (as discussed in Chapter 5). As many of the siRNAs in the combinatorial screen panel were transition zone targets, it would be interesting to broaden the targets of the siRNA panel to include all ciliary compartments. This should include additional IFT and motor proteins, as these were some of the strongest

synthetic genetic interactions identified in the combinatorial screen, and are supported by evidence from previously published data (72).

The current 87 defined transition zone proteins would be too many to screen in a single sitting. Therefore a panel of CRISPR/Cas9 edited cell lines of the most commonly mutated genes in ciliopathies, or genes that specifically cause a spectrum of disorders, such as CEP290, would make up an ideal screening panel for the large scale combinatorial screen. The over 1000 proteins in the ciliome could then easily be made into a custom siRNA screening panel. This larger scale combinatorial screen could be used to identify cilia incidence and length as tested but also the high-throughput format can easily be adapted for screening signalling responses. Cell lines which stably express Gli reporter assay systems could be edited using CRISRP/Cas9 and then transfected with the ciliome siRNA panel. It's important to note that RPE-1 cells are not an ideal model to assess Gli response because they have cilia in deep pockets that have been do not respond strongly to Shh signalling. A possible ciliopathy cell model for signalling assays would be ARPE-19 cells. By using genes that are already known to cause a spectrum of disorders and by including signalling response assays, the combinatorial screen would have the potential to identify any, if not all, genetic interactions of ciliary genes that influence the spectrum of phenotypes in ciliopathies.

Of high importance in the follow up work would be an examination of patient genome data to see if it correlates with any of the synergistic interactions identified. It may be that patients with more severe ciliopathy phenotypes have a second mutation or SNP in one of the suggested interacting pairs, with the primary disease causing mutation.

6.8 Final Remarks

6.8.1 Impact and Significance

Although the role of actin remodelling in ciliogenesis is well-described, this is the first report of the specific negative regulation of this remodelling by ROCK2. Furthermore, this regulation by ROCK2 is not compensated for by its isozyme ROCK1. This work also highlights the important role of inhibition of acto-myosin

contraction in inducing ciliogenesis, a ROCK2-regulated pathway that has otherwise received little previous attention in this context.

The work also demonstrates the value of re-tasking primary whole genome siRNA screens. Often, there is more to be learnt from these large data sets, even when looking at phenotypes for which the screens were not originally designed.

6.8.1.1 ROCK2 and actin remodelling as a therapeutic target in ciliopathies

Work in this thesis has shown that specific inhibition of ROCK2 is enough to provide a rescue of cilia incidence in some cell models of cilia loss such as *IFT88* knock-downs (Figure 3.23). In contrast, ROCK2 inhibition was unable to rescue cilia loss in *RPGRIP1L* knock-downs. There are no known patients with *IFT88* mutations, whereas there is a clinical need for a drug to restore cilia in patients with *RPGRIP1L* mutations. Therefore the applicability of KD025 or ROCK2 as potential drug targets with other inhibitors would need to be tested in additional disease models. It is unclear if the inhibition of off-target kinases, such as observed with other non-specific ROCK inhibitors that include Y27632, may further benefit cilia rescue. The current evidence and data presented in this thesis suggest that specific ROCK2 inhibition has the potential for high clinical impact.

The value of small molecule inhibitors in rescuing ciliogenesis has been shown previously in *CEP290* knock-out RPE-1 cells. These cells were unable to produce visible cilia, but a natural and synthetic compound screen identified that plant flavonoids were able to restore ciliogenesis in these cells through interaction with NPHP5. They specifically identified eupatilin, which has previously been approved for clinical use to treat gastritis and peptic ulcers (447). However, these gene knock-outs have also been shown to be rescued by targeting actin stability with cytochalasin D and lantrunculin B. In parallel, these drugs were also able to partially rescue cilia in *IFT88* knock-downs (448). Thus, targeting specific protein interactions, or non-specifically targeting the actin cytoskeleton, could both be of value to patients with Senior-Loken syndrome, Joubert syndrome, or Leber Congenital amaurosis, all caused by mutations in *CEP290* or *NPHP5*.

Other work on glomerulocystic kidney disease in mice caused by mutations in *Arhgap35* showed that the ROCK1 inhibitor GSK 429286A or cytochalasin D were able to partially recuse loss of cilia incidence and length in these mice models (286). This is consistent with the data presented in Figure 3.14, showing that mIMCD3 wild-type cilia were elongated following ROCK1 knock-down.

Independently, results from a small molecule inhibitor screen looking to rescue cilia in *IFT88* and *RPGRIP1L* knock-down conditions, showed that a non-specific ROCK inhibitor was amongst the top hits (personal communications with Dr. Claire E.L. Smith, University of Leeds). These findings suggest that ROCK pathways are a potential therapeutic target for ciliopathy patients.

With such promising independent results and the case for drug repurposing, further pre-clinical work will not be extensive before a proposal could be presented to industry partners to start clinical trials using ROCK inhibitors. Providing a huge opportunity to increase the quality of life for ciliopathy patients.

6.8.1.2 A new technique for investigating genetic interactions influencing ciliary phenotypes

Genetic interactions and modifier alleles are thought to contribute to variations in Bardet-Biedl syndrome and thus have been the focus of several studies looking at human ciliopathy phenotypes (359, 371, 449). Genetic interactions and modifiers have also been suggested to contribute to retinal phenotype variation in ciliopathies (450). However, there have been very few studies looking at the impact of genetic interactions in general mammalian ciliary biology, which could in turn relate to our molecular understanding of ciliogenesis. This is the first work that looks at potential genetic interactions that perturb cilia incidence and size in a high-throughput format with a focus on the cellular and molecular level of ciliary biology.

The combinatorial screen identified several potentially biologically important interactions for follow-up work which could significantly contribute to the growing evidence of the role of genetic interactions in ciliopathy phenotypes. Thus providing proof of concept that a large scale screen could be developed from this techniques with some further optimisation and development of cell lines.

As this work was completed in cell lines that were assumed to lack relevant clinical phenotypes, it is possible that complete knock-outs do not have the same genetic interactions as seen for the heterozygote cells lines and that the molecular mechanisms would therefore differ in ciliopathy patients. This does not minimise the value of this data as this work still gives novel insight into the molecular understanding of ciliary biology and has provided further evidence of genetic interactions between IFT and the transition zone. The main advantage of this technique to identify genetic interactions over big data *in silico* genetic interaction studies and genome-wide association studies (451, 452), is that this technique, although more laborious, provides biological data and presents the exact phenotype of the genetic interactions tested.

A large scale screen would not only aid our understanding of ciliogenesis and ciliopathy disease pathology but allow the improvement of genetic counselling services for patients. With an understanding of the influence of different alleles and their interactions with primary disease causing mutations the severity of phenotypes could be predicted. Helping patients not only better understand their disease compared to the ciliopathy community but also allow parents of these patients to be more informed for future family planning.

6.8.2 Summary of findings

Through the chapters of this thesis, work has been presented to show novel regulators and synthetic genetic interactions that influence ciliogenesis. In Chapter 3 it was shown that ROCK2 is a specific regulator of the actin remodelling required in ciliogenesis and that the isozyme ROCK1 cannot compensate for the loss of ROCK2 in actin regulation of ciliogenesis. The role of acto-myosin contractions in ciliogenesis was presented, highlighting a previously under-appreciated means of actin remodelling in the negative regulation of ciliogenesis, and providing further evidence to support an essential role in dynamic actin remodelling during ciliogenesis. Rudimentary testing of the ROCK2-specific inhibitor KD025 also suggested ROCK2 as a potential therapeutic target for ciliary disease. The previously highlighted role of actin remodelling in the pathogenesis of several ciliopathies further shows the potential clinical impact of taking a ROCK2 inhibitor forward for pre-clinical testing.

In Chapter 4 the link between centrosome maturation and supernumerary cilia was investigated. The mechanism highlighted in that chapter supports previous reports that centrosome over duplication, or retention of centrioles, is the main molecular mechanism that causes supernumerary cilia. However, this is the first work showing that RACGAP1-mediated cytokinesis is not a prerequisite for centriole maturation and the formation of supernumerary cilia.

In Chapter 5, novel synthetic genetic interactions were identified across a range of structural ciliary compartments that influence cilia incidence and cilia length. A triad of synergistic reciprocal interactions were identified between *IFT88, TMEM67* and *RPGRIP1L*, alongside data showing biochemical associations between these proteins. Another novel synergistic genetic interaction was also identified between RPGRIP1L and TMEM107 which affected ciliary structure, and implicated TMEM107 in ciliary gate function or membrane tethering. However, further investigation into potential biochemical interactions are required.

6.8.3 Conclusion

In summary, reverse genetics techniques and whole genome siRNA screen data sets have been shown to be highly valuable in a hypothesis-neutral strategy for identifying novel regulatory pathways in ciliogenesis throughout this thesis.

References

1. Beales, P. and Jackson, P.K. Cilia - the prodigal organelle. *Cilia.* 2012, **1**(1), p.1.

2. Larusso, N.F. and Masyuk, T.V. The role of cilia in the regulation of bile flow. *Digestive diseases (Basel, Switzerland).* 2011, **29**(1), pp.6-12.

3. Silflow, C.D. and Lefebvre, P.A. Assembly and Motility of Eukaryotic Cilia and Flagella. Lessons from *Chlamydomonas reinhardtii*. *Plant Physiology.* 2001, **127**(4), pp.1500-1507.

4. Fawcett, D.W. and Porter, K.R. A study of the fine structure of ciliated epithelia. *Journal of Morphology.* 1954, **94**(2), pp.221-281.

5. Meunier, A. and Azimzadeh, J. Multiciliated Cells in Animals. *Cold Spring Harbor perspectives in biology.* 2016, **8**(12), p.a028233.

6. Marshall, W.F. and Kintner, C. Cilia orientation and the fluid mechanics of development. *Current opinion in cell biology.* 2008, **20**(1), pp.48-52.

7. Singla, V. and Reiter, J.F. The primary cilium as the cell's antenna: signaling at a sensory organelle. *Science.* 2006, **313**(5787), pp.629-633.

8. Molla-Herman, A., Ghossoub, R., Blisnick, T., Meunier, A., Serres, C., Silbermann, F., Emmerson, C., Romeo, K., Bourdoncle, P., Schmitt, A., Saunier, S., Spassky, N., Bastin, P. and Benmerah, A. The ciliary pocket: an endocytic membrane domain at the base of primary and motile cilia. *Journal of Cell Science.* 2010, **123**(10), pp.1785-1795.

9. Nauli, S.M., Alenghat, F.J., Luo, Y., Williams, E., Vassilev, P., Li, X., Elia, A.E.H., Lu, W., Brown, E.M., Quinn, S.J., Ingber, D.E. and Zhou, J. Polycystins 1 and 2 mediate mechanosensation in the primary cilium of kidney cells. *Nature Genetics.* 2003, **33**(2), pp.129-137.

10. Kindt, K.S., Finch, G. and Nicolson, T. Kinocilia mediate mechanosensitivity in developing zebrafish hair cells. *Developmental Cell.* 2012, **23**(2), pp.329-341.

11. Jenkins, P.M., McEwen, D.P. and Martens, J.R. Olfactory cilia: linking sensory cilia function and human disease. *Chemical senses.* 2009, **34**(5), pp.451-464.

12. Molday, R.S. and Moritz, O.L. Photoreceptors at a glance. *Journal of Cell Science.* 2015, **128**(22), pp.4039-4045.

13. Pazour, G.J., Baker, S.A., Deane, J.A., Cole, D.G., Dickert, B.L., Rosenbaum, J.L., Witman, G.B. and Besharse, J.C. The intraflagellar transport protein, IFT88, is essential for vertebrate photoreceptor assembly and maintenance. *The Journal of Cell Biology.* 2002, **157**(1), pp.103-113.

14. Okada, Y., Takeda, S., Tanaka, Y., Belmonte, J.-C.I. and Hirokawa, N. Mechanism of Nodal Flow: A Conserved Symmetry Breaking Event in Left-Right Axis Determination. *Cell.* 2005, **121**(4), pp.633-644.

15. Khanna, H. Photoreceptor Sensory Cilium: Traversing the Ciliary Gate. *Cells.* 2015, **4**(4), pp.674-686.

16. Kramer-Zucker, A.G., Olale, F., Haycraft, C.J., Yoder, B.K., Schier, A.F. and Drummond, I.A. Cilia-driven fluid flow in the zebrafish pronephros, brain and Kupffer's vesicle is required for normal organogenesis. *Development.* 2005, **132**(8), pp.1907-1921.

17. Yoshiba, S., Shiratori, H., Kuo, I.Y., Kawasumi, A., Shinohara, K., Nonaka, S., Asai, Y., Sasaki, G., Belo, J.A., Sasaki, H., Nakai, J., Dworniczak, B., Ehrlich, B.E., Pennekamp, P. and Hamada, H. Cilia at the node of mouse embryos sense fluid flow for left-right determination via Pkd2. *Science.* 2012, **338**(6104), pp.226-231.

18. Currie, A.R. and Wheatley, D.N. Cilia of a Distinctive Structure (9 + 0) in Endocrine and other Tissues. *Postgraduate Medical Journal.* 1966, **42**(489), pp.403-408.

19. Sorokin, S. Centrioles and the formation of rudimentary cilia by fibroblasts and smooth muscle cells. *The Journal of Cell Biology.* 1962, **15**(2), pp.363-377.

20. Flood, P.R. and Totland, G.K. Substructure of solitary cilia in mouse kidney. *Cell Tissue Res.* 1977, **183**(2), pp.281-290.

21. Warner, F.D. Ciliary inter-microtubule bridges. *Journal of Cell Science.* 1976, **20**(1), pp.101-114.

22. Anderson, R.G. The three-dimensional structure of the basal body from the rhesus monkey oviduct. *J Cell Biol.* 1972, **54**(2), pp.246-265.

23. Garcia, G., 3rd, Raleigh, D.R. and Reiter, J.F. How the Ciliary Membrane Is Organized Inside-Out to Communicate Outside-In. *Curr Biol.* 2018, **28**(8), pp.R421-r434.

24. Tanos, B.E., Yang, H.-J., Soni, R., Wang, W.-J., Macaluso, F.P., Asara, J.M. and Tsou, M.-F.B. Centriole distal appendages promote membrane docking, leading to cilia initiation. *Genes & Development.* 2013, **27**(2), pp.163-168.

25. Breslow, D.K. and Holland, A.J. Mechanism and Regulation of Centriole and Cilium Biogenesis. *Annual review of biochemistry.* 2019, **88**, pp.691-724.

26. Nachury, M.V., Seeley, E.S. and Jin, H. Trafficking to the Ciliary Membrane: How to Get Across the Periciliary Diffusion Barrier? *Annual Review of Cell and Developmental Biology.* 2010, **26**(1), pp.59-87.

27. Rattner, J.B., Sciore, P., Ou, Y., van der Hoorn, F.A. and Lo, I.K. Primary cilia in fibroblast-like type B synoviocytes lie within a cilium pit: a site of endocytosis. *Histol Histopathol.* 2010, **25**(7), pp.865-875.

28. Dawe, H.R., Farr, H. and Gull, K. Centriole/basal body morphogenesis and migration during ciliogenesis in animal cells. *Journal of Cell Science.* 2007, **120**(1), pp.7-15.

29. Linck, R.W., Chemes, H. and Albertini, D.F. The axoneme: the propulsive engine of spermatozoa and cilia and associated ciliopathies leading to infertility. *Journal of Assisted Reproduction and Genetics.* 2016, **33**(2), pp.141-156.

30. Galati, Domenico F., Mitchell, Brian J. and Pearson, Chad G. Subdistal Appendages Stabilize the Ups and Downs of Ciliary Life. *Developmental Cell.* 2016, **39**(4), pp.387-389.

31. Allen, R.A. Isolated cilia in inner retinal neurons and in retinal pigment epithelium. *Journal of Ultrastructure Research.* 1965, **12**(5), pp.730-747.

32. Kellogg, D.R., Moritz, M. and Alberts, B.M. THE CENTROSOME AND CELLULAR ORGANIZATION. *Annual review of biochemistry.* 1994, **63**(1), pp.639-674.

33. Mazo, G., Soplop, N., Wang, W.-J., Uryu, K. and Tsou, M.F.B. Spatial Control of Primary Ciliogenesis by Subdistal Appendages Alters Sensation-Associated Properties of Cilia. *Developmental Cell.* 2016, **39**(4), pp.424-437.

34. Shi, X., Garcia, G., Van De Weghe, J.C., McGorty, R., Pazour, G.J., Doherty, D., Huang, B. and Reiter, J.F. Super-resolution microscopy reveals that disruption of ciliary transition-zone architecture causes Joubert syndrome. *Nat Cell Biol.* 2017, **19**(10), pp.1178-1188.

35. Garcia-Gonzalo, F.R. and Reiter, J.F. Open Sesame: How Transition Fibers and the Transition Zone Control Ciliary Composition. *Cold Spring Harbor perspectives in biology.* 2017, **9**(2).

36. Geimer, S. and Melkonian, M. The ultrastructure of the Chlamydomonas reinhardtii basal apparatus: identification of an early marker of radial asymmetry inherent in the basal body. *Journal of Cell Science.* 2004, **117**(13), pp.2663-2674.

37. Dummer, A., Poelma, C., DeRuiter, M.C., Goumans, M.-J.T.H. and Hierck, B.P. Measuring the primary cilium length: improved method for unbiased high-throughput analysis. *Cilia.* 2016, **5**(1), p.7.

38. Lechtreck, K.F. IFT-Cargo Interactions and Protein Transport in Cilia. *Trends Biochem Sci.* 2015, **40**(12), pp.765-778.

39. Roepman, R., Ueffing, M., Kremer, H., Huynen, M., Gibson, T., Katsanis, N., Walz, G., Wolfrum, U., Franco, B., Giles, R., Beales, P., Johnson, C., Blacque, O., Pontoglio, M., Képès, F., Apic, G., Russell, R. and Omran,

H. SYSCILIA, “A systems biology approach to dissect cilia function and its disruption in human genetic disease”. *Cilia.* 2012, **1**(Suppl 1), p.P41.

40. Gupta, G.D., Coyaud, E., Goncalves, J., Mojarad, B.A., Liu, Y., Wu, Q., Gheiratmand, L., Comartin, D., Tkach, J.M., Cheung, S.W., Bashkurov, M., Hasegan, M., Knight, J.D., Lin, Z.Y., Schueler, M., Hildebrandt, F., Moffat, J., Gingras, A.C., Raught, B. and Pelletier, L. A Dynamic Protein Interaction Landscape of the Human Centrosome-Cilium Interface. *Cell.* 2015, **163**(6), pp.1484-1499.

41. Mick, D.U., Rodrigues, R.B., Leib, R.D., Adams, C.M., Chien, A.S., Gygi, S.P. and Nachury, M.V. Proteomics of Primary Cilia by Proximity Labeling. *Dev Cell.* 2015, **35**(4), pp.497-512.

42. Martell, J.D., Deerinck, T.J., Sancak, Y., Poulos, T.L., Mootha, V.K., Sosinsky, G.E., Ellisman, M.H. and Ting, A.Y. Engineered ascorbate peroxidase as a genetically encoded reporter for electron microscopy. *Nature Biotechnology.* 2012, **30**(11), pp.1143-1148.

43. Martell, J.D., Deerinck, T.J., Sancak, Y., Poulos, T.L., Mootha, V.K., Sosinsky, G.E., Ellisman, M.H. and Ting, A.Y. Engineered ascorbate peroxidase as a genetically-encoded reporter for electron microscopy. *Nat Biotechnol.* 2012, **30**(11), pp.1143-1148.

44. Yang, T.T., Chong, W.M. and Liao, J.C. STED and STORM Superresolution Imaging of Primary Cilia. *Methods Mol Biol.* 2016, **1454**, pp.169-192.

45. Kandachar, V., Tam, B.M., Moritz, O.L. and Deretic, D. An interaction network between the SNARE VAMP7 and Rab GTPases within a ciliary membrane-targeting complex. *Journal of Cell Science.* 2018, **131**(24), p.jcs222034.

46. Lu, Q., Insinna, C., Ott, C., Stauffer, J., Pintado, P.A., Rahajeng, J., Baxa, U., Walia, V., Cuenca, A., Hwang, Y.-S., Daar, I.O., Lopes, S., Lippincott-Schwartz, J., Jackson, P.K., Caplan, S. and Westlake, C.J. Early steps in primary cilium assembly require EHD1/EHD3-dependent ciliary vesicle formation. *Nat Cell Biol.* 2015, **17**(3), pp.228-240.

47. Das, A. and Guo, W. Rabs and the exocyst in ciliogenesis, tubulogenesis and beyond. *Trends in Cell Biology.* 2011, **21**(7), pp.383-386.

48. Barral, D.C., Garg, S., Casalou, C., Watts, G.F.M., Sandoval, J.L., Ramalho, J.S., Hsu, V.W. and Brenner, M.B. Arl13b regulates endocytic recycling traffic. *Proceedings of the National Academy of Sciences.* 2012, **109**(52), pp.21354-21359.

49. Revenkova, E., Liu, Q., Gusella, G.L. and Iomini, C. The Joubert syndrome protein ARL13B binds tubulin to maintain uniform distribution of proteins along the ciliary membrane. *Journal of Cell Science.* 2018, **131**(9), p.jcs212324.

50. Phua, S.C., Chiba, S., Suzuki, M., Su, E., Roberson, E.C., Pusapati, G.V., Setou, M., Rohatgi, R., Reiter, J.F., Ikegami, K. and Inoue, T.

Dynamic Remodeling of Membrane Composition Drives Cell Cycle through Primary Cilia Excision. *Cell.* 2017, **168**(1-2), pp.264-279.e215.

51. Young, R.W. and Bok, D. Participation of the retinal pigment epithelium in the rod outer segment renewal process. *J Cell Biol.* 1969, **42**(2), pp.392-403.

52. Hogan, M.C., Manganelli, L., Woollard, J.R., Masyuk, A.I., Masyuk, T.V., Tammachote, R., Huang, B.Q., Leontovich, A.A., Beito, T.G., Madden, B.J., Charlesworth, M.C., Torres, V.E., LaRusso, N.F., Harris, P.C. and Ward, C.J. Characterization of PKD protein-positive exosome-like vesicles. *Journal of the American Society of Nephrology : JASN.* 2009, **20**(2), pp.278-288.

53. Nager, A.R., Goldstein, J.S., Herranz-Pérez, V., Portran, D., Ye, F., Garcia-Verdugo, J.M. and Nachury, M.V. An Actin Network Dispatches Ciliary GPCRs into Extracellular Vesicles to Modulate Signaling. *Cell.* 2017, **168**(1), pp.252-263.e214.

54. Mirvis, M., Stearns, T. and James Nelson, W. Cilium structure, assembly, and disassembly regulated by the cytoskeleton. *The Biochemical journal.* 2018, **475**(14), pp.2329-2353.

55. Taschner, M., Bhogaraju, S. and Lorentzen, E. Architecture and function of IFT complex proteins in ciliogenesis. *Differentiation; research in biological diversity.* 2012, **83**(2), pp.S12-S22.

56. Follit, J.A., Xu, F., Keady, B.T. and Pazour, G.J. Characterization of mouse IFT complex B. *Cell motility and the cytoskeleton.* 2009, **66**(8), pp.457-468.

57. Katoh, Y., Terada, M., Nishijima, Y., Takei, R., Nozaki, S., Hamada, H. and Nakayama, K. Overall Architecture of the Intraflagellar Transport (IFT)-B Complex Containing Cluap1/IFT38 as an Essential Component of the IFT-B Peripheral Subcomplex. *J Biol Chem.* 2016, **291**(21), pp.10962-10975.

58. Bhogaraju, S., Engel, B.D. and Lorentzen, E. Intraflagellar transport complex structure and cargo interactions. *Cilia.* 2013, **2**(1), p.10.

59. Taschner, M., Bhogaraju, S., Vetter, M., Morawetz, M. and Lorentzen, E. Biochemical mapping of interactions within the intraflagellar transport (IFT) B core complex: IFT52 binds directly to four other IFT-B subunits. *J Biol Chem.* 2011, **286**(30), pp.26344-26352.

60. Tony Yang, T., Su, J., Wang, W.-J., Craige, B., Witman, G.B., Bryan Tsou, M.-F. and Liao, J.-C. Superresolution Pattern Recognition Reveals the Architectural Map of the Ciliary Transition Zone. *Scientific Reports.* 2015, **5**(1), p.14096.

61. Pazour, G.J., Wilkerson, C.G. and Witman, G.B. A Dynein Light Chain Is Essential for the Retrograde Particle Movement of Intraflagellar Transport (IFT). *The Journal of Cell Biology.* 1998, **141**(4), pp.979-992.

62. Lechtreck, K.-F., Johnson, E.C., Sakai, T., Cochran, D., Ballif, B.A., Rush, J., Pazour, G.J., Ikebe, M. and Witman, G.B. The Chlamydomonas reinhardtii BBSome is an IFT cargo required for export of specific signaling proteins from flagella. *Journal of Cell Biology.* 2009, **187**(7), pp.1117-1132.

63. Williams, C.L., McIntyre, J.C., Norris, S.R., Jenkins, P.M., Zhang, L., Pei, Q., Verhey, K. and Martens, J.R. Direct evidence for BBSome-associated intraflagellar transport reveals distinct properties of native mammalian cilia. *Nat Commun.* 2014, **5**, p.5813.

64. Klink, B.U., Zent, E., Juneja, P., Kuhlee, A., Raunser, S. and Wittinghofer, A. A recombinant BBSome core complex and how it interacts with ciliary cargo. *Elife.* 2017, **6**, p.e27434.

65. Mukhopadhyay, S., Wen, X., Chih, B., Nelson, C.D., Lane, W.S., Scales, S.J. and Jackson, P.K. TULP3 bridges the IFT-A complex and membrane phosphoinositides to promote trafficking of G protein-coupled receptors into primary cilia. *Genes Dev.* 2010, **24**(19), pp.2180-2193.

66. Cole, D.G., Diener, D.R., Himelblau, A.L., Beech, P.L., Fuster, J.C. and Rosenbaum, J.L. Chlamydomonas Kinesin-II–dependent Intraflagellar Transport (IFT): IFT Particles Contain Proteins Required for Ciliary Assembly in Caenorhabditis elegans Sensory Neurons. *The Journal of Cell Biology.* 1998, **141**(4), pp.993-1008.

67. Takahara, M., Kunii, M., Nakamura, K., Harada, A., Hirano, T., Katoh, Y. and Nakayama, K. C11ORF74 interacts with the IFT-A complex and participates in ciliary BBSome localization. *The Journal of Biochemistry.* 2018, **165**(3), pp.257-267.

68. Liem, K.F., Jr., Ashe, A., He, M., Satir, P., Moran, J., Beier, D., Wicking, C. and Anderson, K.V. The IFT-A complex regulates Shh signaling through cilia structure and membrane protein trafficking. *J Cell Biol.* 2012, **197**(6), pp.789-800.

69. Picariello, T., Brown, J.M., Hou, Y., Swank, G., Cochran, D.A., King, O.D., Lechtreck, K., Pazour, G.J. and Witman, G.B. A global analysis of IFT-A function reveals specialization for transport of membrane-associated proteins into cilia. *Journal of Cell Science.* 2019, **132**(3), p.jcs220749.

70. Fu, W., Wang, L., Kim, S., Li, J. and Dynlacht, B.D. Role for the IFT-A Complex in Selective Transport to the Primary Cilium. *Cell reports.* 2016, **17**(6), pp.1505-1517.

71. Caparrós-Martín, J.A., De Luca, A., Cartault, F., Aglan, M., Temtamy, S., Otaify, G.A., Mehrez, M., Valencia, M., Vázquez, L., Alessandri, J.L., Nevado, J., Rueda-Arenas, I., Heath, K.E., Digilio, M.C., Dallapiccola, B., Goodship, J.A., Mill, P., Lapunzina, P. and Ruiz-Perez, V.L. Specific variants in WDR35 cause a distinctive form of Ellis-van Creveld syndrome by disrupting the recruitment of the EvC complex and SMO into the cilium. *Hum Mol Genet.* 2015, **24**(14), pp.4126-4137.

72. Jensen, V.L., Lambacher, N.J., Li, C., Mohan, S., Williams, C.L., Inglis, P.N., Yoder, B.K., Blacque, O.E. and Leroux, M.R. Role for intraflagellar transport in building a functional transition zone. *EMBO reports.* 2018, **19**(12), p.e45862.

73. Szymanska, K. and Johnson, C.A. The transition zone: an essential functional compartment of cilia. *Cilia.* 2012, **1**(1), p.10.

74. Ashburner, M., Ball, C.A., Blake, J.A., Botstein, D., Butler, H., Cherry, J.M., Davis, A.P., Dolinski, K., Dwight, S.S., Eppig, J.T., Harris, M.A., Hill, D.P., Issel-Tarver, L., Kasarskis, A., Lewis, S., Matese, J.C., Richardson, J.E., Ringwald, M., Rubin, G.M. and Sherlock, G. Gene ontology: tool for the unification of biology. The Gene Ontology Consortium. *Nat Genet.* 2000, **25**(1), pp.25-29.

75. The Gene Ontology Resource: 20 years and still GOing strong. *Nucleic acids research.* 2019, **47**(D1), pp.D330-d338.

76. Carbon, S., Ireland, A., Mungall, C.J., Shu, S., Marshall, B. and Lewis, S. AmiGO: online access to ontology and annotation data. *Bioinformatics.* 2009, **25**(2), pp.288-289.

77. Robichaux, M.A., Potter, V.L., Zhang, Z., He, F., Liu, J., Schmid, M.F. and Wensel, T.G. Defining the layers of a sensory cilium with STORM and cryoelectron nanoscopy. *Proceedings of the National Academy of Sciences.* 2019, **116**(47), pp.23562-23572.

78. Czarnecki, P.G. and Shah, J.V. The ciliary transition zone: from morphology and molecules to medicine. *Trends in Cell Biology.* 2012, **22**(4), pp.201-210.

79. Wiegering, A., Dildrop, R., Kalfhues, L., Spychala, A., Kuschel, S., Lier, J.M., Zobel, T., Dahmen, S., Leu, T., Struchtrup, A., Legendre, F., Vesque, C., Schneider-Maunoury, S., Saunier, S., Rüther, U. and Gerhardt, C. Cell type-specific regulation of ciliary transition zone assembly in vertebrates. *The EMBO Journal.* 2018, **37**(10), p.e97791.

80. Williams, C.L., Li, C., Kida, K., Inglis, P.N., Mohan, S., Semenec, L., Bialas, N.J., Stupay, R.M., Chen, N., Blacque, O.E., Yoder, B.K. and Leroux, M.R. MKS and NPHP modules cooperate to establish basal body/transition zone membrane associations and ciliary gate function during ciliogenesis. *Journal of Cell Biology.* 2011, **192**(6), pp.1023-1041.

81. Lambacher, N.J., Bruel, A.-L., van Dam, T.J.P., Szymańska, K., Slaats, G.G., Kuhns, S., McManus, G.J., Kennedy, J.E., Gaff, K., Wu, K.M., van der Lee, R., Burglen, L., Doummar, D., Rivière, J.-B., Faivre, L., Attié-Bitach, T., Saunier, S., Curd, A., Peckham, M., Giles, R.H., Johnson, C.A., Huynen, M.A., Thauvin-Robinet, C. and Blacque, O.E. TMEM107 recruits ciliopathy proteins to subdomains of the ciliary transition zone and causes Joubert syndrome. *Nat Cell Biol.* 2016, **18**(1), pp.122-131.

82. Wiegering, A., Dildrop, R., Vesque, C., Schneider-Maunoury, S. and Gerhardt, C. Rpgrip1l controls ciliary gating by ensuring the proper

amount of Cep290 at the vertebrate transition zone. *bioRxiv.* 2020, p.2020.2002.2010.942300.

83. Ford, M.J., Yeyati, P., Mali, G., Keighren, M., Waddell, S., Mjoseng, H.K., Douglas, A.T., Hall, E., Sakaue-Sawano, A., Miyawaki, A., Meehan, R., Boulter, L., Jackson, I., Mill, P. and Mort, R. A cell/cilia cycle biosensor for single cell kinetics reveals persistence of cilia after the G1/ S transition is a general property in cells and mice. *Developmental Cell.* 2018.

84. Anderson, C.T. and Stearns, T. Centriole age underlies asynchronous primary cilium growth in mammalian cells. *Curr Biol.* 2009, **19**(17), pp.1498-1502.

85. Sonnen, K.F., Schermelleh, L., Leonhardt, H. and Nigg, E.A. 3D-structured illumination microscopy provides novel insight into architecture of human centrosomes. *Biology open.* 2012, **1**(10), pp.965-976.

86. Kim, J., Krishnaswami, S.R. and Gleeson, J.G. CEP290 interacts with the centriolar satellite component PCM-1 and is required for Rab8 localization to the primary cilium. *Hum Mol Genet.* 2008, **17**(23), pp.3796-3805.

87. Lopes, C.A.M., Prosser, S.L., Romio, L., Hirst, R.A., O'Callaghan, C., Woolf, A.S. and Fry, A.M. Centriolar satellites are assembly points for proteins implicated in human ciliopathies, including oral-facial-digital syndrome 1. *Journal of Cell Science.* 2011, **124**(Pt 4), pp.600-612.

88. Graser, S., Stierhof, Y.-D., Lavoie, S.B., Gassner, O.S., Lamla, S., Le Clech, M. and Nigg, E.A. Cep164, a novel centriole appendage protein required for primary cilium formation. *The Journal of Cell Biology.* 2007, **179**(2), pp.321-330.

89. Westlake, C.J., Baye, L.M., Nachury, M.V., Wright, K.J., Ervin, K.E., Phu, L., Chalouni, C., Beck, J.S., Kirkpatrick, D.S., Slusarski, D.C., Sheffield, V.C., Scheller, R.H. and Jackson, P.K. Primary cilia membrane assembly is initiated by Rab11 and transport protein particle II (TRAPPII) complex-dependent trafficking of Rabin8 to the centrosome. *Proceedings of the National Academy of Sciences of the United States of America.* 2011, **108**(7), pp.2759-2764.

90. Wu, C.-T., Chen, H.-Y. and Tang, T.K. Myosin-Va is required for preciliary vesicle transportation to the mother centriole during ciliogenesis. *Nat Cell Biol.* 2018, **20**(2), pp.175-185.

91. Kobayashi, T., Tsang, William Y., Li, J., Lane, W. and Dynlacht, Brian D. Centriolar Kinesin Kif24 Interacts with CP110 to Remodel Microtubules and Regulate Ciliogenesis. *Cell.* 2011, **145**(6), pp.914-925.

92. Kim, J., Jo, H., Hong, H., Kim, M.H., Kim, J.M., Lee, J.-K., Heo, W.D. and Kim, J. Actin remodelling factors control ciliogenesis by regulating YAP/TAZ activity and vesicle trafficking. *Nature Communications.* 2015, **6**(1), p.6781.

93. Kim, J.H., Ki, S.M., Joung, J.-G., Scott, E., Heynen-Genel, S., Aza-Blanc, P., Kwon, C.H., Kim, J., Gleeson, J.G. and Lee, J.E. Genome-wide screen identifies novel machineries required for both ciliogenesis and cell cycle arrest upon serum starvation. *Biochimica et Biophysica Acta (BBA) - Molecular Cell Research.* 2016, **1863**(6, Part A), pp.1307-1318.

94. Copeland, S.J., McRae, A., Guarguaglini, G., Trinkle-Mulcahy, L. and Copeland, J.W. Actin-dependent regulation of cilia length by the inverted formin FHDC1. *Mol Biol Cell.* 2018, **29**(13), pp.1611-1627.

95. Pitaval, A., Senger, F., Letort, G., Gidrol, X., Guyon, L., Sillibourne, J. and Théry, M. Microtubule stabilization drives 3D centrosome migration to initiate primary ciliogenesis. *Journal of Cell Biology.* 2017, **216**(11), pp.3713-3728.

96. Kim, J., Lee, J.E., Heynen, S., Suyama, E., Ono, K., Lee, K.Y., Ideker, T., Aza-Blac, P. and Gleeson, J.G. Functional genomic screen for modulators of ciliogenesis and cilium length. *Nature.* 2010, **464**(7291), pp.1048-1051.

97. Barbelanne, M., Song, J., Ahmadzai, M. and Tsang, W.Y. Pathogenic NPHP5 mutations impair protein interaction with Cep290, a prerequisite for ciliogenesis. *Hum Mol Genet.* 2013, **22**(12), pp.2482-2494.

98. Kim, J., Jo, H., Hong, H., Kim, M.H., Kim, J.M., Lee, J.-K., Heo, W.D. and Kim, J. Actin remodelling factors control ciliogenesis by regulating YAP/TAZ activity and vesicle trafficking. *Nature Communications.* 2015, **6**, p.6781.

99. Valente, E.M., Logan, C.V., Mougou-Zerelli, S., Lee, J.H., Silhavy, J.L., Brancati, F., Iannicelli, M., Travaglini, L., Romani, S., Illi, B., Adams, M., Szymanska, K., Mazzotta, A., Lee, J.E., Tolentino, J.C., Swistun, D., Salpietro, C.D., Fede, C., Gabriel, S., Russ, C., Cibulskis, K., Sougnez, C., Hildebrandt, F., Otto, E.A., Held, S., Diplas, B.H., Davis, E.E., Mikula, M., Strom, C.M., Ben-Zeev, B., Lev, D., Sagie, T.L., Michelson, M., Yaron, Y., Krause, A., Boltshauser, E., Elkhartoufi, N., Roume, J., Shalev, S., Munnich, A., Saunier, S., Inglehearn, C., Saad, A., Alkindy, A., Thomas, S., Vekemans, M., Dallapiccola, B., Katsanis, N., Johnson, C.A., Attié-Bitach, T. and Gleeson, J.G. Mutations in TMEM216 perturb ciliogenesis and cause Joubert, Meckel and related syndromes. *Nature Genetics.* 2010, **42**(7), pp.619-625.

100. Hong, H., Kim, J. and Kim, J. Myosin heavy chain 10 (MYH10) is required for centriole migration during the biogenesis of primary cilia. *Biochemical and Biophysical Research Communications.* 2015, **461**(1), pp.180-185.

101. Rao, Y., Hao, R., Wang, B. and Yao, T.P. A Mec17-Myosin II Effector Axis Coordinates Microtubule Acetylation and Actin Dynamics to Control Primary Cilium Biogenesis. *PloS one.* 2014, **9**(12), p.e114087.

102. Cao, J., Shen, Y., Zhu, L., Xu, Y., Zhou, Y., Wu, Z., Li, Y., Yan, X. and Zhu, X. miR-129-3p controls cilia assembly by regulating CP110 and actin dynamics. *Nat Cell Biol.* 2012, **14**(7), pp.697-706.

103. Pan, J., You, Y., Huang, T. and Brody, S.L. RhoA-mediated apical actin enrichment is required for ciliogenesis and promoted by Foxj1. *J Cell Sci.* 2007, **120**(Pt 11), pp.1868-1876.

104. Kim, H., Xu, H., Yao, Q., Li, W., Huang, Q., Outeda, P., Cebotaru, V., Chiaravalli, M., Boletta, A., Piontek, K., Germino, G.G., Weinman, E.J., Watnick, T. and Qian, F. Ciliary membrane proteins traffic through the Golgi via a Rabep1/GGA1/Arl3-dependent mechanism. *Nature Communications.* 2014, **5**, pp.5482-5482.

105. Follit, J.A., Li, L., Vucica, Y. and Pazour, G.J. The cytoplasmic tail of fibrocystin contains a ciliary targeting sequence. *The Journal of Cell Biology.* 2010, **188**(1), pp.21-28.

106. Knödler, A., Feng, S., Zhang, J., Zhang, X., Das, A., Peränen, J. and Guo, W. Coordination of Rab8 and Rab11 in primary ciliogenesis. *Proceedings of the National Academy of Sciences of the United States of America.* 2010, **107**(14), pp.6346-6351.

107. Kim, J., Lee, J.E., Heynen-Genel, S., Suyama, E., Ono, K., Lee, K., Ideker, T., Aza-Blanc, P. and Gleeson, J.G. Functional genomic screen for modulators of ciliogenesis and cilium length. *Nature.* 2010, **464**(7291), pp.1048-1051.

108. DePina, A.S. and Langford, G.M. Vesicle transport: the role of actin filaments and myosin motors. *Microsc Res Tech.* 1999, **47**(2), pp.93-106.

109. Ojeda Naharros, I., Gesemann, M., Mateos, J.M., Barmettler, G., Forbes, A., Ziegler, U., Neuhauss, S.C.F. and Bachmann-Gagescu, R. Loss-of-function of the ciliopathy protein Cc2d2a disorganizes the vesicle fusion machinery at the periciliary membrane and indirectly affects Rab8-trafficking in zebrafish photoreceptors. *PLoS genetics.* 2017, **13**(12), p.e1007150.

110. Szymanska, K. *Molecular genetics and cell biology of ciliopathies*. PhD thesis, University of Leeds, 2015.

111. Follit, J.A., Tuft, R.A., Fogarty, K.E. and Pazour, G.J. The intraflagellar transport protein IFT20 is associated with the Golgi complex and is required for cilia assembly. *Molecular Biology of the Cell.* 2006, **17**(9), pp.3781-3792.

112. Molla-Herman, A., Ghossoub, R., Blisnick, T., Meunier, A., Serres, C., Silbermann, F., Emmerson, C., Romeo, K., Bourdoncle, P., Schmitt, A., Saunier, S., Spassky, N., Bastin, P. and Benmerah, A. The ciliary pocket: an endocytic membrane domain at the base of primary and motile cilia. *J Cell Sci.* 2010, **123**(Pt 10), pp.1785-1795.

113. Yeyati, P., Schiller, R., Mali, G., Kasioulis, I., Kawamura, A., Adams, I., Playfoot, C., Gilbert, N., van Heyningen, V., Wills, J., Von Kriegsheim, A.,

Finch, A., Sakai, J., Schofield, C.J., Jackson, I. and Mill, P. KDM3A coordinates actin dynamics with intraflagellar transport to regulate cilia stability. *The Journal of Cell Biology.* 2017, **216**(4), pp.999-1013.

114. Ishizaki, T., Maekawa, M., Fujisawa, K., Okawa, K., Iwamatsu, A., Fujita, A., Watanabe, N., Saito, Y., Kakizuka, A., Morii, N. and Narumiya, S. The small GTP-binding protein Rho binds to and activates a 160 kDa Ser/Thr protein kinase homologous to myotonic dystrophy kinase. *Embo j.* 1996, **15**(8), pp.1885-1893.

115. Leung, T., Manser, E., Tan, L. and Lim, L. A novel serine/threonine kinase binding the Ras-related RhoA GTPase which translocates the kinase to peripheral membranes. *J Biol Chem.* 1995, **270**(49), pp.29051-29054.

116. Huang, L., Szymanska, K., Jensen, V.L., Janecke, A.R., Innes, A.M., Davis, E.E., Frosk, P., Li, C., Willer, J.R., Chodirker, B.N., Greenberg, C.R., McLeod, D.R., Bernier, F.P., Chudley, A.E., Müller, T., Shboul, M., Logan, C.V., Loucks, C.M., Beaulieu, C.L., Bowie, R.V., Bell, S.M., Adkins, J., Zuniga, F.I., Ross, K.D., Wang, J., Ban, M.R., Becker, C., Nürnberg, P., Douglas, S., Craft, C.M., Akimenko, M.-A., Hegele, R.A., Ober, C., Utermann, G., Bolz, H.J., Bulman, D.E., Katsanis, N., Blacque, O.E., Doherty, D., Parboosingh, J.S., Leroux, M.R., Johnson, C.A. and Boycott, K.M. TMEM237 is mutated in individuals with a Joubert syndrome related disorder and expands the role of the TMEM family at the ciliary transition zone. *Am J Hum Genet.* 2011, **89**(6), pp.713-730.

117. Hernandez-Hernandez, V., Pravincumar, P., Diaz-Font, A., May-Simera, H., Jenkins, D., Knight, M. and Beales, P.L. Bardet-Biedl syndrome proteins control the cilia length through regulation of actin polymerization. *Hum Mol Genet.* 2013, **22**(19), pp.3858-3868.

118. Adams, M., Dawe, H., Wheway, G., Szymanska, K., Logan, C., Noegel, A., Gull, K. and Johnson, C. 16-P005 Mutations in the lethal ciliopathy Meckel–Gruber syndrome alter the subcellular distribution of actin-binding proteins and disrupt the actin cytoskeleton. *Mechanisms of Development.* 2009, **126**, p.S263.

119. Hernandez-Hernandez, V., Pravincumar, P., Diaz-Font, A., May-Simera, H., Jenkins, D., Knight, M. and Beales, P.L. Bardet-Biedl syndrome proteins control the cilia length through regulation of actin polymerization. *Hum Mol Genet.* 2013, **22**(19), pp.3858-3868.

120. Vuolo, L., Stevenson, N.L., Heesom, K.J. and Stephens, D.J. Dynein-2 intermediate chains play crucial but distinct roles in primary cilia formation and function. *Elife.* 2018, **7**, p.e39655.

121. Kim, S. and Tsiokas, L. Cilia and cell cycle re-entry: more than a coincidence. *Cell cycle (Georgetown, Tex.).* 2011, **10**(16), pp.2683-2690.

122. Pugacheva, E.N., Jablonski, S.A., Hartman, T.R., Henske, E.P. and Golemis, E.A. HEF1-Dependent Aurora A Activation Induces Disassembly of the Primary Cilium. *Cell.* 2007, **129**(7), pp.1351-1363.

123. Jacoby, M., Cox, J.J., Gayral, S., Hampshire, D.J., Ayub, M., Blockmans, M., Pernot, E., Kisseleva, M.V., Compère, P., Schiffmann, S.N., Gergely, F., Riley, J.H., Pérez-Morga, D., Woods, C.G. and Schurmans, S. INPP5E mutations cause primary cilium signaling defects, ciliary instability and ciliopathies in human and mouse. *Nature Genetics.* 2009, **41**(9), pp.1027-1031.

124. Mirvis, M., Siemers, K.A., Nelson, W.J. and Stearns, T.P. Primary cilium loss in mammalian cells occurs predominantly by whole-cilium shedding. *PLOS Biology.* 2019, **17**(7), p.e3000381.

125. Hirokawa, N., Tanaka, Y., Okada, Y. and Takeda, S. Nodal Flow and the Generation of Left-Right Asymmetry. *Cell.* 2006, **125**(1), pp.33-45.

126. Gerdes, J.M., Davis, E.E. and Katsanis, N. The vertebrate primary cilium in development, homeostasis, and disease. *Cell.* 2009, **137**(1), pp.32-45.

127. Huangfu, D., Liu, A., Rakeman, A.S., Murcia, N.S., Niswander, L. and Anderson, K.V. Hedgehog signalling in the mouse requires intraflagellar transport proteins. *Nature.* 2003, **426**(6962), pp.83-87.

128. Corbit, K.C., Aanstad, P., Singla, V., Norman, A.R., Stainier, D.Y.R. and Reiter, J.F. Vertebrate Smoothened functions at the primary cilium. *Nature.* 2005, **437**(7061), pp.1018-1021.

129. Logan, C.Y. and Nusse, R. THE WNT SIGNALING PATHWAY IN DEVELOPMENT AND DISEASE. *Annual Review of Cell and Developmental Biology.* 2004, **20**(1), pp.781-810.

130. Shillingford, J.M., Murcia, N.S., Larson, C.H., Low, S.H., Hedgepeth, R., Brown, N., Flask, C.A., Novick, A.C., Goldfarb, D.A., Kramer-Zucker, A., Walz, G., Piontek, K.B., Germino, G.G. and Weimbs, T. The mTOR pathway is regulated by polycystin-1, and its inhibition reverses renal cystogenesis in polycystic kidney disease. *Proceedings of the National Academy of Sciences.* 2006, **103**(14), pp.5466-5471.

131. Habbig, S., Bartram, M.P., Müller, R.U., Schwarz, R., Andriopoulos, N., Chen, S., Sägmüller, J.G., Hoehne, M., Burst, V., Liebau, M.C., Reinhardt, H.C., Benzing, T. and Schermer, B. NPHP4, a cilia-associated protein, negatively regulates the Hippo pathway. *The Journal of Cell Biology.* 2011, **193**(4), pp.633-642.

132. Mykytyn, K. and Askwith, C. G-Protein-Coupled Receptor Signaling in Cilia. *Cold Spring Harbor perspectives in biology.* 2017, **9**(9), p.a028183.

133. Du, E., Li, H., Jin, S., Hu, X., Qiu, M. and Han, R. Evidence that TMEM67 causes polycystic kidney disease through activation of JNK/ERK-dependent pathways. *Cell biology international.* 2013, **37**(7), pp.694-702.

134. Clement, C.A., Ajbro, K.D., Koefoed, K., Vestergaard, M.L., Veland, I.R., Henriques de Jesus, M.P., Pedersen, L.B., Benmerah, A., Andersen, C.Y., Larsen, L.A. and Christensen, S.T. TGF-beta signaling is associated with endocytosis at the pocket region of the primary cilium. *Cell reports.* 2013, **3**(6), pp.1806-1814.

135. Zullo, A., Iaconis, D., Barra, A., Cantone, A., Messaddeq, N., Capasso, G., Dollé, P., Igarashi, P. and Franco, B. Kidney-specific inactivation of Ofd1 leads to renal cystic disease associated with upregulation of the mTOR pathway. *Hum Mol Genet.* 2010, **19**(14), pp.2792-2803.

136. Bell, P.D., Fitzgibbon, W., Sas, K., Stenbit, A.E., Amria, M., Houston, A., Reichert, R., Gilley, S., Siegal, G.P., Bissler, J., Bilgen, M., Chou, P.C.-t., Guay-Woodford, L., Yoder, B., Haycraft, C.J. and Siroky, B. Loss of primary cilia upregulates renal hypertrophic signaling and promotes cystogenesis. *Journal of the American Society of Nephrology : JASN.* 2011, **22**(5), pp.839-848.

137. Shillingford, J.M., Murcia, N.S., Larson, C.H., Low, S.H., Hedgepeth, R., Brown, N., Flask, C.A., Novick, A.C., Goldfarb, D.A., Kramer-Zucker, A., Walz, G., Piontek, K.B., Germino, G.G. and Weimbs, T. The mTOR pathway is regulated by polycystin-1, and its inhibition reverses renal cystogenesis in polycystic kidney disease. *Proceedings of the National Academy of Sciences of the United States of America.* 2006, **103**(14), pp.5466-5471.

138. Kim, M., Kim, M., Lee, M.-S., Kim, C.-H. and Lim, D.-S. The MST1/2-SAV1 complex of the Hippo pathway promotes ciliogenesis. *Nature Communications.* 2014, **5**(1), p.5370.

139. Grampa, V., Delous, M., Zaidan, M., Odye, G., Thomas, S., Elkhartoufi, N., Filhol, E., Niel, O., Silbermann, F., Lebreton, C., Collardeau-Frachon, S., Rouvet, I., Alessandri, J.-L., Devisme, L., Dieux-Coeslier, A., Cordier, M.-P., Capri, Y., Khung-Savatovsky, S., Sigaudy, S., Salomon, R., Antignac, C., Gubler, M.-C., Benmerah, A., Terzi, F., Attié-Bitach, T., Jeanpierre, C. and Saunier, S. Novel NEK8 Mutations Cause Severe Syndromic Renal Cystic Dysplasia through YAP Dysregulation. *PLoS genetics.* 2016, **12**(3), pp.e1005894-e1005894.

140. Christensen, S.T., Morthorst, S.K., Mogensen, J.B. and Pedersen, L.B. Primary Cilia and Coordination of Receptor Tyrosine Kinase (RTK) and Transforming Growth Factor β (TGF-β) Signaling. *Cold Spring Harbor perspectives in biology.* 2017, **9**(6), p.a028167.

141. Jang, H.-S., Han, S.J., Kim, J.I., Lee, S., Lipschutz, J.H. and Park, K.M. Activation of ERK accelerates repair of renal tubular epithelial cells, whereas it inhibits progression of fibrosis following ischemia/reperfusion injury. *Biochimica et Biophysica Acta (BBA) - Molecular Basis of Disease.* 2013, **1832**(12), pp.1998-2008.

142. Lindbæk, L., Warzecha, C.B., Koefoed, K., Mogensen, J.B., Schmid, F., Pedersen, L.B., Larsen, L.A. and Christensen, S. Coordination of TGFβ/BMP signaling is associated with the primary cilium. *Cilia.* 2015, **4**(1), p.P17.

143. Foulkes, W.D., Kamihara, J., Evans, D.G.R., Brugieres, L., Bourdeaut, F., Molenaar, J.J., Walsh, M.F., Brodeur, G.M. and Diller, L. Cancer Surveillance in Gorlin Syndrome and Rhabdoid Tumor Predisposition Syndrome. *Clin Cancer Res.* 2017, **23**(12), pp.e62-e67.

144. Beachy, P.A., Hymowitz, S.G., Lazarus, R.A., Leahy, D.J. and Siebold, C. Interactions between Hedgehog proteins and their binding partners come into view. *Genes & Development.* 2010, **24**(18), pp.2001-2012.

145. Briscoe, J. and Thérond, P.P. The mechanisms of Hedgehog signalling and its roles in development and disease. *Nature Reviews Molecular Cell Biology.* 2013, **14**(7), pp.416-429.

146. Nozawa, Y.I., Lin, C. and Chuang, P.-T. Hedgehog signaling from the primary cilium to the nucleus: an emerging picture of ciliary localization, trafficking and transduction. *Current Opinion in Genetics & Development.* 2013, **23**(4), pp.429-437.

147. Kibar, Z., Torban, E., McDearmid, J.R., Reynolds, A., Berghout, J., Mathieu, M., Kirillova, I., De Marco, P., Merello, E., Hayes, J.M., Wallingford, J.B., Drapeau, P., Capra, V. and Gros, P. Mutations in VANGL1 Associated with Neural-Tube Defects. *New England Journal of Medicine.* 2007, **356**(14), pp.1432-1437.

148. Zhan, T., Rindtorff, N. and Boutros, M. Wnt signaling in cancer. *Oncogene.* 2017, **36**(11), pp.1461-1473.

149. Huang, H.-C. and Klein, P.S. The Frizzled family: receptors for multiple signal transduction pathways. *Genome biology.* 2004, **5**(7), pp.234-234.

150. MacDonald, B.T., Tamai, K. and He, X. Wnt/beta-catenin signaling: components, mechanisms, and diseases. *Developmental Cell.* 2009, **17**(1), pp.9-26.

151. Shtutman, M., Zhurinsky, J., Simcha, I., Albanese, C., D'Amico, M., Pestell, R. and Ben-Ze'ev, A. The cyclin D1 gene is a target of the β-catenin/LEF-1 pathway. *Proceedings of the National Academy of Sciences.* 1999, **96**(10), pp.5522-5527.

152. van Amerongen, R. Alternative Wnt pathways and receptors. *Cold Spring Harbor perspectives in biology.* 2012, **4**(10), p.a007914.

153. Corbit, K.C., Shyer, A.E., Dowdle, W.E., Gaulden, J., Singla, V. and Reiter, J.F. Kif3a constrains β-catenin-dependent Wnt signalling through dual ciliary and non-ciliary mechanisms. *Nat Cell Biol.* 2008, **10**(1), pp.70-76.

154. Huang, P. and Schier, A.F. Dampened Hedgehog signaling but normal Wnt signaling in zebrafish without cilia. *Development.* 2009, **136**(18), pp.3089-3098.

155. Ocbina, P.J.R., Tuson, M. and Anderson, K.V. Primary cilia are not required for normal canonical Wnt signaling in the mouse embryo. *PloS one.* 2009, **4**(8), pp.e6839-e6839.

156. Lienkamp, S., Ganner, A. and Walz, G. Inversin, Wnt signaling and primary cilia. *Differentiation.* 2012, **83**(2), pp.S49-S55.

157. Wheway, G., Nazlamova, L. and Hancock, J.T. Signaling through the Primary Cilium. *Frontiers in Cell and Developmental Biology.* 2018, **6**, pp.8-8.

158. Lancaster, M.A., Schroth, J. and Gleeson, J.G. Subcellular spatial regulation of canonical Wnt signalling at the primary cilium. *Nat Cell Biol.* 2011, **13**(6), pp.700-707.

159. Wheway, G., Nazlamova, L. and Hancock, J.T. Signaling through the Primary Cilium. *Frontiers in Cell and Developmental Biology.* 2018, **6**(8).

160. Alliance, C. *CIliopathies* [Online]. [Accessed May]. Available from: http://www.ciliopathyalliance.org/ciliopathies.html

161. Zaki, M.S., Sattar, S., Massoudi, R.A. and Gleeson, J.G. Co-occurrence of distinct ciliopathy diseases in single families suggests genetic modifiers. *American journal of medical genetics. Part A.* 2011, **155A**(12), pp.3042-3049.

162. Roosing, S., Cremers, F.P.M., Riemslag, F.C.C., Zonneveld-Vrieling, M.N., Talsma, H.E., Klessens-Godfroy, F.J.M., den Hollander, A.I. and van den Born, L.I. A Rare Form of Retinal Dystrophy Caused by Hypomorphic Nonsense Mutations in CEP290. *Genes.* 2017, **8**(8), p.208.

163. Frank, V., den Hollander, A.I., Brüchle, N.O., Zonneveld, M.N., Nürnberg, G., Becker, C., Du Bois, G., Kendziorra, H., Roosing, S., Senderek, J., Nürnberg, P., Cremers, F.P., Zerres, K. and Bergmann, C. Mutations of the CEP290 gene encoding a centrosomal protein cause Meckel-Gruber syndrome. *Hum Mutat.* 2008, **29**(1), pp.45-52.

164. Judge, D.P. and Dietz, H.C. Marfan's syndrome. *Lancet (London, England).* 2005, **366**(9501), pp.1965-1976.

165. Myers, R.H. Huntington's disease genetics. *NeuroRx : the journal of the American Society for Experimental NeuroTherapeutics.* 2004, **1**(2), pp.255-262.

166. Kay, C., Collins, J.A., Miedzybrodzka, Z., Madore, S.J., Gordon, E.S., Gerry, N., Davidson, M., Slama, R.A. and Hayden, M.R. Huntington disease reduced penetrance alleles occur at high frequency in the general population. *Neurology.* 2016, **87**(3), pp.282-288.

167. Moore, J.H. The ubiquitous nature of epistasis in determining susceptibility to common human diseases. *Hum Hered.* 2003, **56**(1-3), pp.73-82.

168. Devuyst, O., Persu, A. and Vo-Cong, M.-T. Autosomal dominant polycystic kidney disease: modifier genes and endothelial dysfunction. *Nephrology Dialysis Transplantation.* 2003, **18**(11), pp.2211-2215.

169. Kousi, M. and Katsanis, N. Genetic modifiers and oligogenic inheritance. *Cold Spring Harbor perspectives in medicine.* 2015, **5**(6), p.a017145.

170. Nadeau, J.H. Modifier genes in mice and humans. *Nat Rev Genet.* 2001, **2**(3), pp.165-174.

171. Wu, G., Tian, X., Nishimura, S., Markowitz, G.S., D'Agati, V., Hoon Park, J., Yao, L., Li, L., Geng, L., Zhao, H., Edelmann, W. and Somlo, S. Trans-heterozygous Pkd1 and Pkd2 mutations modify expression of polycystic kidney disease. *Hum Mol Genet.* 2002, **11**(16), pp.1845-1854.

172. Rao, K.N., Zhang, W., Li, L., Ronquillo, C., Baehr, W. and Khanna, H. Ciliopathy-associated protein CEP290 modifies the severity of retinal degeneration due to loss of RPGR. *Hum Mol Genet.* 2016, **25**(10), pp.2005-2012.

173. Khanna, H., Davis, E.E., Murga-Zamalloa, C.A., Estrada-Cuzcano, A., Lopez, I., den Hollander, A.I., Zonneveld, M.N., Othman, M.I., Waseem, N., Chakarova, C.F., Maubaret, C., Diaz-Font, A., MacDonald, I., Muzny, D.M., Wheeler, D.A., Morgan, M., Lewis, L.R., Logan, C.V., Tan, P.L., Beer, M.A., Inglehearn, C.F., Lewis, R.A., Jacobson, S.G., Bergmann, C., Beales, P.L., Attié-Bitach, T., Johnson, C.A., Otto, E.A., Bhattacharya, S.S., Hildebrandt, F., Gibbs, R.A., Koenekoop, R.K., Swaroop, A. and Katsanis, N. A common allele in RPGRIP1L is a modifier of retinal degeneration in ciliopathies. *Nature Genetics.* 2009, **41**(6), pp.739-745.

174. Li, Z. and Srivastava, P. Heat-shock proteins. *Curr Protoc Immunol.* 2004, **Appendix 1**, p.Appendix 1T.

175. Schell, R., Mullis, M. and Ehrenreich, I.M. Modifiers of the Genotype–Phenotype Map: Hsp90 and Beyond. *PLOS Biology.* 2016, **14**(11), p.e2001015.

176. Young, J.C. The role of the cytosolic HSP70 chaperone system in diseases caused by misfolding and aberrant trafficking of ion channels. *Disease Models & Mechanisms.* 2014, **7**(3), pp.319-329.

177. Kim, J.C., Ou, Y.Y., Badano, J.L., Esmail, M.A., Leitch, C.C., Fiedrich, E., Beales, P.L., Archibald, J.M., Katsanis, N., Rattner, J.B. and Leroux, M.R. MKKS/BBS6, a divergent chaperonin-like protein linked to the obesity disorder Bardet-Biedl syndrome, is a novel centrosomal component required for cytokinesis. *Journal of Cell Science.* 2005, **118**(5), pp.1007-1020.

178. Álvarez-Satta, M., Castro-Sánchez, S. and Valverde, D. Bardet-Biedl Syndrome as a Chaperonopathy: Dissecting the Major Role of Chaperonin-Like BBS Proteins (BBS6-BBS10-BBS12). *Frontiers in molecular biosciences.* 2017, **4**, pp.55-55.

179. Shaheen, R., Szymanska, K., Basu, B., Patel, N., Ewida, N., Faqeih, E., Al Hashem, A., Derar, N., Alsharif, H., Aldahmesh, M.A., Alazami, A.M., Hashem, M., Ibrahim, N., Abdulwahab, F.M., Sonbul, R., Alkuraya, H., Alnemer, M., Al Tala, S., Al-Husain, M., Morsy, H., Seidahmed, M.Z., Meriki, N., Al-Owain, M., AlShahwan, S., Tabarki, B., Salih, M.A., Ciliopathy, W., Faquih, T., El-Kalioby, M., Ueffing, M., Boldt, K., Logan,

C.V., Parry, D.A., Al Tassan, N., Monies, D., Megarbane, A., Abouelhoda, M., Halees, A., Johnson, C.A. and Alkuraya, F.S. Characterizing the morbid genome of ciliopathies. *Genome biology.* 2016, **17**(1), pp.242-242.

180. Phelps, I.G., Dempsey, J.C., Grout, M.E., Isabella, C.R., Tully, H.M., Doherty, D. and Bachmann-Gagescu, R. Interpreting the clinical significance of combined variants in multiple recessive disease genes: systematic investigation of Joubert syndrome yields little support for oligogenicity. *Genet Med.* 2018, **20**(2), pp.223-233.

181. Eichers, E., Lewis, R.A., Katsanis, N. and Lupski, J. Triallelic inheritance: a bridge between Mendelian and multifactorial traits. *Annals of Medicine.* 2004, **36**(4), pp.262-272.

182. Katsanis, N., Ansley, S.J., Badano, J.L., Eichers, E.R., Lewis, R.A., Hoskins, B.E., Scambler, P.J., Davidson, W.S., Beales, P.L. and Lupski, J.R. Triallelic Inheritance in Bardet-Biedl Syndrome, a Mendelian Recessive Disorder. *Science.* 2001, **293**(5538), pp.2256-2259.

183. Beales, P.L., Badano, J.L., Ross, A.J., Ansley, S.J., Hoskins, B.E., Kirsten, B., Mein, C.A., Froguel, P., Scambler, P.J., Lewis, R.A., Lupski, J.R. and Katsanis, N. Genetic Interaction of BBS1 Mutations with Alleles at Other BBS Loci Can Result in Non-Mendelian Bardet-Biedl Syndrome. *The American Journal of Human Genetics.* 2003, **72**(5), pp.1187-1199.

184. Menzl, I., Lebeau, L., Pandey, R., Hassounah, N.B., Li, F.W., Nagle, R., Weihs, K. and McDermott, K.M. Loss of primary cilia occurs early in breast cancer development. *Cilia.* 2014, **3**(1), p.7.

185. Paquette, M., El-Houjeiri, L. and Pause, A. mTOR Pathways in Cancer and Autophagy. *Cancers.* 2018, **10**(1), p.18.

186. Zhao, X., Pak, E., Ornell, K.J., Pazyra-Murphy, M.F., MacKenzie, E.L., Chadwick, E.J., Ponomaryov, T., Kelleher, J.F. and Segal, R.A. A Transposon Screen Identifies Loss of Primary Cilia as a Mechanism of Resistance to SMO Inhibitors. *Cancer Discovery.* 2017, **7**(12), pp.1436-1449.

187. Higgins, M., Obaidi, I. and McMorrow, T. Primary cilia and their role in cancer. *Oncology letters.* 2019, **17**(3), pp.3041-3047.

188. Gradilone, S.A., Pisarello, M.J.L. and LaRusso, N.F. Primary Cilia in Tumor Biology: The Primary Cilium as a Therapeutic Target in Cholangiocarcinoma. *Current drug targets.* 2017, **18**(8), pp.958-963.

189. Fabbri, L., Bost, F. and Mazure, N.M. Primary Cilium in Cancer Hallmarks. *International journal of molecular sciences.* 2019, **20**(6), p.1336.

190. Stratigopoulos, G., Martin Carli, J.F., O'Day, D.R., Wang, L., Leduc, C.A., Lanzano, P., Chung, W.K., Rosenbaum, M., Egli, D., Doherty, D.A. and Leibel, R.L. Hypomorphism for RPGRIP1L, a ciliary gene vicinal to the

FTO locus, causes increased adiposity in mice. *Cell metabolism.* 2014, **19**(5), pp.767-779.

191. Aughsteen, A.A. The ultrastructure of primary cilia in the endocrine and excretory duct cells of the pancreas of mice and rats. *Eur J Morphol.* 2001, **39**(5), pp.277-283.

192. Stratigopoulos, G., Martin Carli, J.F., O'Day, D.R., Wang, L., Leduc, C.A., Lanzano, P., Chung, W.K., Rosenbaum, M., Egli, D., Doherty, D.A. and Leibel, R.L. Hypomorphism for RPGRIP1L, a ciliary gene vicinal to the FTO locus, causes increased adiposity in mice. *Cell metabolism.* 2014, **19**(5), pp.767-779.

193. Rahmouni, K., Fath, M.A., Seo, S., Thedens, D.R., Berry, C.J., Weiss, R., Nishimura, D.Y. and Sheffield, V.C. Leptin resistance contributes to obesity and hypertension in mouse models of Bardet-Biedl syndrome. *J Clin Invest.* 2008, **118**(4), pp.1458-1467.

194. Gerdes, J.M., Christou-Savina, S., Xiong, Y., Moede, T., Moruzzi, N., Karlsson-Edlund, P., Leibiger, B., Leibiger, I.B., Ostenson, C.G., Beales, P.L. and Berggren, P.O. Ciliary dysfunction impairs beta-cell insulin secretion and promotes development of type 2 diabetes in rodents. *Nat Commun.* 2014, **5**, p.5308.

195. Volta, F. and Gerdes, J.M. The role of primary cilia in obesity and diabetes. *Ann N Y Acad Sci.* 2017, **1391**(1), pp.71-84.

196. Beales, P.L., Elcioglu, N., Woolf, A.S., Parker, D. and Flinter, F.A. New criteria for improved diagnosis of Bardet-Biedl syndrome: results of a population survey. *Journal of Medical Genetics.* 1999, **36**(6), pp.437-446.

197. Hughes, J.W., Cho, J.H., Conway, H.E., DiGruccio, M.R., Ng, X.W., Roseman, H.F., Abreu, D., Urano, F. and Piston, D.W. Primary cilia control glucose homeostasis via islet paracrine interactions. *Proceedings of the National Academy of Sciences.* 2020, **117**(16), pp.8912-8923.

198. Klena, N.T., Gibbs, B.C. and Lo, C.W. Cilia and Ciliopathies in Congenital Heart Disease. *Cold Spring Harbor perspectives in biology.* 2017, **9**(8).

199. Pala, R., Jamal, M., Alshammari, Q. and Nauli, S.M. The Roles of Primary Cilia in Cardiovascular Diseases. *Cells.* 2018, **7**(12), p.233.

200. Luu, V.Z., Chowdhury, B., Al-Omran, M., Hess, D.A. and Verma, S. Role of endothelial primary cilia as fluid mechanosensors on vascular health. *Atherosclerosis.* 2018, **275**, pp.196-204.

201. Dinsmore, C. and Reiter, J.F. Endothelial primary cilia inhibit atherosclerosis. *EMBO reports.* 2016, **17**(2), pp.156-166.

202. Cook, S.A., Collin, G.B., Bronson, R.T., Naggert, J.K., Liu, D.P., Akeson, E.C. and Davisson, M.T. A Mouse Model for Meckel Syndrome Type 3. *Journal of the American Society of Nephrology : JASN.* 2009, **20**(4), pp.753-764.

203. Yokobayashi, S., Okita, K., Nakagawa, M., Nakamura, T., Yabuta, Y., Yamamoto, T. and Saitou, M. Clonal variation of human induced pluripotent stem cells for induction into the germ cell fate†. *Biology of Reproduction.* 2017, **96**(6), pp.1154-1166.

204. Kozminski, K.G., Johnson, K.A., Forscher, P. and Rosenbaum, J.L. A motility in the eukaryotic flagellum unrelated to flagellar beating. *Proceedings of the National Academy of Sciences of the United States of America.* 1993, **90**(12), pp.5519-5523.

205. Pedersen, L.B., Geimer, S. and Rosenbaum, J.L. Dissecting the molecular mechanisms of intraflagellar transport in chlamydomonas. *Curr Biol.* 2006, **16**(5), pp.450-459.

206. Rajagopalan, V., Corpuz, E.O., Hubenschmidt, M.J., Townsend, C.R., Asai, D.J. and Wilkes, D.E. Analysis of properties of cilia using Tetrahymena thermophila. *Methods Mol Biol.* 2009, **586**, pp.283-299.

207. Pan, X., Ou, G., Civelekoglu-Scholey, G., Blacque, O.E., Endres, N.F., Tao, L., Mogilner, A., Leroux, M.R., Vale, R.D. and Scholey, J.M. Mechanism of transport of IFT particles in C. elegans cilia by the concerted action of kinesin-II and OSM-3 motors. *J Cell Biol.* 2006, **174**(7), pp.1035-1045.

208. Song, Z., Zhang, X., Jia, S., Yelick, P.C. and Zhao, C. Zebrafish as a Model for Human Ciliopathies. *Journal of Genetics and Genomics.* 2016, **43**(3), pp.107-120.

209. Coxam, B., Sabine, A., Bower, N.I., Smith, K.A., Pichol-Thievend, C., Skoczylas, R., Astin, J.W., Frampton, E., Jaquet, M., Crosier, P.S., Parton, R.G., Harvey, N.L., Petrova, T.V., Schulte-Merker, S., Francois, M. and Hogan, B.M. Pkd1 regulates lymphatic vascular morphogenesis during development. *Cell reports.* 2014, **7**(3), pp.623-633.

210. *Why Mouse Matters.* [Online]. 2010. [Accessed]. Available from: https://www.genome.gov/10001345/importance-of-mouse-genome

211. Norris, D.P. and Grimes, D.T. Mouse models of ciliopathies: the state of the art. *Dis Model Mech.* 2012, **5**(3), pp.299-312.

212. Halbritter, J., Porath, J.D., Diaz, K.A., Braun, D.A., Kohl, S., Chaki, M., Allen, S.J., Soliman, N.A., Hildebrandt, F. and Otto, E.A. Identification of 99 novel mutations in a worldwide cohort of 1,056 patients with a nephronophthisis-related ciliopathy. *Hum Genet.* 2013, **132**(8), pp.865-884.

213. Jiang, S.T., Chiou, Y.Y., Wang, E., Lin, H.K., Lee, S.P., Lu, H.Y., Wang, C.K., Tang, M.J. and Li, H. Targeted disruption of Nphp1 causes male infertility due to defects in the later steps of sperm morphogenesis in mice. *Hum Mol Genet.* 2008, **17**(21), pp.3368-3379.

214. Ajzeberg, H., Slaats, G., Stokman, M., Logister, I., Knoers, N. and Giles, R. Urine-derived Renal Epithelial Cells (URECs) as a source of

biomaterial from ciliopathy patients for functional studies and diagnostics. *Cilia.* 2015, **4**(Suppl 1), pp.P51-P51.

215. Mead, B.E. and Karp, J.M. All models are wrong, but some organoids may be useful. *Genome biology.* 2019, **20**(1), p.66.

216. Sato, T., Vries, R.G., Snippert, H.J., van de Wetering, M., Barker, N., Stange, D.E., van Es, J.H., Abo, A., Kujala, P., Peters, P.J. and Clevers, H. Single Lgr5 stem cells build crypt-villus structures in vitro without a mesenchymal niche. *Nature.* 2009, **459**(7244), pp.262-265.

217. Parfitt, D.A., Lane, A., Ramsden, C.M., Carr, A.J., Munro, P.M., Jovanovic, K., Schwarz, N., Kanuga, N., Muthiah, M.N., Hull, S., Gallo, J.M., da Cruz, L., Moore, A.T., Hardcastle, A.J., Coffey, P.J. and Cheetham, M.E. Identification and Correction of Mechanisms Underlying Inherited Blindness in Human iPSC-Derived Optic Cups. *Cell Stem Cell.* 2016, **18**(6), pp.769-781.

218. Hanaoka, K. and Guggino, W.B. cAMP regulates cell proliferation and cyst formation in autosomal polycystic kidney disease cells. *Journal of the American Society of Nephrology : JASN.* 2000, **11**(7), pp.1179-1187.

219. *Genetics*. s.v.

220. Zou, Y. Charles Darwin's Theory of Pangenesis. *Embryo Project Encyclopedia.* 2014.

221. Mendel, G.J. "Versuche über Pflanzen-Hybriden" [Experiments Concerning Plant Hybrids]. *Verhandlungen des naturforschenden Vereines in Brünn [Proceedings of the Natural History Society of Brünn]* 1865, pp.3-47.

222. Maderspacher, F. Theodor Boveri and the natural experiment. *Current Biology.* 2008, **18**(7), pp.R279-R286.

223. Hall, A.D. Hugo de Vries, 1848-1935. *Obituary Notices of Fellows of the Royal Society.* 1935, **1**(4), pp.371-373.

224. Beadle, G.W. and Tatum, E.L. Genetic Control of Biochemical Reactions in Neurospora. *Proceedings of the National Academy of Sciences of the United States of America.* 1941, **27**(11), pp.499-506.

225. Watson, J.D. and Crick, F.H.C. Molecular Structure of Nucleic Acids: A Structure for Deoxyribose Nucleic Acid. *Nature.* 1953, **171**(4356), pp.737-738.

226. Saiki, R.K., Scharf, S., Faloona, F., Mullis, K.B., Horn, G.T., Erlich, H.A. and Arnheim, N. Enzymatic amplification of beta-globin genomic sequences and restriction site analysis for diagnosis of sickle cell anemia. *Science.* 1985, **230**(4732), pp.1350-1354.

227. International Human Genome Sequencing, C. Finishing the euchromatic sequence of the human genome. *Nature.* 2004, **431**(7011), pp.931-945.

228. Fire, A., Albertson, D., Harrison, S.W. and Moerman, D.G. Production of antisense RNA leads to effective and specific inhibition of gene expression in C. elegans muscle. *Development.* 1991, **113**(2), pp.503-514.

229. Agrawal, N., Dasaradhi, P.V.N., Mohmmed, A., Malhotra, P., Bhatnagar, R.K. and Mukherjee, S.K. RNA Interference: Biology, Mechanism, and Applications. *Microbiology and Molecular Biology Reviews.* 2003, **67**(4), pp.657-685.

230. Fire, A., Xu, S., Montgomery, M.K., Kostas, S.A., Driver, S.E. and Mello, C.C. Potent and specific genetic interference by double-stranded RNA in Caenorhabditis elegans. *Nature.* 1998, **391**(6669), pp.806-811.

231. Kamath, R.S. and Ahringer, J. Genome-wide RNAi screening in Caenorhabditis elegans. *Methods.* 2003, **30**(4), pp.313-321.

232. Wang, W., Liu, H., Zhao, H., Luo, Z. and Shi, Y. Design, construction, and analysis of specific zinc finger nucleases for microphthalmia - associate transcription factor. *Brazilian Archives of Biology and Technology.* 2012, **55**, pp.559-568.

233. Joung, J.K. and Sander, J.D. TALENs: a widely applicable technology for targeted genome editing. *Nature reviews. Molecular cell biology.* 2013, **14**(1), pp.49-55.

234. Jinek, M., Chylinski, K., Fonfara, I., Hauer, M., Doudna, J.A. and Charpentier, E. A Programmable Dual-RNA–Guided DNA Endonuclease in Adaptive Bacterial Immunity. *Science.* 2012, **337**(6096), pp.816-821.

235. Ran, F.A., Hsu, P.D., Wright, J., Agarwala, V., Scott, D.A. and Zhang, F. Genome engineering using the CRISPR-Cas9 system. *Nature Protocols.* 2013, **8**(11), pp.2281-2308.

236. Video animation: RNA interference. *Nature.* 2011.

237. Kanasty, R.L., Whitehead, K.A., Vegas, A.J. and Anderson, D.G. Action and reaction: the biological response to siRNA and its delivery vehicles. *Molecular therapy : the journal of the American Society of Gene Therapy.* 2012, **20**(3), pp.513-524.

238. El-Brolosy, M.A. and Stainier, D.Y.R. Genetic compensation: A phenomenon in search of mechanisms. *PLoS genetics.* 2017, **13**(7), pp.e1006780-e1006780.

239. Lemos, B.R., Kaplan, A.C., Bae, J.E., Ferrazzoli, A.E., Kuo, J., Anand, R.P., Waterman, D.P. and Haber, J.E. CRISPR/Cas9 cleavages in budding yeast reveal templated insertions and strand-specific insertion/deletion profiles. *Proceedings of the National Academy of Sciences.* 2018, **115**(9), pp.E2040-E2047.

240. Rath, D., Amlinger, L., Rath, A. and Lundgren, M. The CRISPR-Cas immune system: Biology, mechanisms and applications. *Biochimie.* 2015, **117**, pp.119-128.

241. Chu, V.T., Weber, T., Wefers, B., Wurst, W., Sander, S., Rajewsky, K. and Kuhn, R. Increasing the efficiency of homology-directed repair for CRISPR-Cas9-induced precise gene editing in mammalian cells. *Nat Biotech.* 2015, **33**(5), pp.543-548.

242. Maruyama, T., Dougan, S.K., Truttmann, M., Bilate, A.M., Ingram, J.R. and Ploegh, H.L. Inhibition of non-homologous end joining increases the efficiency of CRISPR/Cas9-mediated precise [TM: inserted] genome editing. *Nat Biotechnol.* 2015, **33**(5), pp.538-542.

243. Zetsche, B., Gootenberg, J.S., Abudayyeh, O.O., Slaymaker, I.M., Makarova, K.S., Essletzbichler, P., Volz, S.E., Joung, J., van der Oost, J., Regev, A., Koonin, E.V. and Zhang, F. Cpf1 is a single RNA-guided endonuclease of a class 2 CRISPR-Cas system. *Cell.* 2015, **163**(3), pp.759-771.

244. Suzuki, K., Tsunekawa, Y., Hernandez-Benitez, R., Wu, J., Zhu, J., Kim, E.J., Hatanaka, F., Yamamoto, M., Araoka, T., Li, Z., Kurita, M., Hishida, T., Li, M., Aizawa, E., Guo, S., Chen, S., Goebl, A., Soligalla, R.D., Qu, J., Jiang, T., Fu, X., Jafari, M., Esteban, C.R., Berggren, W.T., Lajara, J., Nuñez-Delicado, E., Guillen, P., Campistol, J.M., Matsuzaki, F., Liu, G.-H., Magistretti, P., Zhang, K., Callaway, E.M., Zhang, K. and Belmonte, J.C.I. In vivo genome editing via CRISPR/Cas9 mediated homology-independent targeted integration. *Nature.* 2016, **540**(7631), pp.144-149.

245. Hu, P., Zhao, X., Zhang, Q., Li, W. and Zu, Y. Comparison of Various Nuclear Localization Signal-Fused Cas9 Proteins and Cas9 mRNA for Genome Editing in Zebrafish. *G3 (Bethesda, Md.).* 2018, **8**(3), pp.823-831.

246. Hu, J.H., Miller, S.M., Geurts, M.H., Tang, W., Chen, L., Sun, N., Zeina, C.M., Gao, X., Rees, H.A., Lin, Z. and Liu, D.R. Evolved Cas9 variants with broad PAM compatibility and high DNA specificity. *Nature.* 2018, **556**(7699), pp.57-63.

247. O'Brien, A.R., Wilson, L.O.W., Burgio, G. and Bauer, D.C. Unlocking HDR-mediated nucleotide editing by identifying high-efficiency target sites using machine learning. *Scientific Reports.* 2019, **9**(1), p.2788.

248. Li, X.-L., Li, G.-H., Fu, J., Fu, Y.-W., Zhang, L., Chen, W., Arakaki, C., Zhang, J.-P., Wen, W., Zhao, M., Chen, W.V., Botimer, G.D., Baylink, D., Aranda, L., Choi, H., Bechar, R., Talbot, P., Sun, C.-K., Cheng, T. and Zhang, X.-B. Highly efficient genome editing via CRISPR-Cas9 in human pluripotent stem cells is achieved by transient BCL-XL overexpression. *Nucleic acids research.* 2018, **46**(19), pp.10195-10215.

249. Supharattanasitthi, W., Carlsson, E., Sharif, U. and Paraoan, L. CRISPR/Cas9-mediated one step bi-allelic change of genomic DNA in iPSCs and human RPE cells in vitro with dual antibiotic selection. *Scientific Reports.* 2019, **9**(1), p.174.

250. Suzuki, K. and Izpisua Belmonte, J.C. In vivo genome editing via the HITI method as a tool for gene therapy. *Journal of Human Genetics.* 2018, **63**(2), pp.157-164.

251. Bakondi, B., Lv, W., Lu, B., Jones, M.K., Tsai, Y., Kim, K.J., Levy, R., Akhtar, A.A., Breunig, J.J., Svendsen, C.N. and Wang, S. In Vivo CRISPR/Cas9 Gene Editing Corrects Retinal Dystrophy in the S334ter-3 Rat Model of Autosomal Dominant Retinitis Pigmentosa. *Mol Ther.* 2016, **24**(3), pp.556-563.

252. Chrenek, M.A., Nickerson, J.M. and Boatright, J.H. Clustered Regularly Interspaced Short Palindromic Repeats: Challenges in Treating Retinal Disease. *Asia-Pacific journal of ophthalmology (Philadelphia, Pa.).* 2016, **5**(4), pp.304-308.

253. Gaudelli, N.M., Komor, A.C., Rees, H.A., Packer, M.S., Badran, A.H., Bryson, D.I. and Liu, D.R. Programmable base editing of A•T to G•C in genomic DNA without DNA cleavage. *Nature.* 2017, **551**(7681), pp.464-471.

254. Krokan, H.E., Drabløs, F. and Slupphaug, G. Uracil in DNA – occurrence, consequences and repair. *Oncogene.* 2002, **21**(58), pp.8935-8948.

255. Komor, A.C., Kim, Y.B., Packer, M.S., Zuris, J.A. and Liu, D.R. Programmable editing of a target base in genomic DNA without double-stranded DNA cleavage. *Nature.* 2016, **533**(7603), pp.420-424.

256. Komor, A.C., Zhao, K.T., Packer, M.S., Gaudelli, N.M., Waterbury, A.L., Koblan, L.W., Kim, Y.B., Badran, A.H. and Liu, D.R. Improved base excision repair inhibition and bacteriophage Mu Gam protein yields C:G-to-T:A base editors with higher efficiency and product purity. *Science advances.* 2017, **3**(8), pp.eaao4774-eaao4774.

257. Kim, Y.B., Komor, A.C., Levy, J.M., Packer, M.S., Zhao, K.T. and Liu, D.R. Increasing the genome-targeting scope and precision of base editing with engineered Cas9-cytidine deaminase fusions. *Nature Biotechnology.* 2017, **35**(4), pp.371-376.

258. Anzalone, A.V., Randolph, P.B., Davis, J.R., Sousa, A.A., Koblan, L.W., Levy, J.M., Chen, P.J., Wilson, C., Newby, G.A., Raguram, A. and Liu, D.R. Search-and-replace genome editing without double-strand breaks or donor DNA. *Nature.* 2019, **576**(7785), pp.149-157.

259. Wheway, G., Schmidts, M., Mans, D.A., Szymanska, K., Nguyen, T.T., Racher, H., Phelps, I.G., Toedt, G., Kennedy, J., Wunderlich, K.A., Sorusch, N., Abdelhamed, Z.A., Natarajan, S., Herridge, W., van Reeuwijk, J., Horn, N., Boldt, K., Parry, D.A., Letteboer, S.J.F., Roosing, S., Adams, M., Bell, S.M., Bond, J., Higgins, J., Morrison, E.E., Tomlinson, D.C., Slaats, G.G., van Dam, T.J.P., Huang, L., Kessler, K., Giessl, A., Logan, C.V., Boyle, E.A., Shendure, J., Anazi, S., Aldahmesh, M., Al Hazzaa, S., Hegele, R.A., Ober, C., Frosk, P., Mhanni, A.A., Chodirker, B.N., Chudley, A.E., Lamont, R., Bernier, F.P., Beaulieu, C.L., Gordon, P., Pon, R.T., Donahue, C., Barkovich, A.J., Wolf, L., Toomes,

C., Thiel, C.T., Boycott, K.M., McKibbin, M., Inglehearn, C.F., Stewart, F., Omran, H., Huynen, M.A., Sergouniotis, P.I., Alkuraya, F.S., Parboosingh, J.S., Innes, A.M., Willoughby, C.E., Giles, R.H., Webster, A.R., Ueffing, M., Blacque, O., Gleeson, J.G., Wolfrum, U., Beales, P.L., Gibson, T., Doherty, D., Mitchison, H.M., Roepman, R. and Johnson, C.A. An siRNA-based functional genomics screen for the identification of regulators of ciliogenesis and ciliopathy genes. *Nat Cell Biol.* 2015, **17**(8), pp.1074-1087.

260. Kim, J., Lee, J.E., Heynen-Genel, S., Suyama, E., Ono, K., Lee, K., Ideker, T., Aza-Blanc, P. and Gleeson, J.G. Functional genomic screen for modulators of ciliogenesis and cilium length. *Nature.* 2010, **464**(7291), pp.1048-1051.

261. Balestra, Fernando R., Strnad, P., Flückiger, I. and Gönczy, P. Discovering Regulators of Centriole Biogenesis through siRNA-Based Functional Genomics in Human Cells. *Developmental Cell.* 2013, **25**(6), pp.555-571.

262. Roosing, S., Hofree, M., Kim, S., Scott, E., Copeland, B., Romani, M., Silhavy, J.L., Rosti, R.O., Schroth, J., Mazza, T., Miccinilli, E., Zaki, M.S., Swoboda, K.J., Milisa-Drautz, J., Dobyns, W.B., Mikati, M.A., Incecik, F., Azam, M., Borgatti, R., Romaniello, R., Boustany, R.M., Clericuzio, C.L., D'Arrigo, S., Stromme, P., Boltshauser, E., Stanzial, F., Mirabelli-Badenier, M., Moroni, I., Bertini, E., Emma, F., Steinlin, M., Hildebrandt, F., Johnson, C.A., Freilinger, M., Vaux, K.K., Gabriel, S.B., Aza-Blanc, P., Heynen-Genel, S., Ideker, T., Dynlacht, B.D., Lee, J.E., Valente, E.M., Kim, J. and Gleeson, J.G. Functional genome-wide siRNA screen identifies KIAA0586 as mutated in Joubert syndrome. *Elife.* 2015, **4**, p.e06602.

263. Tsai, I.C., Adams, K.A., Tzeng, J.A., Shennib, O., Tan, P.L. and Katsanis, N. Genome-wide suppressor screen identifies USP35/USP38 as therapeutic candidates for ciliopathies. *JCI insight.* 2019, **4**(22), p.e130516.

264. Breslow, D.K., Hoogendoorn, S., Kopp, A.R., Morgens, D.W., Vu, B.K., Kennedy, M.C., Han, K., Li, A., Hess, G.T., Bassik, M.C., Chen, J.K. and Nachury, M.V. A CRISPR-based screen for Hedgehog signaling provides insights into ciliary function and ciliopathies. *Nature Genetics.* 2018, **50**(3), pp.460-471.

265. Grant, G.P. *Rho GTPase Signalling in Cilia and Blood Vessel Lumen Formation.* . PhD thesis, Univeristy of Leeds, 2017.

266. Wheway, G., Schmidts, M., Mans, D.A., Szymanska, K., Nguyen, T.-M.T., Racher, H., Phelps, I.G., Toedt, G., Kennedy, J., Wunderlich, K.A., Sorusch, N., Abdelhamed, Z.A., Natarajan, S., Herridge, W., van Reeuwijk, J., Horn, N., Boldt, K., Parry, D.A., Letteboer, S.J.F., Roosing, S., Adams, M., Bell, S.M., Bond, J., Higgins, J., Morrison, E.E., Tomlinson, D.C., Slaats, G.G., van Dam, T.J.P., Huang, L., Kessler, K., Giessl, A., Logan, C.V., Boyle, E.A., Shendure, J., Anazi, S., Aldahmesh, M., Al Hazzaa, S., Hegele, R.A., Ober, C., Frosk, P., Mhanni, A.A.,

Chodirker, B.N., Chudley, A.E., Lamont, R., Bernier, F.P., Beaulieu, C.L., Gordon, P., Pon, R.T., Donahue, C., Barkovich, A.J., Wolf, L., Toomes, C., Thiel, C.T., Boycott, K.M., McKibbin, M., Inglehearn, C.F., Consortium, U.K., University of Washington Center for Mendelian, G., Stewart, F., Omran, H., Huynen, M.A., Sergouniotis, P.I., Alkuraya, F.S., Parboosingh, J.S., Innes, A.M., Willoughby, C.E., Giles, R.H., Webster, A.R., Ueffing, M., Blacque, O., Gleeson, J.G., Wolfrum, U., Beales, P.L., Gibson, T., Doherty, D., Mitchison, H.M., Roepman, R. and Johnson, C.A. An siRNA-based functional genomics screen for the identification of regulators of ciliogenesis and ciliopathy genes. *Nat Cell Biol.* 2015, **17**, p.1074.

267. Valente, E.M., Logan, C.V., Mougou-Zerelli, S., Lee, J.H., Silhavy, J.L., Brancati, F., Iannicelli, M., Travaglini, L., Romani, S., Illi, B., Adams, M., Szymanska, K., Mazzotta, A., Lee, J.E., Tolentino, J.C., Swistun, D., Salpietro, C.D., Fede, C., Gabriel, S., Russ, C., Cibulskis, K., Sougnez, C., Hildebrandt, F., Otto, E.A., Held, S., Diplas, B.H., Davis, E.E., Mikula, M., Strom, C.M., Ben-Zeev, B., Lev, D., Sagie, T.L., Michelson, M., Yaron, Y., Krause, A., Boltshauser, E., Elkhartoufi, N., Roume, J., Shalev, S., Munnich, A., Saunier, S., Inglehearn, C., Saad, A., Alkindy, A., Thomas, S., Vekemans, M., Dallapiccola, B., Katsanis, N., Johnson, C.A., Attie-Bitach, T. and Gleeson, J.G. Mutations in TMEM216 perturb ciliogenesis and cause Joubert, Meckel and related syndromes. *Nat Genet.* 2010, **42**(7), pp.619-625.

268. Schindelin, J., Arganda-Carreras, I., Frise, E., Kaynig, V., Longair, M., Pietzsch, T., Preibisch, S., Rueden, C., Saalfeld, S., Schmid, B., Tinevez, J.-Y., White, D.J., Hartenstein, V., Eliceiri, K., Tomancak, P. and Cardona, A. Fiji: an open-source platform for biological-image analysis. *Nature Methods.* 2012, **9**(7), pp.676-682.

269. Bolte, S. and Cordelieres, F.P. A guided tour into subcellular colocalization analysis in light microscopy. *J Microsc.* 2006, **224**(Pt 3), pp.213-232.

270. Costes, S.V., Daelemans, D., Cho, E.H., Dobbin, Z., Pavlakis, G. and Lockett, S. Automatic and quantitative measurement of protein-protein colocalization in live cells. *Biophysical journal.* 2004, **86**(6), pp.3993-4003.

271. Cost, G.J. Enzymatic ligation assisted by nucleases: simultaneous ligation and digestion promote the ordered assembly of DNA. *Nat Protoc.* 2007, **2**(9), pp.2198-2202.

272. Szklarczyk, D., Gable, A.L., Lyon, D., Junge, A., Wyder, S., Huerta-Cepas, J., Simonovic, M., Doncheva, N.T., Morris, J.H., Bork, P., Jensen, L.J. and Mering, C.V. STRING v11: protein-protein association networks with increased coverage, supporting functional discovery in genome-wide experimental datasets. *Nucleic acids research.* 2019, **47**(D1), pp.D607-d613.

273. Franceschini, A., Szklarczyk, D., Frankild, S., Kuhn, M., Simonovic, M., Roth, A., Lin, J., Minguez, P., Bork, P., von Mering, C. and Jensen, L.J.

STRING v9.1: protein-protein interaction networks, with increased coverage and integration. *Nucleic acids research.* 2013, **41**(Database issue), pp.D808-D815.

274. Sharma, S. and Rao, A. RNAi screening: tips and techniques. *Nature immunology.* 2009, **10**(8), pp.799-804.

275. Liu, P., Dodson, M., Fang, D., Chapman, E. and Zhang, D.D. NRF2 negatively regulates primary ciliogenesis and hedgehog signaling. *PLoS Biol.* 2020, **18**(2), p.e3000620.

276. Kasahara, K., Kawakami, Y., Kiyono, T., Yonemura, S., Kawamura, Y., Era, S., Matsuzaki, F., Goshima, N. and Inagaki, M. Ubiquitin-proteasome system controls ciliogenesis at the initial step of axoneme extension. *Nature Communications.* 2014, **5**(1), p.5081.

277. Drummond, M.L., Li, M., Tarapore, E., Nguyen, T.T.L., Barouni, B.J., Cruz, S., Tan, K.C., Oro, A.E. and Atwood, S.X. Actin polymerization controls cilia-mediated signaling. *Journal of Cell Biology.* 2018, **217**(9), pp.3255-3266.

278. Wang, L. and Dynlacht, B.D. The regulation of cilium assembly and disassembly in development and disease. *Development.* 2018, **145**(18), p.dev151407.

279. Binns, D., Dimmer, E., Huntley, R., Barrell, D., O'Donovan, C. and Apweiler, R. QuickGO: a web-based tool for Gene Ontology searching. *Bioinformatics.* 2009, **25**(22), pp.3045-3046.

280. Szklarczyk, D., Morris, J.H., Cook, H., Kuhn, M., Wyder, S., Simonovic, M., Santos, A., Doncheva, N.T., Roth, A., Bork, P., Jensen, L.J. and von Mering, C. The STRING database in 2017: quality-controlled protein-protein association networks, made broadly accessible. *Nucleic acids research.* 2017, **45**(D1), pp.D362-d368.

281. Hannus, M., Beitzinger, M., Engelmann, J.C., Weickert, M.-T., Spang, R., Hannus, S. and Meister, G. siPools: highly complex but accurately defined siRNA pools eliminate off-target effects. *Nucleic acids research.* 2014, **42**(12), pp.8049-8061.

282. Zimmer, A.M., Pan, Y.K., Chandrapalan, T., Kwong, R.W.M. and Perry, S.F. Loss-of-function approaches in comparative physiology: is there a future for knockdown experiments in the era of genome editing? *The Journal of Experimental Biology.* 2019, **222**(7), p.jeb175737.

283. Thumkeo, D., Keel, J., Ishizaki, T., Hirose, M., Nonomura, K., Oshima, H., Oshima, M., Taketo, M.M. and Narumiya, S. Targeted disruption of the mouse rho-associated kinase 2 gene results in intrauterine growth retardation and fetal death. *Mol Cell Biol.* 2003, **23**(14), pp.5043-5055.

284. Nakagawa, O., Fujisawa, K., Ishizaki, T., Saito, Y., Nakao, K. and Narumiya, S. ROCK-I and ROCK-II, two isoforms of Rho-associated coiled-coil forming protein serine/threonine kinase in mice. *FEBS Lett.* 1996, **392**(2), pp.189-193.

285. Kakiuchi, A., Kohno, T., Kakuki, T., Kaneko, Y., Konno, T., Hosaka, Y., Hata, T., Kikuchi, S., Ninomiya, T., Himi, T., Takano, K. and Kojima, T. Rho-kinase and PKCalpha Inhibition Induces Primary Cilia Elongation and Alters the Behavior of Undifferentiated and Differentiated Temperature-sensitive Mouse Cochlear Cells. *J Histochem Cytochem.* 2019, **67**(7), pp.523-535.

286. Stewart, K., Gaitan, Y., Shafer, M.E.R., Aoudjit, L., Hu, D., Sharma, R., Tremblay, M., Ishii, H., Marcotte, M., Stanga, D., Tang, Y.C., Boualia, S.K., Nguyen, A.H.T., Takano, T., Lamarche-Vane, N., Vidal, S. and Bouchard, M. A Point Mutation in p190A RhoGAP Affects Ciliogenesis and Leads to Glomerulocystic Kidney Defects. *PLoS genetics.* 2016, **12**(2), p.e1005785.

287. Davies, S.P., Reddy, H., Caivano, M. and Cohen, P. Specificity and mechanism of action of some commonly used protein kinase inhibitors. *The Biochemical journal.* 2000, **351**(Pt 1), pp.95-105.

288. Boerma, M., Fu, Q., Wang, J., Loose, D.S., Bartolozzi, A., Ellis, J.L., McGonigle, S., Paradise, E., Sweetnam, P., Fink, L.M., Vozenin-Brotons, M.-C. and Hauer-Jensen, M. Comparative gene expression profiling in three primary human cell lines after treatment with a novel inhibitor of Rho kinase or atorvastatin. *Blood coagulation & fibrinolysis : an international journal in haemostasis and thrombosis.* 2008, **19**(7), pp.709-718.

289. Amano, M., Ito, M., Kimura, K., Fukata, Y., Chihara, K., Nakano, T., Matsuura, Y. and Kaibuchi, K. Phosphorylation and activation of myosin by Rho-associated kinase (Rho-kinase). *J Biol Chem.* 1996, **271**(34), pp.20246-20249.

290. McMullan, R., Lax, S., Robertson, V.H., Radford, D.J., Broad, S., Watt, F.M., Rowles, A., Croft, D.R., Olson, M.F. and Hotchin, N.A. Keratinocyte differentiation is regulated by the Rho and ROCK signaling pathway. *Curr Biol.* 2003, **13**(24), pp.2185-2189.

291. Goddette, D.W. and Frieden, C. Actin polymerization. The mechanism of action of cytochalasin D. *J Biol Chem.* 1986, **261**(34), pp.15974-15980.

292. Bhadriraju, K., Yang, M., Alom Ruiz, S., Pirone, D., Tan, J. and Chen, C.S. Activation of ROCK by RhoA is regulated by cell adhesion, shape, and cytoskeletal tension. *Exp Cell Res.* 2007, **313**(16), pp.3616-3623.

293. Kovacs, M., Toth, J., Hetenyi, C., Malnasi-Csizmadia, A. and Sellers, J.R. Mechanism of blebbistatin inhibition of myosin II. *J Biol Chem.* 2004, **279**(34), pp.35557-35563.

294. Epting, D., Slanchev, K., Boehlke, C., Hoff, S., Loges, N.T., Yasunaga, T., Indorf, L., Nestel, S., Lienkamp, S.S., Omran, H., Kuehn, E.W., Ronneberger, O., Walz, G. and Kramer-Zucker, A. The Rac1 regulator ELMO controls basal body migration and docking in multiciliated cells through interaction with Ezrin. *Development.* 2015, **142**(1), pp.174-184.

295. Iwasaki, T., Murata-Hori, M., Ishitobi, S. and Hosoya, H. Diphosphorylated MRLC is required for organization of stress fibers in interphase cells and the contractile ring in dividing cells. *Cell Struct Funct.* 2001, **26**(6), pp.677-683.

296. Zhou, H., Wertz, I., O'Rourke, K., Ultsch, M., Seshagiri, S., Eby, M., Xiao, W. and Dixit, V.M. Bcl10 activates the NF-kappaB pathway through ubiquitination of NEMO. *Nature.* 2004, **427**(6970), pp.167-171.

297. Kaneko, Y., Kohno, T., Kakuki, T., Takano, K.I., Ogasawara, N., Miyata, R., Kikuchi, S., Konno, T., Ohkuni, T., Yajima, R., Kakiuchi, A., Yokota, S.I., Himi, T. and Kojima, T. The role of transcriptional factor p63 in regulation of epithelial barrier and ciliogenesis of human nasal epithelial cells. *Sci Rep.* 2017, **7**(1), p.10935.

298. Petryszak, R., Keays, M., Tang, Y.A., Fonseca, N.A., Barrera, E., Burdett, T., Füllgrabe, A., Fuentes, A.M.-P., Jupp, S., Koskinen, S., Mannion, O., Huerta, L., Megy, K., Snow, C., Williams, E., Barzine, M., Hastings, E., Weisser, H., Wright, J., Jaiswal, P., Huber, W., Choudhary, J., Parkinson, H.E. and Brazma, A. Expression Atlas update—an integrated database of gene and protein expression in humans, animals and plants. *Nucleic acids research.* 2015, **44**(D1), pp.D746-D752.

299. Li Xiaobin, Y.H., Li Ting, Jia Sansan, Wen Limin, Bai Xinyan,Wang Hailong, Guo Rui Fancd2os gene and its encoded protein bioinformatics analysis and expression profile identification. *Chinese Journal of Biologicals.* 2015, **6630**(7), pp.670-676.

300. Li Ting, J.S., Wen Limin, Bai Xinyan, Wang Yujing, Wang Hailong, Xie Jun, Guo Rui Cell-specific Analysis and Preliminary Functional Study of Fancd2os Highly Expressed Gene in Testis. *Chinese Journal of Biologicals.* 2016.

301. Ampah, K.K., Greaves, J., Shun-Shion, A.S., Asnawi, A.W., Lidster, J.A., Chamberlain, L.H., Collins, M.O. and Peden, A.A. S-acylation regulates the trafficking and stability of the unconventional Q-SNARE STX19. *Journal of Cell Science.* 2018, **131**(20), p.jcs212498.

302. Ampah, K.K., Greaves, J., Shun-Shion, A.S., Asnawi, A.W., Lidster, J.A., Chamberlain, L.H., Collins, M.O. and Peden, A.A. S-acylation regulates the trafficking and stability of the unconventional Q-SNARE STX19. *J Cell Sci.* 2018, **131**(20).

303. Knodler, A., Feng, S., Zhang, J., Zhang, X., Das, A., Peranen, J. and Guo, W. Coordination of Rab8 and Rab11 in primary ciliogenesis. *Proc Natl Acad Sci U S A.* 2010, **107**(14), pp.6346-6351.

304. Patrussi, L. and Baldari, C.T. The Rab GTPase Rab8 as a shared regulator of ciliogenesis and immune synapse assembly: From a conserved pathway to diverse cellular structures. *Small GTPases.* 2016, **7**(1), pp.16-20.

305. Jacobs, M., Hayakawa, K., Swenson, L., Bellon, S., Fleming, M., Taslimi, P. and Doran, J. The structure of dimeric ROCK I reveals the mechanism for ligand selectivity. *J Biol Chem.* 2006, **281**(1), pp.260-268.

306. Dvorsky, R., Blumenstein, L., Vetter, I.R. and Ahmadian, M.R. Structural insights into the interaction of ROCKI with the switch regions of RhoA. *J Biol Chem.* 2004, **279**(8), pp.7098-7104.

307. Shimizu, T., Ihara, K., Maesaki, R., Amano, M., Kaibuchi, K. and Hakoshima, T. Parallel coiled-coil association of the RhoA-binding domain in Rho-kinase. *J Biol Chem.* 2003, **278**(46), pp.46046-46051.

308. Amano, M., Chihara, K., Nakamura, N., Kaneko, T., Matsuura, Y. and Kaibuchi, K. The COOH terminus of Rho-kinase negatively regulates rho-kinase activity. *J Biol Chem.* 1999, **274**(45), pp.32418-32424.

309. Hartmann, S., Ridley, A.J. and Lutz, S. The Function of Rho-Associated Kinases ROCK1 and ROCK2 in the Pathogenesis of Cardiovascular Disease. *Front Pharmacol.* 2015, **6**, p.276.

310. Shi, J., Surma, M., Zhang, L. and Wei, L. Dissecting the roles of ROCK isoforms in stress-induced cell detachment. *Cell cycle (Georgetown, Tex.).* 2013, **12**(10), pp.1492-1500.

311. Nardone, G., Oliver-De La Cruz, J., Vrbsky, J., Martini, C., Pribyl, J., Skládal, P., Pešl, M., Caluori, G., Pagliari, S., Martino, F., Maceckova, Z., Hajduch, M., Sanz-Garcia, A., Pugno, N.M., Stokin, G.B. and Forte, G. YAP regulates cell mechanics by controlling focal adhesion assembly. *Nature Communications.* 2017, **8**(1), p.15321.

312. Tojkander, S., Gateva, G. and Lappalainen, P. Actin stress fibers – assembly, dynamics and biological roles. *Journal of Cell Science.* 2012, **125**(8), pp.1855-1864.

313. Ridley, A.J. Rho GTPases and cell migration. *Journal of Cell Science.* 2001, **114**(15), pp.2713-2722.

314. Sumi, T., Matsumoto, K. and Nakamura, T. Specific activation of LIM kinase 2 via phosphorylation of threonine 505 by ROCK, a Rho-dependent protein kinase. *J Biol Chem.* 2001, **276**(1), pp.670-676.

315. Maekawa, M., Ishizaki, T., Boku, S., Watanabe, N., Fujita, A., Iwamatsu, A., Obinata, T., Ohashi, K., Mizuno, K. and Narumiya, S. Signaling from Rho to the actin cytoskeleton through protein kinases ROCK and LIM-kinase. *Science.* 1999, **285**(5429), pp.895-898.

316. Kimura, K., Ito, M., Amano, M., Chihara, K., Fukata, Y., Nakafuku, M., Yamamori, B., Feng, J., Nakano, T., Okawa, K., Iwamatsu, A. and Kaibuchi, K. Regulation of myosin phosphatase by Rho and Rho-associated kinase (Rho-kinase). *Science.* 1996, **273**(5272), pp.245-248.

317. Chrzanowska-Wodnicka, M. and Burridge, K. Rho-stimulated contractility drives the formation of stress fibers and focal adhesions. *J Cell Biol.* 1996, **133**(6), pp.1403-1415.

318. Matsui, T., Maeda, M., Doi, Y., Yonemura, S., Amano, M., Kaibuchi, K., Tsukita, S. and Tsukita, S. Rho-kinase phosphorylates COOH-terminal threonines of ezrin/radixin/moesin (ERM) proteins and regulates their head-to-tail association. *The Journal of Cell Biology.* 1998, **140**(3), pp.647-657.

319. Melak, M., Plessner, M. and Grosse, R. Actin visualization at a glance. *J Cell Sci.* 2017, **130**(3), pp.525-530.

320. Pitaval, A., Tseng, Q., Bornens, M. and Théry, M. Cell shape and contractility regulate ciliogenesis in cell cycle-arrested cells. *The Journal of Cell Biology.* 2010, **191**(2), pp.303-312.

321. Pitaval, A., Tseng, Q., Bornens, M. and Thery, M. Cell shape and contractility regulate ciliogenesis in cell cycle-arrested cells. *J Cell Biol.* 2010, **191**(2), pp.303-312.

322. Pitaval, A., Senger, F., Letort, G., Gidrol, X., Guyon, L., Sillibourne, J. and Thery, M. Microtubule stabilization drives 3D centrosome migration to initiate primary ciliogenesis. *J Cell Biol.* 2017, **216**(11), pp.3713-3728.

323. Satir, P., Pedersen, L.B. and Christensen, S.T. The primary cilium at a glance. *Journal of Cell Science.* 2010, **123**(4), pp.499-503.

324. Brooks, E.R. and Wallingford, J.B. Multiciliated cells. *Curr Biol.* 2014, **24**(19), pp.R973-982.

325. Ishikawa, H. and Marshall, W.F. Ciliogenesis: building the cell's antenna. *Nature Reviews Molecular Cell Biology.* 2011, **12**, p.222.

326. Tang, T.K. Centriole biogenesis in multiciliated cells. *Nat Cell Biol.* 2013, **15**(12), pp.1400-1402.

327. Zhao, H., Zhu, L., Zhu, Y., Cao, J., Li, S., Huang, Q., Xu, T., Huang, X., Yan, X. and Zhu, X. The Cep63 paralogue Deup1 enables massive de novo centriole biogenesis for vertebrate multiciliogenesis. *Nat Cell Biol.* 2013, **15**(12), pp.1434-1444.

328. Ma, L., Quigley, I., Omran, H. and Kintner, C. Multicilin drives centriole biogenesis via E2f proteins. *Genes Dev.* 2014, **28**(13), pp.1461-1471.

329. Stubbs, J.L., Vladar, E.K., Axelrod, J.D. and Kintner, C. Multicilin promotes centriole assembly and ciliogenesis during multiciliate cell differentiation. *Nat Cell Biol.* 2012, **14**(2), pp.140-147.

330. Klos Dehring, Deborah A., Vladar, Eszter K., Werner, Michael E., Mitchell, Jennifer W., Hwang, P. and Mitchell, Brian J. Deuterosome-Mediated Centriole Biogenesis. *Developmental Cell.* 2013, **27**(1), pp.103-112.

331. Brown, N.J., Marjanović, M., Lüders, J., Stracker, T.H. and Costanzo, V. Cep63 and Cep152 Cooperate to Ensure Centriole Duplication. *PloS one.* 2013, **8**(7), p.e69986.

332. Gomperts, B.N., Gong-Cooper, X. and Hackett, B.P. Foxj1 regulates basal body anchoring to the cytoskeleton of ciliated pulmonary epithelial cells. *Journal of Cell Science.* 2004, **117**(8), p.1329.

333. Tammachote, R., Hommerding, C.J., Sinders, R.M., Miller, C.A., Czarnecki, P.G., Leightner, A.C., Salisbury, J.L., Ward, C.J., Torres, V.E., Gattone, V.H., 2nd and Harris, P.C. Ciliary and centrosomal defects associated with mutation and depletion of the Meckel syndrome genes MKS1 and MKS3. *Hum Mol Genet.* 2009, **18**(17), pp.3311-3323.

334. Battini, L., Macip, S., Fedorova, E., Dikman, S., Somlo, S., Montagna, C. and Gusella, G.L. Loss of polycystin-1 causes centrosome amplification and genomic instability. *Hum Mol Genet.* 2008, **17**(18), pp.2819-2833.

335. Mahjoub, M.R. and Stearns, T. Supernumerary centrosomes nucleate extra cilia and compromise primary cilium signaling. *Curr Biol.* 2012, **22**(17), pp.1628-1634.

336. Nikonova, A.S., Deneka, A.Y., Kiseleva, A.A., Korobeynikov, V., Gaponova, A., Serebriiskii, I.G., Kopp, M.C., Hensley, H.H., Seeger-Nukpezah, T.N., Somlo, S., Proia, D.A. and Golemis, E.A. Ganetespib limits ciliation and cystogenesis in autosomal-dominant polycystic kidney disease (ADPKD). *Faseb j.* 2018, **32**(5), pp.2735-2746.

337. Difilippantonio, M.J., Ghadimi, B.M., Howard, T., Camps, J., Nguyen, Q.T., Ferris, D.K., Sackett, D.L. and Ried, T. Nucleation capacity and presence of centrioles define a distinct category of centrosome abnormalities that induces multipolar mitoses in cancer cells. *Environmental and molecular mutagenesis.* 2009, **50**(8), pp.672-696.

338. Seeley, E.S., Carriere, C., Goetze, T., Longnecker, D.S. and Korc, M. Pancreatic cancer and precursor pancreatic intraepithelial neoplasia lesions are devoid of primary cilia. *Cancer Res.* 2009, **69**(2), pp.422-430.

339. Werner, S., Pimenta-Marques, A. and Bettencourt-Dias, M. Maintaining centrosomes and cilia. *Journal of Cell Science.* 2017, **130**(22), p.3789.

340. Li, L., Grausam, K.B., Wang, J., Lun, M.P., Ohli, J., Lidov, H.G.W., Calicchio, M.L., Zeng, E., Salisbury, J.L., Wechsler-Reya, R.J., Lehtinen, M.K., Schüller, U. and Zhao, H. Sonic Hedgehog promotes proliferation of Notch-dependent monociliated choroid plexus tumour cells. *Nat Cell Biol.* 2016, **18**(4), pp.418-430.

341. Faggioli, F., Vezzoni, P. and Montagna, C. Single-Cell Analysis of Ploidy and Centrosomes Underscores the Peculiarity of Normal Hepatocytes. *PloS one.* 2011, **6**(10), p.e26080.

342. Grisham, J.W., Nopanitaya, W., Compagno, J. and Nägel, A.E.H. Scanning electron microscopy of normal rat liver: The surface structure of its cells and tissue components. *American Journal of Anatomy.* 1975, **144**(3), pp.295-321.

343. Huang, B.Q., Masyuk, T.V., Muff, M.A., Tietz, P.S., Masyuk, A.I. and LaRusso, N.F. Isolation and characterization of cholangiocyte primary

cilia. *American Journal of Physiology-Gastrointestinal and Liver Physiology.* 2006, **291**(3), pp.G500-G509.

344. Stearns, T. Centrosome duplication. a centriolar pas de deux. *Cell.* 2001, **105**(4), pp.417-420.

345. Lianga, N., Dore, C., Kennedy, E.K., Yeh, E., Williams, E.C., Fortinez, C.M., Wang, A., Bloom, K.S. and Rudner, A.D. Cdk1 phosphorylation of Esp1/Separase functions with PP2A and Slk19 to regulate pericentric Cohesin and anaphase onset. *PLoS genetics.* 2018, **14**(3), p.e1007029.

346. Toure, A., Mzali, R., Liot, C., Seguin, L., Morin, L., Crouin, C., Chen-Yang, I., Tsay, Y.G., Dorseuil, O., Gacon, G. and Bertoglio, J. Phosphoregulation of MgcRacGAP in mitosis involves Aurora B and Cdk1 protein kinases and the PP2A phosphatase. *FEBS Lett.* 2008, **582**(8), pp.1182-1188.

347. Brown, N.R., Korolchuk, S., Martin, M.P., Stanley, W.A., Moukhametzianov, R., Noble, M.E.M. and Endicott, J.A. CDK1 structures reveal conserved and unique features of the essential cell cycle CDK. *Nature Communications.* 2015, **6**, pp.6769-6769.

348. Enserink, J.M. and Kolodner, R.D. An overview of Cdk1-controlled targets and processes. *Cell Division.* 2010, **5**(1), p.11.

349. Bertoli, C., Skotheim, J.M. and de Bruin, R.A.M. Control of cell cycle transcription during G1 and S phases. *Nature reviews. Molecular cell biology.* 2013, **14**(8), pp.518-528.

350. Wirth, K.G., Wutz, G., Kudo, N.R., Desdouets, C., Zetterberg, A., Taghybeeglu, S., Seznec, J., Ducos, G.M., Ricci, R., Firnberg, N., Peters, J.-M. and Nasmyth, K. Separase: a universal trigger for sister chromatid disjunction but not chromosome cycle progression. *The Journal of Cell Biology.* 2006, **172**(6), pp.847-860.

351. D'Avino, P.P., Giansanti, M.G. and Petronczki, M. Cytokinesis in animal cells. *Cold Spring Harbor perspectives in biology.* 2015, **7**(4), pp.a015834-a015834.

352. Mishima, M. Chapter 22 - Preparation of centralspindlin as an active heterotetramer of kinesin and GTPase activating protein subunits for in vitro structural and functional assays. In: Echard, A. ed. *Methods in Cell Biology*. Academic Press, 2017, pp.371-385.

353. Jantsch-Plunger, V., Gönczy, P., Romano, A., Schnabel, H., Hamill, D., Schnabel, R., Hyman, A.A. and Glotzer, M. CYK-4: A Rho family gtpase activating protein (GAP) required for central spindle formation and cytokinesis. *The Journal of Cell Biology.* 2000, **149**(7), pp.1391-1404.

354. Mishima, M., Kaitna, S. and Glotzer, M. Central spindle assembly and cytokinesis require a kinesin-like protein/RhoGAP complex with microtubule bundling activity. *Dev Cell.* 2002, **2**(1), pp.41-54.

355. Yüce, Ö., Piekny, A. and Glotzer, M. An ECT2–centralspindlin complex regulates the localization and function of RhoA. *The Journal of Cell Biology.* 2005, **170**(4), p.571.

356. Weigel, A., Schild, D. and Zeug, A. Resolution in the ApoTome and the confocal laser scanning microscope: comparison. *J Biomed Opt.* 2009, **14**(1), p.014022.

357. Fouquet, C., Gilles, J.-F., Heck, N., Dos Santos, M., Schwartzmann, R., Cannaya, V., Morel, M.-P., Davidson, R.S., Trembleau, A. and Bolte, S. Improving axial resolution in confocal microscopy with new high refractive index mounting media. *PloS one.* 2015, **10**(3), pp.e0121096-e0121096.

358. Huff, J. The Airyscan detector from ZEISS: confocal imaging with improved signal-to-noise ratio and super-resolution. *Nature Methods.* 2015, **12**(12), pp.i-ii.

359. Tayeh, M.K., Yen, H.-J., Beck, J.S., Searby, C.C., Westfall, T.A., Griesbach, H., Sheffield, V.C. and Slusarski, D.C. Genetic interaction between Bardet-Biedl syndrome genes and implications for limb patterning. *Hum Mol Genet.* 2008, **17**(13), pp.1956-1967.

360. Yee, L.E., Garcia-Gonzalo, F.R., Bowie, R.V., Li, C., Kennedy, J.K., Ashrafi, K., Blacque, O.E., Leroux, M.R. and Reiter, J.F. Conserved Genetic Interactions between Ciliopathy Complexes Cooperatively Support Ciliogenesis and Ciliary Signaling. *PLoS genetics.* 2015, **11**(11), p.e1005627.

361. Novas, R., Cardenas-Rodriguez, M., Lepanto, P., Fabregat, M., Rodao, M., Fariello, M.I., Ramos, M., Davison, C., Casanova, G., Alfaya, L., Lecumberry, F., González-Sapienza, G., Irigoín, F. and Badano, J.L. Kinesin 1 regulates cilia length through an interaction with the Bardet-Biedl syndrome related protein CCDC28B. *Scientific Reports.* 2018, **8**(1), p.3019.

362. Warburton-Pitt, S.R.F., Jauregui, A.R., Li, C., Wang, J., Leroux, M.R. and Barr, M.M. Ciliogenesis in *Caenorhabditis elegans* requires genetic interactions between ciliary middle segment localized NPHP-2 (inversin) and transition zone-associated proteins. *Journal of Cell Science.* 2012, **125**(11), p.2592.

363. Pazour, G.J., Dickert, B.L., Vucica, Y., Seeley, E.S., Rosenbaum, J.L., Witman, G.B. and Cole, D.G. Chlamydomonas IFT88 and its mouse homologue, polycystic kidney disease gene tg737, are required for assembly of cilia and flagella. *The Journal of Cell Biology.* 2000, **151**(3), pp.709-718.

364. Vierkotten, J., Dildrop, R., Peters, T., Wang, B. and Rüther, U. Ftm is a novel basal body protein of cilia involved in Shh signalling. *Development.* 2007, **134**(14), p.2569.

365. Abdelhamed, Z.A., Natarajan, S., Wheway, G., Inglehearn, C.F., Toomes, C., Johnson, C.A. and Jagger, D.J. The Meckel-Gruber

syndrome protein TMEM67 controls basal body positioning and epithelial branching morphogenesis in mice via the non-canonical Wnt pathway. *Disease Models & Mechanisms.* 2015, **8**(6), p.527.

366. Lehner, B. Modelling genotype–phenotype relationships and human disease with genetic interaction networks. *Journal of Experimental Biology.* 2007, **210**(9), pp.1559-1566.

367. Tory, K., Lacoste, T., Burglen, L., Moriniere, V., Boddaert, N., Macher, M.A., Llanas, B., Nivet, H., Bensman, A., Niaudet, P., Antignac, C., Salomon, R. and Saunier, S. High NPHP1 and NPHP6 mutation rate in patients with Joubert syndrome and nephronophthisis: potential epistatic effect of NPHP6 and AHI1 mutations in patients with NPHP1 mutations. *Journal of the American Society of Nephrology : JASN.* 2007, **18**(5), pp.1566-1575.

368. Hartill, V., Szymanska, K., Sharif, S.M., Wheway, G. and Johnson, C.A. Meckel-Gruber Syndrome: An Update on Diagnosis, Clinical Management, and Research Advances. *Front Pediatr.* 2017, **5**, p.244.

369. *Online Mendelian Inheritance in Man, OMIM®.* [Online database].

370. Chekuri, A., Guru, A.A., Biswas, P., Branham, K., Borooah, S., Soto-Hermida, A., Hicks, M., Khan, N.W., Matsui, H., Alapati, A., Raghavendra, P.B., Roosing, S., Sarangapani, S., Mathavan, S., Telenti, A., Heckenlively, J.R., Riazuddin, S.A., Frazer, K.A., Sieving, P.A. and Ayyagari, R. IFT88 mutations identified in individuals with non-syndromic recessive retinal degeneration result in abnormal ciliogenesis. *Hum Genet.* 2018, **137**(6-7), pp.447-458.

371. Badano, J.L., Leitch, C.C., Ansley, S.J., May-Simera, H., Lawson, S., Lewis, R.A., Beales, P.L., Dietz, H.C., Fisher, S. and Katsanis, N. Dissection of epistasis in oligogenic Bardet-Biedl syndrome. *Nature.* 2006, **439**(7074), pp.326-330.

372. Guschin, D.Y., Waite, A.J., Katibah, G.E., Miller, J.C., Holmes, M.C. and Rebar, E.J. A rapid and general assay for monitoring endogenous gene modification. *Methods Mol Biol.* 2010, **649**, pp.247-256.

373. Schwarz, J.M., Cooper, D.N., Schuelke, M. and Seelow, D. MutationTaster2: mutation prediction for the deep-sequencing age. *Nat Methods.* 2014, **11**(4), pp.361-362.

374. Boldt, K., van Reeuwijk, J., Lu, Q., Koutroumpas, K., Nguyen, T.-M.T., Texier, Y., van Beersum, S.E.C., Horn, N., Willer, J.R., Mans, D.A., Dougherty, G., Lamers, I.J.C., Coene, K.L.M., Arts, H.H., Betts, M.J., Beyer, T., Bolat, E., Gloeckner, C.J., Haidari, K., Hetterschijt, L., Iaconis, D., Jenkins, D., Klose, F., Knapp, B., Latour, B., Letteboer, S.J.F., Marcelis, C.L., Mitic, D., Morleo, M., Oud, M.M., Riemersma, M., Rix, S., Terhal, P.A., Toedt, G., van Dam, T.J.P., de Vrieze, E., Wissinger, Y., Wu, K.M., Apic, G., Beales, P.L., Blacque, O.E., Gibson, T.J., Huynen, M.A., Katsanis, N., Kremer, H., Omran, H., van Wijk, E., Wolfrum, U., Kepes, F., Davis, E.E., Franco, B., Giles, R.H., Ueffing, M., Russell, R.B.,

Roepman, R. and Group, U.K.R.D. An organelle-specific protein landscape identifies novel diseases and molecular mechanisms. *Nature Communications.* 2016, **7**, pp.11491-11491.

375. Williams, C.L., Li, C., Kida, K., Inglis, P.N., Mohan, S., Semenec, L., Bialas, N.J., Stupay, R.M., Chen, N., Blacque, O.E., Yoder, B.K. and Leroux, M.R. MKS and NPHP modules cooperate to establish basal body/transition zone membrane associations and ciliary gate function during ciliogenesis. *J Cell Biol.* 2011, **192**(6), pp.1023-1041.

376. Garcia-Gonzalo, F.R., Corbit, K.C., Sirerol-Piquer, M.S., Ramaswami, G., Otto, E.A., Noriega, T.R., Seol, A.D., Robinson, J.F., Bennett, C.L., Josifova, D.J., García-Verdugo, J.M., Katsanis, N., Hildebrandt, F. and Reiter, J.F. A transition zone complex regulates mammalian ciliogenesis and ciliary membrane composition. *Nature Genetics.* 2011, **43**(8), pp.776-784.

377. Iomini, C., Li, L., Esparza, J.M. and Dutcher, S.K. Retrograde intraflagellar transport mutants identify complex A proteins with multiple genetic interactions in Chlamydomonas reinhardtii. *Genetics.* 2009, **183**(3), pp.885-896.

378. Katoh, Y., Michisaka, S., Nozaki, S., Funabashi, T., Hirano, T., Takei, R. and Nakayama, K. Practical method for targeted disruption of cilia-related genes by using CRISPR/Cas9-mediated, homology-independent knock-in system. *Molecular Biology of the Cell.* 2017, **28**(7), pp.898-906.

379. Hanke-Gogokhia, C., Wu, Z., Sharif, A., Yazigi, H., Frederick, J.M. and Baehr, W. The guanine nucleotide exchange factor Arf-like protein 13b is essential for assembly of the mouse photoreceptor transition zone and outer segment. *J Biol Chem.* 2017, **292**(52), pp.21442-21456.

380. Rachel, R.A., Yamamoto, E.A., Dewanjee, M.K., May-Simera, H.L., Sergeev, Y.V., Hackett, A.N., Pohida, K., Munasinghe, J., Gotoh, N., Wickstead, B., Fariss, R.N., Dong, L., Li, T. and Swaroop, A. CEP290 alleles in mice disrupt tissue-specific cilia biogenesis and recapitulate features of syndromic ciliopathies. *Hum Mol Genet.* 2015, **24**(13), pp.3775-3791.

381. Craige, B., Tsao, C.-C., Diener, D.R., Hou, Y., Lechtreck, K.-F., Rosenbaum, J.L. and Witman, G.B. CEP290 tethers flagellar transition zone microtubules to the membrane and regulates flagellar protein content. *The Journal of Cell Biology.* 2010, **190**(5), pp.927-940.

382. Boldt, K., van Reeuwijk, J., Lu, Q., Koutroumpas, K., Nguyen, T.-M.T., Texier, Y., van Beersum, S.E.C., Horn, N., Willer, J.R., Mans, D.A., Dougherty, G., Lamers, I.J.C., Coene, K.L.M., Arts, H.H., Betts, M.J., Beyer, T., Bolat, E., Gloeckner, C.J., Haidari, K., Hetterschijt, L., Iaconis, D., Jenkins, D., Klose, F., Knapp, B., Latour, B., Letteboer, S.J.F., Marcelis, C.L., Mitic, D., Morleo, M., Oud, M.M., Riemersma, M., Rix, S., Terhal, P.A., Toedt, G., van Dam, T.J.P., de Vrieze, E., Wissinger, Y., Wu, K.M., Apic, G., Beales, P.L., Blacque, O.E., Gibson, T.J., Huynen, M.A., Katsanis, N., Kremer, H., Omran, H., van Wijk, E., Wolfrum, U.,

Kepes, F., Davis, E.E., Franco, B., Giles, R.H., Ueffing, M., Russell, R.B., Roepman, R., Al-Turki, S., Anderson, C., Antony, D., Barroso, I., Bentham, J., Bhattacharya, S., Carss, K., Chatterjee, K., Cirak, S., Cosgrove, C., Danecek, P., Durbin, R., Fitzpatrick, D., Floyd, J., Reghan Foley, A., Franklin, C., Futema, M., Humphries, S.E., Hurles, M., Joyce, C., McCarthy, S., Mitchison, H.M., Muddyman, D., Muntoni, F., O'Rahilly, S., Onoufriadis, A., Payne, F., Plagnol, V., Raymond, L., Savage, D.B., Scambler, P., Schmidts, M., Schoenmakers, N., Semple, R., Serra, E., Stalker, J., van Kogelenberg, M., Vijayarangakannan, P., Walter, K., Whittall, R., Williamson, K. and Group, U.K.R.D. An organelle-specific protein landscape identifies novel diseases and molecular mechanisms. *Nature Communications.* 2016, **7**(1), p.11491.

383. Finn, R.D., Attwood, T.K., Babbitt, P.C., Bateman, A., Bork, P., Bridge, A.J., Chang, H.Y., Dosztanyi, Z., El-Gebali, S., Fraser, M., Gough, J., Haft, D., Holliday, G.L., Huang, H., Huang, X., Letunic, I., Lopez, R., Lu, S., Marchler-Bauer, A., Mi, H., Mistry, J., Natale, D.A., Necci, M., Nuka, G., Orengo, C.A., Park, Y., Pesseat, S., Piovesan, D., Potter, S.C., Rawlings, N.D., Redaschi, N., Richardson, L., Rivoire, C., Sangrador-Vegas, A., Sigrist, C., Sillitoe, I., Smithers, B., Squizzato, S., Sutton, G., Thanki, N., Thomas, P.D., Tosatto, S.C., Wu, C.H., Xenarios, I., Yeh, L.S., Young, S.Y. and Mitchell, A.L. InterPro in 2017-beyond protein family and domain annotations. *Nucleic acids research.* 2017, **45**(D1), pp.D190-D199.

384. Gerhardt, C., Lier, J.M., Burmühl, S., Struchtrup, A., Deutschmann, K., Vetter, M., Leu, T., Reeg, S., Grune, T. and Rüther, U. The transition zone protein Rpgrip1l regulates proteasomal activity at the primary cilium. *The Journal of Cell Biology.* 2015, **210**(1), pp.115-133.

385. Garcia-Gonzalo, F.R., Corbit, K.C., Sirerol-Piquer, M.S., Ramaswami, G., Otto, E.A., Noriega, T.R., Seol, A.D., Robinson, J.F., Bennett, C.L., Josifova, D.J., Garcia-Verdugo, J.M., Katsanis, N., Hildebrandt, F. and Reiter, J.F. A transition zone complex regulates mammalian ciliogenesis and ciliary membrane composition. *Nat Genet.* 2011, **43**(8), pp.776-784.

386. Moon, S.B., Kim, D.Y., Ko, J.-H. and Kim, Y.-S. Recent advances in the CRISPR genome editing tool set. *Experimental & Molecular Medicine.* 2019, **51**(11), p.130.

387. Banan, M. Recent advances in CRISPR/Cas9-mediated knock-ins in mammalian cells. *Journal of Biotechnology.* 2020, **308**, pp.1-9.

388. Pickar-Oliver, A. and Gersbach, C.A. The next generation of CRISPR–Cas technologies and applications. *Nature Reviews Molecular Cell Biology.* 2019, **20**(8), pp.490-507.

389. Shi, X., Garcia, G., 3rd, Van De Weghe, J.C., McGorty, R., Pazour, G.J., Doherty, D., Huang, B. and Reiter, J.F. Super-resolution microscopy reveals that disruption of ciliary transition-zone architecture causes Joubert syndrome. *Nat Cell Biol.* 2017, **19**(10), pp.1178-1188.

390. Vuolo, L., Stevenson, N.L., Heesom, K.J. and Stephens, D.J. Dynein-2 is required for a functional transition zone and bidirectional ciliary trafficking. *bioRxiv.* 2018, p.251694.

391. Roosing, S., Hofree, M., Kim, S., Scott, E., Copeland, B., Romani, M., Silhavy, J.L., Rosti, R.O., Schroth, J., Mazza, T., Miccinilli, E., Zaki, M.S., Swoboda, K.J., Milisa-Drautz, J., Dobyns, W.B., Mikati, M.A., İncecik, F., Azam, M., Borgatti, R., Romaniello, R., Boustany, R.-M., Clericuzio, C.L., D'Arrigo, S., Strømme, P., Boltshauser, E., Stanzial, F., Mirabelli-Badenier, M., Moroni, I., Bertini, E., Emma, F., Steinlin, M., Hildebrandt, F., Johnson, C.A., Freilinger, M., Vaux, K.K., Gabriel, S.B., Aza-Blanc, P., Heynen-Genel, S., Ideker, T., Dynlacht, B.D., Lee, J.E., Valente, E.M., Kim, J. and Gleeson, J.G. Functional genome-wide siRNA screen identifies KIAA0586 as mutated in Joubert syndrome. *Elife.* 2015, **4**, p.e06602.

392. Kondo, S. and Perrimon, N. A Genome-Wide RNAi Screen Identifies Core Components of the G₂-M DNA Damage Checkpoint. *Science Signaling.* 2011, **4**(154), pp.rs1-rs1.

393. Kavanaugh, G., Ye, F., Mohni, K.N., Luzwick, J.W., Glick, G. and Cortez, D. A whole genome RNAi screen identifies replication stress response genes. *DNA Repair.* 2015, **35**, pp.55-62.

394. Ma, Z., Kanai, M., Kawamura, K., Kaibuchi, K., Ye, K. and Fukasawa, K. Interaction between ROCK II and nucleophosmin/B23 in the regulation of centrosome duplication. *Mol Cell Biol.* 2006, **26**(23), pp.9016-9034.

395. Chevrier, V., Piel, M., Collomb, N., Saoudi, Y., Frank, R., Paintrand, M., Narumiya, S., Bornens, M. and Job, D. The Rho-associated protein kinase p160ROCK is required for centrosome positioning. *The Journal of Cell Biology.* 2002, **157**(5), pp.807-817.

396. Iizuka, M., Kimura, K., Wang, S., Kato, K., Amano, M., Kaibuchi, K. and Mizoguchi, A. Distinct Distribution and Localization of Rho-kinase in Mouse Epithelial, Muscle and Neural Tissues. *Cell Structure and Function.* 2012, **37**(2), pp.155-175.

397. Leung, T., Chen, X.Q., Manser, E. and Lim, L. The p160 RhoA-binding kinase ROK alpha is a member of a kinase family and is involved in the reorganization of the cytoskeleton. *Mol Cell Biol.* 1996, **16**(10), pp.5313-5327.

398. Stroeken, P.J., Alvarez, B., Van Rheenen, J., Wijnands, Y.M., Geerts, D., Jalink, K. and Roos, E. Integrin cytoplasmic domain-associated protein-1 (ICAP-1) interacts with the ROCK-I kinase at the plasma membrane. *J Cell Physiol.* 2006, **208**(3), pp.620-628.

399. Yoneda, A., Multhaupt, H.A. and Couchman, J.R. The Rho kinases I and II regulate different aspects of myosin II activity. *J Cell Biol.* 2005, **170**(3), pp.443-453.

400. Jensen, V.L., Li, C., Bowie, R.V., Clarke, L., Mohan, S., Blacque, O.E. and Leroux, M.R. Formation of the transition zone by Mks5/Rpgrip1L

establishes a ciliary zone of exclusion (CIZE) that compartmentalises ciliary signalling proteins and controls PIP2 ciliary abundance. *The EMBO Journal.* 2015, **34**(20), pp.2537-2556.

401. Chávez, M., Ena, S., Van Sande, J., de Kerchove d'Exaerde, A., Schurmans, S. and Schiffmann, Serge N. Modulation of Ciliary Phosphoinositide Content Regulates Trafficking and Sonic Hedgehog Signaling Output. *Developmental Cell.* 2015, **34**(3), pp.338-350.

402. Lowery, D.M., Clauser, K.R., Hjerrild, M., Lim, D., Alexander, J., Kishi, K., Ong, S.E., Gammeltoft, S., Carr, S.A. and Yaffe, M.B. Proteomic screen defines the Polo-box domain interactome and identifies Rock2 as a Plk1 substrate. *Embo j.* 2007, **26**(9), pp.2262-2273.

403. Lee, H.H., Tien, S.C., Jou, T.S., Chang, Y.C., Jhong, J.G. and Chang, Z.F. Src-dependent phosphorylation of ROCK participates in regulation of focal adhesion dynamics. *J Cell Sci.* 2010, **123**(Pt 19), pp.3368-3377.

404. Riento, K., Totty, N., Villalonga, P., Garg, R., Guasch, R. and Ridley, A.J. RhoE function is regulated by ROCK I-mediated phosphorylation. *Embo j.* 2005, **24**(6), pp.1170-1180.

405. Hu, Q., Milenkovic, L., Jin, H., Scott, M.P., Nachury, M.V., Spiliotis, E.T. and Nelson, W.J. A Septin Diffusion Barrier at the Base of the Primary Cilium Maintains Ciliary Membrane Protein Distribution. *Science.* 2010, **329**(5990), pp.436-439.

406. Ghossoub, R., Hu, Q., Failler, M., Rouyez, M.C., Spitzbarth, B., Mostowy, S., Wolfrum, U., Saunier, S., Cossart, P., Jamesnelson, W. and Benmerah, A. Septins 2, 7 and 9 and MAP4 colocalize along the axoneme in the primary cilium and control ciliary length. *J Cell Sci.* 2013, **126**(Pt 12), pp.2583-2594.

407. Sharma, N., Kosan, Z.A., Stallworth, J.E., Berbari, N.F. and Yoder, B.K. Soluble levels of cytosolic tubulin regulate ciliary length control. *Molecular Biology of the Cell.* 2011, **22**(6), pp.806-816.

408. Yoshizaki, H., Ohba, Y., Parrini, M.C., Dulyaninova, N.G., Bresnick, A.R., Mochizuki, N. and Matsuda, M. Cell type-specific regulation of RhoA activity during cytokinesis. *J Biol Chem.* 2004, **279**(43), pp.44756-44762.

409. D'Avino, P.P., Savoian, M.S. and Glover, D.M. Mutations in sticky lead to defective organization of the contractile ring during cytokinesis and are enhanced by Rho and suppressed by Rac. *The Journal of Cell Biology.* 2004, **166**(1), pp.61-71.

410. Miller, A.L. and Bement, W.M. Regulation of cytokinesis by Rho GTPase flux. *Nat Cell Biol.* 2009, **11**(1), pp.71-77.

411. Warga, R.M., Wicklund, A., Webster, S.E. and Kane, D.A. Progressive loss of RacGAP1/ogre activity has sequential effects on cytokinesis and zebrafish development. *Dev Biol.* 2016, **418**(2), pp.307-322.

412. van Dam, T.J.P., Wheway, G., Slaats, G.G., Huynen, M.A., Giles, R.H. and Group, S.S. The SYSCILIA gold standard (SCGSv1) of known ciliary components and its applications within a systems biology consortium. *Cilia.* 2013, **2**(1), p.7.

413. Smith, K.R., Kieserman, E.K., Wang, P.I., Basten, S.G., Giles, R.H., Marcotte, E.M. and Wallingford, J.B. A role for central spindle proteins in cilia structure and function. *Cytoskeleton (Hoboken, N.J.).* 2011, **68**(2), pp.112-124.

414. van Wijk, S.J. and Timmers, H.T. The family of ubiquitin-conjugating enzymes (E2s): deciding between life and death of proteins. *Faseb j.* 2010, **24**(4), pp.981-993.

415. Iconomou, M. and Saunders, D.N. Systematic approaches to identify E3 ligase substrates. *The Biochemical journal.* 2016, **473**(22), pp.4083-4101.

416. Wiegering, A., Rüther, U. and Gerhardt, C. The Role of Primary Cilia in the Crosstalk between the Ubiquitin⁻Proteasome System and Autophagy. *Cells.* 2019, **8**(3).

417. Malicki, J.J. and Johnson, C.A. The Cilium: Cellular Antenna and Central Processing Unit. *Trends in Cell Biology.* 2017, **27**(2), pp.126-140.

418. Shearer, R.F., Frikstad, K.-A.M., McKenna, J., McCloy, R.A., Deng, N., Burgess, A., Stokke, T., Patzke, S. and Saunders, D.N. The E3 ubiquitin ligase UBR5 regulates centriolar satellite stability and primary cilia. *Molecular Biology of the Cell.* 2018, **29**(13), pp.1542-1554.

419. Nagai, T., Mukoyama, S., Kagiwada, H., Goshima, N. and Mizuno, K. Cullin-3-KCTD10-mediated CEP97 degradation promotes primary cilium formation. *J Cell Sci.* 2018, **131**(24).

420. Coon, T.A., McKelvey, A.C., Lear, T., Rajbhandari, S., Dunn, S.R., Connelly, W., Zhao, J.Y., Han, S., Liu, Y., Weathington, N.M., McVerry, B.J., Zhang, Y. and Chen, B.B. The proinflammatory role of HECTD2 in innate immunity and experimental lung injury. *Science translational medicine.* 2015, **7**(295), p.295ra109.

421. Hein, M.Y., Hubner, N.C., Poser, I., Cox, J., Nagaraj, N., Toyoda, Y., Gak, I.A., Weisswange, I., Mansfeld, J., Buchholz, F., Hyman, A.A. and Mann, M. A human interactome in three quantitative dimensions organized by stoichiometries and abundances. *Cell.* 2015, **163**(3), pp.712-723.

422. Huttlin, E.L., Ting, L., Bruckner, R.J., Gebreab, F., Gygi, M.P., Szpyt, J., Tam, S., Zarraga, G., Colby, G., Baltier, K., Dong, R., Guarani, V., Vaites, L.P., Ordureau, A., Rad, R., Erickson, B.K., Wuhr, M., Chick, J., Zhai, B., Kolippakkam, D., Mintseris, J., Obar, R.A., Harris, T., Artavanis-Tsakonas, S., Sowa, M.E., De Camilli, P., Paulo, J.A., Harper, J.W. and Gygi, S.P. The BioPlex Network: A Systematic Exploration of the Human Interactome. *Cell.* 2015, **162**(2), pp.425-440.

423. Pao, K.C., Wood, N.T., Knebel, A., Rafie, K., Stanley, M., Mabbitt, P.D., Sundaramoorthy, R., Hofmann, K., van Aalten, D.M.F. and Virdee, S. Activity-based E3 ligase profiling uncovers an E3 ligase with esterification activity. *Nature.* 2018, **556**(7701), pp.381-385.

424. Cox, B., Briscoe, J. and Ulloa, F. SUMOylation by Pias1 regulates the activity of the Hedgehog dependent Gli transcription factors. *PloS one.* 2010, **5**(8), p.e11996.

425. Kopinke, D., Roberson, E.C. and Reiter, J.F. Ciliary Hedgehog Signaling Restricts Injury-Induced Adipogenesis. *Cell.* 2017, **170**(2), pp.340-351.e312.

426. Cevik, S., Hori, Y., Kaplan, O.I., Kida, K., Toivenon, T., Foley-Fisher, C., Cottell, D., Katada, T., Kontani, K. and Blacque, O.E. Joubert syndrome Arl13b functions at ciliary membranes and stabilizes protein transport in Caenorhabditis elegans. *J Cell Biol.* 2010, **188**(6), pp.953-969.

427. Li, Y., Wei, Q., Zhang, Y., Ling, K. and Hu, J. The small GTPases ARL-13 and ARL-3 coordinate intraflagellar transport and ciliogenesis. *The Journal of Cell Biology.* 2010, **189**(6), pp.1039-1051.

428. Blacque, O.E., Reardon, M.J., Li, C., McCarthy, J., Mahjoub, M.R., Ansley, S.J., Badano, J.L., Mah, A.K., Beales, P.L., Davidson, W.S., Johnsen, R.C., Audeh, M., Plasterk, R.H., Baillie, D.L., Katsanis, N., Quarmby, L.M., Wicks, S.R. and Leroux, M.R. Loss of C. elegans BBS-7 and BBS-8 protein function results in cilia defects and compromised intraflagellar transport. *Genes Dev.* 2004, **18**(13), pp.1630-1642.

429. Liu, P. and Lechtreck, K.F. The Bardet-Biedl syndrome protein complex is an adapter expanding the cargo range of intraflagellar transport trains for ciliary export. *Proceedings of the National Academy of Sciences of the United States of America.* 2018, **115**(5), pp.E934-e943.

430. Zhang, Q., Seo, S., Bugge, K., Stone, E.M. and Sheffield, V.C. BBS proteins interact genetically with the IFT pathway to influence SHH-related phenotypes. *Hum Mol Genet.* 2012, **21**(9), pp.1945-1953.

431. Haycraft, C.J., Banizs, B., Aydin-Son, Y., Zhang, Q., Michaud, E.J. and Yoder, B.K. Gli2 and Gli3 localize to cilia and require the intraflagellar transport protein polaris for processing and function. *PLoS genetics.* 2005, **1**(4), p.e53.

432. Scheidel, N. and Blacque, O.E. Intraflagellar Transport Complex A Genes Differentially Regulate Cilium Formation and Transition Zone Gating. *Current Biology.* 2018, **28**(20), pp.3279-3287.e3272.

433. Lin, H., Guo, S. and Dutcher, S.K. RPGRIP1L helps to establish the ciliary gate for entry of proteins. *Journal of Cell Science.* 2018, **131**(20), p.jcs220905.

434. Huang, L., Szymanska, K., Jensen, V.L., Janecke, A.R., Innes, A.M., Davis, E.E., Frosk, P., Li, C., Willer, J.R., Chodirker, B.N., Greenberg, C.R., McLeod, D.R., Bernier, F.P., Chudley, A.E., Muller, T., Shboul, M.,

Logan, C.V., Loucks, C.M., Beaulieu, C.L., Bowie, R.V., Bell, S.M., Adkins, J., Zuniga, F.I., Ross, K.D., Wang, J., Ban, M.R., Becker, C., Nurnberg, P., Douglas, S., Craft, C.M., Akimenko, M.A., Hegele, R.A., Ober, C., Utermann, G., Bolz, H.J., Bulman, D.E., Katsanis, N., Blacque, O.E., Doherty, D., Parboosingh, J.S., Leroux, M.R., Johnson, C.A. and Boycott, K.M. TMEM237 is mutated in individuals with a Joubert syndrome related disorder and expands the role of the TMEM family at the ciliary transition zone. *Am J Hum Genet.* 2011, **89**(6), pp.713-730.

435. Jensen, V.L., Li, C., Bowie, R.V., Clarke, L., Mohan, S., Blacque, O.E. and Leroux, M.R. Formation of the transition zone by Mks5/Rpgrip1L establishes a ciliary zone of exclusion (CIZE) that compartmentalises ciliary signalling proteins and controls PIP2 ciliary abundance. *EMBO J.* 2015, **34**(20), pp.2537-2556.

436. Abdelhamed, Z.A., Abdelmottaleb, D.I., El-Asrag, M.E., Natarajan, S., Wheway, G., Inglehearn, C.F., Toomes, C. and Johnson, C.A. The ciliary Frizzled-like receptor Tmem67 regulates canonical Wnt/β-catenin signalling in the developing cerebellum via Hoxb5. *Scientific Reports.* 2019, **9**(1), p.5446.

437. Zanin-Zhorov, A., Weiss, J.M., Trzeciak, A., Chen, W., Zhang, J., Nyuydzefe, M.S., Arencibia, C., Polimera, S., Schueller, O., Fuentes-Duculan, J., Bonifacio, K.M., Kunjravia, N., Cueto, I., Soung, J., Fleischmann, R.M., Kivitz, A., Lebwohl, M., Nunez, M., Woodson, J., Smith, S.L., West, R.F., Berger, M., Krueger, J.G., Ryan, J.L. and Waksal, S.D. Cutting Edge: Selective Oral ROCK2 Inhibitor Reduces Clinical Scores in Patients with Psoriasis Vulgaris and Normalizes Skin Pathology via Concurrent Regulation of IL-17 and IL-10. *Journal of immunology (Baltimore, Md. : 1950).* 2017, **198**(10), pp.3809-3814.

438. Kola, I. and Landis, J. Can the pharmaceutical industry reduce attrition rates? *Nature Reviews Drug Discovery.* 2004, **3**(8), pp.711-716.

439. Pushpakom, S., Iorio, F., Eyers, P.A., Escott, K.J., Hopper, S., Wells, A., Doig, A., Guilliams, T., Latimer, J., McNamee, C., Norris, A., Sanseau, P., Cavalla, D. and Pirmohamed, M. Drug repurposing: progress, challenges and recommendations. *Nature Reviews Drug Discovery.* 2019, **18**(1), pp.41-58.

440. Talevi, A. and Bellera, C.L. Challenges and opportunities with drug repurposing: finding strategies to find alternative uses of therapeutics. *Expert Opinion on Drug Discovery.* 2020, **15**(4), pp.397-401.

441. E. P. Offer, N.E.G., S. A. Best, T. Pesnot, P. MacFaul, S. Ceccarelli, K. Eckersley, M. R. Box, and N. Hawkins, G.R.P., P.R. Bunyard, C. D. Jones, R. Armer. ROCK2 inhibitors for the treatment of chronic kidney disease. In: *American Society for Nephrology (ASN) Kidney Week*, *San Diego*. 2018: Poster Number: TH-PO877, Redx Pharma, 2018.

442. Nichols, R.J., Dzamko, N., Hutti, J.E., Cantley, L.C., Deak, M., Moran, J., Bamborough, P., Reith, A.D. and Alessi, D.R. Substrate specificity and

inhibitors of LRRK2, a protein kinase mutated in Parkinson's disease. *The Biochemical journal.* 2009, **424**(1), pp.47-60.

443. Huszar, D., Lynch, C.A., Fairchild-Huntress, V., Dunmore, J.H., Fang, Q., Berkemeier, L.R., Gu, W., Kesterson, R.A., Boston, B.A., Cone, R.D., Smith, F.J., Campfield, L.A., Burn, P. and Lee, F. Targeted Disruption of the Melanocortin-4 Receptor Results in Obesity in Mice. *Cell.* 1997, **88**(1), pp.131-141.

444. Loos, R.J.F., Lindgren, C.M., Li, S., Wheeler, E., Zhao, J.H., Prokopenko, I., Inouye, M., Freathy, R.M., Attwood, A.P., Beckmann, J.S., Berndt, S.I., Jacobs, K.B., Chanock, S.J., Hayes, R.B., Bergmann, S., Bennett, A.J., Bingham, S.A., Bochud, M., Brown, M., Cauchi, S., Connell, J.M., Cooper, C., Smith, G.D., Day, I., Dina, C., De, S., Dermitzakis, E.T., Doney, A.S.F., Elliott, K.S., Elliott, P., Evans, D.M., Sadaf Farooqi, I., Froguel, P., Ghori, J., Groves, C.J., Gwilliam, R., Hadley, D., Hall, A.S., Hattersley, A.T., Hebebrand, J., Heid, I.M., Lamina, C., Gieger, C., Illig, T., Meitinger, T., Wichmann, H.E., Herrera, B., Hinney, A., Hunt, S.E., Jarvelin, M.-R., Johnson, T., Jolley, J.D.M., Karpe, F., Keniry, A., Khaw, K.-T., Luben, R.N., Mangino, M., Marchini, J., McArdle, W.L., McGinnis, R., Meyre, D., Munroe, P.B., Morris, A.D., Ness, A.R., Neville, M.J., Nica, A.C., Ong, K.K., O'Rahilly, S., Owen, K.R., Palmer, C.N.A., Papadakis, K., Potter, S., Pouta, A., Qi, L., Kraft, P., Hankinson, S.E., Hunter, D.J., Hu, F.B., Randall, J.C., Rayner, N.W., Ring, S.M., Sandhu, M.S., Scherag, A., Sims, M.A., Song, K., Soranzo, N., Speliotes, E.K., Lyon, H.N., Voight, B.F., Ridderstrale, M., Groop, L., Syddall, H.E., Teichmann, S.A., Timpson, N.J., Tobias, J.H., Uda, M., Scheet, P., Sanna, S., Abecasis, G.R., Albai, G., Nagaraja, R., Schlessinger, D., Ganz Vogel, C.I., Wallace, C., Waterworth, D.M., Weedon, M.N., Willer, C.J., Jackson, A.U., Tuomilehto, J., Collins, F.S., Boehnke, M., Mohlke, K.L., Wraight, V.L., Yuan, X., Zeggini, E., Hirschhorn, J.N., Strachan, D.P., Ouwehand, W.H., Caulfield, M.J., Samani, N.J., Frayling, T.M., Vollenweider, P., Waeber, G., Mooser, V., Deloukas, P., McCarthy, M.I., Wareham, N.J., Barroso, I., The Prostate, L.C., Ovarian Cancer Screening, T., Kora, Nurses' Health, S., Diabetes Genetics, I., The Sardi, N.I.A.S., The Wellcome Trust Case Control, C. and Fusion. Common variants near MC4R are associated with fat mass, weight and risk of obesity. *Nature Genetics.* 2008, **40**(6), pp.768-775.

445. Cideciyan, A.V., Jacobson, S.G., Drack, A.V., Ho, A.C., Charng, J., Garafalo, A.V., Roman, A.J., Sumaroka, A., Han, I.C., Hochstedler, M.D., Pfeifer, W.L., Sohn, E.H., Taiel, M., Schwartz, M.R., Biasutto, P., Wit, W.d., Cheetham, M.E., Adamson, P., Rodman, D.M., Platenburg, G., Tome, M.D., Balikova, I., Nerinckx, F., Zaeytijd, J.D., Van Cauwenbergh, C., Leroy, B.P. and Russell, S.R. Effect of an intravitreal antisense oligonucleotide on vision in Leber congenital amaurosis due to a photoreceptor cilium defect. *Nature Medicine.* 2019, **25**(2), pp.225-228.

446. Kadmon Holdings, I. *Research and Development Pipelin.* [Online]. 2019. [Accessed 19/08/219]. Available from: https://kadmon.com/research-development/pipeline/

447. Kim, Y.J., Kim, S., Jung, Y., Jung, E., Kwon, H.J. and Kim, J. Eupatilin rescues ciliary transition zone defects to ameliorate ciliopathy-related phenotypes. *J Clin Invest.* 2018, **128**(8), pp.3642-3648.

448. Barbelanne, M., Song, J., Ahmadzai, M. and Tsang, W.Y. Pathogenic NPHP5 mutations impair protein interaction with Cep290, a prerequisite for ciliogenesis. *Hum Mol Genet.* 2013, **22**(12), pp.2482-2494.

449. Abu-Safieh, L., Al-Anazi, S., Al-Abdi, L., Hashem, M., Alkuraya, H., Alamr, M., Sirelkhatim, M.O., Al-Hassnan, Z., Alkuraya, B. and Mohamed, J.Y. In search of triallelism in Bardet-Biedl syndrome. *Eur J Hum Genet.* 2012, **20**.

450. Khanna, H., Davis, E.E., Murga-Zamalloa, C.A., Estrada-Cuzcano, A., Lopez, I., den Hollander, A.I., Zonneveld, M.N., Othman, M.I., Waseem, N., Chakarova, C.F., Maubaret, C., Diaz-Font, A., MacDonald, I., Muzny, D.M., Wheeler, D.A., Morgan, M., Lewis, L.R., Logan, C.V., Tan, P.L., Beer, M.A., Inglehearn, C.F., Lewis, R.A., Jacobson, S.G., Bergmann, C., Beales, P.L., Attie-Bitach, T., Johnson, C.A., Otto, E.A., Bhattacharya, S.S., Hildebrandt, F., Gibbs, R.A., Koenekoop, R.K., Swaroop, A. and Katsanis, N. A common allele in RPGRIP1L is a modifier of retinal degeneration in ciliopathies. *Nat Genet.* 2009, **41**(6), pp.739-745.

451. Frånberg, M., Strawbridge, R.J., Hamsten, A., consortium, P., de Faire, U., Lagergren, J. and Sennblad, B. Fast and general tests of genetic interaction for genome-wide association studies. *PLoS computational biology.* 2017, **13**(6), pp.e1005556-e1005556.

452. Frånberg, M., Gertow, K., Hamsten, A., consortium, P., Lagergren, J. and Sennblad, B. Discovering Genetic Interactions in Large-Scale Association Studies by Stage-wise Likelihood Ratio Tests. *PLoS genetics.* 2015, **11**(9), pp.e1005502-e1005502.

Appendix A
siRNA and primer sequences

A.1 siRNAs

A.1.1 mIMCD3 Secondary screen controls

These siRNAs were purchased from Dharmacon™ as 5nmol stocks, in tube format. All siRNAs targeted the mouse orthologue of the genes listed, except MLNR which was used as a negative control as it targeted the human orthologue, and the scrambled negative control which is non-targeting sequence across all species. These control siRNAs were used in Chapters 3 and 4.

Table A.1 mIMCD3 Secondary Screen siRNA Controls

Gene Symbol	***Gene Accession***	***ON-TARGETplus siRNA SMARTpool Target Sequences***
Plk1	NM_011121	CCAACCAAAGUGGAAUAUGA, GCAAUUACAUGAGUGAGCA, GCAAGAUCGUGCCUAAGUC, UCACUCUCCUCAACUAUUU
Mks1	NM_001039684	CGGCGAAUCUUCACUUACA, AGUUUGAAGUCGACCUGUA, CAAUGUACAUCAUGGCGGA, UGGCUGAGCGGAUGGCGAA
Rpgrip1l	NM_173431	GGAUCAAGCUAUUCGACUU, CAGCACAGAUUACGAAACA, GAAUACUGGUCCGAUUAA, CAAUAAAGAUCUAGACCGA
Ift88	NM_009376	CGGAGAAUGUUGAAUGUUU, GCUUGGAGCUUAUUACAUU, CGUCAGCUCUCACUAAUAA, GUAGCUAGCUGCUUUAGAAA
MLNR (Human)	NM_001507	GAAGAUUCGCGGAUGAUGU, CAUCGUCGCUCUGCAACUU, GCGCAUCUAUCAACCCAAU, GCGCUAACGUGAAGACGAU
Scrambled Negative Control	N/A	UGGUUUACAUGUCGACUAA, UGGUUUACAUGUUGUGUGA, UGGUUUACAUGUUUUCUGA, UGGUUUACAUGUUUUCCUA

A.1.2. Increase cilia incidence secondary screen

These siRNAs were purchased from Dharmacon™ as an RNAi Cherry-pick Library, 0.1nmol stocks, in 96 well plate format for screening. All siRNAs targeted the mouse orthologue of the genes listed. These siRNAs were used in Chapter 3.

Table A.2 Increase Cilia Incidence Secondary Screen siRNAs

Gene Symbol	*Gene Accession*	*ON-TARGETplus siRNA SMARTpool Target Sequences*
1700011H14Rik	NM_025956	GCGCAUACUGUUUCUGAUU, CGACAAUAAAUCAGUCAAA, GGACCGGACGAAACGUUUA, UCUAUGUGAUGCCGCAAUA
1700084C01Rik	NM_001033185	GUACUUUGUUACACGGCCA, UGUUCCAGCCAUCGAGAAU, CCGCAACAAACUUGGCUAU, UCACUUUGGUACUGAGCGA
2310057M21Rik	NM_026655	CGACAAUAAAUCAGUCAAA, GGACCGGACGAAACGUUUA, UCUAUGUGAUGCCGCAAUA, AGAUCUGACUGAAUCGGAA
2810403A07Rik	NM_028814	GGCUAGACCAGAACCCAUA, AGUUUUAUCCAGAGAGUAA, GUUCUUAGUACCCGCAGUA, UAAAGAACCCCGAACGUUU
Abcg5	NM_031884	GCUCUAGCUGUGCGAUUAU, AGAAGUUAGUUACGAAGAA, CUUAUCAAGUACUGAGUCU, AGGAAAUCUUGCUGCGCUA
Actr10	NM_019785	CUACAGUUAGUGAGGCGAA, CUGGUUUGCCUGCGGUUUA, CAACUAAAGCACCGUAUAA, UCAGGAUGUAUUACCGAAA
Akap5	XM_989052	UAAAGAACCCCGAACGUUU, GUUAAACCUUCAUGGUAAU, GUAGGAAGUAGAAGUAUCA, GAGCCAAACUGAACCGAGA
Akap8	NM_019774	CUGGUUUGCCUGCGGUUUA, CAACUAAAGCACCGUAUAA, UCAGGAUGUAUUACCGAAA, CGUUAUAGCUGGAGACCGC
Amer1	NM_175179	AGAGAAUAGCUUCGAACCA, ACUCAAGAUGGGUCGCUUU, GCGCAUAGUGGGUGUUUUA, GGCCAGACACUGUGGGUCA
Anapc16	NM_025514	AGUACAGACCUUCGAUUCA, AAAUUAACCCUUACCCGUA, UGGAGAAAGGGUCCCGAAU, GGAAAAGGUCAGACGUCUA
Arc	NM_018790	GAGAAUACAGGGACGCACA, GGCUAGACCAGAACCCAUA, AGUUUUAUCCAGAGAGUAA, GUUCUUAGUACCCGCAGUA
AU019823	NM_212449	CAAACUGCCUGGCGGCUUU, CAAACUUGGUGUACGCCUU, GAUCCUUACAGAAGACGAU, GGACAUAAUCACCGCGUAA
B230217C12Rik	XM_978478	GGCCAGACACUGUGGGUCA, CCAUCAGACUGGAGUUGCA, UGACAACACCCGAGGACGA, GUAUAUAAUUUGUGGCGUG
Bcl10	NM_009740	UGUUCCAGCCAUCGAGAAU, CCGCAACAAACUUGGCUAU, UCACUUUGGUACUGAGCGA, CAAUUAAUCACUUAGGGUA
Bin3	NM_021328	CGUUAUAGCUGGAGACCGC, GAGAAUACAGGGACGCACA, GGCUAGACCAGAACCCAUA, AGUUUUAUCCAGAGAGUAA
Ccser2	NM_028407	CCGCAACAAACUUGGCUAU, UCACUUUGGUACUGAGCGA, CAAUUAAUCACUUAGGGUA, ACUCGAGCUUCUAGUACUA
Cdv3	NM_175833	GAAAUACAGUAGUCGAAGU, CUAAGUGACACCAAGAUAA, CAUGAUGGUCUGAGCUCAA, GAACAUACUUCUACAACAC
Chtop	NM_023215	GGAACCUGGAAGUCGGCAA, UUGAAGACUAACCGAAUCA, AGUACAGACCUUCGAUUCA, AAAUUAACCCUUACCCGUA
Cttnbp2nl	NM_030249	GGAUAUGGGUGUUCCGGGU, AGAGAAUAGCUUCGAACCA, ACUCAAGAUGGGUCGCUUU, GCGCAUAGUGGGUGUUUUA
Cxxc5	NM_133687	UGACAACACCCGAGGACGA, GUAUAUAAUUUGUGGCGUG, GCGCAUACUGUUUCUGAUU, CGACAAUAAAUCAGUCAAA
D430042O09Rik	XM_001002577	GAGGCCAGGGAGAGCGAUU, GAAAUACAGUAGUCGAAGU, CUAAGUGACACCAAGAUAA, CAUGAUGGUCUGAGCUCAA

Dnajc5	NM_016775	CAACUAAAGCACCGUAUAA, UCAGGAUGUAUUACCGAAA, CGUUAUAGCUGGAGACCGC, GAGAAUACAGGGACGCACA
Dym	NM_027727	GAUAUCCAUAGUAGACAUA, GAUCGUUGGUGAUAAAGUA, UUAAGACGCUUGAGACAUA, GGACAGUAGUCAUGGAGUA
Ehd2	NM_153068	GAGUAUAACUAAAGCGACA, GUACUUUGUUACACGGCCA, UGUUCCAGCCAUCGAGAAU, CCGCAACAAACUUGGCUAU
Epb4.1l5	NM_145506	GAGCCAAACUGAACCGAGA, UAGCAAGGCAGCCGAGGAA, CUUCCAUGCUGGUGCUCGA, ACUCAUAUGCUAAAGCUAA
Fam109a	NM_175474	GAUAUUCACUGCACGCUUA, GUGUCAUAGCCACGUAUAA, GGAGAUAAGUGCCGAUGCU, GCAUUACCUUCAACGGAAA
Fam210b	NM_025912	GAUCCUUACAGAAGACGAU, GGACAUAAUCACCGCGUAA, CUGAAUAAAUCUAAGACGC, GGAUAUGGGUGUUCCGGGU
Fam211a	NM_198861	GUUCUUAGUACCCGCAGUA, UAAAGAACCCCGAACGUUU, GUUAAACCUUCAUGGUAAU, GUAGGAAGUAGAAGUAUCA
Fancd2os	NM_027633	CGCGAGACGUUGCGAUACA, AGGCAGUGAUUAUGCGUCU, UAGAAACGUACAAGCGAGU, GUCCAGAACAACACGCUAA
Fancl	NM_025923	CCAUCAGACUGGAGUUGCA, UGACAACACCCGAGGACGA, GUAUAUAAUUUGUGGCGUG, GCGCAUACUGUUUCUGAUU
Fcho2	NM_172591	CAUGAUGGUCUGAGCUCAA, GAACAUACUUCUACAACAC, CGCGAGACGUUGCGAUACA, AGGCAGUGAUUAUGCGUCU
Frmd8	NM_026169	AAAGGAAGUUACGGACAUA, AAGAAGAAGGUCAGCGAAC, CCGAAUGAUGUUAUACUUA, ACUAAUCCGUCAAUUGUAU
Gata4	NM_008092	GAUCGUUGGUGAUAAAGUA, UUAAGACGCUUGAGACAUA, GGACAGUAGUCAUGGAGUA, GGACACACUUCAUAAAGAU
Gbp4	NM_008620	CCGAAUGAUGUUAUACUUA, ACUAAUCCGUCAAUUGUAU, GAGAUAUACCAAUUCAGAUCUACAGUUAGUGAGGCGAA
Gm129	NM_001033302	UUAAGACGCUUGAGACAUA, GGACAGUAGUCAUGGAGUA, GGACACACUUCAUAAAGAU, AAUAAAGCAAGUUCGGAGA
Golt1b	NM_025872	GUAGGAAGUAGAAGUAUCAGAGCCAAACUGAACCGAGA, UAGCAAGGCAGCCGAGGAA, CUUCCAUGCUGGUGCUCGA
Hgsnat	NM_133970	GAACAUACUUCUACAACAC, CGCGAGACGUUGCGAUACA, AGGCAGUGAUUAUGCGUCU, UAGAAACGUACAAGCGAGU
Hist1h2be	NM_178194	CUGAAUAAAUCUAAGACGC, GGAUAUGGGUGUUCCGGGU, AGAGAAUAGCUUCGAACCA, ACUCAAGAUGGGUCGCUUU
Hormad2	XM_987942	CAAACUUGGUGUACGCCUU, GAUCCUUACAGAAGACGAU, GGACAUAAUCACCGCGUAA, CUGAAUAAAUCUAAGACGC
Irgm1	NM_008326	GCAGAAACCAUGCGCGUGA, UGAAAGAGGCCCUGACGCA, GAUAUCCAUAGUAGACAUA, GAUCGUUGGUGAUAAAGUA
Lsm14b	NM_177727	CUGAGGAGAUAUUCCGAGA, CCUCUGUGCACAAGCCGAA, GAUAUUCACUGCACGCUUA, GUGUCAUAGCCACGUAUAA
Lyrm1	NM_029610	AGAUCUGACUGAAUCGGAA, GAGGCCAGGGAGAGCGAUU, GAAAUACAGUAGUCGAAGU, CUAAGUGACACCAAGAUAA
Mab21l3	NM_172295	GGACAUAAUCACCGCGUAA, CUGAAUAAAUCUAAGACGC, GGAUAUGGGUGUUCCGGGU, AGAGAAUAGCUUCGAACCA
Mfi2	NM_013900	GUGUCAUAGCCACGUAUAA, GGAGAUAAGUGCCGAUGCU, GCAUUACCUUCAACGGAAA, GCUGAGCAUAGUAACGGAA

Mob1a	NM_145571	ACUCAUAUGCUAAAGCUAA, UGGUCUAAGUGAAGCGUCU, GAUGGGACCAAGCGAAGUU, CUGAGGAGAUAUUCCGAGA
Mpzl3	NM_176993	ACUCAAGAUGGGUCGCUUU, GCGCAUAGUGGGUGUUUUA, GGCCAGACACUGUGGGUCA, CCAUCAGACUGGAGUUGCA
Mrpl52	NM_026851	ACUAAUCCGUCAAUUGUAU, GAGAUAUACCAAUUCAGAU, CUACAGUUAGUGAGGCGAA, CUGGUUUGCCUGCGGUUUA
Mum1l1	NM_175541	UCAGGAUGUAUUACCGAAA, CGUUAUAGCUGGAGACCGC, GAGAAUACAGGGACGCACA, GGCUAGACCAGAACCCAUA
Mvp	NM_080638	UAGCAAGGCAGCCGAGGAA, CUUCCAUGCUGGUGCUCGA, ACUCAUAUGCUAAAGCUAAUGGUCUAAGUGAAGCGUCU
Mxi1	NM_010847	GCAAAUACUUAACGAAAAG, GCAGAAACCAUGCGCGUGA, UGAAAGAGGCCCUGACGCA, GAUAUCCAUAGUAGACAUA
Mycbpap	NM_170671	AAAUUAACCCUUACCCGUA, UGGAGAAAGGGUCCCGAAU, GGAAAAGGUCAGACGUCUA, GAGUAUAACUAAAGCGACA
Nfasc	NM_182716	CCUCUGUGCACAAGCCGAA, GAUAUUCACUGCACGCUUA, GUGUCAUAGCCACGUAUAA, GGAGAUAAGUGCCGAUGCU
Ngrn	NM_031375	GCGUAGCAUGUGAGCGUUU, GGAACCUGGAAGUCGGCAA, UUGAAGACUAACCGAAUCA, AGUACAGACCUUCGAUUCA
Nrcam	NM_176930	CUAAGUGACACCAAGAUAA, CAUGAUGGUCUGAGCUCAA, GAACAUACUUCUACAACAC, CGCGAGACGUUGCGAUACA
Pdcd1lg2	NM_021396	UGGUCUAAGUGAAGCGUCU, GAUGGGACCAAGCGAAGUU, CUGAGGAGAUAUUCCGAGA, CCUCUGUGCACAAGCCGAA
Pls1	NM_001033210	GUAUAUAAUUUGUGGCGUG, GCGCAUACUGUUUCUGAUU, CGACAAUAAAUCAGUCAAA, GGACCGGACGAAACGUUUA
Poc5	NM_026173	UUGAAGACUAACCGAAUCA, AGUACAGACCUUCGAUUCA, AAAUUAACCCUUACCCGUA, UGGAGAAAGGGUCCCGAAU
Prkrip1	NM_025774	GUCCAGAACAACACGCUAA, GGAACUAAUGCAUGCGAAG, GCGUAGCAUGUGAGCGUUU, GGAACCUGGAAGUCGGCAA
Ptplad1	NM_021345	ACUCGAGCUUCUAGUACUA, AAAGGAAGUUACGGACAUA, AAGAAGAAGGUCAGCGAAC, CCGAAUGAUGUUAUACUUA
Rgag4	NM_183318	AAGAAGAAGGUCAGCGAAC, CCGAAUGAUGUUAUACUUA, ACUAAUCCGUCAAUUGUAU, GAGAUAUACCAAUUCAGAU
Rif1	NM_175238	GUUAAACCUUCAUGGUAAU, GUAGGAAGUAGAAGUAUCA, GAGCCAAACUGAACCGAGA, UAGCAAGGCAGCCGAGGAA
Rock2	NM_009072	UCUAUGUGAUGCCGCAAUA, AGAUCUGACUGAAUCGGAA, GAGGCCAGGGAGAGCGAUU, GAAAUACAGUAGUCGAAGU
S100g	NM_009789	UGAAAGAGGCCCUGACGCA, GAUAUCCAUAGUAGACAUA, GAUCGUUGGUGAUAAAGUA, UUAAGACGCUUGAGACAUA
Sat2	XM_901870	GGACACACUUCAUAAAGAU, AAUAAAGCAAGUUCGGAGA, GCUCUAGCUGUGCGAUUAU, AGAAGUUAGUUACGAAGAA
Sccpdh	NM_178653	AGAAGUUAGUUACGAAGAA, CUUAUCAAGUACUGAGUCU, AGGAAAUCUUGCUGCGCUA, CAAACUGCCUGGCGGCUUU
Sgsm3	NM_134091	GAGAUAUACCAAUUCAGAU, CUACAGUUAGUGAGGCGAA, CUGGUUUGCCUGCGGUUUA, CAACUAAAGCACCGUAUAA
Sh3gl2	NM_019535	GGAACUAAUGCAUGCGAAG, GCGUAGCAUGUGAGCGUUU, GGAACCUGGAAGUCGGCAA, UUGAAGACUAACCGAAUCA

Slain2	NM_153567	GGAAAAGGUCAGACGUCUA, GAGUAUAACUAAAGCGACA, GUACUUUGUUACACGGCCA, UGUUCCAGCCAUCGAGAAU
Srp68	NM_146032	GGACCGGACGAAACGUUUA, UCUAUGUGAUGCCGCAAUA, AGAUCUGACUGAAUCGGAA, GAGGCCAGGGAGAGCGAUU
Stx19	NM_026588	GAUGGGACCAAGCGAAGUU, CUGAGGAGAUAUUCCGAGA, CCUCUGUGCACAAGCCGAA, GAUAUUCACUGCACGCUUA
Tbc1d22b	NM_198647	UAGAAACGUACAAGCGAGU, GUCCAGAACAACACGCUAA, GGAACUAAUGCAUGCGAAG, GCGUAGCAUGUGAGCGUUU
Tchhl1	NM_027762	AAUAAAGCAAGUUCGGAGA, GCUCUAGCUGUGCGAUUAU, AGAAGUUAGUUACGAAGAA, CUUAUCAAGUACUGAGUCU
Tm9sf1	NM_028780	UGGAGAAAGGGUCCCGAAU, GGAAAAGGUCAGACGUCUA, GAGUAUAACUAAAGCGACA, GUACUUUGUUACACGGCCA
Tmco3	NM_172282	GGACAGUAGUCAUGGAGUA, GGACACACUUCAUAAAGAU, AAUAAAGCAAGUUCGGAGA, GCUCUAGCUGUGCGAUUAU
Tmem218	NM_025464	GCGCAUAGUGGGUGUUUUA, GGCCAGACACUGUGGGUCA, CCAUCAGACUGGAGUUGCA, UGACAACACCCGAGGACGA
Tprg	NM_175165	AGGAAAUCUUGCUGCGCUA, CAAACUGCCUGGCGGCUUU, CAAACUUGGUGUACGCCUU, GAUCCUUACAGAAGACGAU
Tspan2	NM_027533	GGAGAUAAGUGCCGAUGCU, GCAUUACCUUCAACGGAAA, GCUGAGCAUAGUAACGGAA, UGAAGAUUGUGGACGCCUU
Tspyl2	NM_029836	AGUUUUAUCCAGAGAGUAA, GUUCUUAGUACCCGCAGUA, UAAAGAACCCCGAACGUUU, GUUAAACCUUCAUGGUAAU
Usp6nl	NM_181399	AGGCAGUGAUUAUGCGUCU, UAGAAACGUACAAGCGAGU, GUCCAGAACAACACGCUAA, GGAACUAAUGCAUGCGAAG
Wdr47	NM_181400	CUUCCAUGCUGGUGCUCGA, ACUCAUAUGCUAAAGCUAA, UGGUCUAAGUGAAGCGUCU, GAUGGGACCAAGCGAAGUU
Zcchc12	NM_028325	CUUAUCAAGUACUGAGUCU, AGGAAAUCUUGCUGCGCUA, CAAACUGCCUGGCGGCUUU, CAAACUUGGUGUACGCCUU
Zfp106	NM_011743	CAAUUAAUCACUUAGGGUA, ACUCGAGCUUCUAGUACUA, AAAGGAAGUUACGGACAUA, AAGAAGAAGGUCAGCGAAC
Zfp799	NM_177359	UCACUUUGGUACUGAGCGA, CAAUUAAUCACUUAGGGUA, ACUCGAGCUUCUAGUACUA, AAAGGAAGUUACGGACAUA

A.1.3 Increase incidence of cells with two or more cilia (supernumerary cilia) secondary screen

These siRNAs were purchased from Dharmacon™ as an RNAi Cherry-pick Library, 0.1nmol stocks, in 96 well plate format for screening. All siRNAs targeted the mouse orthologue of the genes listed and were used in Chapter 4.

Table A.3 Increase incidence of cells with two or more cilia (supernumerary cilia) secondary screen siRNAs

Gene Symbol	*Gene Accession*	*ON-TARGETplus siRNA SMARTpool Target Sequences*
1700029I15Rik	NM_183112	CCAACAUGGCUGACUAUUA, CAGGCCUGGUGGAUGACUA, GCAUAAAGCUAUUCUGGGC, AGCAAUCUGUUCCGGAGGA
9030617O03Rik	NM_145448	GUCAAGUCCAUGAGCGCUA, GGCAAUUACUACAACGCGA, GCAUGGUGAUGGUCCCGAA, GGACAAAGUGAGGCGGUGA
Arglu1	NM_176849	ACAAGGAGCGGGUGCGGAA, AGGAUGAAAUUGAGCGAGA, AGAACAAGAACGACAGCGU, GAGGAACUGGAGCGGAUAU
Arpp21	NM_028755	CGACCAUACUGGAAGAAGG, GUCUGGAUGAGGAGGAGAA, GAAGCUGACCAGAAGUCUU, CAAGUCAGGAGCAGGCAAA
BC031181	NM_001001181	ACAAAUAGAAGGUCCGUGU, AGUUCUUUCUUACGAGUUU, GGGAAACAGUGCCGUCCGA, GCGAUAAGAAUAUGAGCAA
BC089491	NM_175033	GGUAAGCUCUCCACGAUUU, UGUGGGUGCUAUUGACGAA, AAGUGUUUGUGGAUGGGAA, GAAUCUAGGUCGGGUCUUU
Ccdc58	NM_198645	CUGGAUGACUUAACGUUAU, UGAAUUAAACACUACGGUU, AGUCAGAACUAAAUGUCGA, GUGAAGAGUUCGCCGAGUU
Ccdc85a	NM_181577	UAUCUAAAGUGACGGACGA, CGGAAUGUCUACAGCGGCA, GCAUGUUGCUGGACGAGGA, GGCAAAGAUUGGGUCGCUA
Ccnb1	NM_172301	UAACGGAAGUUGUCGAAUU, CUGCCUCACUCUAGUUUAA, CAAACUGUGUGUAACAUAG, AAGGGUGUAUUCUUGUAUA
Cdk1	NM_007659	GAACUUCGACAUCCAAAUA, GUAUAAGGGUAGACACAGA, UGCCAGAGCGUUUGGAAUA, GGCUGUAUCUCAUCUUUGA
Cela2a	NM_007919	CGAGAAACUAUGUCUGCUA, GGUGAUGGCAAGGAACUAA, UCACCAGGGUCUCCAACUA, GCCUGCUGGUUGUGGACUA
Chmp2a	NM_026885	CAAAAGACCUGGUGCGUAC, GAGGAACUACUUCGGCAAA, GAACGACAGAAACUAGAAA, GGAGAUAUGUACGCAAGUU
Clec4b1	NM_027218	AGUAUAUUACCGUCGGAAU, CGAGCUGUGUGGACAAAGU, CACCAUAUGAAGAAAGUGU, GAAUGAUAUCUCUUGCAAU
Cnih3	NM_028408	GAUGCUGGCAGGUGUCGAA, UGAGGAACAUCGAACGCAU, GCAGCAGAACUGUGCGAGU, ACAUAAUCGCCUUUGACGA
Csrnp1	NM_153287	CGGAUAGCCUUGAGACCUU, CGAGUGGAAUUCAAUCAGA, CAGGUCACGUGGCCUUUAA, CCAUCUGGCUGACAUCUUU
Cwh43	NM_145560	GGACUGAUGCUAUCGGGUU, GAAAAGUGACAUCCGGCAA, GGAUUAGGGCUACGGCACA, CAACCAGAAAGUCGUCAUA
Dcps	NM_027030	AGGUAGAACACGUGGCGCA, UGGCUCAAGUGAUCGAGAA, AAGCCAUCCUGAAGCGCUA, UAUCAGAUCACUUCGAGAU

Dnajc9	NM_134081	CUACAGCGCCUUCGUCAAA, AAGAAGAGCUAAACGAUAU, GGUCUUAAUCCUACACGGA, AGACAAAAGGAUCGGCAAA
Dpt	NM_019759	AAUCAGUGCUGGAUCGUGA, GGGUGAAUCUUAACCGCCA, GCGAAUUCGAAAACGUUUA, AGUACCAGGACUACGGUGA
E030002O03Rik	NM_172905	CCCUGAAGCUUCUGGUCGA, GUGGCAAUACCGUGUACAA, GCAAUCUGGUUGUAAGUCU, CCGCAGAAUUCUAGGAUCA
E2f4	NM_148952	GCAUCGGUCUGAUCGAGAA, GCACUGCUGGAUAGUAGUA, UCUGUGAUCUCUUUGAUGU, CUACGUGACUCAUGAAGAC
Ebf3	NM_010096	GCAGCCAGCUAGCCGUUAA, CUUAAUGGCUCCUCCGCUA, GGGCUUAGCUACACGAACA, CCAAUGACCAAGUCGGCUA
Espl1	NM_001014976	CUAGUAACUUGGAGGAAUU, GGUAAUCUCUGGGAUGUGA, GAUGUGCUCUCCAUUCAGA, UCACCGGGAUUGUGUAUGA
Fgf21	NM_020013	GUCAAAGCCUCUAGGUUUC, CUACACAGAUGACGACCAA, UGGAUGAGAUCUAGAGUUG, GAGCAUGGUAGAGCCUUUA
Foxm1	NM_008021	GAGCAUCAUCACAGCGCUA, CUGGAGCAGAAUCGGGUUA, GCGCACGGCGAAAGAUGAA, UGUGAAAGCCUAUUGGAUU
Hbegf	NM_010415	UGCUGAUGUUAGCGUGUAA, CUGAGACAGUGGUUCGUUA, UGAAAUACCGCAAGCUCGA, UGGAUUAGAGUGUCAGCUA
Hectd2	NM_172637	GCACACAGUACGACGGCUA, UGUCAGUACCCAUUCGUUA, GGACACAUCUGGUUAGCGA, CUACACAGCAGCCGAAGAA
Htatip2	NM_016865	GAGAUUAUGUGCUCAAGUC, GAUCGACUCUCAGUGUUUC, CAAAGUAACGCUCAUUGGU, GUCCAGCAGUUUCUUAUAC
Ints5	NM_176843	GGGUAAUAUGCACGAGGUA, CAUUACGGCUAGAACGGAA, GACGGGAACUGUUGCGCAU, CUUCUAAGUCCGUACGUAA
Kif27	NM_175214	GCGAGAAACGGAACGUAAA, GCUUGUACAUUGAACGAUU, CAGAAAGAGUUCCGUAAAA, GCAGAGCAUUGCCGAUAAA
Krtap15	NM_013713	CAGGGAGGCUUUACCGGAU, AGGACUCAGCAUCGUGAUA, GUUUCCGGCCUAAGCAAUA, GAGCUAGCAUUGCAACUAU
Lhb	NM_008497	CAGCAGGUGUUCUAAUCAU, CAGCAUCUGUGCCGGCUAC, UAGCAUGGUCCGAGUACUG, CCUCCCUCCUUCCCAAUAA
Lmx1b	NM_010725	GCGAGAGGCAACUGCGCAA, CAGUGGAGAUGACGGGAAA, GCGAAGAGCUUUCAAGGCA, GGAAGGUCCGAGAGACAUU
Lrrc58	NM_177093	ACCAUUAAGAUCCGAAGUA, AAAGUGUGGUGGAGUCUAU, UUACCUGCCUCGAGAGAUC, CCCUCAGUCUGCACAAUAA
Mapk8ip3	NM_013931	GAUCCAAGAUGCAGCAAGU, GAGGUGGACUGAAAUGAUC, GCUACCCGCUGCAAUGUUC, CAACACUGACUCCUUGUAU
Mcm7	NM_008568	GCUCCUAUCUUACAUCGAC, UGACAAAGAGUGACGAUGA, GGAGAUCUAUGGACAUGAA, GGACAUGAAACUUAUGAGA
Mkl1	NM_153049	GGACCGAGGACUAUUUGAA, GCUGCGUCCUGCUGUCUAA, GGUCAGCUCUUGUAACAGC, GCACAUGGAUGAUCUGUUU
Mrps10	NM_183086	CCGAUGAGCCAGACACGUU, GGAUGCUUGUGUCCCGAUA, GAGUAUAUCCAGCGAAACU, AAACAUUUGUGUAGCGCUG
Narf	NM_026272	GCGUACGGCUUUCGCAACA, GAUAUCAAGUGGUGACAAA, GCGUCAUGAUGGAGUGAGU, CGAGAGGGACUUUCCACUA
Nsl1	NM_198654	UCUCUUACCUGGUGCGUCA, GCUCUGCAUUUCAGCGUGA, CAGCAGGCCUGUGGUAAUU, GGAAUACGGCUGAGUGCCU

Nsmf	NM_020276	CACUGAACAAUGUACGAUA, GGGUGAAGGCCCAGACGUU, CCAAGGUGCCAAAGGCCGA, UGUCCUCGGUAGCGGCCAA
Oca2	NM_021879	GAUCUUAGUAGCCGUAUUU, CUGUAAAGGCAUAUCAACU, GAACAGACUGCCCUACUAA, GUGGAUUGAUUUCGAGACU
Olfr1447	NM_146703	CAUGAAUGGGCUACUAAUA, ACAAAUUCCUCCAUCCAUA, UAAUCAAGUUAGGGAACAU, CCAUCAUGACUAAAAGUAU
Olfr43	NM_146711	CAGGAAUAUUUCUUCUUCA, GGUGAUUGCAAAUGCUAAU, CAUUGAUAACUGUGAUGUA, CAGUGGUGUCCUUGUAUUA
Olfr652	NM_147048	GCAAUUAUCAGCAGGAGCU, CCAUAUACUGUUUGCAAAU, CCAUGUGUGUUCUUGCUAA, UGGCUUUGCAGUACCAAUA
Olfr713	NM_147034	GCAAGAAAUUGUUAUCGUU, CAGCACAGUUUGAAGUCUA, UGGCUUCAAUCUAGUCAUU, UCAGAAACCAUAUCACAUA
Olfr723	NM_001011530	CAACAAGUCAGCUGCACAU, GGGCAACAUCCUUAUUAUA, UGAAAUGACCCUUUUGAUA, CCUAUUAUUUACACACUGA
Phox2a	NM_008887	CAUUUACACUCGCGAGGAA, UCAAGGAGUUGGAGCGCGU, CUGAAGAGUCCCACCGCCA, GCGCAGAGGUUAGACACUA
Pole3	NM_021498	AAGAGAGACUGGACGAGGA, GGAAAGCGCAAGACUCUCA, CCUGAGAUCCUGAGACAUG, GUGCCUGAGAUCAAAAUAA
Pomp	NM_025624	CAGUCACCCUCUCGAGUUA, UCACGAUCUUCUCCGGAAA, ACGUGAUGGUGGAACAUAA, CCAUUGGUUUUGAGGAUAU
Pomt2	NM_153415	GAGUCUAUCUGCUCGGCAA, GGGCCAAUGACACGGACUU, GCGUAUGGCUCUGUAAUCA, CAAAGAAACUACUCGGAAC
Prim2	NM_008922	GCAAGAUUUCCUUAGAUCA, UCUUACAAUAUCCGGCAUA, ACAUAUCGUUGACGGAGUU, GAGUAUGAGCCACGGCGAA
Prtg	NM_175485	CUUUCUACAUUGUGGCGUA, GGAGCAAAAUUGUCCGAAA, GUGUGGAGCUUUAGCGAAC, AAACAGAUAUAGACUCGAA
Psg27	NM_001037168	GCGUAGAUAGCAAUCCAUA, GGUAUUCCAUGCUCAUUGG, UGUGAAAGUUGAAACCUUG, GCACUACAUUUACUGGACU
Psma7	NM_011969	AGUCUGAAGCAGCGUUAUA, ACAUCGAACUUGCCGUCAU, GCGCAGGCCAUUUGGUAUC, GGUCCAGUCAGGUGGCAAA
Racgap1	NM_012025	CCAGGCAAAUGAAUCAAUA, UGACACAUCUGGCAGUAUU, GGACACCGGUUAAGAUUGG, GUAAUCAAGUGGACGUGGA
Raet1e	NM_198193	GCUCAGUGGAUGAAAUAAC, ACCCAGGGAAGAUGGCAAA, GCCAGGAGUUGAGGGACAA, CCGCAAAGCCAGGGCCAAA
Ranbp9	NM_019930	GAAGACUACAUGCGAGAAU, GAAGAUUGUGACACCGAAA, CUAAACAUGACCACGAAAU, GGUCACAGCAAGUUAAUAA
Rasgrp1	NM_011246	CAAAUUAAUUCUCGAGACU, CUUGUAAAUAGCUGCGUAA, GAGAGAGGCUCCGCGGAAA, UCAAUAAGGUUCUGGGCGA
Rimklb	XM_981743	GGAUAUAUGCUCUGUUAAU, CUGCGAGGCCAAUGCAAAU, AGGAUUAUUUGGAGUCAUA, GUAUAUAUGUCGCAUGCAA
Rita1	NM_029096	GUGCAGAAUUGUAACCGAU, CCUCCUUGGAAGUGAGAUU, CCUCACACCAAGGAAGAAA, CGAAGGGCUCUCUGGCCAA
Rnps1	NM_009070	GCAGGGACAUUGAUUCGUA, GCUCCAACUCCUCCCGAUA, GUUUGAGAAUCCCGAUGAA, GGAAAAGGCGGCACGUUCA
Rplp0	NM_007475	GGACAAAGAUUUUCCAGGU, AGAUGGAAAUAAAGGCUUA, CGCCAAAGCAACCAAGUCA, GAGGAAUCAGAUGAGGAUA

Rps7	NM_011300	CGGAAAAGCCGUACGAAAA, GCGAGAAGCCGGACGAGUU, AGUUGGUGGUGGUCGGAAA, CAGCAGUGCACGACGCCAU
Scg5	NM_009162	GAUGAUGGAUGUCUAGAAA, CCAAAUCACUGUCCUCUUG, GGUUGAUGUUUGAGUGGAA, GGAACAAGAAACUCCUUUA
Sec22c	NM_178677	GCAUCGUACGGGUGAGGGA, CUUCAUAGCUUCCUACGAC, GGCCUUACGCCUUUCUUGA, UUACUACGCCCAGGAGUUU
Slitrk1	NM_199065	UGUAACAACCGGAACGUGA, UGGAGUACAACGCGAUUCA, UCACAAGUCUGCAGCGCUU, CCGAGGUGCUGAUGAGCGA
Sord	NM_146126	UCUCAAACUCGUCGCAUAA, GCUAGAAGGGGAAGCCGUA, GCACGCAGCCAUUCGGGAA, GAUGGGUAUCACAGCGUAA
Sox2	NM_011443	GAAGAAGGAUAAGUACACG, GCACCCGGAUUAUAAAUAC, GCUCGCAGACCUACAUGAA, GGACAGCUACGCGCACAUG
Spopl	NM_029773	GGGAUUAGAUGACGAAAGU, GUGCAGUGUUCUUCGACAA, GAUGACAAGCUUACGUUAU, UGAAUGAGUGGGCCGAUUA
Ssrp1	NM_182990	GCGAGAAGAUCAAGUCGGA, GCGUACAUGCUGUGGCUUA, CGAAUCGGAGUUUGAGAAA, GCAUUAGGCCAUGGGCUUA
Stat5a	NM_011488	GCAACGAGCUGGUGUUCCA, GGACCGAAACCUCUGGAAU, UGAACUACCUUAUCUACGU, GAACACGUAUGACCGCUGU
Stk10	NM_009288	GGCAUGACCUGCUGCGUAA, CAAAGAAACGGGCUCAUUG, AAAGCGAGACUCCUUCAUA, GCAAUAAGGCUCUUCGGGA
Supt7l	NM_028150	GAACCUGGCUCACGUGAAA, AUGCAAUAUAUGACGUCUA, GCGCUUUGCUGUCGACCGA, AGGCAAUGUGUCUGCGCAU
Sval3	NM_001003952	CUUGAAUAGAUCCGAGUCA, CAGGACAAAUGAAGUUAUA, CUGCCUAUGGUCAAGACAA, GGUACUACUGGGAGAAUAU
Taf6	NM_009315	CGACAGAAGCUCACUACCA, UGAGCAACAUCGACCGUAU, GAUGUGAUUAAGACGCUAA, AGAGCUGGGUCGACGAGAA
Tagap1	NM_147155	AGCUCAGAGUCCAGCGUUA, CAACAAGACAGGCGGUUCU, ACGAAGAGGCCAUUUAUUA, CGACAACACGUUCCAGUUA
Tas2r106	NM_207016	GCAGAAUCUUUGUCAUAUG, UCUCAACCUGGGAGUUAUA, GGGUAAUUAUCAAUCAUAC, GAUAGAAACAUUGAGCUUU
Tfdp1	NM_009361	CGUUUGAGAUCCACGAUGA, CGACGAGGAGGAUUGAUUA, CAAACGAAUCAGCUUAUGA, AGAAGGAGAUCAAAUGGAU
Tmed6	NM_025458	GCUACGAGGUUCAGCGCAU, ACACUCUGGAUGCGAUUAA, CCGUGGAGCUGAUCGGAAU, UCGAAUGUUUCUGGCAAUU
Tmem144	NM_027495	CAACAUUGCUGUCGUUCCA, CUGGAAUACUCUACGGAUC, UAGACUACGUGUUCGCACA, GCUCAAAGGCAUAUCGGAU
Tpmt	NM_016785	AGGCCAGAGUGGACUGCGA, GAUGAAAUGGUUCGCAGAU, GGUGUGGAAAUCAGUGAAA, GGCUAUCAAUCCAGGCGAU
Tshr	NM_011648	CAGUACAACCCUCGAGAUA, ACCAGAAGCUUAACCUAUA, AGGAUGAGGUCGUUGGUUU, CCAAGUCGGACGAGUUUAA
Ttf1	NM_009442	GCGUGAAACAGGAGAGCUG, GGAUAUGGAAACUGGGAUC, CCUUCUAGCUGUUCCCAUA, CAUAGUUCCUCCAGCAUAU
Ubn2	NM_177185	GAACACAGGGUGCUACUAA, ACACUAAGUUACCACGGAA, GUAAAGAAGCGGAAGCGGA, ACUCAGAGGCUUAUGACGA
Vpreb3	NM_009514	CGGAGGAUGAUGCCGAUUA, ACUGUUAGAUCCUGUGUAA, CUAUUACGCAGAAGAGGAA, CCCGACAGAUUCUCAGCUA

Vps53	NM_026664	GAGCCUGACUGAACGAAUU, CUGAGAACAUUACGGUUAU, AAAGAGAUCACCCGAGAUA, GAGUGGUGCAUGACGGAGA
Ypel1	NM_023249	GGUAAAGUGAAGCGGUCCA, GAUUGGAAGGCUGGUAAUA, UGAUGUAGAAGGCGAGUGA, UUGAAUCCCUGUCGUGUAA
Zfp622	NM_144523	CAUAAGGUGGGAAACGCAA, GAUACUACAAACAGCGAUU, GGUCAAAGCUAGGACGUUC, UCGAACAGCAGGCGAAGAA
Zfp790	NM_146185	ACAAACAGCACGUGCGCAA, GUAAGAAAUCACACGAAUU, GGUAAGAAGCUGUACGAGU, CCUCAGACCUCUCUCGACA
Zfp804a	XM_001000810	AGAGAGAAUUUGCUCGAAA, CAAAGAAAGCCACGGUGAA, ACUACAAACAGUAACGAAA, GGAGAUGGAACUACGAAAA

A.1.4 Combinatorial screen

Table A.4 Combinatorial Screen siRNAs

These siRNAs were purchased from Dharmacon™ as 5nmol stocks, in tube format. All siRNAs targeted the human orthologue of the genes listed, except the scrambled negative control which is non-targeting sequence across all species. The siRNAs were diluted before and used in both the combinatorial screen and downstream validation work in Chapter 5.

Gene Symbol	***Gene Accession***	***ON-TARGETplus siRNA SMARTpool Target Sequences***
ARL13B	NM_182896	CUUUAAGUGUACAUCGUAA, UGAACGAGUGCGAAAAUUA, AGACACAAGGCCAGGUUAA, GCUACAUGUUAUUGCAAGA
CEP290	NM_025114	GGAUUCGGAUGAAAUGAAA, GGAAUUGACUUACCUGAUG, GAAAGUUAAUGAGCAAUUG, GAAGUAGAGUCCCUCAGAA
IFT88	NM_175605	AGUAAAGGUGAACGACUAA, AGGAAGUGCUAGCGGUGAU, AGGCAAAUGGAACGUGAAA, GAGAAUUAUAUGAUCGUGA
PLK1	NM_005030	GCACAUACCGCCUGAGUCU, CCACCAAGGUUUUCGAUUG, GCUCUUCAAUGACUCAACA, UCUCAAGGCCUCCUAAUAG
RPGRIP1L	NM_015272	GAAUACUGGUUCCGAUUAA, UAAUACGGCUAGUUAAUGA, GAGCUGCAGGAUAGAAUUA, GAAGGUAUCUUUCGUGGAU
TMEM67	NM_153704	CAUGAAUUCUUACGACUUU, GCAGUAAGUGGACGAGAAA, CCUUAAAAGAGAAGCGGAA, UGACUUAACUGCCGAAGGA
TMEM107	NM_032354	GUAAAUAGAAAGUGCGUAC, GCACGUAACUGAUCGGAGC, CAACUGGAAGGACGCUAAA, UGGGAGUGCACUACGUAUU
TMEM216	NM_016499	CCACAUGCUCCCUGUACGA, GGCAAGCAACUCAGCAUAA, CAGGCUGACACCACACAUA, GAAACCUCUGCCAGCGAAA
TMEM237	NM_001044385	GCAAUGAGCCAUCAACUAA, AAGGCUACCUCUUGAAUUG, CAGUAGCAAUCCGAAAUUU, GAGAUCAGCUAUCCAACCU
Scrambled Negative Control	N/A	UGGUUUACAUGUCGACUAA, UGGUUUACAUGUUGUGUGA, UGGUUUACAUGUUUUCUGA, UGGUUUACAUGUUUUCCUA

A.1.5 Other siRNAS

Table A.5 Other Human siRNAs used

These siRNAs were purchased from Dharmacon™ as 5nmol stocks, in tube format. All siRNAs targeted the human orthologue of the genes listed. The siRNAs were diluted and used in downstream tertiary validation work of the secondary screens in Chapters 3 and 4.

Gene Symbol	***Gene Accession***	***ON-TARGETplus siRNA. SMARTpool Target Sequences***
ROCK1	NM_005406.2	CUACAAGUGUUGCUAGUUU, UAGCAAUCGUAGAUACUUA, CCAGGAAGGUAUAUGCUAU, GCCAAUGACUUACUUAGGA
ROCK2	NM_004850	GCAACUGGCUCGUUCAAUU, UAGAAUAUGUGGCCUAGAA, GAAACUAAUAGGACACUAA, CAAACUUGUUAAAGAAUUG
RACGAP1	NM_013277	UAAAUGAGAUUGAGCAAAG, GCGAAGUGCUCUGGAUGUU, CCACAGACACCAGAUAUUA, GAAGUCACAUCUGCCUGUU

Table A.6 Other Mouse siRNAs used

These siRNAs were purchased from Dharmacon™ as 5nmol stocks, in tube format. All siRNAs targeted the mouse orthologue of the genes listed. The siRNAs were diluted and used in downstream tertiary validation work of the secondary screens in Chapters 3 and 4.

Gene Symbol	***Gene Accession***	***ON-TARGETplus siRNA SMARTpool Target Sequences***
Rock1	NM_009071	UGUCGAAGAUGCCAUGUUA, GCGGUUAGAACAAGAAGUA, GCACCAAUCUAUCGAAGAG, GACCUUCAAGCACGAAUUA
Rock2	NM_009072	GCAAUGAAGCUUCUUAGUA, GGACAUGAGUUUAUUCCUA, GCAAUGAAGCUUCUUAGUA, CACAACAGAUGAUCAAAUA
Racgap1	NM_012025	CCAGGCAAAUGAAUCAAUA, UGACACAUCUGGCAGUAUU, GGACACCGGUUAAGAUUGG, GUAAUCAAGUGGACGUGGA

Table A.7 Other control siRNAs used

These siRNAs were purchased from Dharmacon™ as 5nmol stocks, in tube format. *PLK1* was used as a positive control for transfection as knock-down causes significant cell loss. The siRNAs were diluted and used as controls in downstream tertiary validation work of the secondary screens in Chapters 3,4 and 5.

Gene Symbol	***Gene Accession***	***ON-TARGETplus siRNA SMARTpool Target Sequences***
PLK1 (Human)	NM_005030	GCACAUACCGCCUGAGUCU, CCACCAAGGUUUUCGAUUG, GCUCUUCAAUGACUCAACA, UCUCAAGGCCUCCUAAUAG
Plk1 (Mouse)	NM_011121	UCACUCUCCUCAACUAUUU, GCAAGAUCGUGCCUAAGUC, GCAAUUACAUGAGUGAGCA, CAACCAAAGUGGAAUAUGA
Scrambled Negative Control	N/A	UGGUUUACAUGUCGACUAA, UGGUUUACAUGUUGUGUGA, UGGUUUACAUGUUUUCUGA, UGGUUUACAUGUUUUCCUA

A.2 Primers

A.2.2 PCR, Sequencing and T7 Primers

These primers were designed and optimised specifically for use within this project. Other universal sequencing primers were used for cloning validation throughout the project.

Table A.8 PCR Primer Sequences

Primers designed for PCR, sequencing and T7 assay of CRISPR/Cas9 edited genes for use in Chapter 5. Primers were designed using Primer3 (http://bioinfo.ut.ee/primer3/) to amplify exons and adjacent intronic junctions to generate a final product 500-800bp in size.

Gene Symbol	***Exon Target***	***Forward Sequence***	***Reverse Sequence***
ARL13B	1	CAGGACTCTCCAGCCACTCA	GACACCCTGGGAATGAAAGC
CEP290	2	GATCAAGGCTATTTTGCCCA	TTTCCCCTACACACCCTTTT
CEP290	2	ATGATTGTCGGCCTTCCA	AGAACACTTCCAGATTGTGACA
CEP290	2	TACAGAGGTGGAGCACAGTG	TCCCCTACACACCCTTTTAGA
IFT88	7	TGAAATAGCTTATGCGAGGTTTT	TATGTGAGCTGGTGTGGTGG
RPGRIP1L	2	AAGCAGCACATGTGGACAAT	CCAGGCAATTCAGTTTGGAG
TMEM67	1	TTGAAAATATCGCTGGGCTC	TGAAACTCCATTTACGGGGA
TMEM67	1	GATGGGTTTATTGCGGGGAG	TGCCTTGGCTTCCTCTACAA
TMEM67	1	TATGCTCAAACCTGGCAGGA	TGCCTTGGCTTCCTCTACAA
TMEM216	2	GACTGGAAGCAGGACCTCTG	AGGAAAGGCAATCCCATAGC

A.2.2 RT -PCR Primers

Table A.9 RT-PCR Primer Sequences

These primers were designed to target an intron-exon boundary across all known and predicted transcripts of each gene to produce a product less than 250bp in size. These primers were used within this project to validate siRNA knock-downs and CRISPR/Cas9 edited cell-lines. Primers conditions were optimised individually and work is presented in Chapters 4 and 5.

Gene Symbol	Exon Target	Forward Sequence	Reverse Sequence
ACTB	*3*	*CACCACTGGGACGACAT*	*ACAGCCTGGATAGCAACG*
GAPDH	*5*	*TTCACCACCATGGAGAAGGC*	*TGCAGGAGGCATTGCTGATG*
RACGAP1	2	CTGCCGTTGGAAAGATGGATACT	GGTCAGTCCTCTGCCACTTTT
TMEM216	2	GCGCCGCGAGGTAAA	GCTGTTGGATATGGTAGCAGG
TMEM107	4	ATGACAAGCAGGACATTCATCCACT	GGCACTGCAGAAGACAAAAATGT

Appendix B

FIJI Macro Script for Cilia Recognition and Quantification

B.1 Fiji Macro Script

This script was adapted from a script kindly shared by Thomas Stevenson, University of Bristol. Before the macro was run, the DAPI channel was adjusted to optimal brightness and maximum contrast.

```
run("Z Project...", "projection=[Max Intensity]");
//run("Channels Tool...");
title Get Title();
run("Split Channels");
selectWindow("C1-" + title);
run("8-bit");
run("Auto Threshold", "method=Huang)");
run("Convert to Mask");
run("Dilate");
run("Fill Holes");
run("Watershed");
run("Analyze Particles...", "size=30-infinity
circularity=0.30-1.00 show=Nothing display exclude clear
summarize");
selectImage("C2-" + title);
run("Subtract Background...", "rolling=5"); // removes
background. If this is too harsh increase the "rolling"
value.
run("Median...", "radius=3");
//run("Gamma...", "value=0.70"); //optional line may help
to include for some noisy images.
setAutoThreshold("Yen dark");
setOption("BlackBackground", false);
run("Convert to Mask"); // Generate binary image.
run("Dilate");
run("Dilate"); // makes each thresholded cilia one pixel
wider, to join any gaps. Possible to omit if results show
cilia are too long.
run("Skeletonize");
run("Set Measurements...", "area perimeter redirect=None
decimal=3");
run("Analyze Particles...", "size=0.05-100 show=[Overlay
Masks] display exclude clear include summarize add
in_situ");
        for(n=0; n<nResults;n++) {
             setResult("Cilia Length", n,
((getResult("Perim.", n))/2));        } // this for loop
takes the results of each cilia perimeter, divides by 2 to
give the length and adds it to the results table.
```

Appendix C

gRNA Sequences

C.1 CRISPR Guide RNAs

The guide RNA sequences used were cloned into pX458 plasmid and expressed as a full sgRNA under a U6 promoter.

Table C.1 CRISPR Guide Sequences

Guides were designed using crispr.mit.edu (no longer available) and were designed to the first coding exon. To ensure good expression from the U6 promoter a G was added to the start of every guide sequence. These were used to make the CRISPR heterozygote cell lines used in Chapter 5.

Gene Symbol	Exon Target	Guide Sequence
ARL13B	1	GCGGCTGGTTCAAGCGGTGGC
CEP290	2	GCCAGTTCTTCTTGACGGGGC
IFT88	7	GGGGCCCCTTGACTGACTAAG
RPGRIP1L	2	GGGTCCAACTGATGAGACTGC
TMEM67	1	GCACGGCCCGGGCGGATAAGA
TMEM216	2	GGATGCCGCTCAGTATTAGCG

Appendix D

Screen Plate Maps

D.1 Secondary screen plates

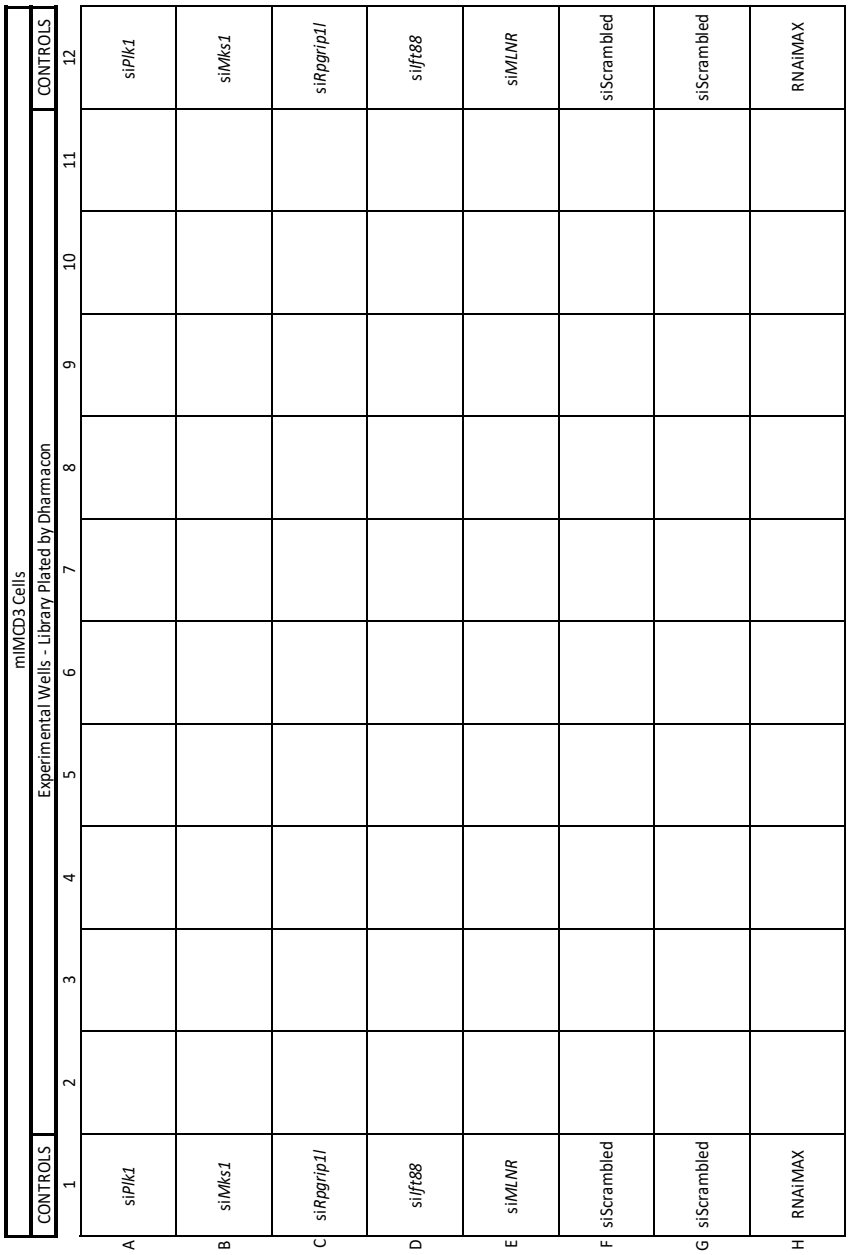

Figure D.1 Secondary Screen Plate Map

Dharmacon™ Library plates were purchased with columns 1 and 12 blank for manual addition of control siRNAs. Library plates were sub plated into working assay plates (PerkinElmer View Plates) for experimental use using a Agilent Bravo liquid handling platform. Any central wells without an experimental siRNA was treated with RNAiMax.

D.2 Combinatorial screen plates

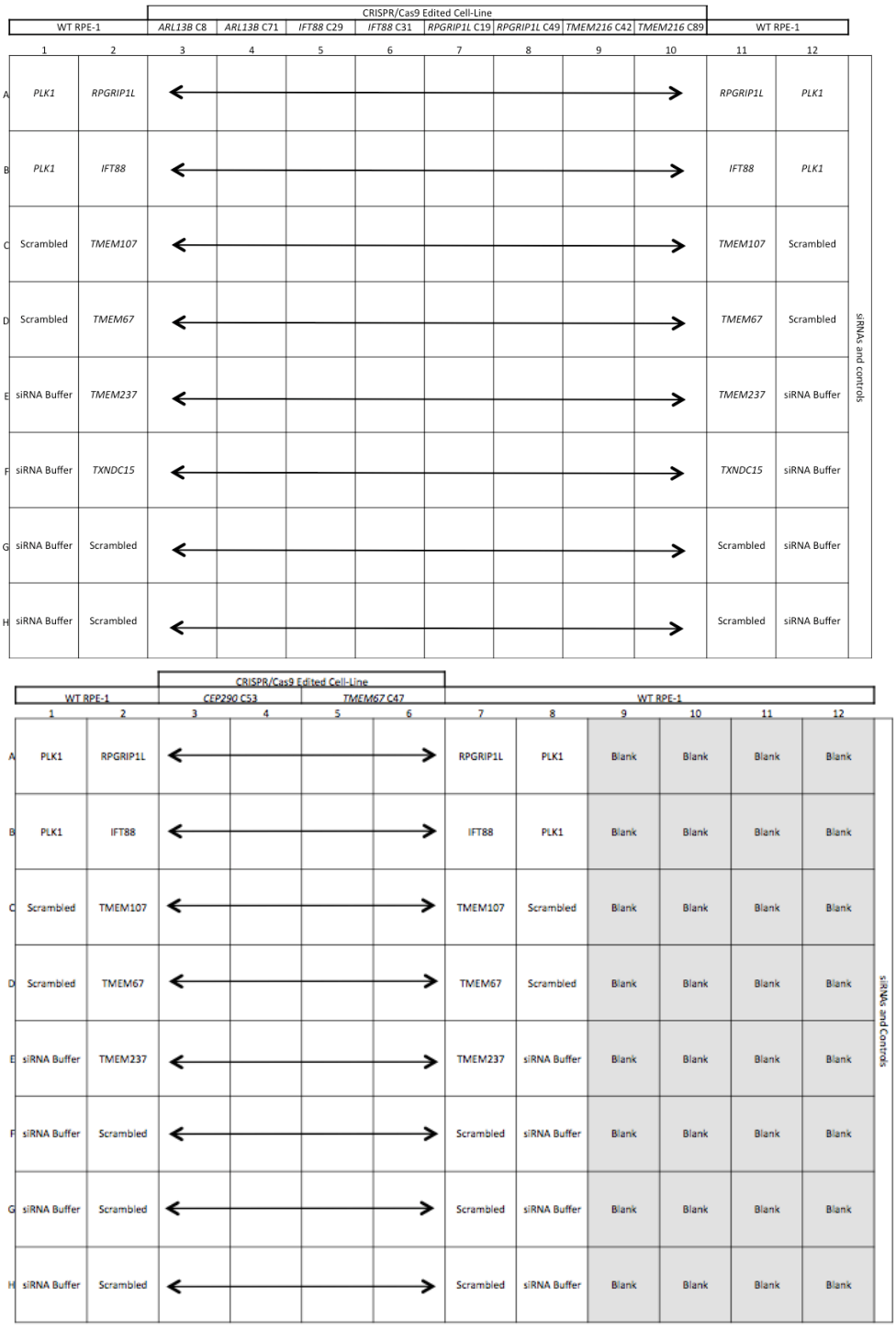

Figure D.2 Combinatorial screen plate maps

A) This layout was used to screen *ARL13B, IFT88, RPGRIP1L* and *TMEM216* CRISPR/Cas9 edited cell-lines. **B)** This layout was used to screen CEP90 and TMEM67 CRISRP/Cas9 edited cell lines. All plates were done in duplicate to ensure two technical replicates per run. All siRNAs and cell lines were plated manually using and 8-channel multi-pipette.

Appendix E

Automated Columbus™ Recognition Protocols

E.1 Increase cilia incidence screen recognition protocol

Analysis Sequence "Alice_IMCD3_v4"

Input Image	**Stack Processing :** Individual Planes **Flatfield Correction :** None		
Find Nuclei	**Channel :** DAPI **ROI :** None	**Method :** C Common Threshold : 0.4 Area : > 30 µm² Split Factor : 7 Individual Threshold : 0.4 Contrast : > 0.1	Output Population : All nuclei
Find Cytoplasm	**Channel :** DRAQ5 **Nuclei :** All nuclei	**Method :** D Individual Threshold : 0.15	
Select Population	**Population :** All nuclei	**Method :** Common Filters Remove Border Objects Region : Cell	Output Population : Whole cells
Find Spots	**Channel :** Alexa 488 **ROI :** Whole cells	**Method :** C Radius : ≤ 22 px Contrast : > 0.08 Uncorrected Spot to Region Intensity : > 1 Distance : ≥ 5.6 px Spot Peak Radius : 1 px Calculate Spot Properties	Output Population : Cilia
Calculate Intensity Properties	**Channel :** Alexa 546 **Population :** Whole cells **Region :** Nucleus	**Method :** Standard Mean	Output Properties : Intensity Nucleus Alexa 546
Select Population (2)	**Population :** Whole cells	**Method :** Filter by Property Number of Spots : == 1	Output Population : Cells with single cilium
Select Population (3)	**Population :** Whole cells	**Method :** Filter by Property Number of Spots : >= 2	Output Population : Cells with 2 or more cilia

Define Results

Method : List of Outputs
Population : Whole cells
Number of Objects
Apply to All :
Total Spot Area :
Relative Spot Intensity :
Number of Spots :
Number of Spots per Area of Cell :
Intensity Nucleus Alexa 546 Mean : Mean
Cells with single cilium :
Cells with 2 or more cilia :

Population : All nuclei
Apply to All :
Whole cells :

Population : Cilia
Apply to All :
Relative Spot Intensity :
Corrected Spot Intensity :
Uncorrected Spot Peak Intensity :
Spot Contrast :
Spot Background Intensity :
Spot Area [px²] :
Region Intensity :
Spot to Region Intensity :

Population : Cells with single cilium
Number of Objects
Apply to All :
Total Spot Area :
Relative Spot Intensity :
Number of Spots :
Number of Spots per Area of Cell :
Intensity Nucleus Alexa 546 Mean :

Population : Cells with 2 or more cilia
Number of Objects
Apply to All :
Total Spot Area :
Relative Spot Intensity :
Number of Spots :
Number of Spots per Area of Cell :
Intensity Nucleus Alexa 546 Mean :
Cells with single cilium :

Method : Formula Output
Formula : (100/a)*b
Population Type : Objects
Variable A : Whole cells - Number of Objects
Variable B : Cells with single cilium - Number of Objects
Output Name : % cells with single cilium

Method : Formula Output
Formula : (100/a)*b
Population Type : Objects
Variable A : Whole cells - Number of Objects
Variable B : Cells with 2 or more cilia - Number of Objects
Output Name : % cells with 2 or more cilia

Population : Whole cells : None
Population : All nuclei : None
Population : Cilia : None
Population : Cells with single cilium : None
Population : Cells with 2 or more cilia : None

E.2 Increase incidence of cells with two or more cilia (supernumerary cilia) screen recognition protocol

Analysis Sequence "2MoreCilia_IMCD3_Screen"

Input Image	**Stack Processing :** Individual Planes **Flatfield Correction :** None		
Find Nuclei	**Channel :** DAPI **ROI :** None	**Method :** C Common Threshold : 0.4 Area : > 30 µm² Split Factor : 7 Individual Threshold : 0.4 Contrast : > 0.1	Output Population : All nuclei
Find Cytoplasm	**Channel :** DRAQ5 **Nuclei :** All nuclei	**Method :** D Individual Threshold : 0.15	
Select Population	**Population :** All nuclei	**Method :** Common Filters Remove Border Objects Region : Cell	Output Population : Whole cells
Find Spots	**Channel :** Alexa 488 **ROI :** Whole cells	**Method :** C Radius : ≤ 12.7 px Contrast : > 0.1 Uncorrected Spot to Region Intensity : > 1 Distance : ≥ 6.3 px Spot Peak Radius : 1 px Calculate Spot Properties	Output Population : Cilia
Select Population (2)	**Population :** Whole cells	**Method :** Filter by Property Number of Spots : == 1	Output Population : Cells with single cilium
Select Population (3)	**Population :** Whole cells	**Method :** Filter by Property Number of Spots : >= 2	Output Population : Cells with 2 or more cilia

Define Results **Method :** List of Outputs

Population : Whole cells
Number of Objects
Apply to All :
Total Spot Area :
Relative Spot Intensity :
Number of Spots :
Number of Spots per Area of Cell :
Cells with single cilium :
Cells with 2 or more cilia :

Population : All nuclei
Apply to All :
Whole cells :

Population : Cilia
Apply to All :
Relative Spot Intensity : Mean
Corrected Spot Intensity :
Uncorrected Spot Peak Intensity :
Spot Contrast :
Spot Background Intensity :
Spot Area [px²] : Mean
Region Intensity :
Spot to Region Intensity :

Population : Cells with single cilium
Number of Objects
Apply to All :
Total Spot Area :
Relative Spot Intensity :
Number of Spots :
Number of Spots per Area of Cell :

Population : Cells with 2 or more cilia
Number of Objects
Apply to All :
Total Spot Area :
Relative Spot Intensity :
Number of Spots :
Number of Spots per Area of Cell :
Cells with single cilium :

Method : Formula Output
Formula : (100/a)*b
Population Type : Objects
Variable A : Whole cells - Number of Objects
Variable B : Cells with single cilium - Number of Objects
Output Name : % cells with single cilium

Method : Formula Output
Formula : (100/a)*b
Population Type : Objects
Variable A : Whole cells - Number of Objects
Variable B : Cells with 2 or more cilia - Number of Objects
Output Name : % cells with 2 or more cilia

Population : Whole cells : None
Population : All nuclei : None
Population : Cilia : None
Population : Cells with single cilium : None
Population : Cells with 2 or more cilia : None

E.3 Combinatorial screens recognition protocol

Analysis Sequence "Cilia count and intensity"

Input Image	**Stack Processing :** Individual Planes **Flatfield Correction :** None		
Find Nuclei	**Channel :** DAPI **ROI :** None	**Method :** C Common Threshold : 0.4 Area : > 30 µm² Split Factor : 7 Individual Threshold : 0.4 Contrast : > 0.1	Output Population : All nuclei
Find Cytoplasm	**Channel :** DRAQ5 **Nuclei :** All nuclei	**Method :** A Individual Threshold : 0.15	
Select Population	**Population :** All nuclei	**Method :** Common Filters Remove Border Objects Region : Cell	Output Population : Whole cells
Find Spots	**Channel :** Alexa 488 **ROI :** Whole cells	**Method :** C Radius : ≤ 24.4 px Contrast : > 0.11 Uncorrected Spot to Region Intensity : > 1.5 Distance : ≥ 4.1 px Spot Peak Radius : 0.7 px Calculate Spot Properties	Output Population : Cilia
Select Population (2)	**Population :** Whole cells	**Method :** Filter by Property Number of Spots : == 1	Output Population : Cells with single cilium
Select Population (3)	**Population :** Whole cells	**Method :** Filter by Property Number of Spots : >= 2	Output Population : Cells with 2 or more cilia
Calculate Intensity Properties	**Channel :** Alexa 488 **Population :** Cilia **Region :** Spot	**Method :** Standard Mean	Output Properties : Cilia Intensity

Define Results

Method : List of Outputs
Population : Whole cells
Number of Objects
Apply to All :
Total Spot Area :
Relative Spot Intensity :
Number of Spots :
Number of Spots per Area of Cell :
Cells with single cilium :
Cells with 2 or more cilia :

Population : All nuclei
Apply to All :
Whole cells :

Population : Cells with single cilium
Number of Objects
Apply to All :
Total Spot Area :
Relative Spot Intensity :
Number of Spots :
Number of Spots per Area of Cell :

Population : Cells with 2 or more cilia
Number of Objects
Apply to All :
Total Spot Area :
Relative Spot Intensity :
Number of Spots :
Number of Spots per Area of Cell :
Cells with single cilium :

Population : Cilia
Apply to All :
Relative Spot Intensity :
Corrected Spot Intensity :
Uncorrected Spot Peak Intensity :
Spot Contrast :
Spot Background Intensity :
Spot Area [px²] : Mean
Region Intensity :
Spot to Region Intensity :
Cilia Intensity Mean : Mean

Method : Formula Output
Formula : (100/a)*b
Population Type : Objects
Variable A : Whole cells - Number of Objects
Variable B : Cells with single cilium - Number of Objects
Output Name : % cells with single cilium

Method : Formula Output
Formula : (100/a)*b
Population Type : Objects
Variable A : Whole cells - Number of Objects
Variable B : Cells with 2 or more cilia - Number of Objects
Output Name : % cells with 2 or more cilia

Population : Whole cells : None
Population : All nuclei : None
Population : Cells with single cilium : None
Population : Cells with 2 or more cilia : None
Population : Cilia : None

Appendix F

Inconsistent results from phosphorylated myosin light chain antibodies

F.1 p-MLC (Ser19)

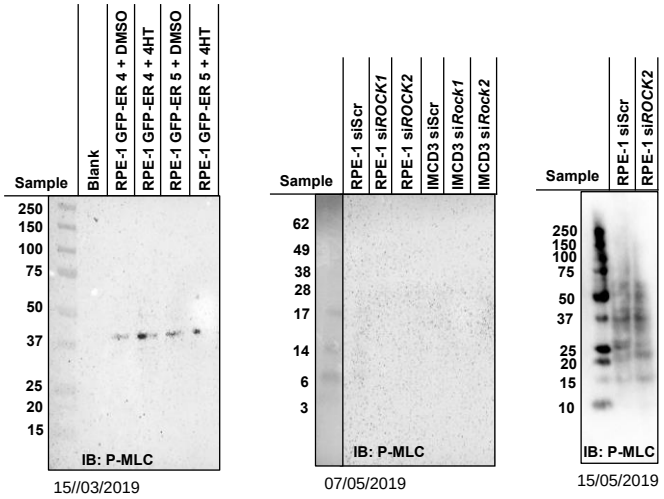

Figure F.1 Immunoblotting results for p-MLC

Example images of the different staining patterns received with CST Phospho-Myosin Light Chain 2 (Ser19) Antibody #3671. Expected single band size was 18kDa.

F.2 pp-MLC (Ser19/Thr18)

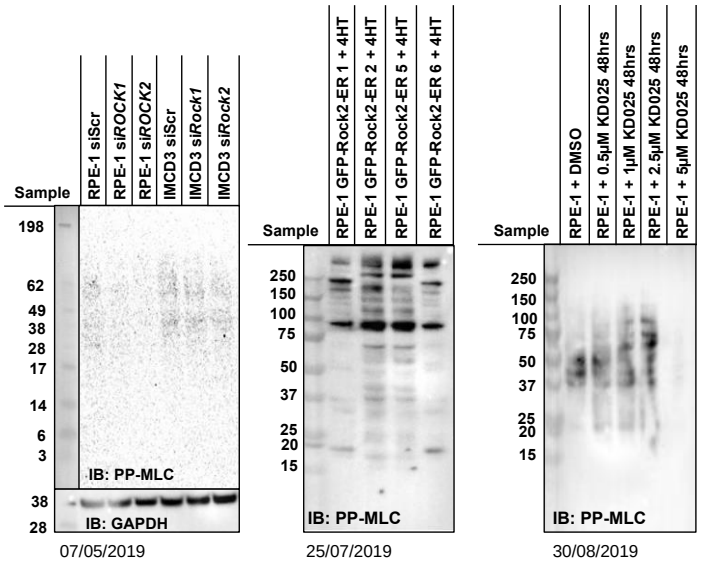

Figure F.2 Immunoblotting results for pp-MLC

Example images of the different staining patterns received with CST Phospho-Myosin Light Chain 2 (Thr18/Ser19) Antibody #3674. Expected single band size was 18kDa.

Appendix G

KD025 treatment of cell-lines

G.1 RPE-1 Cells: p-MLC structure

G.1.1 48hr KD025 treatment raw image data

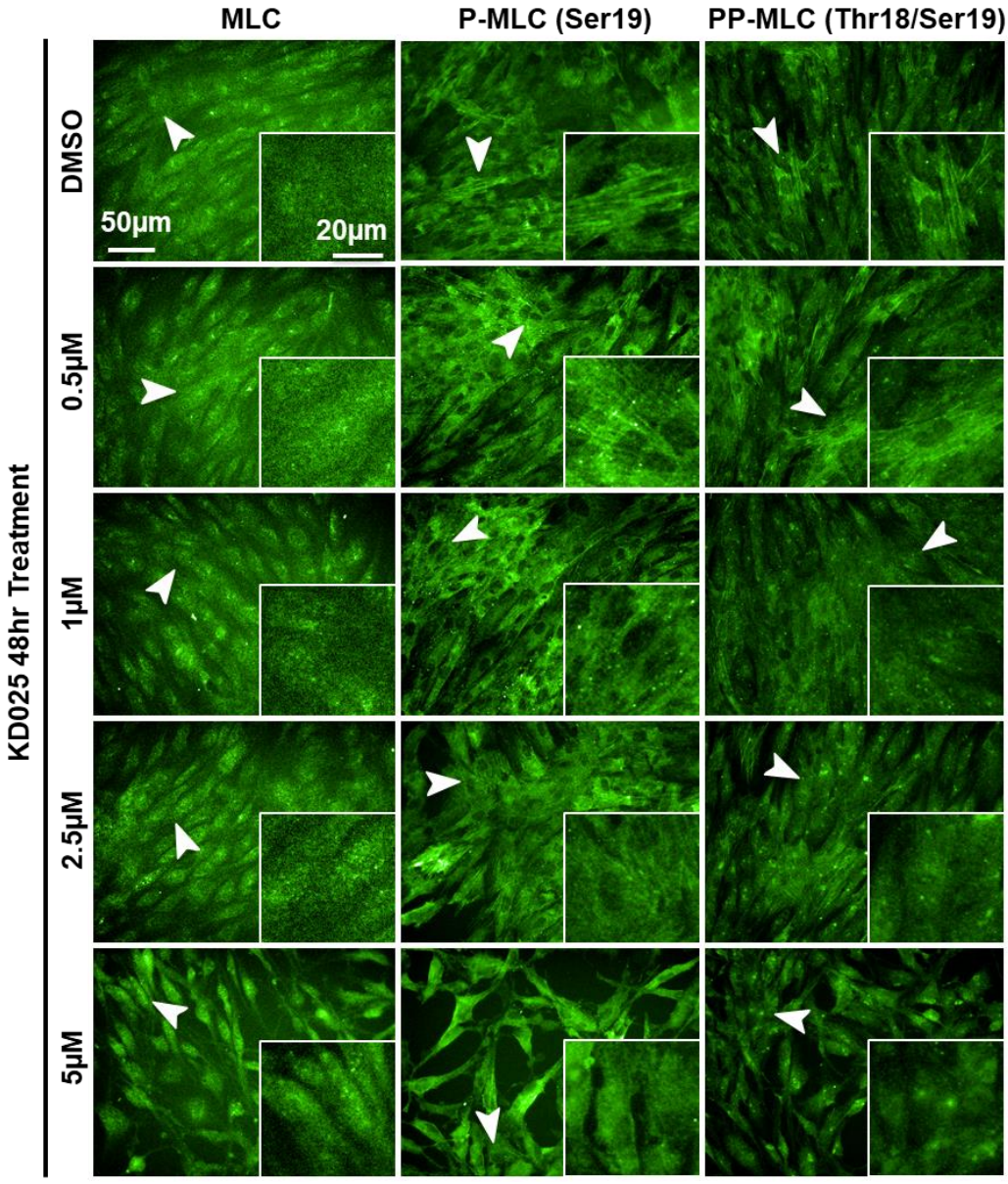

Figure G.1 Raw image data p-MLC structure in RPE-1 cells with 48hr KD025 treatment

A qualitative difference can be seen in the presence of fibre like structures in both p-MLC and pp-MLC immunostaining. There is also a change in cell shape and cell number per field of view after 48hrs KD025treatment at 5µM concentration.

G.2 mIMCD3 cells: p-MLC structure

G.2.1 2hr and 48hr KD025 Treatment

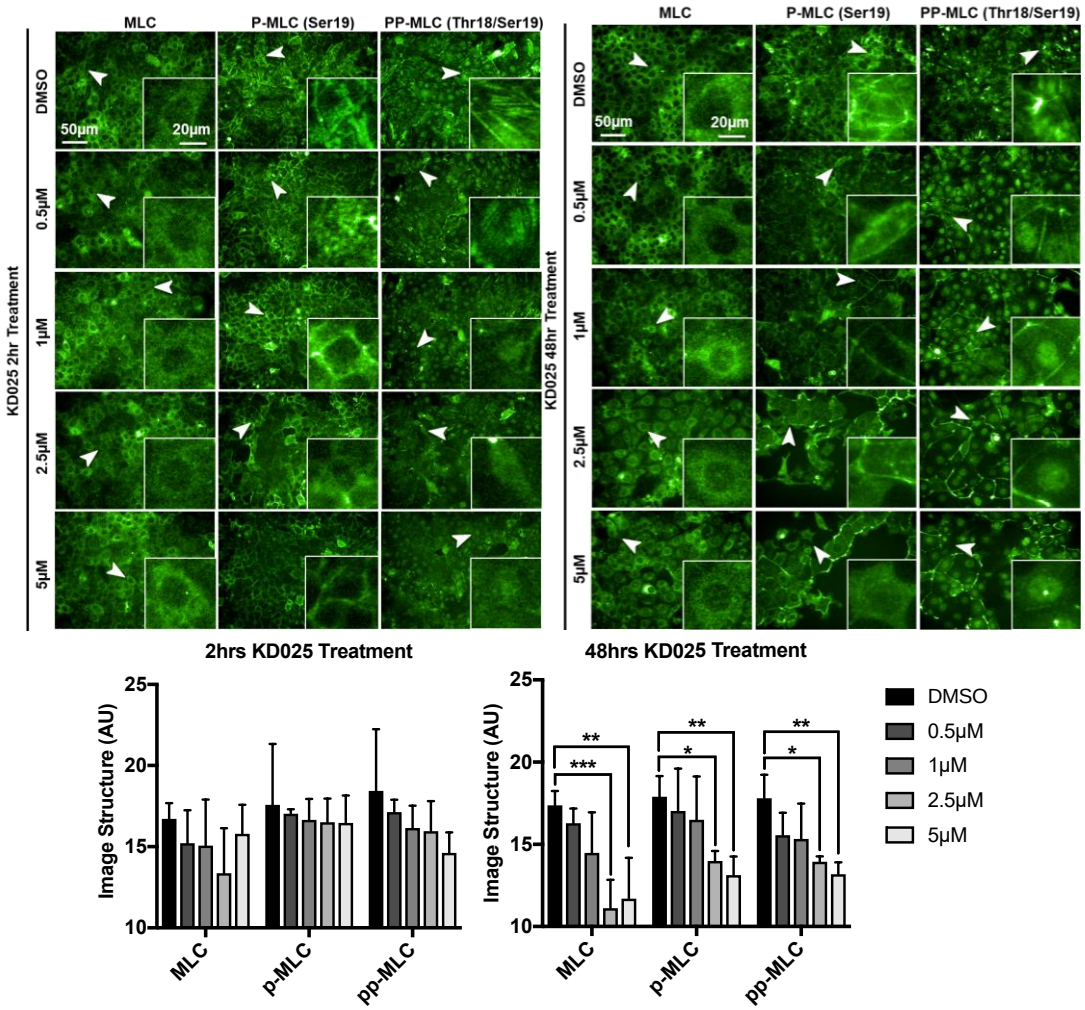

Figure G.2 p-MLC structures in mIMCD3 cells treated with KD025

2hr KD025 treatment of IMCD3s showed a qualitative loss of p-MLC and pp-MLC structures. 48hr KD025 treatment showed a both a qualitative and a significant loss in p-MLC and pp-MLC structures. However, there was also a loss of structure in MLC, suggesting general dispersal of MLC throughout the cell.

G.3 mIMCD3 cells: cilia incidence and length

G.3.1 2hr KD025 treatment

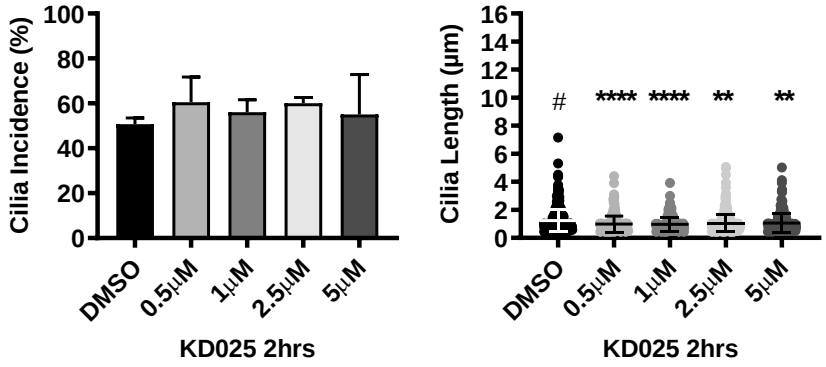

Figure G.3 mIMCD3 cilia incidence and length after 2hrs KD025

mIMCD3 cells treated for 2hrs with KD025 had no significant increase in cilia incidence. There was a significant decrease in cilia length (n=3 and at least 100 cilia measured per replicate), however this was assumed to be an artefact from the FIJI analysis macro as it best measured cilia lying flat, whereas mIMCD3 cilia extend through the Z-stacks of images taken. Qualitatively there was a large increase in cilia length. Significance calculated with one-way ANOVA with Dunnett's test for multiple corrections (cilia incidence) and Kruskal-Wallis test with Dunn's multiple comparisons test (cilia length). **=p<0.01, ****=p<0.0001. # Is the control all data sets were compared to in statistical tests.

G.3.2 48hr KD025 treatment

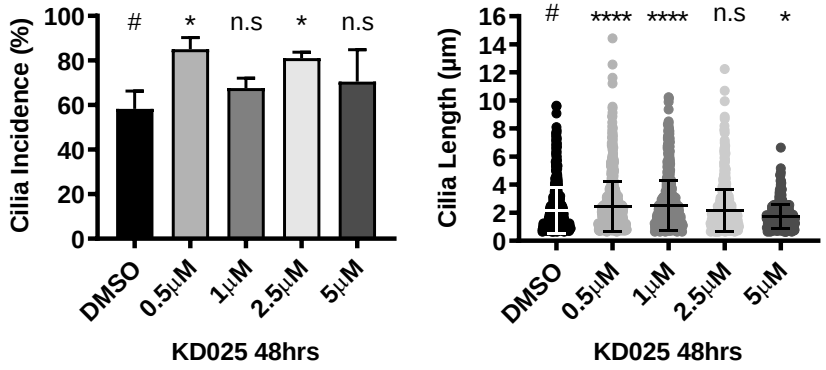

Figure G.4 mIMCD3 Cilia incidence and length after 48hrs KD025 treatment

There was a significant increase in both cilia incidence and length in mIMCD3 cells treated for 48hrs with KD025. Samples were prepared to ensure cilia lay flat for accurate length measurements (n=3 and at least 100 cilia measured per replicate). Significance calculated with one-way ANOVA with Dunnett's test for multiple corrections (cilia incidence) and Kruskal-Wallis test with Dunn's multiple comparisons test (cilia length). *=p<0.05, ****=p<0.0001. # Is the control all data sets were compared to in statistical tests.

Appendix H

Sanger sequencing of CRISPR/Cas9 edited cell lines

H.1 Sanger sequencing results

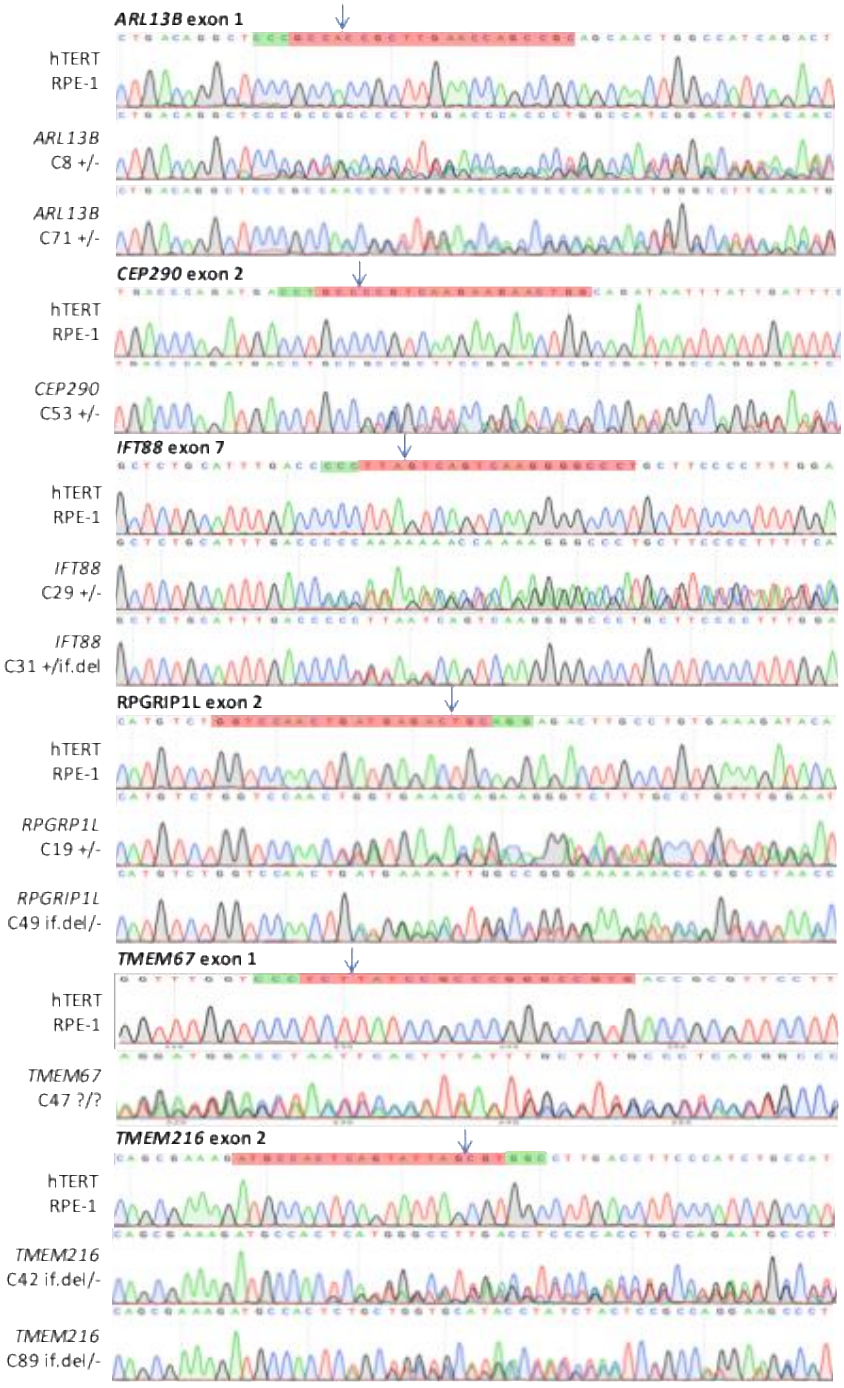

Figure H.1 Electropherogram results from CRISPR/Cas9 edited cell lines

Sequencing data from CRISPR/Cas9 edited cell lines used in Chapter 5. Green highlights = PAM sequence, Red highlights = gRNA target sequence, Blue arrows = Predicted cut site.